# DOSIMETRY FOR ABSOLUTE BIOLOGICAL EFFECTIVENESS OF IONISING RADIATIONS

Lawal Abdul Kadiri

A Thesis Submitted for the Degree of PhD
at the
University of St Andrews

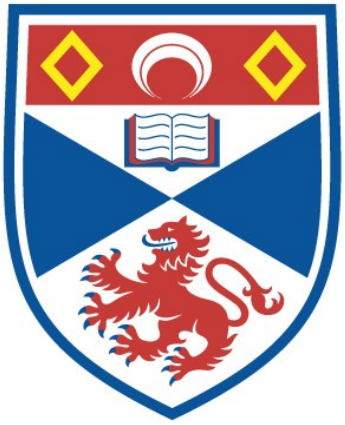

1991

# DOSIMETRY FOR ABSOLUTE BIOLOGICAL EFFECTIVENESS OF IONISING RADIATIONS.

BY

Lawal Abdul KADIRI

B.Sc., M.Sc.(ABU, Zaria, Nigeria)

A thesis presented for the degree of Doctor of Philosophy.

University of St.Andrews.

St.Andrews, Fife, KY16 9SS,

United Kingdom.

May, 1990



ProQuest LLC.
789 East Eisenhower Parkway
P.O. Box 1346
Ann Arbor, MI 48106 – 1346

Th A1228

## CONTENTS OF THE THESIS.

# DECLARATION.

I Lawal Abdul KADIRI hereby declare that this thesis has been composed by myself, that it is a record of my own work, and that it has not been accepted in partial or complete fulfilment of any other degree or professional qualification.

This research was carried out in the Department of Physics and Astronomy in the University of St.Andrews under the supervision of Dr. D. E. Watt.

Lawal Kadiri. Date.....

I was admitted to the Faculty of Science of the university of St. Andrews under Ordinance General No 12 on 3rd Febuary, 1987 and as a candidate for the degree of Ph.D on 1st October, 1987.

Lawal Kadiri. Date.....

# CERTIFICATION

I hereby certify that the candidate Lawal Abdul KADIRI, has fulfilled the conditions of the Resolutions and Regulations of the University of St.Andrews appropriate to the Degree of Doctor of Philosophy.

David E. Watt
Research Supervisor

Date 27/8/90

## LIST OF PUBLICATIONS.

D.E.Watt, C.Z.Chen, L.A.Kadiri and A.Younis. Towards a unified system for the expression of Biological damage by ionising radiation. IN: Health effects of low dose of ionising radiation-Recent advances and their implications. BNES, London, 1988, pages 37-41.

D.E. Watt and L.A. Kadiri. Physical quantification of the biological effectiveness of ionising radiations. Int. J. Quantum Chemistry. In press.

L.A.Kadiri and D.E.Watt. Common mechanism in the induction of various biological effects of ionising radiations. Presented at the ARR meeting. St.Andrews, 3-5 January, 1990. Abstract published in *Int. J. Radiat. Biology* , **57** (1990) 1259.

L.A.Kadiri, D.E. Watt and I.A.M. Al-Affan. Biophysical calculations of the initial yield of DNA double strand breaks in irradiated mammalian cells. Presented at the ARR meeting. St.Andrews, 3-5 January, 1990. Abstract published in *Int. J. Radiat. Biology* , **57** (1990) 1253.

## ACKNOWLEDGEMENTS

"Yettore tabbitino ha Jaumirawo". I wish to express my gratitude to the following.

My supervisor, Dr. D. E. Watt, for the valuable guidance, help, advice, encouragement and stimulating discussions throughout the course of this work. His accessibility, friendliness, willingness to assist in both academic and nonacademic matters are exemplary manners of a supervisor and a gentleman.

The academic staff and students of Physics and other departments of the University of St.Andrews for a variety of assistance. Messes R. McGraw, Myles White, Tom McQueen, J. Clark, M. Robertson and their collaborators at the Mechanical and Electronic workshops who have offered valuable technical assistance. E. Bell and L. Mordi of the Library and many other supporting staff of the Physics Department for excellent services.

Elias, Chen, Younis, Yusuf, Aba-Umar, Ibrahim and many fellow colleagues at the Radiation Research Laboratory for their understanding, discussions, and encouragement which provided an atmosphere conducive for research. Aminu, Abdullahi, Garba, JK, Yahya, ThankGod, Ralphel, Wale and many other friends who have made my stay in St. Andrews easier.

Ahmadu Bello University, Zaria, in collaboration with the Federal Government of Nigeria, for the fellowship that enabled this work to be done.

Dr. S. B. Elegba, Dr. J. Adetunji, Prof. J. Kiefer, Prof. D.E. Ajakaiye, Mallam H. Mijinyawa and many other teachers, supervisors and friends at Zaria and elsewhere for providing continuing moral and academic guidance.

Jika, Sa'ad, Habu, Mahmud and many other friends for offering me cushions of support at difficult times.

Last, but not the least, my parents and other relatives for providing me with motivation at an early stage, support and encouragement all along. To all 'miyetti sosai' and thanks.

# *DEDICATION.*

*This work is to dedicated to Bappa,*

*Nandu, Hamma and Mallum.*

## ABSTRACT

It was shown that the conventional radiation dosimetric system which is based on RBE and LET is incapable of determining the likely consequences of ionising radiation exposure. Analyses of data on the induction of the chromosome aberrations, mutations and transformation in mammalian cells by radiations of different types and energies has indicated that (a) the induction of double strand breaks (dsb) in the DNA is their common critical lesion. (b) Fast ions and neutrons radiations are by order of magnitude more damaging than photons and electrons of equal mean free path. (c) Damage is through intra track action of the charged particles.

A new system of radiation dosimetry, which does not require a radiation quality parameter, was proposed. It was based on the observation that for each of the biological endpoints considered an Absolute Biological Effectiveness (ABE) for damage by the charged particles can be defined as the product of the charged particle fluence and the saturation effect cross section, scaled with the efficiency ($\varepsilon$) of damage by radiation of mean free path ($\lambda$). $\varepsilon$ is given by $1-\exp-(\lambda o/\lambda)$, where $\lambda_o$, about 1.8nm, is the mean inter-strand distance of the DNA.

The physical requirements for its instrumentation, basically the emulation and quantification of the induction of dsb in the DNA, were defined. The feasibility for its realisation using detectors based on gas ionisation, superconductivity, secondary electron emission, and semiconductivity was assessed. Ultrathin films of rectified, organic semiconductors appeared to have the best potential, but such materials are not yet available in the physically characterised form as may be required for detector construction; investigations were made with available films of plastic scintillators.

Experimental investigations have shown that by using coincidence techniques, plastic scintillator films can be used as a single volume 'microdosimeter', that is as counters of single strand breaks. Its use as a single volume 'nanodosimeter' is handicapped by light losses in the detector assembly which reduces the detector's sensitivity, efficiency and resolution. Semi-empirical analysis showed that the production of light from a phosphor differs fundamentally from the induction of biological damage. It was inferred that the plastic scintillators are unsuitable for instrumentation of the proposed system of dosimetry. Suggestions for future investigations were made.

# TABLE OF TEXT CONTEXT

# LIST OF TABLES

# LIST OF FIGURES

# LIST OF ABBREVIATIONS

| | |
|---|---|
| ABE | Absolute biological effectiveness |
| ADC | Analouge digital converter |
| AC (or DC) | Alternating (or Direct) current |
| DNA | Deoxyribonucleic acid |
| dsb | double strand break |
| CHO | Chinese hamster ovary (cells). |
| csda | continous slowing down approximation |
| cps | counts per second |
| FWHM | Full width at half maximum |
| HPRT | hypoxanthinetransferabusyl |
| HVL | Half value layer |
| ICRP | International commission on radiological protection |
| ICRU | International commission on radiological measurements and units |
| LET | Linear energy transfer |
| MCA | Multichannel analyser |
| MSAC | Mutistep avalanche counter |
| MWPC | Mutiwire proportional counter |
| PM | Photomultiplier |
| PPAC | Parrallel plate avalanche counter |
| RBE | Relative Biological Effectiveness |
| RQI | Radiation Quality Index |
| QE | Quantum efficiency |
| SBD | Surface Barrier Detector |
| sc | sacchramomyces cerevisiae |
| SCA | Single Channel Analyser |
| SEE | secondary electron emission |
| SNR | signal-to-noise ratio |
| ssb | single strand break |
| STJ | Superconductive tunnel junction |
| TE | Tissue equivalent |
| TFD | Thin film detector (plastic scintillator) |
| 6-TG$^r$ | 6-thioguanine ressistance |
| UNSCEAR | United Nations Scientific Committee on Effects of Atomic Radiations |
| VDN | Voltage divider network (to a photomultiplier). |

# CHAPTER ONE
# INTRODUCTION AND SCOPE.

## 1.1 THE NEED FOR AND THE PROBLEMS OF RADIATION DOSIMETRY

The basic objective of radiation dosimetry is to predict the most probable effects of radiation perturbations on an object of interest. The attainment of this goal is complicated by the various physical and chemical effects induced in the interaction of ionising radiations with matter. The nature and the extent of the effects under a given irradiation condition depend on the characteristics of that radiation (energy, momentum, etc) and of the object irradiated (its constitution, size, etc). In principle, any phenomenon which results from the action of radiation may be relevant for radiation detection. The phenomena which may be practically employed for radiation dosimetry are limited, mainly due to the requirement that, for the detector's response to be a useful indicator of radiation action on an object of interest, it should emulate it.

This restriction is particularly severe when living matter, say man, is exposed, for the initial physical and chemical effects can interact with the complex processes of life and may lead to complicated biological responses being manifested over a wide time scale (Boag, 1975). Genetic effects such as leukemia are manifested a decade or more after exposure. Biological detectors such as the retrospective scoring of dicentric aberrations (Lloyd and Purrot, 1981) can be used, but are of limited value due to poor reproducibility and durability. With physical detectors, on the other hand, problems arise not in the detection and quantification of the radiation exposure, but in the interpretation of the observed changes in terms of the probability of inducing significant genetic and somatic effects.

In the modern world, man is increasingly exposed to ionising radiations either as a part of his natural environment or in the process of utilising it as a tool for realising other ends. The fields in which ionising radiations are beneficially used is wide and is increasing. They are industrially used in quality measurements, sample analysis, sterilisation of products, food preservation, plastic modification etc. At research level, radiations are used as probes for investigating molecular, atomic and nuclear configuration as in X-ray diffraction, radiography and in electron microscopy. Other research applications include neutron activation analysis, proton induced X-ray fluorescence, micro-analysis and auger electron spectroscopy. In agriculture radiations are used in mutating seedlings for improving yield.

Medically they are used in therapy, tomography, diagnosis of bone fracture, determination of bone mineral content and volumes of body fluids, etc.

In order to sustain this expansion it is necessary to minimise the associated health risks and to optimise the efficiency of the radiations. Both objectives can be realised through a comprehensive understanding of the mechanisms of radiation interaction with matter, and with living tissue in particular. The knowledge will then be used in the design of
(a) relevant and reliable radiation detectors,
(b) a system for the interpretation of the detector response in terms of the likelihood of inducing significant health hazards to man, and
(c) a set of rules and regulations for radiation protection.

## 1.2 THE ROLE OF RADIOBIOLOGICAL MODELS.

The knowledge hitherto available on the deleterious action of ionising radiation with living matter is limited and inconclusive. There are two sources of data: Epidemiological survey and experimentation with rodents and cultured cells. The data available from uranium mine workers, accidental over-exposures and from atomic bomb survivors of Hiroshima and Nagasaki is difficult to assess (UNSCEAR, 1977). Due to the length of the observation periods, complications with other factors such as carcinogens create uncertainties. Experimental investigations with rodents could be informative, but large number of animals and high doses have to employed, and their relevance to man is in doubt. Except for occasional, accidental exposures and in fractionation high dose therapy (Elkind, 1984), the situation of usual interest is that of low doses (less than 0.1Gy) of prolonged exposure, as exist in the vicinities of nuclear power reactors, radioactive waste containments, X-ray sources, accelerators etc. The biological effects of radiations at such doses is not well known. Extrapolation of their likely consequences from data obtained with high doses (more than 1Gy) is difficult and may not be based on sound grounds (Upton, 1977). The improvisational approach is to develop biophysical models of radiation action based on the statistically more reliable high dose data. The models are then used as a guide in the extrapolation of the possible effects of low doses (e.g., Kellerer and Rossi, 1972).

In-vitro experimentation with viruses, bacteria, yeast and cultured mammalian cells can yield the desired statistical accuracy and provide data on which biophysical models can be developed and tested. The fact that the cells are the basic units with which organised

systems are built and that all manifestable effects may be initiated at cellular level provides justification for their use. Furthermore, in these systems, the conditions of exposure and in some cases the cells themselves can be manipulated and modified in a predetermined manner. The biological end point most widely employed is cellular inactivation or inhibition of reproductive capacity (e.g., Cox et al, 1977). The other effects sometimes investigated are the induction mutations (Kiefer et al, 1982), strand breakage (Kampf and Eichhorn, 1983), chromosomal aberrations (Edwards et al, 1985) and transformations (Miller et al, 1989).

The general methodology is to determine the yield of a specified endpoint as a function of the absorbed dose, D, defined loosely as the energy absorbed per unit mass, for radiations of different types and/or energies. Often the exposure conditions may be varied. The analysis of the relationship between the radiation dose and the manifested biological response is the basis of most biophysical models of radiation action and dosimetry. Two basic types of dose response are observed. In one the increment in effect is linearly proportional to a dose (D) increment.

$$Y = \alpha_0 + \alpha .D \qquad 1.1.1$$

Where Y is the yield of specified effect. $\alpha_0$, the spontaneous frequencies of the specified end point, is often negligible. In the other the response is a non linear function of the dose and is a polynomial of the type

$$Y = \alpha_0 + \alpha D + \beta D^2 \qquad 1.1.2$$

The actual values of the empirical parameters $\alpha$, $\alpha_0$, and $\beta$ depend upon the system and the end point, the dose rates and dose range used.

The shape of the dose-response curves is often associated with the mechanism of radiation injury (for example: Chadwick and Leenhouts, 1981). Dose response data describable by expressions of the type (1.1.1) and (1.1.2) are associated with the induction of damage by the passage of a single and multiple charged particles across the radiation susceptible site, respectively (Kellerer and Rossi, 1972; Neary, 1965). But more complicated dose response curves have been observed (Elkind, 1984). There are also alternative interpretations based on the involvement of cellular repair processes (Alper, 1979; Goodhead et al, 1980).

It is also expected of biophysical models to determine the possibility of a threshold in the

induction of biological damage. Currently dose-effect relationship are assumed to have no threshold (ICRU-40, 1986). Of particular relevance to the theme of the present study is the need for models to identify the critical radiosensitive sites and their sizes. This is significant in the design of radiation dosimeters, for the interaction of radiation with matter is a random process. Consequently, the ability of characterising the interaction with mean quantities such as the absorbed dose depends on the volume of the absorber. For volumes with mean diameter of micron or less energy deposition by both low and high LET radiations can not be described with mean values (Rossi, 1968).

## 1.3 RADIATION QUALITY: THE LET.

Figure 1.1 illustrates a typical set of dose response curves obtained by irradiating mammalian cells with radiations of different type.

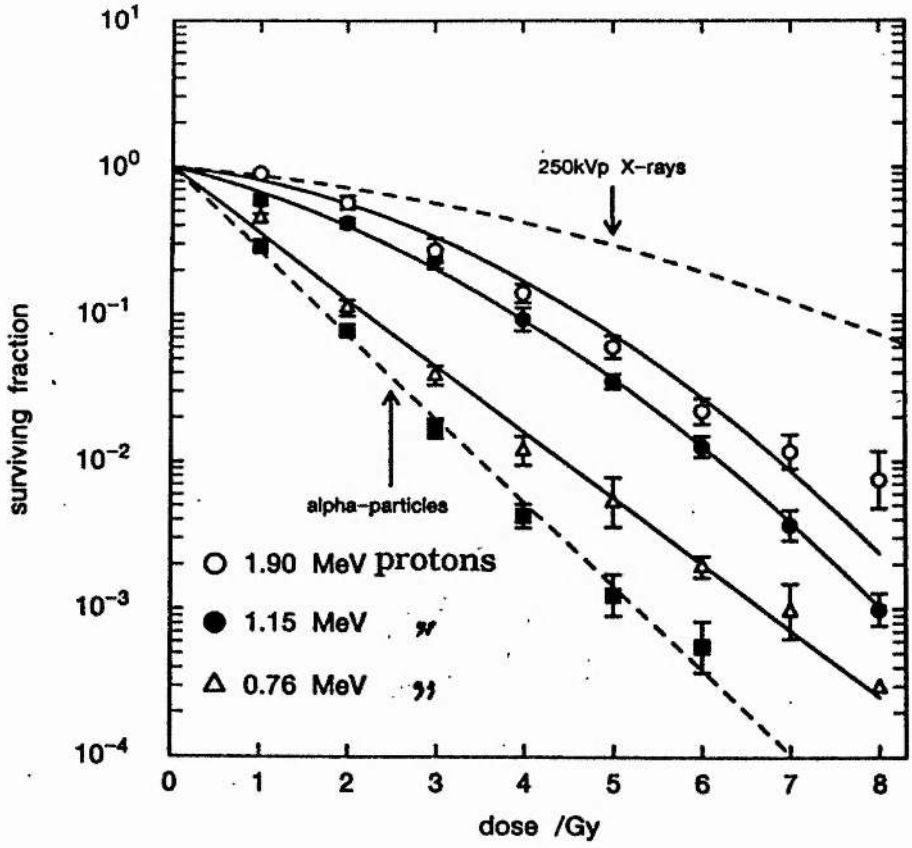


FIGURE 1.1: The survival fraction of V79 cells irradiated with radiations of different type and energy plotted as a function of dose. Adapted from Folkard et al (1989).

It has been generally observed that the yield of lesions depends on the type of radiation for a given dose. Photon and electron radiations are generally less efficient than fast charged particles and neutrons on a unit dose basis. The inherent damage capability of different radiations in inducing a specified endpoint, in a given system, under given conditions of exposure is referred to as the radiation quality. An ideal quality parameter should be capable of predicting the biological response to different radiations and provide a functional relationship between the responses of physical or biological detectors to a given radiation. But such a parameter is yet to be unambiguously identified. Various parameters such as lineal energy (ICRU-36, 1983), $Z^{*2}/\beta^2$ (Butts and Katz, 1967) and linear primary ionisation (Watt et al, 1985) have been proposed. The present system of radiation dosimetry, used for legislation purposes, is based on the parameter linear energy transfer (LET).

In its original form (ICRU-16, 1970), the LET is defined as the energy transferred per unit length of the primary particle track. In this form, it is termed as the total LET, $L_\infty$. It is quantitatively equal to, but conceptually different from, the collisional stopping power (dE/dX). The dE/dX refers to the loss of energy by the incoming charged particle whereas the LET characterises energy transfer to the absorber. In close collisions, energetic electrons (δ-rays) having ranges that exceed the dimension of the absorber may be ejected. Thus not all the energy lost by the incoming particle is absorbed "locally" in the medium of interest, and the two parameters are not equal.

The difference depends on the radiation type and the size of the absorber. For photon and electron irradiation a maximum of half the kinetic energy of the primary particle may be transferred to the secondary electron. The maximum energy transferable to the δ-ray ($T_{\delta,max}$) in the case of heavy charged particles of mass M and energy E is

$$T_{\delta,max} = \frac{(m+M)^2}{(4m.M)}E$$

Where m is the mass of the electron. The δ–rays can in turn ionise and generate other electrons or escape from the system. In consideration of this, the restricted LET ($L_\Delta$) is introduced (ICRU-16, 1970).

The restricted LET is defined as the quotient of ΔE to Δx, where Δx is the distance

traversed by the particle and $\Delta E$ is the mean energy loss due to collisions with energy transfers less than some specified value $\Delta$. The limit, $\Delta$, usually 100eV; is the energy of secondary electrons considered to have ranges exceeding the dimensions of the pertinent site. The δ–rays having energies greater than the cut off are considered as separate tracks (ICRU-16, 1970) and their LET is appropriately evaluated. Although an energy cut off is normally employed a radial distance cut off may also be imposed (ICRU-16, 1970).

Practical radiation fields, except in the case of photon or electron irradiation, are usually comprised of a mixture of charged particles of different type, energy and, therefore, LET. Nuclear reactor workers are for instance exposed to gamma rays and neutrons having energies ranging from a few hundreds of keV to a few MeV. Thus the LET is not single valued. Two LET averages are defined (RBE Committee, 1963); the track averaged or frequency averaged LET ($L_T$):

$$L_T = \frac{\int_0^\infty L\, t(L)dL}{\int_0^\infty t(L)dL} \qquad 1.1.3$$

and the dose averaged LET ($L_D$):

$$L_D = \frac{\int_0^\infty L^2 t(L)dL}{\int_0^\infty L\, t(L)dL} \qquad 1.1.4$$

where t(L) is the fraction of track length with LET between L and L+dL. Restricted dose averaged LET and restricted frequency averaged LET can be analogously defined (ICRU-16, 1970). One problem with the use of these quantities is that whereas the total LET distributions are measurable the restricted LET distributions have to be calculated analytically for a given situation (ICRU-16,1970; Howard-Flanders, 1958). This, therefore, creates complications in the implementation and limits the usefulness of the present radiation dosimetric system.

## 1.4 THE CONVENTIONAL DOSIMETRIC SYSTEM: ITS HANDICAPS.

In the current radiation dosimetric system used for legislation purposes (ICRU-16, 1970;

ICRU-40, 1986) radiations are primary characterised in terms of the absorbed dose, and the linear energy transfer (LET). The latter is used for the specification of radiation quality. The parameter conventionally used for expressing the biological effectiveness of ionising radiations is the relative biological effectiveness (RBE).

The RBE of a radiation for a given type and severity of effect, is the ratio of the absorbed dose of some reference radiation which produces that effect, to the absorbed dose of the test radiation that produces an identical effect under similar conditions of irradiation. The reference radiation can be any stated radiation but is usually 250kV X-rays or $^{60}Co$ gamma rays. Thus, under the present practices, correlation between the biological effectiveness of radiation and the physical quantities measurable and/or derivable from physical radiation detectors, is obtained by taking the RBE as a function of the total LET or one of the LET averages. The RBE generally varies with the type and severity of biological effect, the cell type and its physiological condition. It also varies with the ionising density of the radiation and its rate of delivery.

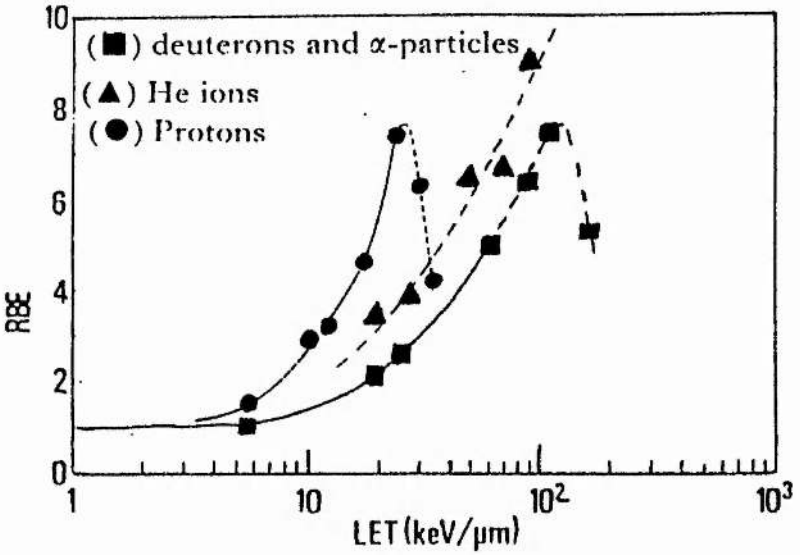


FIGURE 1.2: The relationship between RBE and LET for the induction of cellular inactivation by radiations of different quality and type. Adapted from Belli et al (1989).

However, using data obtained from track segment experiments (whose distribution of LET is narrow) several investigators explored the functional relationship between the RBE and

LET. It was observed (Barendsen, 1964) that in the case of loss of reproductive capacity of asynchronous human cells, the RBE initially increases with LET until a maximum value (greater than one), at about 100keV/μm to 200keV/μm, is attained, after which it decreases or increases less rapidly. Similar trend was observed for other biological endpoints. But a unique functional relationship between the two parameters was not obtained. Recent investigations (see Figure 1.2 ) have shown that at the same LET protons are more damaging than α-particles. Other results (Kraft, 1987) have shown that the value of the LET at which the efficiency of cellular inactivation saturates depends on the ion type and the RBE maxima shifted to higher LET values for heavier ions. These suggest, and it is shown in Chapter two, that the parameters LET and RBE are unsuitabile for a clear characterisation of biological damage.

It is expected that $L_D$ would be a suitable quality parameter if RBE is a linear function of LET, and the $L_T$, if RBE is independent of LET or decreases with the inverse of the frequency mean LET. Bewley (1968) has shown that neither the total LET nor either the $L_D$ or $L_T$ uniquely determines the biological effectiveness of fast neutrons. A wide relationship was also reported between the induction of chromosome aberration in lymphocytes and LET by Edwards et al (1985).

The limitations of LET are both conceptual and practical (Kellerer, 1987; Kellerer and Chemlevsky, 1975; ICRU-16, 1970). It is a mean value pertaining to a single particle of specified charge and velocity which degrades its energy in accordance with the continuous slowing down approximation (csda). It describes neither random fluctuations in the interaction of a given particle nor fluctuations among identical particles. For the more usual heterogeneous radiation fields, the mean values and restrictions are not conclusive since the weighting factors of the different components are usually unknown and the selection of the energy cut off limit for delta rays has to be done with due consideration of the size of sensitive targets. The smaller the size of the site considered, the greater the variation in the absorbed dose and LET. The implications of these in radiotherapy and practical instrumentation for radiation protection are as follows.

The basic requirement of radiotherapy is to deposit appropriate doses of radiation energy to the tumour site with minimum damage to the surrounding tissue. In conventional photon beam therapy a description of treatment regions with isodose contours having a resolution of the order of a millimetre is sufficient; inhomogeneity of energy resolution within cellular

or subcellular dimensions of micrometers or nanometers is unimportant, due to the diffused pattern of ionisation of these radiations. Oxygen effects are however important in the interactions of these low LET radiations (Raju, 1980). In radiotherapy treatment with high LET radiations oxygen effects are reduced and better depth-dose distribution can be obtained, but fluctuations of energy deposition at subcellular level are of practical significance, particularly towards the end of the particle's ranges. Isodose contours having resolution of the order of nanometers are therefore needed. In this respect LET and conventional ionisation chambers are inadequate.

The existing system legislation for radiation protection is based on the concept of dose-equivalent (H), with which limits for the exposure to radiation under given circumstances are set. By definition

$$H = N \cdot Q_F \cdot D \qquad 1.1.5$$

where N is equal to one, except in the case of exposure to the eyes; D is the absorbed dose of a given radiation type (in grays) and $Q_F$ is the quality factor. The quality factor is a fixed value but selected in such a way as to represent a conservative judgment of the maximum RBE. The quality factors currently recommended by the ICRP (1977) are specified as a function of the total LET as follows;

$$Q_f = 0.8 + 1.6 L_\infty \qquad 1.1.6$$

There is a subjective judgment in the the selection of the in built safety factors (Rossi, 1977). The practical implementation of this guideline is also beset by the problem of determining the effective LET and of assigning a suitable quality factor. In the case of a single radiation field of low LET radiation, say $\gamma$- or X-rays, a linear averaged LET deduced from the absorbed dose provides an adequate description of the radiation field for the practical assessment of radiation exposures.

However, in many situations of practical relevance, for instance in the vicinity of a nuclear reactor where a mixed neutron and photon radiation fields exists, a range of LET values are involved, linear averaged LET determined by integration over the LET distribution cannot provide a reliable description of the radiation field. A common expedient is to separate the absorbed dose into low and high LET components and then assign a quality factor to the high LET component allowing a suitable margin. It is inconvenient as it requires a preknowledge of the radiation type(s), which is often not available. The other impractical alternative is to provide different types of dose equivalent instruments for the different types of radiations that constitute the field. These limitations indicate the inability of the

parameter H in correlating the effectiveness of any radiation field in a unified way, and is due to the inappropriateness of the concepts of dose and LET as a basis of the radiation dosimetric system.

There are also inherent problems in the application of the concepts of absorbed dose in internal dosimetry as in nuclear medicine where auger emitting electron capture radionuclides are incorporated into the body. There are also problems in the dosimetry of alpha particles ingested through radioactive aerosols. Furthermore, the quality factors assigned to neutrons having energy in the range of MeV do not explicitly take into account the influence of neutron energy on biological effectiveness (ICRU-26, 1977). The present system does not cater for the dosimetry at interferences, eg bone-tissue, and cannot describe the recently observed phenomenon of reverse dose effect (Sykes and Watt, 1989).

## 1.5. THE NEED FOR AN ALTERNATIVE RADIATION DOSIMETRIC SYSTEM.

The problems cited above suggest the need for a new system of radiation dosimetery with appropriate detectors, based on the recently improved understanding of radiobiological action (see chapter two). The new system should overcome the problems inherent in the existing system and enable the direct assessment of absolute biological effectiveness (ABE) of ionising radiation without preknowledge of the radiation type or intensity. The proposed system would be a system of unified dosimetry (termed unidosimetry, in this work ).

There are at present various radiation dosimeters which are based on various physical principles and with which quantities of interest are measured by modifying the response of some radiation detection system in a suitable manner. Thus absorbed dose in tissue is determined from ionisation chambers and proportional counters made tissue equivalent. The dose equivalent to neutron exposure can be directly obtained by modifying the response with neutron moderators.

These conventional devices have relatively large sensitive volumes (mean diameter > 10μm) and can be referred to as macrodosimeters. By their principle of operation, size and configuration they are meant to measure quantities related to the mean energy deposited in their sensitive volume and do not indicate the stochastic of the energy deposition processes. The latter is an inherent feature of ionising radiation interaction with matter, and is significant for small doses, with densely ionising radiations and in small

volumes.

It is now well established that the biological effects of ionising radiations are determined by its interaction within the cellular and subcellular components of living matter (see Chapter two). The diameters of a typical mammalian cell and of the DNA, the carrier of genetic information, are respectively of the order of micrometer and nanometer. In volumes of such order of magnitude the stochastic in the energy deposition processes are significant. Macrodosimeters and the concepts of dose and LET which are mean values are not suitable. Realisation of this has lead to the introduction of microdosimetry and microdosimeters for use in radiobiology, heavy particle therapy, radiation protection in mixed radiation fields, microelectronics, etc.

Two parameters introduced by Rossi (1968) as microdosimetric counterparts to the absorbed dose and LET are the specific energy (z), and the lineal energy (y). The specific energy is defined as the ratio of the energy imparted ($\varepsilon$) to the matter in a given volume by a single energy deposition event divided by the mass (m) of the matter in that volume:

$$z_1 = \varepsilon / m \qquad 1.3.1$$

The lineal energy is defined as the energy imparted to the matter in a specified volume by a single energy deposition event divided by the mean chord length (l) through that volume:

$$y = \varepsilon / l \qquad 1.3.2$$

To enable the measurement of these quantities and their distributions in volumes of less than 10μm mean diameter, Rossi and collaborators (Rossi, 1968) introduced gas based microdosimeters. Basically, these are tissue equivalent, spherical proportional counters which simulate the radiation's interaction, with tissues of 0.3-10μm diameter, by appropriate reduction of the gas pressure (see section 3.2). The micron is the order of size of the critical cellular structures deduced from the 'The Dual Theory of Radiation Action' in its 'site' version (Kellerer and Rossi, 1972).

Experiments with ultra-soft X-rays and deductions of some models based on the empirically observed RBE-LET relationship (Barendsen et al 1966, Oda and Iwanami, 1984; Guenther and Schultz, 1983; Holt, 1974) indicate that the dimension of cellular radiosensitive sites is of the order of nanometer. The 'Dual radiation action model' was modified to accommodate this (Kellerer and Rossi, 1978). The need therefore arose for radiation nanodosimeters. Various attempts were made towards the realisation of such a detector (see Chapter Three) but in most the measured quantity is the energy deposited in

the specified volume and its distribution.

Recently Watt and co-investigators (Cannell and Watt, 1985; Chen and Watt, 1986; Watt et al 1985, Watt, 1989) showed that the dominant mechanism of radiation action as manifested by loss of cellular clonegenic capacity is determined by the probability that the mean interionisation distance of the charged particle tracks matches the DNA strand separation. It was deduced that the DNA double strand breaks are the critical lesions. This contention was extended and confirmed for chromosome aberration, mutation and transformation in the present work (Chapter Two). These data provide an overwhelming justification for radiation nanodosimeters but with a much more subtle requirement, that is, it should simulate the simultanoes damage to both DNA strands by the ionising radiation. Because of this difference and that in the proposed system of dosimetry, the quality parameter is irrelevant. The terms unidosimetry (shortened from unified dosimetry) and unidosimeter are preferably used in this work.

## 1.6. SCOPE OF THE THESIS.

In the formulation of the unified dosimetric system three related aspects have to be considered. First, a clear justification for the new system has to be presented. Second, appropriate physical and biological parameters (radiation quality) with which the biological effectiveness of radiation can be unambiguously predicted have to identified. Third, an appropriate physical system for its instrumentation, and for interpretation of the instrument's response, have to be presented. The objective of this work is to consider these requirements.

In Chapter two the dominant determinants of radiation damage as may be manifested through cellular mutagenesis, chromosome damage, oncogenic transformation and DNA strand breakage are identified. In this, radiation tracks were used as probes for investigating the radiosensitive sites. It is shown that for all endpoints investigated, as well as for cellular death, the critical cellular entity susceptible to radiation damage is the DNA and the critical lesions are most likely to be the DNA double strand breaks. Damage is optimally induced when the mean free path of ionisation of the charged particles matches the mean separation of the DNA strands. Radiation damage is determined by the frequency of interactions and not by the energy deposited by the primary particle track or by the delta rays. These findings constitute a basis for the new 'unified dosimetric system'.

In chapter three the requirements for appropriate instrumentation based on the deductions of chapter two are defined. It is inferred that the appropriate detector need not measure the total energy deposited in the sensitive volume, but to count the frequencies of coincident interactions in two nanometer size volumes that simulate the DNA duplex. The threshold of energy deposits that need to be detected is that corresponding to the energy involved in the induction of a DNA single-strand break (about 30eV).

Also made in chapter three is an appraisal of the potentials of various radiation detection systems in satisfying the outlined criteria. It is deduced that gas based detectors may not satisfy the geometrical requirements of the detector. Radiation detection based on secondary electron emission, thermoluminescence, radiopholuminescence were judged to lack the required sensitivity. On the other hand detectors based on superconductivity do have the desired configuration, have the advantage of high sensitivity but the role of the substrate on which they are supported is not clear. Films of semiconductors made using modern techniques of fabricating submicron films may be useful, if they can be facilitated with rectifying contacts. The organic semiconductors appear to have the best potential. For reasons of availability, only thin film scintillator detectors were practically assessed.

The objective of chapter four is to determine whether the response of a scintillator to the presence of ionising radiation bears a resemblance to the response of a cell (a biological detector) to the same radiation. In other words, the degree to which the physical detector can simulate the interaction of radiations with cellular targets as shown in the second chapter is sought. It is deduced that the two differ considerably. This indicates a fundamental weakness in the use of detectors based on light response for unidosimetry.

Reported in the fifth chapter is an experimental assessment of organic scintillators in the form of thin film plastic detectors. The method of fabricating the high quality films, the assessment of its quality and the ability to mount the films into a detector assembly are discussed. The response of thin films of various thickness to the passage of natural alpha particles of different energies was determined. The data were used to determine the minimum thicknesses that can give a detectable signal and the detection efficiency of the system. Methods of modifying the system in such a way as to obtain a nanodosimeter were sought.

The inferences made and suggestions for future investigations are given in chapter 6.

# CHAPTER TWO
# FUNDAMENTAL PHYSICAL MECHANISM OF RADIATION ACTION

## 2.0 PREFATORY REMARKS.

Radiations of interest in dosimetry are γ-rays, hard and soft X-rays, electrons, protons, neutrons, natural α-particles and accelerated nuclei. Their minimum energies may be considered as 10eV (Inokuti, 1983 ); accelerated ions may have kinetic energies up to the order of their rest mass energy. The interaction of these radiations with matter is predominantly with the electrons of the target medium. Electrons, natural α-particles and accelerated nuclei are directly ionising. Photons act through the agency of secondary electrons produced in compton and photoelectric interactions and the subsequently generated electrons. Neutrons induce damage mainly via the interaction of the recoil protons. The carbon, hydrogen and oxygen recoils may play a smaller role (ICRU-26, 1977).

Table 2.1 The seven most common elements of a 'reference' man, according to ICRP-23 (1974).

| Element | Atomic number | %weight of the total body |
|---|---|---|
| Oxygen | 8 | 16 |
| Carbon | 6 | 23 |
| Hydrogen | 2 | 10 |
| Nitrogen | 7 | 2.6 |
| Calcium | 20 | 1.4 |
| Phosphorous | 16 | 1.1 |

The seven elements which individually constitute more than one percent of the total body weight of "reference" man are given in Table 2.1. They are low atomic weight elements that are usually in the form of water molecules and organic compounds, like proteins and nucleic acids. Significant damage can be induced when energy deposition events are large enough to break the molecular bonds in the nucleic acids or proteins. With these low

atomic number (Z) constituents the contribution to the total energy loss through Bremsstrahlung and Cerenkov radiation generation is small and and therefore neglected. Rutherford scattering which may play a fundamental role in determining the scattering of charged particles, makes a trivial contribution to the total energy loss. The density or polarisation effect (ICRU-37, 1984) can also ignored. At the other end of the energy range, it can be inferred that direct transfer of energy to translational, rotational or vibrational modes of the target electrons is also insignificant (Inokuti, 1983). The energy involved in the attachment of an electron is too small for ionisation of biological matter. In superexcitations energies in excess of the mean ionisation potential of water (about 12.6eV) are involved, but they are never more than 30eV (the mean energy expected to ionise a water molecule, the main constituent of the cell). In water, superexcited states may form a third of the nonionising primary events (Platzman, 1967), but are most probably irrelevant in terms of inducing biological effects.

Excitations events, involving energies of one to ten electronvolts, are generally considered less effective than ionisations in the induction of significant biological effects. Experimental investigations (Jagger, 1967) with ultraviolet (UV) radiation, which has insufficient energy for ionising biological molecules show that they are an order of magnitude less effective for inactivation of viruses than ionising radiations. Thus, it is probable that only ionisation may play a significant role in biological damage (Rossi, 1970).

Within these outlined limits the interaction of radiation with matter is, at least in principle, well described by the Bethe-Bloch quantum theory of stopping power (ICRU-37, 1984). The theory is however primarily aimed at characterising the fate of the radiation; its use for characterising the fate of the absorber is much more involved, even if only an isolated water molecule is considered (Inokuti, 1983; Sonntag, 1987). In more complex biological systems, there are, in addition, the processes of metabolism, cellular repair, recovery and propagation. Thus in order to formulate a theory from which the biological effects can be predicted at molecular and cellular level, elucidation has to be made of all physicochemical and biochemical processes that intervene between the initial radiation energy deposition event and manifestation of the damage. A complicated, if not an impossible task. The most pragmatic approach is to identify those processes that are dominant. This can be achieved (as described later) by correlating the biological effects, quantified in a suitable manner, with physical parameters characteristic of the radiation.

However, a given manifested effect, such as the exhibition of exponential dose-response curves (Elkind, 1984) may be prompted by different basic mechanisms, each having a separate kind of dependence on some physical factors of the radiation. So the deductions are valid only if supported by separately obtained evidence.

The objective of the present chapter is to discern the fundamental physical properties of the radiation which determine the biological action, and to identify the characteristics which need to be considered in the design of detectors for a unified system of radiation dosimetry. The three aspects of the problem are the identification of the dominant mechanisms, the radiosensitive sites and a suitable quality parameter. Previous attempts at fulfilling some of these objectives (section 2.3) and current understanding of the role of water molecules, the main constituent of cellular mass, and its radiolysis products are first briefly reviewed.

## 2.1. DIRECT AND INDIRECT ACTION.

The direct interaction of radiation with water molecules results in excitation, superexcitation and ionisation. Their respective G-values (the yield per 100eV of absorbed energy) are 0.54, 0.92 and 0.48 (Platzman, 1967). Excitation and ionisation lead mainly to H and OH radicals and the hydrated electron ( $e_{aq}$). Some of the radicals recombine to form $H_2$ and $H_2O$. These radiolytic products diffuse about and react with the DNA, proteins and other biological molecules by extracting the side groups such as H, $CH_3$, OH, COOH, $NH_2$, SH and $H_2PO_4$ forming solute (DNA) radicals. Solute radicals may also be formed through dissociation and addition reaction. Stable products of the reactions may be formed through demerisation and addition, disproportionate reactions, hydrolysis, oxygen addition and hydrogen transfer. Thus, various products, many of which may have little significance in the induction of manifested cellular effects may be produced (For reviews: Sonntag, 1987 and Hutchinson, 1985).

The yield of the primary chemical species produced in water, at pH of 7.00, within three pico seconds after energy deposition are given in Table 2.2.

TABLE 2.2: The yield of the primary radiolytic products. Adapted from Sonntag (1987).

| Product | G-value. |
|---|---|
| OH | 5.08 |
| $H^+$ | 0.88 |
| $e_{aq}$ | 5.00 |
| $H_3O^+$ | 5.00 |

The OH radical is produced at all times; the production of the reducing radicals is dominated by the hydrated electron. The $H_3O^+$ usually dissociates into $H^+$ and $H_2O$. In aerated solutions $H_2O_2$ is produced but its concentration is so low that it may have little significance (Prise et al, 1989). In oxygenated conditions, H atoms also add to double bonds or extract an H atom from a C-H bond. The hydrated electron may form a negative ion in conjugated systems. The $e_{aq}$ is known for reacting quickly with bases, but not with sugars (Sonntag, 1987), while H atoms react more slowly (Hutchinson, 1985).

The hydrated electron does not extract H atoms from C-H bonds and it does not produce strand breaks (Sonntag, 1987). However, Alper (1979) suggested that $e_{aq}$ may play an important role in damaging the cell membranes, unless oxygen (a scavenger) is present. Since the yield of the $H^-$ is much smaller than of $e_{aq}$, it may therefore be expected that it is only the OH radical that may be significant in damaging the DNA.

The OH radical attacks mainly the bases, but it can also induce single strand breaks, whose role may depend on the type of cell. In viruses with single stranded DNA a single break may lead to cell death, the radicals formed in the medium may therefore cause inactivation. Johansen and Howard-Flanders (1965) showed that in the killing of bacteria the OH radicals play an important role. Mammalian cells have much lower surface-to-volume ratio than viruses and have double stranded DNA. For the radicals to induce inactivation they should be capable of inducing a double strand break (dsb) either by one radical action or two radical acting together. It is probable that in aqueous cell suspensions of more organised cellular systems that it is only the endogenous radicals (those formed from the water molecules that are bound to the DNA) that are pertinent. The exogenous radicals

(those from the bulk water radicals) may have little significance on cellular inactivation (Jacobs et al, 1983). There are studies which in broad terms appear to concur with this.

Roots and Okada (1975) reported experimental and analytical investigations on the radiolysis of water with hard X-rays in the presence and absence of radical scavengers. Their results show that the interactions, which occur within a few nanoseconds after irradiation, of the free radicals and molecular products, the OH radical in particular, largely (75%) determine the loss of the reproductive capacity of the cell in the case of the low LET radiations. In subsequent work Roots et al (1985) showed that the OH free radicals causing the damage are produced within 4 and 9nm of the target. However, there are studies that cast doubts on the mechanism of the radical action.

Chatterjee and Magee (1985) reported results of Monte Carlo simulation of the production of strand breaks in dilute aqueous solution of SV40 DNA exposed to high energy electrons. The major radicals were followed from their point of production to the various reaction sites on the DNA molecule. They scored a double-strand break as the occurrence of two breaks on opposite strands separated by less than 10 or 12 base pairs. Their results indicate that there is a negligible probability for the production of a double-strand break through the action of two OH radicals from the same track or through OH radicals from two different tracks, and concluded that double-strand break induction must depend on some other mechanisms. Ward (1985) argued that a fast radical can induce a break in the first strand, but will be subsequently slowed and interference by scavengers may hinder it from interacting with the next strand. He inferred that the production of a double-strand break by a single radical action is not plausible except within the interaction volumes of high radiation energy deposition.

The conclusion that can be made from the foregoing is that the action of radiations on cells is too complicated as simply to be classified into direct and indirect actions. The so called indirect effects may play a significant role in the case of irradiations with sparsely ionising radiations. But in general it may be less significant than direct ionisation events with the DNA. Although the cited investigations refer to cellular death, the deductions may apply to chromososmal abberation induction and other endpoints.

## 2.2 REVIEW: RADIOSENSITIVE SITES AND LESIONS FOR CELL DEATH

Okada (1970) had made an externsive review of experimental investigations that indicates that the critical radiation target is the nuclear DNA. The following is a brief summary of the more recent data.

### 2.2.1 RADIOSENSITIVE SITES AND THE CELL NUCLEUS

Cole and collaborators (Cole et al, 1980) used radiation beams of different penetration depth to irradiate cultured mammalian cells, yeast cells and dry and wet bacteria. They inferred that the cell membrane and cytoplasm are less likely to be targets, and belittled the role of water radicals, for the cellular loss of reproductive capacity.

Table 2.3 : Doses required in the nucleus, cytoplasm and membrane for inactivation of chinese hamster ovary cells at at 50 per cent survival level. Adapted from Sonntag (1987):

| Radiation source | Mode of irradiation | Doses to the nuclues | Doses to the cytoplasm | Doses to membrane |
|---|---|---|---|---|
| X-rays | External | 3.3 | 3.3 | 3.3 |
| $^{3}$H-TdR | Internal | 3.8 | 0.27 | 0.01 |
| $^{125}$I-concavalin | Internal | 4.1 | 24.7 | 516.7 |

Evidence indicative of the significance of the nucleus have also been obtained from the so called "suicide" experiments. Warters et al (1977) compared the level of damage made to cells when their DNA, their outer membrane-bound protein and their cytoplasm are labelled. Table 2.3, which is based on their results, suggests that, compared to the cytoplasm and the nucleus, the outer membrane is not a sensitive target, and that the nucleus is more sensitive than the cytoplasm. Yusui and Hofer (1986) extended this work and showed that the nuclear DNA is more sensitive than mitochondrial DNA. Using $^{105}$IUdR-labelled cells, a non random distribution of radiosensitive sites within the nucleus was also shown by Yusui et al (1985) and Burki (1976).

There is also evidence obtained from measurements of the effect cross section for the

inactivation of cells with fast ions of different quality. By comparing the estimated cross sections for inactivation with independently obtained areas of various cellular organelles, information on the nature of the radiosensitive component is obtained (e.g. Barendsen, 1964). However, the inferences made from this approach are often inconclusive, for the derived cross-sections depends on the ion type, particularly when the ions are saturated (Kraft, 1987; Todd, 1967). It will be shown in subsequent sections that by correlating the effect cross-section to the mean free path of the radiations such ambiguities will be removed.

### 2.2.2 DNA AS THE TARGET.

The role of the DNA as the critical target for reproductive death is better established in viruses than in mammalian cells. Viruses have essentially three components: the coat (the capsid and tail), some proteins and the nucleic acids (which may be DNA or RNA). Depending on the viruses, the nucleic acids could be single or double stranded. To proliferate, viruses inject their DNA into host cell within which they multiply. The inactivation of viruses may therefore arise from damage to proteins that form the injection system, crosslinking between the nucleic acids with the proteins or one nucleic acid with another, and damage to the nucleic acid itself.

By irradiating the double-stranded viruses, Bacteriophage T1, prior to their injection into their bacterial host, Bohne et al (1970) reported that only one in twenty of the inactivated phages fail to attach to their host. This indicates that in the case of this system the damage to the coat and the proteins are of minor importance, compared to that of the nucleic acids. However, Ward (1980) reported that in the case of polivirus injection into heLa cells about a third of the exposed viruses failed to infect their HeLa cell hosts, suggesting that damage to the proteins, though smaller, is not negligible.

The basis for deducing that the DNA is also the important target in mammalian and other cells is provided by studies (for review: Okada, 1970) that correlate the cellular mass with radiosensitivity ($D_0$). For example, Kaplan and Moses (1964) showed that the logarithms of the nucleic acids volume of viruses, bacteria, yeast and mammalian cells are proportional to the logarithm of their radiosensitivity, and that four classes of microorganisms can be distinguished purely on the basis of the ratio of their target volume to nucleic acid content. The ratio decreases as the complexity of the organism increases.

A related approach was followed by Sparrow et al (1967) who showed that for 79 organisms there was a linear relationship between the radiosensitivity and the chromosome volume.

2.2.3. DNA STRAND BREAKS AS THE CRITICAL LESIONS FOR CELL DEATH

The alterations that ionising radiations can induce in the DNA includes single-strand breaks (ssb), double-strand breaks (dsb), base changes, base losses, denatured zones, intermolecular cross links, intramolecular cross links such as DNA-proteins, etc. The occurrence of these lesions is not mutually exclusive. Many, for example ssb with dsb, and base losses with denatured zones, occur concomitantly. It is therefore impractical to isolate the lesions for quantitative analysis. The ssb and dsb are probably the most important and better quantified lesions (Kiefer, 1985).

Frankenberg et al (1981) showed that in yeasts, killing is related to unrepaired dsb. In the case of mammalian cells most of the evidence on the role of dsb as the critical lesions for loss of reproductive capacity is largely circumstantial. Ritter et al (1977) showed that the level of cell killing correlated with the yield of nonrejoined breaks. Radford (1986) reported a series of investigations which strongly suggested that DNA dsb were the critical lesion in mouse cells exposed under a number of different environmental conditions; in all the level of cell killing is directly proportional to the observed yield of DNA dsb. He also showed that DNA single strand breaks, base damage, and DNA-proteins cross links have little or no effect on the level of cell killing.

2.2.4 THE POSSIBILITY OF OTHER TARGETS FOR CELL DEATH

The organelles of the cell (nucleus, mitochondria, lysomes, etc) are bounded by membranes that selectively enable and deter the transfer of needed and undesired substances into and out of the organelles. Since damage to these membranes by radiation may distort their permeability, the resulting unbalanced metabolism may lead to loss of reproductive capacity (Alper, 1970). Furthermore, the experiments of Cole et al (1980) indicate that portions of the cell near the nuclear membrane are more sensitive to radiation as assessed through inactivation than the interior. This however, only reflects the established distribution of chromatin within the nucleus (von Sonntag, 1987) and the role of the membranes was inferred to be untenable (Okada, 1970).

The role of the sulphryl groups was also inferred by Okada (1970) to be as modifiers of radiosensitivity but not as important targets for loss of reproductive capability. The DNA is, therefore, the most significant target for loss of reproductive capability. Other evidences, obtained from different considerations on the role of the DNA as the target for loss of reproductive capacity in mammalian cells is given in section 2.3. The extension and confirmation of the role of the DNA in the induction of other cellular endpoints, carried out by the present author is given sections 2.5 to 2.8.

## 2.3 REVIEW OF PREVIOUS WORK OF WATT AND COLLABORATORS.

The main impetus to the reanalysis of published biophysical data by Watt and Coworkers is an earlier theoretical treatment of the hit and target theory (Watt, 1975) which indicated that energy based parameters may not be the most appropriate for the description of radiation effects in biological systems. This contention was later proved experimentally through the inactivation of enzymes in the dry state and in vacuum (Watt et al, 1984 and 1981). The results showed that for fast charged particles, the whole enzyme molecule constituted the target; inactivation followed the single hit in the single target model, where the hit is a single ionisation and the target is the entire biomolecule; the LET appeared as a reasonable indicator of radiation action; the δ-rays could efficiently induce damage. However for slow heavy particles in an energy region where the LET is approximately constant, but where the type of physical interaction changed from mainly ionising to predominantly elastic events, the effect cross-section could differ by an order of magnitude. This demonstrated that the degree of radiation damage was determined predominantly by the frequency of the physical interaction and not necessarily by the amount of energy transfer.

In their subsequent work a reanalysis of published data was made. The objective was to identify the main mechanism responsible for radiation damage and to determine physical parameters that better specify radiation quality. The analysis was made for the inactivation of enzymes, viruses, yeast and mammalian cells with fast ions (Cannell and Watt, 1985) and mammalian cells with photons (Chen and Watt, 1986) over a wide energy range. With appropriate modifications it was extended to the inactivation of metallo-enzymes by characteristic X-rays (Jawad and Watt, 1987) and by incorporated radionuclides (Younis and Watt, 1989).

The philosophy of approach in that analysis, was to avoid energy based parameters and to represent the general trends of radiation effect in a manner which, ideally, would be independent of both the target and radiation type. The degree of radiation damage was therefore expressed in terms of the intrinsic efficiency $\varepsilon_i$, which represents the total probability that a charged particle track entering the radiosensitive target will induce the biological end point of interest. Thus

$$\varepsilon_i = \sigma_e / \sigma_g \qquad 2.2a$$

Where $\sigma_e$ is the effect cross section for induction of the biological effect. In the case of track segment experiments with fast ions it was obtained directly (from values given by respective authors), otherwise the following conversion relation was used:

$$\sigma_e = 1.6 \times 10^{-9} . L_T . (\frac{1}{\rho}) . \frac{1}{D_0} \qquad 2.2$$

Where $\rho$, the density, is taken as $1 gmcm^{-3}$; $D_0$ (grays ) is the mean inactivation dose (or $D_{37}$ in some cases) is taken from the dose-response curve. $L_T(kev/\mu m)$ is the track-averaged LET for the pertinent charged particles, in the case of accelerated ions in track segment experiments it refers to the primary ion's energy. For photon radiations it was for the electrons in the slowing down equilibrium spectrum.

The geometrical cross sections, $\sigma_g$ are normalising factors representative of the radiosensitive sites for killing of the different cells and biomolecules. For enzymes it is taken as the whole biomolecule; for viruses it is assumed to be the whole system less the projected area of the protein coat; for more organised cells it is unknown. Watt et al (1985) and Watt (1989) took it to be the projected area of intra nuclear DNA. The basis of the selection of $\sigma_g$ for eukaryotic cells is discussed in Watt (1989). With biological effectiveness expressed in terms of intrinsic efficiencies, its correlation with various parameters which may be considered for the specification of radiation quality, such as $L_\infty$, $L_D$, $L_T$ and the $I_i$ was made. Some of the results (see also figure 2.1) are the following:

a) Poor correlation was obtained between the conventional radiosensitive parameter $1/D_0$ with $L_D$, or with $L_T$, or with $I_i$ compared to the correlation between the intrinsic efficiency and the same physical parameters. This, they inferred, suggests that absorbed dose is an

inferior parameter for dosimetric purposes. The parameter linear primary ionisation ($I_i$) was identified as suitable for the specification of radiation quality.

b). Plot of the intrinsic efficiency against the $I_i$ of radiations changes slope at $I_i$ about 0.55 per nm when double stranded DNA is present in the cells, or in T1-phage, but not in enzymes, or in $\phi$X-174 phage with single stranded DNA. This was interpreted as an indication that DNA double strand breaks were the critical lesions for the inactivation of cells containing double-stranded DNA.

c) electrons and photons have intrinsic efficiencies of damage approaching an order of magnitude less than those of heavy ions at equal values of $I_i$ and could also just attain saturation when at their most damaging state with $I_i$ of 0.55 per nm.

d) There was an order of magnitude difference between the intrinsic efficiency for the inactivation of targets containing double stranded DNA compared to those biomolecules containing single stranded nucleic acids. This was interpreted as an indication that a single strand break might lead to the inactivation of the single-stranded objects, but for more organised cells the critical lesions were the DNA double strand breaks whose probability of occurrence depended on the matching of the strand separation with the ionisation mean free path.

The analysis was however restricted to cellular inactivation as the biological endpoint. Because of the important implications of the results for radiation dosimetry, protection and therapy (Watt et al, 1985) it is essential that the validity of the inferences with respect to other cellular effects of radiations be tested. Therefore, in the present work, the analysis of data was extended to mutation induction, chromosome aberrations, strand breakage and transformations. A discourse of the radiobiological significance of the other endpoints, the treatment of the respective data and the results is preceded by a brief description of the calculations of the physical data required for the analyses.

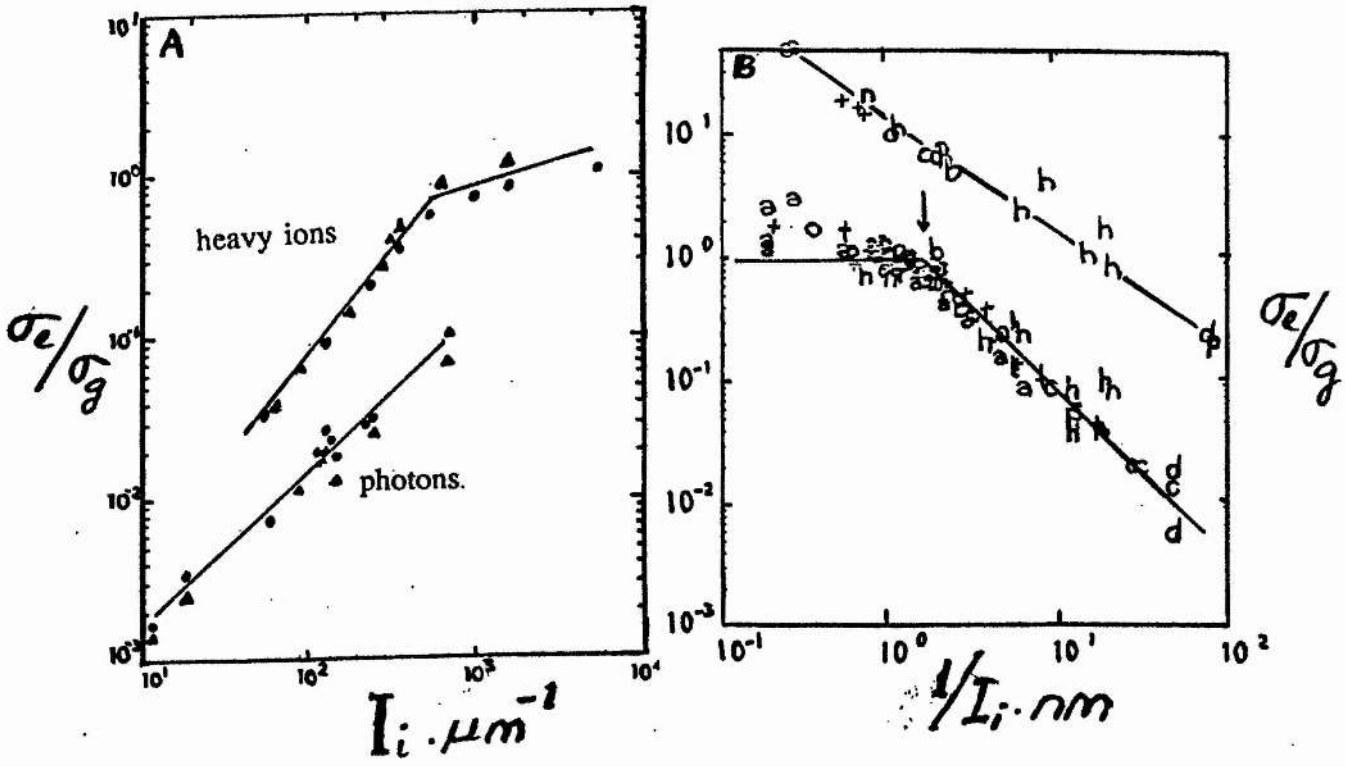


FIGURE 2.1: In (A) The "normalised" effect cross section for cellular loss of reproductive capacity plotted against $I_i$. The difference in the damage capability of the photons relative to the heavy ions, of the same $I_i$ is clearly evident. In 2.1(B) the same cross sections are plotted against the radiation's mean free path ($1/I_i$). Note the monophasic behaviour of the upper curve which pertains to the inactivation of phages containing single stranded DNA. The figures were adapted from Chen and Watt (1986) and Watt and Kadiri (1990) where the sources of the original data are given.

## 2.4 CALCULATION OF PHYSICAL DATA.

### 2.4.1. MEDIUM

All the calculations in this chapter refers to water as the absorbing medium. Table 2.4 give the physical data assumed for this absorber.

Table 2.4: The values of physical parameters taken for liquid water as the main component of cellular mass.

| Parameter | Value assumed |
|---|---|
| Density ($\rho$) | $1.00 g/cm^2$ |
| Mean excitation potential | 68.998eV |
| Avogadros number (Na) | $6.024.10^{23}$ |
| Molecular Mass ($M_a$) | 18.06g/mol. |
| Molecular density | $3.343.10^{20}$moles/gm |
| Ionization potential ($I_p$) | 30.0eV |
| Average (z/A) | 0.551 |

The frequency-averaged LET ($L_T$), Dose-averaged LET ($L_D$) and other physical parameters were calculated with respect to the energies of the relevant charged particles within the cell nucleus. Energy losses in the intervening media were corrected according to the information provided in the original publications.

### 2.4.2. FAST IONS.

The instantaneous energy of the incident ions was used in the case of irradiations with fast ions. The calculation of the LET, $\delta$-ray energy distribution and yields, maximum energies and range-energy relations were made according to the standard Bethe expressions (ICRU-37, 1984) with some refinements. The inner shell corrections were made, where appropriate. The Barkas ($Z_1^3$) and Bloch ($Z_1^4$) corrections were however neglected. The effective charge of the ions, determined essentially following Zeigler's formalism, were employed in scaling the data for protons to heavier ions (Ziegler et al, 1985). Continuous

slowing down approximation (csda) data for protons were obtained from the stopping power data of Janni (1982). For ions with energies between 500keV/amu and 100keV/amu, the data of Anderson and Ziegler (1977) and Ziegler et al (1985) in combination with Bragg additively rule was used. The compilation of Al-Affan (1989) was used for determination of the ranges and effective stopping powers of ions with energies less than 500kev/amu The production of δ-rays was assumed to be uniform for electrons with energies between 100eV and a threshold of 30eV.

The linear primary ionisation ($I_i$) for accelerated ions was calculated from Bohr's relation:

$$I_i = k\,(z^{2*}/\beta^2)\left[\frac{1}{I_p} - \frac{1}{T_{\delta,\,max}}\right]$$

where $I_P$, the ionisation potential, was taken as 30eV. $T_{\delta,max}$ is the maximum energy of the delta-ray spectrum. The constant k is given by:

$$k = \rho\,\frac{N_\alpha Z}{M_\alpha}\,\frac{2\pi e^4}{mc^2}$$

where $N_\alpha$ and $M_\alpha$ are the Avogadros number and the mass of the ions, respectively. In order to provide a self consistency check, $I_i$ was also calculated from the relation

$$I_i = \frac{L}{[\,T_\delta + W\,]}$$

where $T_\delta$ is the average energy transferred to the delta rays in a collision. The mean energy required to produce an ion pair (W) was calculated from ICRU-31(1979) for heavy ions with energy greater than 500keV/amu. The semi emperical relation provided by Goodman (1978) was applied for ions with energies between 2keV/amu and 500keV/amu.

## 2.4.3. PHOTONS AND ELECTRON.

The instantaneous energy was used in the case of exposures with electrons. The calculations of collisional stopping power and ranges of electrons with E>10eV were

based on ICRU-37 (1984). For electrons with E<10keV, the data of Iskef et al (1983), Al-Ahmad and Watt (1984) and Ashley (1982) were used.

Radiation damage by photon radiations is through the agency of electrons produced from the primary Compton and photoelectrons interaction and from the the subsequently generated electrons. For γ-rays from $^{137}Cs$ and $^{60}Co$ the effective energy of the photons was taken to be 662keV and 1252keV respectively. The effective energy ($E_{eff}$) of the Bremsstrahlung spectra for X-rays were obtained from the half-value layer (HVL) or from the degree of filtration quoted by the original authors and by reference to a catalogue of standard X-ray spectra (Seelantag et al, 1979). The equilibrium slowing down spectrum produced by the primary electron source was determined basically, following McGinnies (1959) work. The modifications made are as follows.

The lower threshold cut-off was extended to 30eV electron energy using theoretical and experimental relationships (Ashley, 1982; Al-Ahmad and Watt, 1984). From the distribution and the mean LET, the effective electron energy ( $E_{eff}$) was determined. The relevant energy was used to calculate the linear primary ionisation of the electrons either in the equilibrium slowing down spectrum, or in the primary spectrum, if required, for electrons with energies greater than 10keV, viz

$$I_i = \frac{0.3387}{2\beta^2} \ln (2.325.10^4\beta^2) \text{ ionizations per micrometer.}$$

The data of Tung and Chen (1983) was used for electrons with energy less than 10keV.

## 2.4.4. NEUTRONS.

Damage by neutrons occurs through the interactions of recoil charged particles. Only the proton recoils were considered. The (n, p) scattering cross sections were determined following ICRU-26 (1977). The degradation recoil spectrum was calculated following ICRU-13 (1969). The ranges and collision stopping power, linear primary ionisation etc, of the recoil protons were obtained in the same manner as for fast ions. For fission neutrons the detailed spectrum was considered if known. Otherwise the mean energies as provided in the pertinent publications, were used.

## 2.5. CHROMOSOME ABERRATIONS:

### 2.5.1 SIGNIFICANCE AND DATA TREATMENT.

The genetic material of eukaryotes is organised in the form of chromosomes, which are visible during the mitosis phase of the cell cycle. The observation of chromosome damage therefore offers the possibility of direct (cytological) observation of cellular damage. It also provides an early indication of radiation effects, in comparison to other quantifiable endpoints such as cellular inactivation, mutation induction and transformation. The induction of chromosome aberrations is used as a diagnostic tool for determining, retrospectively, radiation exposure, that is as a biological dosimeter. It is an effective system in which both in-vitro and in-vivo investigations can be made, and are closely related, in so far as the dose uniformity problems are properly considered (Lloyd and Purrot, 1981).

Ionising radiations may induce various forms of chromosome alterations. The induction of dicentric aberrations in $G_0$ human lymphocytes are the most extensively investigated alteration. It is readily inducible by radiations, can be scored less ambiguously and generally occur less frequently spontaneously. In addition there is a vast body of published investigations of the dicentric rings by fast ions, very heavy ions, neutrons, hard and soft X-rays,etc, under standardised experimental procedures (Lloyd and Edwards, 1983). Furthermore, the sensitivity of a cell depends on the stage of the cell cycle; most of the data for other endpoints pertain to asynchronous cells but many cells in the body do not grow exponentially but exist in a nondividing $G_0$ state.

On the weight of these factors the present reevaluation of published data on chromosome alterations by ionising radiations is restricted to data that refers: (a) to the exposure of human peripheral blood lymphocytes at about 35 degrees centigrade of temperature; (b) to irradiated cells which were incubated for two days and for which only dicentric rings were scored.

The radiosensitive parameter (corresponding to the parameter $1/D_0$ in relation 2.2) is taken to be represented by parameter, $\alpha$ (per gray) of the yield of dicentrics per absorbed dose; obtained by fitting dose-response data either to simple linear polynomial (type 1.1.1) or to

to a linear quadratic (type 1.1.2). In the following analysis only the linear coefficient, $\alpha$, is used, irrespective of the fitting (see subsequent discussion on this). In most of the publications the fitted coefficients are provided by the authors and were directly used. For those data for which coefficients are not quoted, the fitted parameters reported in the review work of Lloyd and Edwards (1983) were used. The latter investigators observed that the value of the coefficients may depend on the type of fitting, but this factor is thought to be small and is ignored in this analysis.

For all the considered data, the doses and dose rates vary, respectively, from 0.05Gy to 8.0Gy and from 0.3Gy/min to 0.6Gy/min in the case of electron and photon exposures. Neutron irradiations are within 0.01Gy to 7.0Gy and from 0.01Gy/min to 2.60Gy/min. All are external exposures that last less than 20minutes.

---

TABLE 2.5: Radiation types and sources of data collated for figures 2.2 to 2.7.

| Radiation Type | Reference |
|---|---|
| $^{60}$Co-60, x-rays, fission neutrons | Edwards et al (1985 and |
| $\alpha$–particles, $^{2}$H ions, $^{3}$H ions, | 1986), Lloyd et al (1975). |
| $\pi$–peak, $\pi$-plateau. | |
| $C_k$, $Al_k$, $Ag_k$, $Cr_k$, $Mo_k$ and $W_k$ X-rays, | Virsik et al (1978 and 1983). |
| 13MeV electrons. | |
| $^{60}$Co, Monoenergetic neutrons with mean | Sevankaev et al (1979)* |
| energies of 0.04, 0.09, 0.35, 0.85 MeV | |
| and 14.7MeV D-T neutrons. | |
| X-rays and neutrons (20MeV) | Barjaktorovic and Savage (1980) |
| $^{1}$H ions (4.9MeV) | Takatsuji et al (1983) |
| $^{4}$He ions (23MeV) | Takatsuji and Sasaki (1984) |
| 15MeV electrons | Purrot et al (1977) |
| 3MeV electrons | Schmid et al (1974) |
| $^{137}$Cs $\gamma$-rays | Takahasi et al (1982)* |

*The fitted parameters reported in Lloyd and Edwards (1983) were used.
Unless explicidly stated otherwise neutrons are fission spectrum neutrons.

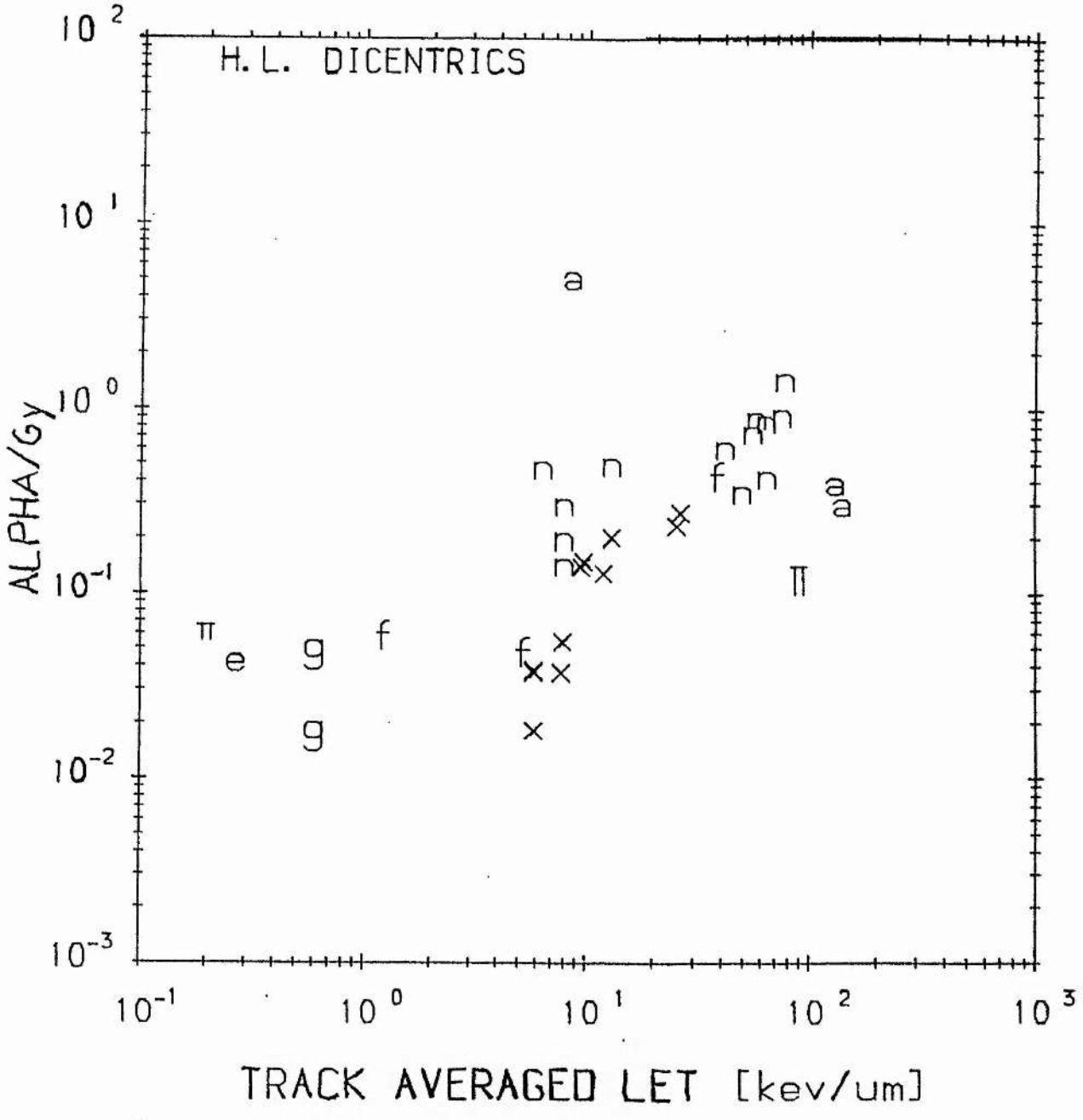


FIGURE 2.2: The linear coefficient, $\alpha$ ($Gy^{-1}$) for the induction of dicentric aberrations plotted against the track-averaged LETof the different radiations. The sources of data are given in table 2.5. The designation of the symbols are as follows: **f:** fast ions; **n :** neutrons (monoenergetic and fission); **X:** hard and soft X-rays; **g:** $\gamma$-rays; **Π:** pion-peak; **$\pi$ :** pion-plateau; **e:** electrons; **a :** natural $\alpha$- particles.

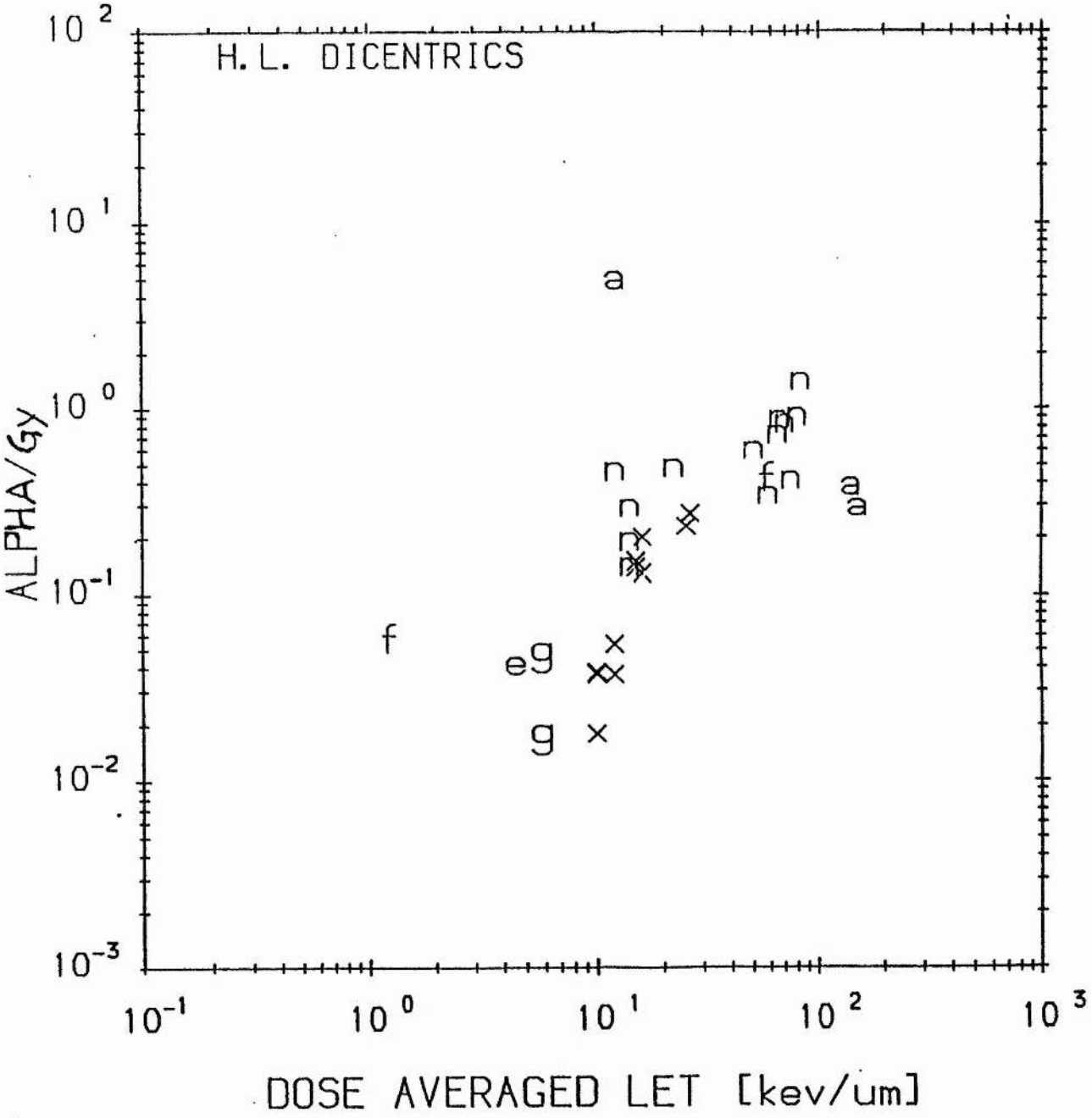


FIGURE 2.3: The linear coefficient, $\alpha$ ($Gy^{-1}$) for the induction of dicentric aberrations plotted against the dose-averaged LET of the different radiations. The sources of data are given in table 2.5. The designation of the symbols are as in figure 2.2.

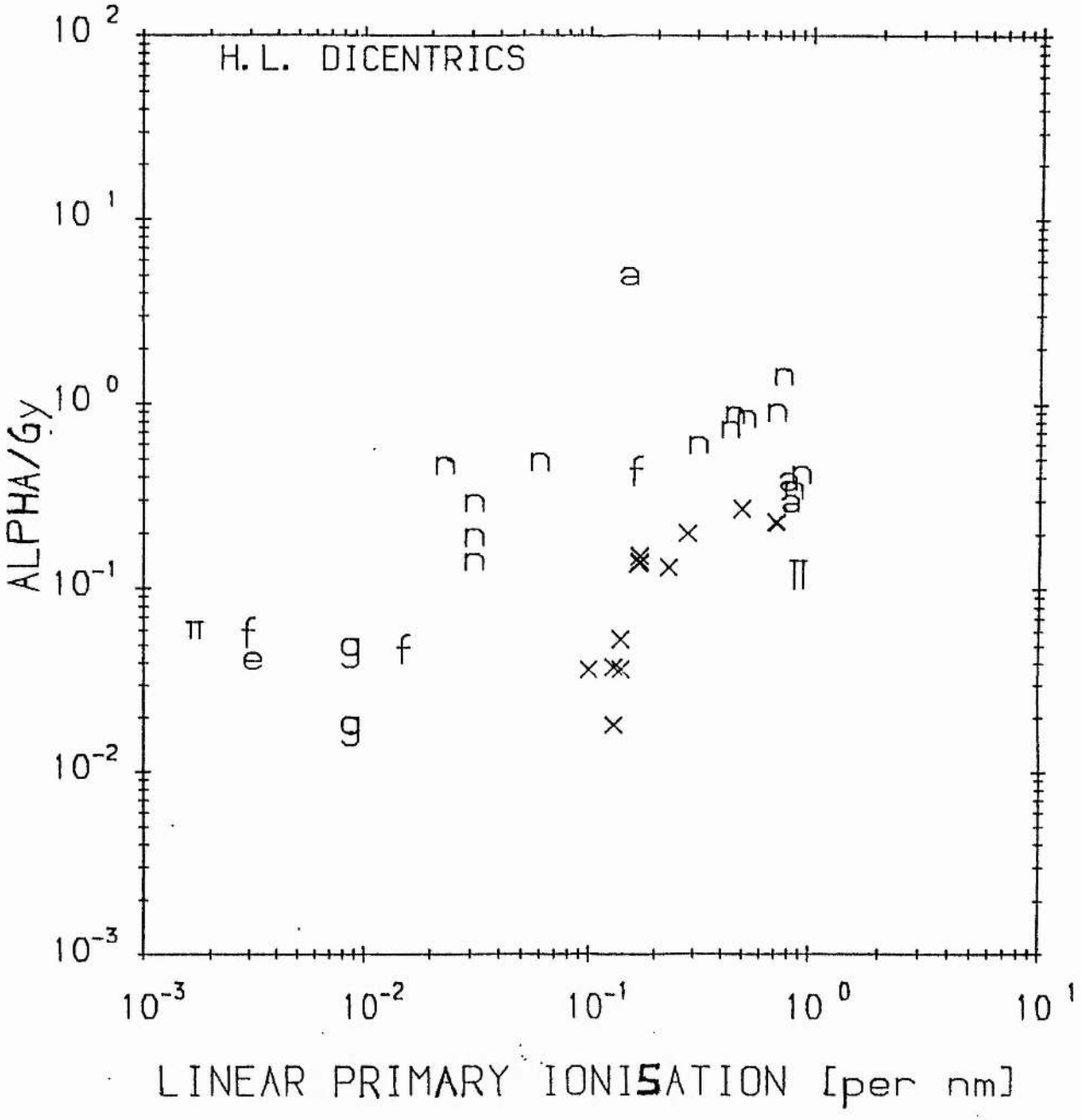


FIGURE 2.4: The linear coefficient, $\alpha$ ($Gy^{-1}$) for the induction of dicentric aberrations plotted against the linear primary ionisation of the different radiations. The sources of data are given in table 2.5. The designation of the symbols are as in figure 2.2.

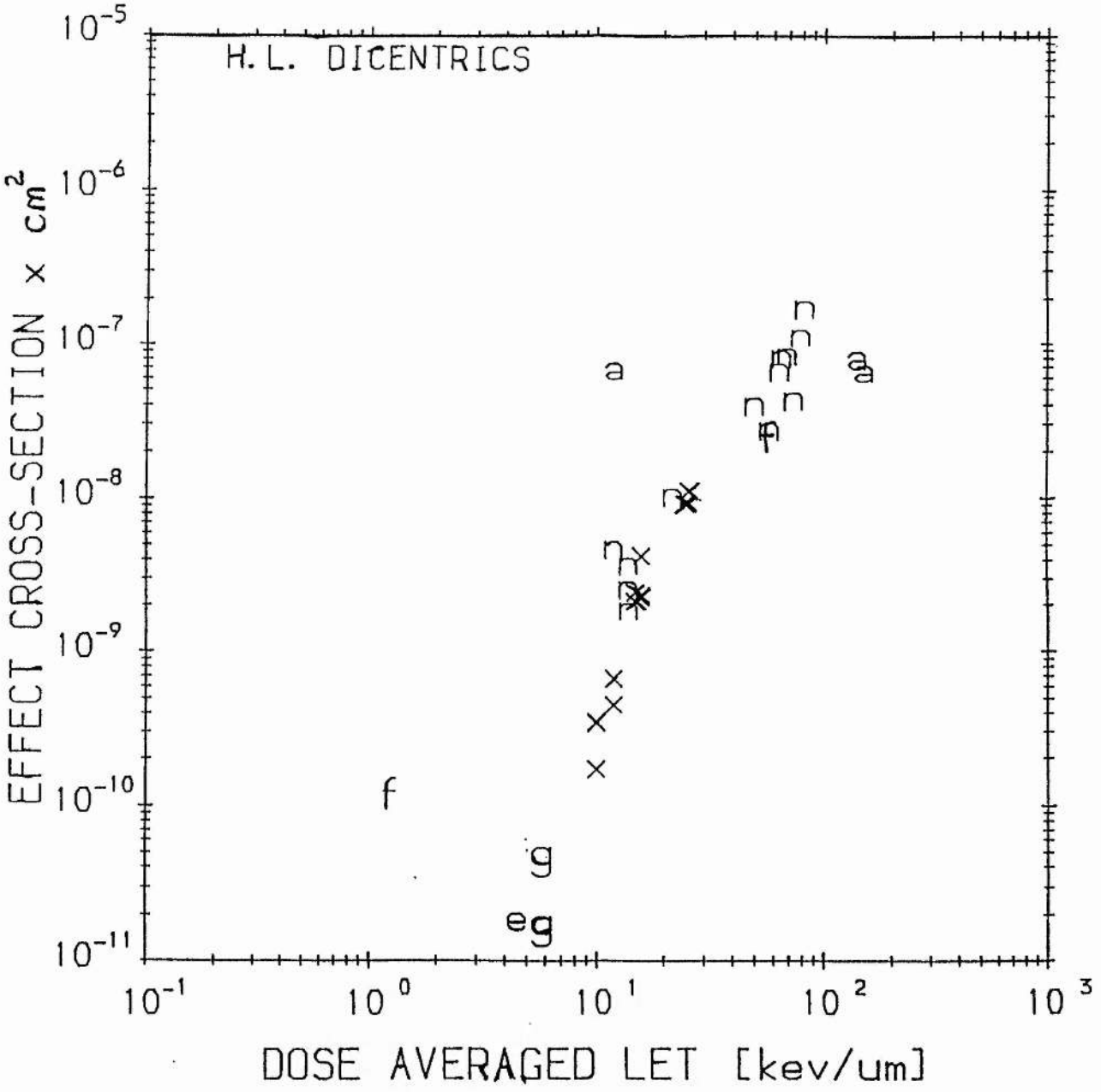


FIGURE 2.5: The effect cross section for the induction of dicentric aberrations plotted against the dose-averaged LET of the different radiations. The sources of data are given in table 2.5. The designation of the symbols are as in figure 2.2.

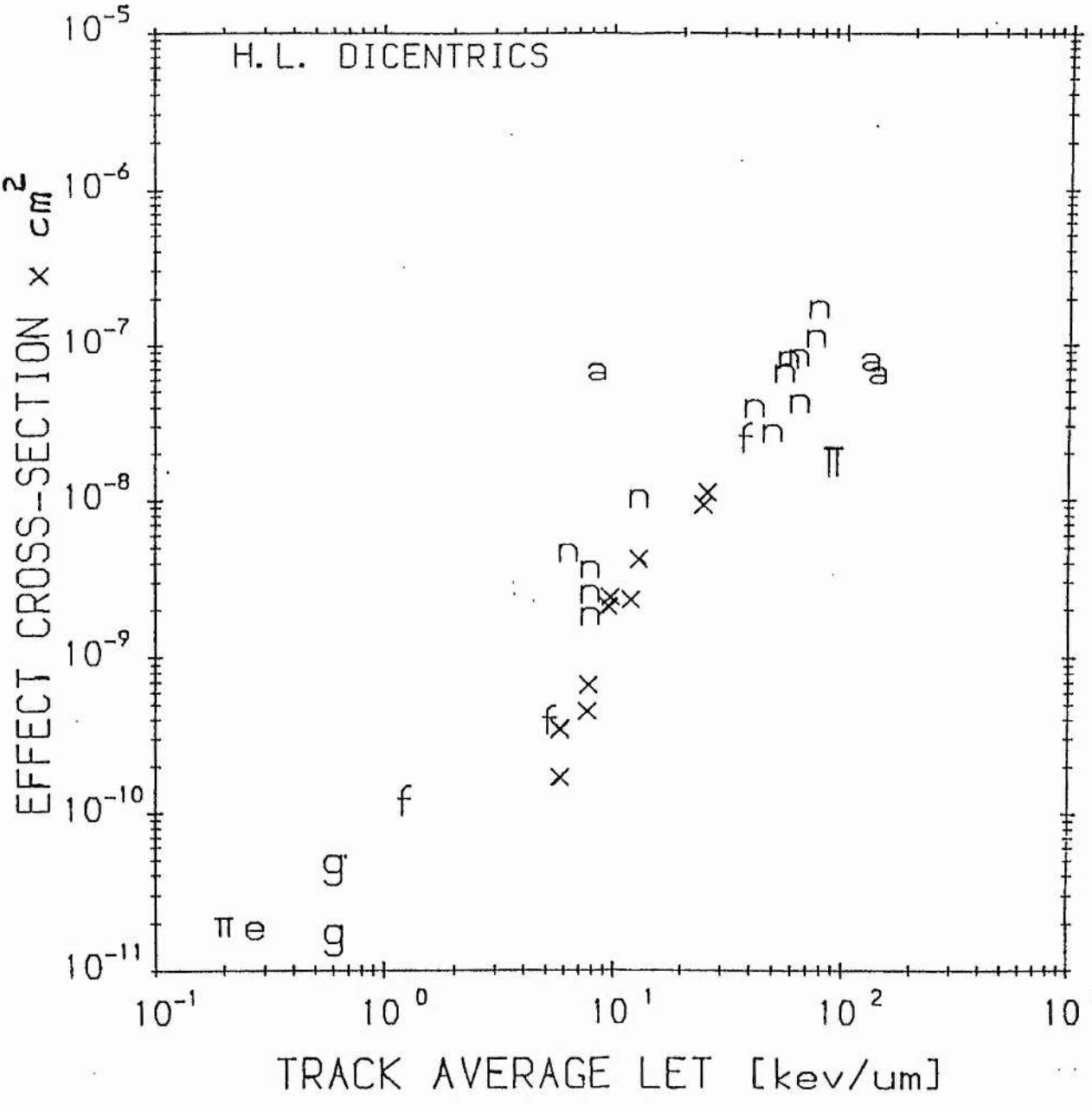


FIGURE 2.6: The effect cross section for the induction of dicentric aberrations plotted against the track-averaged LET of the different radiations. The sources of data are given in table 2.5. The designation of the symbols are as in figure 2.2.

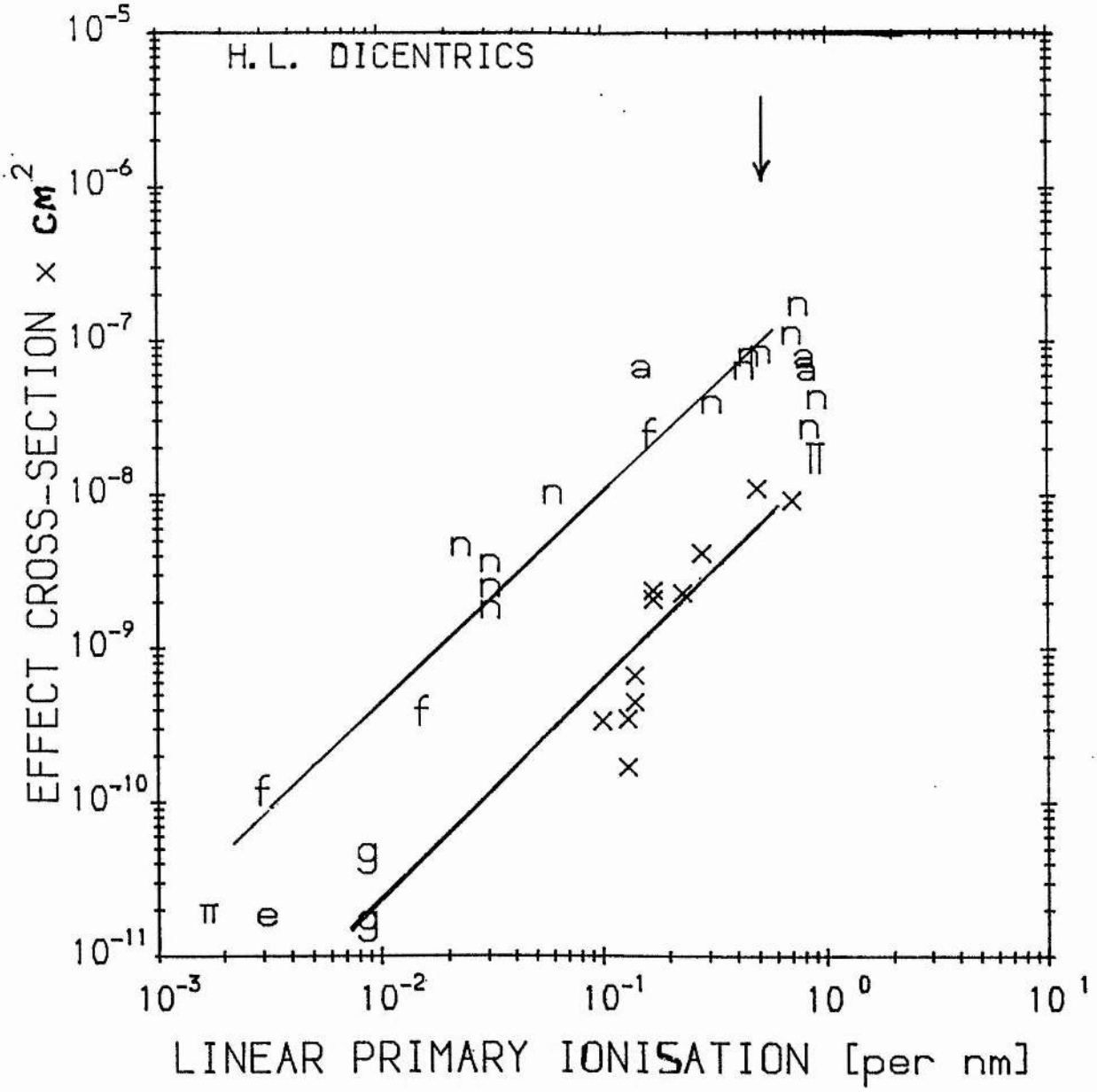


FIGURE 2.7: The effect cross-section for the induction of dicentric aberrations plotted against the linear primary ionisation of the different radiations. The sources of data are given in table 2.5. The designation of the symbols are as in figure 2.2.

## 2.5.2 CHROMOSOME ABERRATIONS : RESULTS.

The linear coefficient, $\alpha$, for the induction of dicentric rings in unstimulated human lymphocytes collated from the various publications is plotted against track-averaged LET (figure 2.2), dose-averaged LET (figure 2.3) and linear primary ionisation (figure 2.4) of the respective radiations. The sources of data, type of radiations, and symbolic designation are given in table 2.5 and in the figure captions. It is evident from these figures that there is, as a whole, no clear trend in the variation of the parameter $\alpha$ as a function of any one of the three physical parameters. Consequently simple and reliable relationships may not established. The implications of this for the appropriateness of the concepts of absorbed dose, RBE and LET as characterising parameters in the current conventional system of radiation dosimetry is discussed in section 2.9.2.

The effect cross sections, $\sigma_e$ , of the same data are plotted against the same physical quantities $L_D$ (figure 2.5), $L_T$ (figure 2.6) and $I_i$ (figure 2.7). With the latter set of presentations a better pattern from which comparisons can be made and quantitative relationships between the the biological effectiveness and the physical variables characteristic of the perturbing radiation fields can be explored. It is apparent that both $L_D$ and $L_T$ correlates closely with the effect cross section for dicentric induction. The dose-averaged LET appears to have a closer relationship to the $\sigma_e$ than the frequency weighted LET.

The pattern observed in figures 2.5 and 2.6 compares sharply with those of effect cross section versus the $I_i$ (figure 2.7). In the former two, for both sparsely and densely ionising radiation a single curve relates the effect cross section to the mean values of LET. In the case of figure 2.7 two curves can be distinguished, one for fast ions and neutron irradiations and another for $\gamma$-rays, hard X-rays, soft X-rays and electron radiations. This indicates a clear difference in the biological effectiveness of the two types of radiation. At equal values of $I_i$, the $\sigma_e$ ($cm^2$) for the production of dicentric aberrations by the ionic type of radiations (fast ions and neutrons) is by one order of magnitude greater than those by the electronic radiations (photons and x-rays). The clear indication of this difference is unique to this type of presentation. The probable reasons for the difference are discussed in section 2.9.3.

The curves drawn through figure 2.7 were fitted by eye to assist visualization. The arrow indicates the position of equal to per nm. The indication of a change in slope of the upper curve, which pertains to neutrons, fast ions and α–particles radiations, at the marked value of linear primary ionisation can be discerned. There is some scatter, due to inter laboratory variations, and limitation of data for radiations with $l_i > 0.55$/nm, nonetheless, the existence of the point of inflection and the tendency for $\sigma_e$ to decrease with further increase in $I_i$, for $I_i > 0.55$per nm is evident. The reciprocal of $I_i$ , the mean free path, λ, of the charged particles at the point of inflection is 1.8nm. The mean inter strand distance, of the DNA is also about 1.8nm. It can therefore be suggested that the occurrence of the point of inflection represents an onset of saturation of biological damage, which occurs when the λ of the radiations matches the mean diameter of the DNA.

Similar observations were made in the case of cellular death (section 2.3 and figure 2.1) which have more extensive and with fast ions under track segment conditions. The absence of a point of inflection at $I_i$ =0.55per nm in the case of inactivation of phages containing single stranded nucleic acids (figure 2.1B) for which ssb are important for death but its presence in the case of double stranded phages inactivation is one evidence supporting this inference. The other strengthening evidence was cited as observation (d) in section 2.3. Other evidences indicative that the nuclear DNA and dsb are respectively the critical sites and lesions for loss of reproductive capacity of mammalian cells were reviewed in section 2.2. Taken together, these suggests a common dominant mechanism may be involved in the induction of the two endpoints.

The inference that dsb are the critical lesions in the induction of chromosome damage such as dicentric aberrations is supported by a number of experimental observations. Okada (1970) had reviewed the earlier data. More recently Bryant (1984), among others, provided evidence suggesting that chromosome aberrations originate from dsb. Correlation between the level of cell killing and chromosome aberration induction in mammalian cells irradiated with γ-rays, X-rays, fast neutrons and ions was also shown by Roberts and Holt (1985) and by Tolkendorf and Eichhorn (1983).

## 2.6. CELLULAR MUTATIONS:

### 2.6.1. TREATMENT OF DATA.

Mutation assays are quantified in terms of the number of mutants per survivor; the radiosensitive parameter, $\alpha$(per gray), is therefore, the mean number of mutants induced per survivor per absorbed dose, obtained as a fitted coefficient of the dose response curves. Empirically fitted coefficients reported in the various publications were used in determining the effect cross sections according to relation 2.3. Some investigators (Kiefer et al 1982, Kranert et al, 1987) reported data in terms of the effect cross sections, these were directly used. For some of the data the original investigators fitted their dose response curves to some form of linear-quadratic function. Irrespective of the fitting, it is only the linear coefficients that are used in this investigation (see section 2.9.1).

Mutation induction assays are characterised by some experimental uncertainties, such as the appropriate expression time and cell density (Thacker et al 1976, Kranert et al 1987). Consequently this analysis is restricted to selected sets of experimental results obtained under well established procedures (Thacker et al 1976). Preference was given to those data sets obtained from the same laboratory. All the data pertains to asynchronous mammalian and yeast cells irradiated in air. In the case of mammalian cells it is restricted to 6-thioguanine resistance ($6\text{-TG}^r$) in V79 and human fibroblast, HF19, cells. All the irradiations are external and acute (lasting less than or about 20 minutes). The sources of data, cell lines, mutational assays, types of radiations employed in the various investigations reanalysed in this section were given in the figure captions.

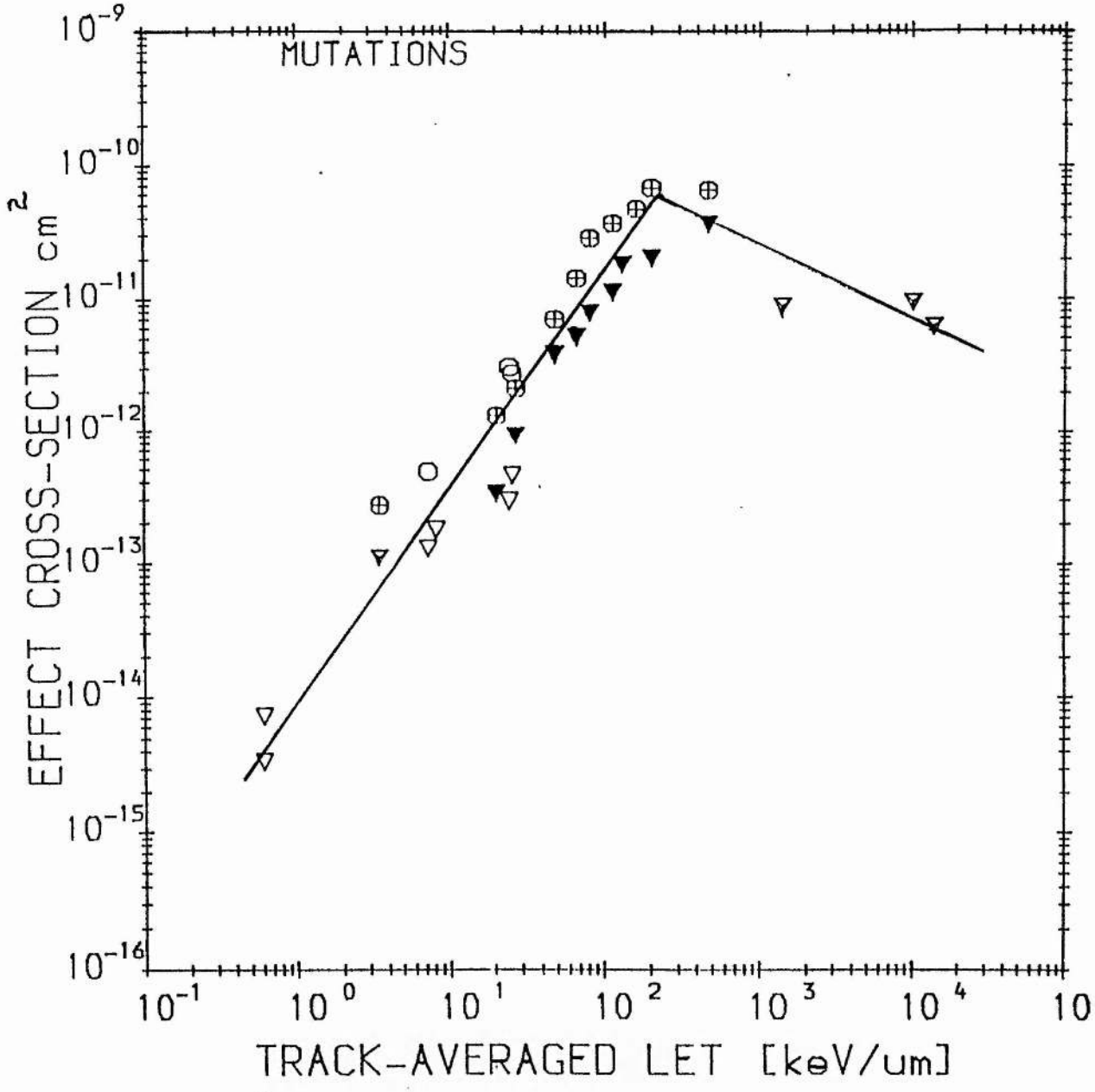


FIGURE 2.8: The effect cross section for the induction of 6-TG$^r$ mutation in mammalian cells plotted against the $L_T$ of the different radiations. Data were obtained from Cox et al al (1977a, 1977b), Thacker et al (1982), Goodhead et al (1979), for V79 cells exposed to fast ions (▼) and to photons (▽), HF19 cells irradiated with fast ions (⬭) and Photons (⊕); and from Kranert et al (1987) for V79 cells (▽) treated with heavy ions.

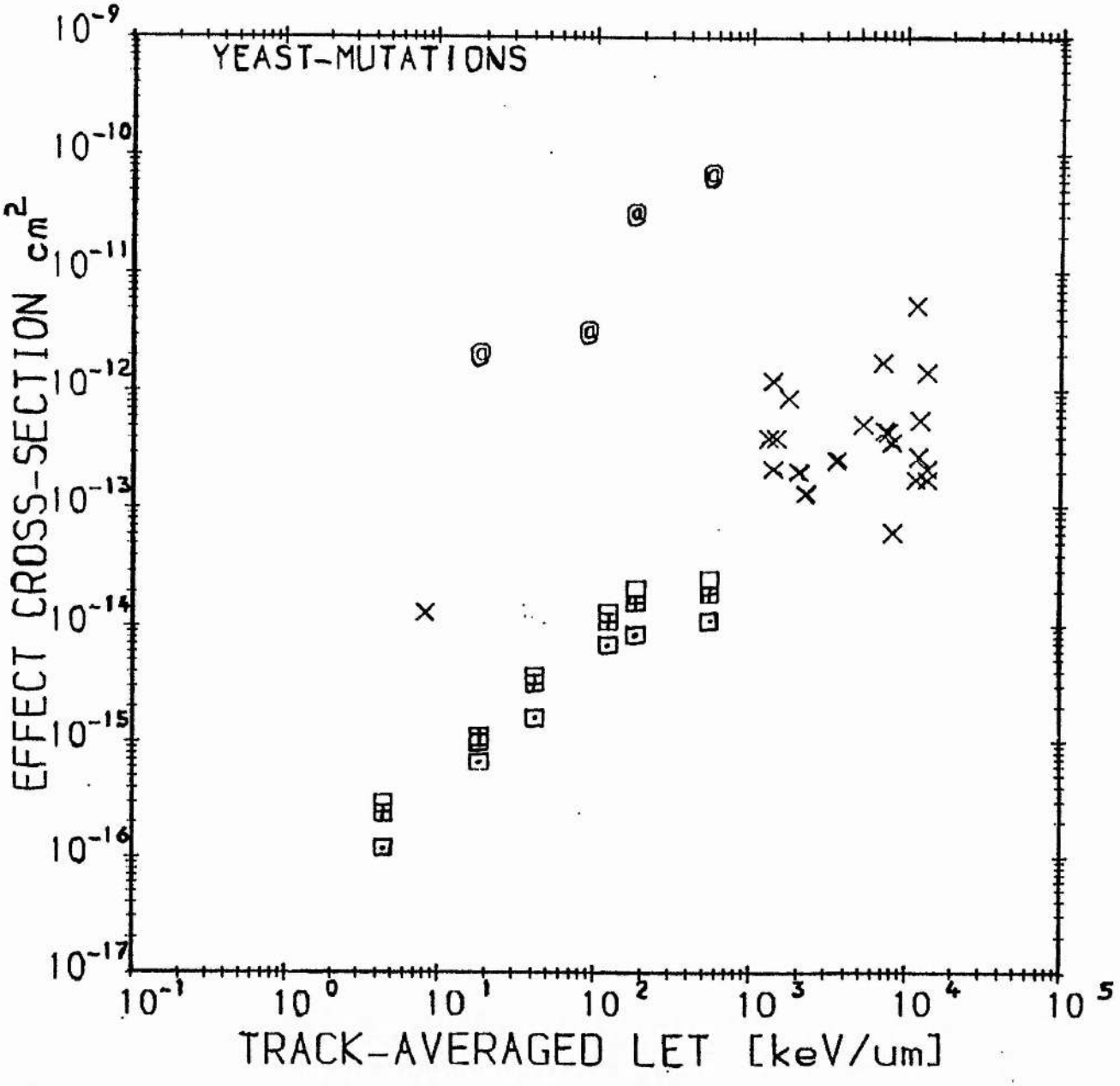


FIGURE 2.9: The effect cross section for the induction of mutations in yeast cells plotted against the $L_T$ of the different radiations. Data were obtained from Kiefer et al (1982) for canavanine resistance in sc 211-1a (X), Raju et al (1971) for arginine dependence in sc BZ34 (@), Mortimer et al (1965) for sc X841's dependence on histidine (⊞), dependence on tryptophan (⊡), and independence from trpytophan (□).

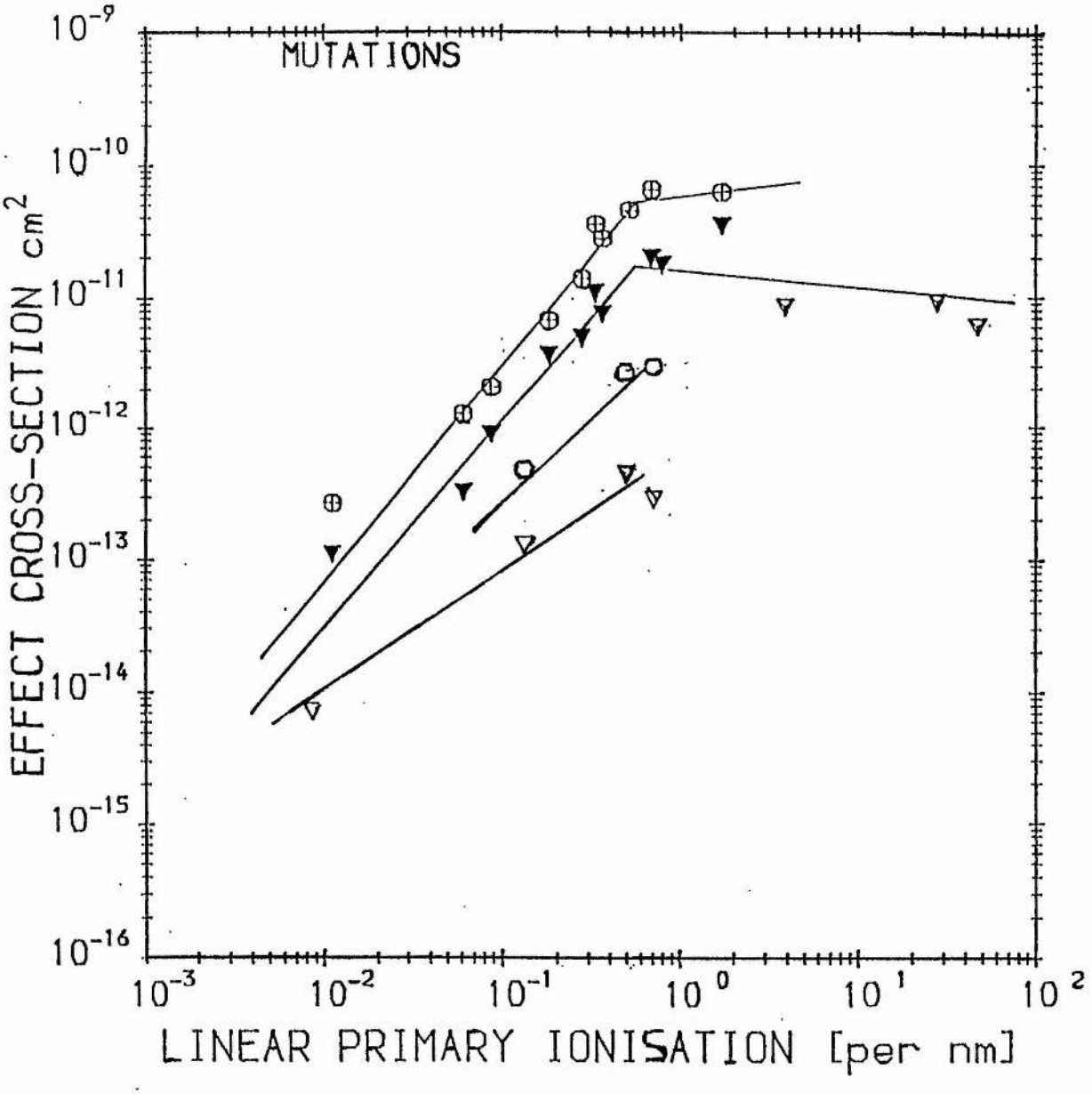


FIGURE 2.10: The effect cross section for the induction of 6-TG$^r$ mutation in mammalian cells plotted against the linear primary ionisation of the different radiations. Sources of data and symbolic designation is similar to figure 2.8.

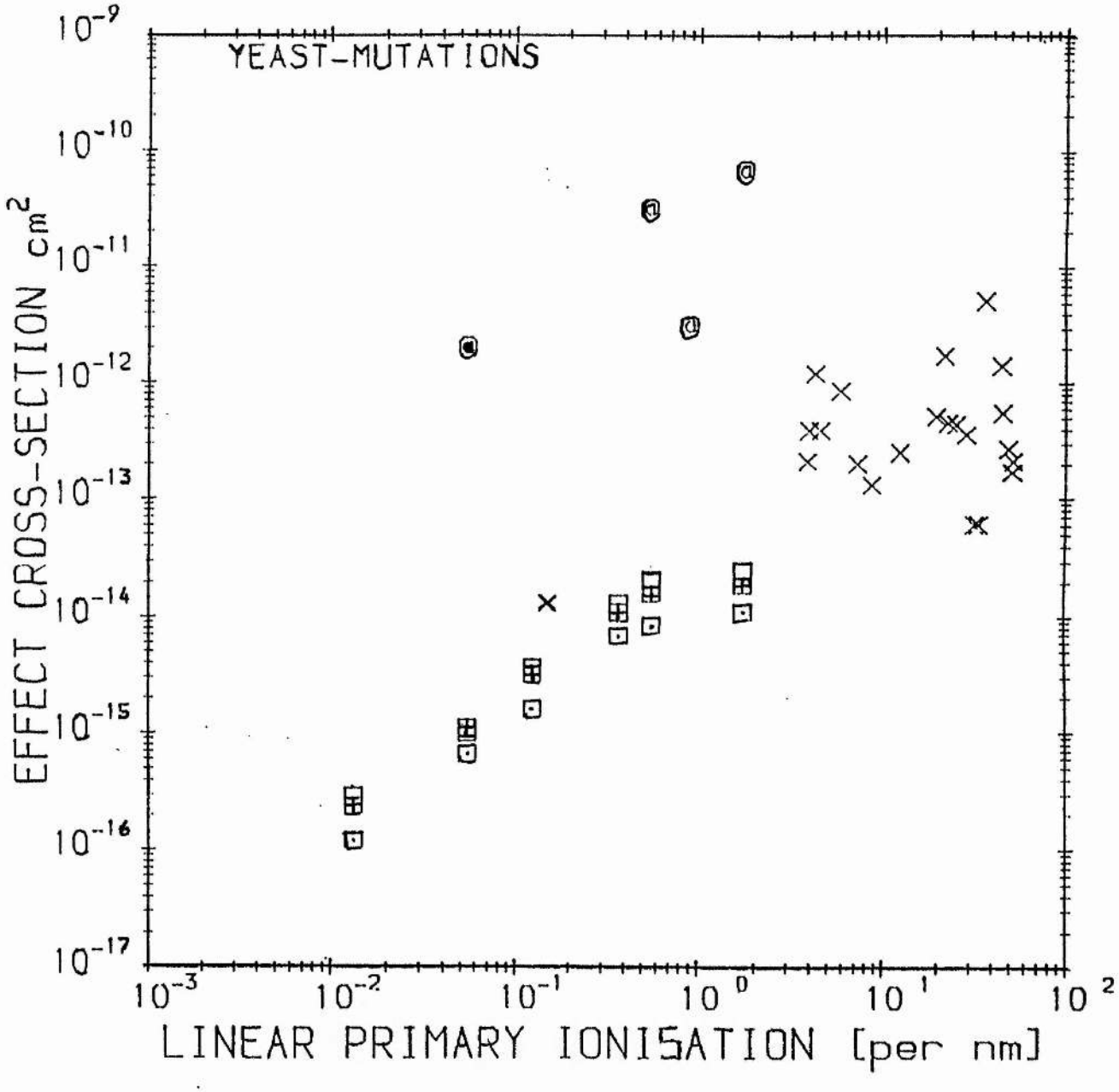


FIGURE 2.11: The effect cross section for the induction of mutation in yeast cells plotted against the linear primary ionisation of the different radiations. Sources of data and symbolic designation is similar to figure 2.9.

## 2.6.2. MUTATION INDUCTION: RESULTS.

The effect cross section for the induction of mutations in yeast and mammalian cells is plotted against the $L_T$ in figures 2.8 and 2.9; against the $I_i$ in figures 2.10 and 2.11 and agginst the maximum energy of the δ-rays generated by the pertinent charged particles in figures 2.12 and 2.13. The same data was used in each of the three charts. The sources of data, the symbolic designations, the type of radiations involved is provided in the figure captions. Most of the high LET particles in these figures are fast ions and very heavy ions. Since under track segment irradiation the $L_T$ and the $L_D$ can both be approximated to the total LET, representation as a function of dose-averaged LET is not necessary. The $L_T$ in figure 2.9 to 2.11 can be taken as synonymous with the total LET or $L_D$, except in the case of the 14MeV neutrons datum and of the photons or electrons exposure.

Figures 2.8 and 2.9 indicate that the $\sigma_e$ for the induction of mutations in eukaryotic cells increase with the LET of the radiation until LET values of about 100KeV/μm and 200KeV/μm are attained. Thereafter it decreases. A similar trend is evident in the auxotrophic assay of the yeast strain X841 reported by Mortimer et al (1965). There are fewer data points in the case of mutational assay data of Raju et al (1971), hence the attainment of saturation in biological effectiveness with increase in LET is inconclusive. The very heavy ions used by Kiefer et al (1982) have a very high ionising density and, with the exception for the single datum of $^{241}Am$ α-particles, are saturated. The yield of δ-rays by those saturated ions is very high and is discussed in subsection 2.9.3.

The two inferences that can be drawn from figures 2.8 and 2.9 are: firstly, the $\sigma_e$ for the induction of mutation depends on the cell type and mutational assay. Secondly, if biological effectiveness for the induction of 6-$TG^r$ in a cell is expressed as a function of LET, a single curve emerges for both photons and heavy ions radiations.

In figures 2.10 the $\sigma_e$ for 6-$TG^r$ mutation induction in mammalian cells are plotted against the $I_i$ of the relevant charged particles. The distinction in the biological effectiveness of photons on one hand from those of fast ions and neutrons on the other is evident. At the same values of $I_i$ the $\sigma_e$ for 6-$TG^r$ mutation by the 'electronic' radiations are about an order of magnitude less than those of the 'ionic' radiations. The curves pertaining to damage by

fast ions (the upper two curve in the figure) shows a clear biphasic behaviour. The effect cross sections initially increase with the increase in $I_i$ until the radiation's linear primary ionisation is about 0.55per nm is attained, thereafter the $\sigma_e$ appears to remain unchanged or decrease with further increase in the charged particle's linear primary ionisation, that is, it saturates. The lower two curves in figure 2.10, which refers to mutation induction by photons, also showed an indication for saturation at $I_i$ of about 0.55per nm, within the limitation of the data.

In figure 2.11 the $\sigma_e$ for the induction of various mutations in yeast cells were plotted against the $I_i$ of the the fast ions. The data of Kiefer et al (1982) are, with the exception of one datum, saturated (that is the charged particle's $I_i$ is greater than 0.55per nm). Hence the possibility for a biphasic behaviour in the relationship between $\sigma_e$ and $I_i$ of the ions can not be discerned. The data of Raju et al (1971) on the other hand are very few. The biphasic behaviour was however clearly indicated in the curves pertaining to the induction of the three different types of mutation reported by Mortimer et al (1965). The change in slope of those curves occurred at $I_i$ of about 0.55 per nm. As was observed in figure 2.10, the $\sigma_e$ initially increase with increase of $I_i$, but for $I_i > 0.55$ per nm it saturates.

In order to provide a quantitative indication of the role of secondary electrons, the $\sigma_e$ for the induction of mutations in the eukaryotic cells are related to the maximum energy of the δ-rays of the fast / heavy ions in figures 2.12 and 2.13. Figure 2.12 indicates that in the case of exposure of mammalian cells to fast ions the $\sigma_e$ hardly increases with the increase in the maximum energy of the δ-rays. However, in the case of the smaller yeast cells (figure 2.13) the relationship between the two parameters depends on whether the ions are saturated or not. For unsaturated ions the $\sigma_e$ decreases by two orders of magnitude with an increase of δ-rays maximum energy from 10keV to 20keV. Saturated ions have a large yield of δ-rays. The data showed that for an increase in the δ-rays maximum energy from 3keV to 20keV the effect cross section increases by two orders of magnitude. Further discussions on the role of δ-rays were made in section 2.9.3.

The observed occurrence of a point of inflection at a mean free path of about 1.8nm suggests that the induction of mutations, chromosome aberration and inactivation have a common dominant mechanism. In each DNA dsb is the critical lesion and its induction is

optimal when the mean interionisation distance of the pertinent charged particles matches the DNA inter strand distance. The role of DNA as the critical targets for cellular mutagenesis is shown by other investigations using incorporated radionuclides (Miyazaki and Fujiwara, 1981; Cleaver, 1977). Association between DNA double strand breaks and mutations was shown recently (Mussa et al, 1990).

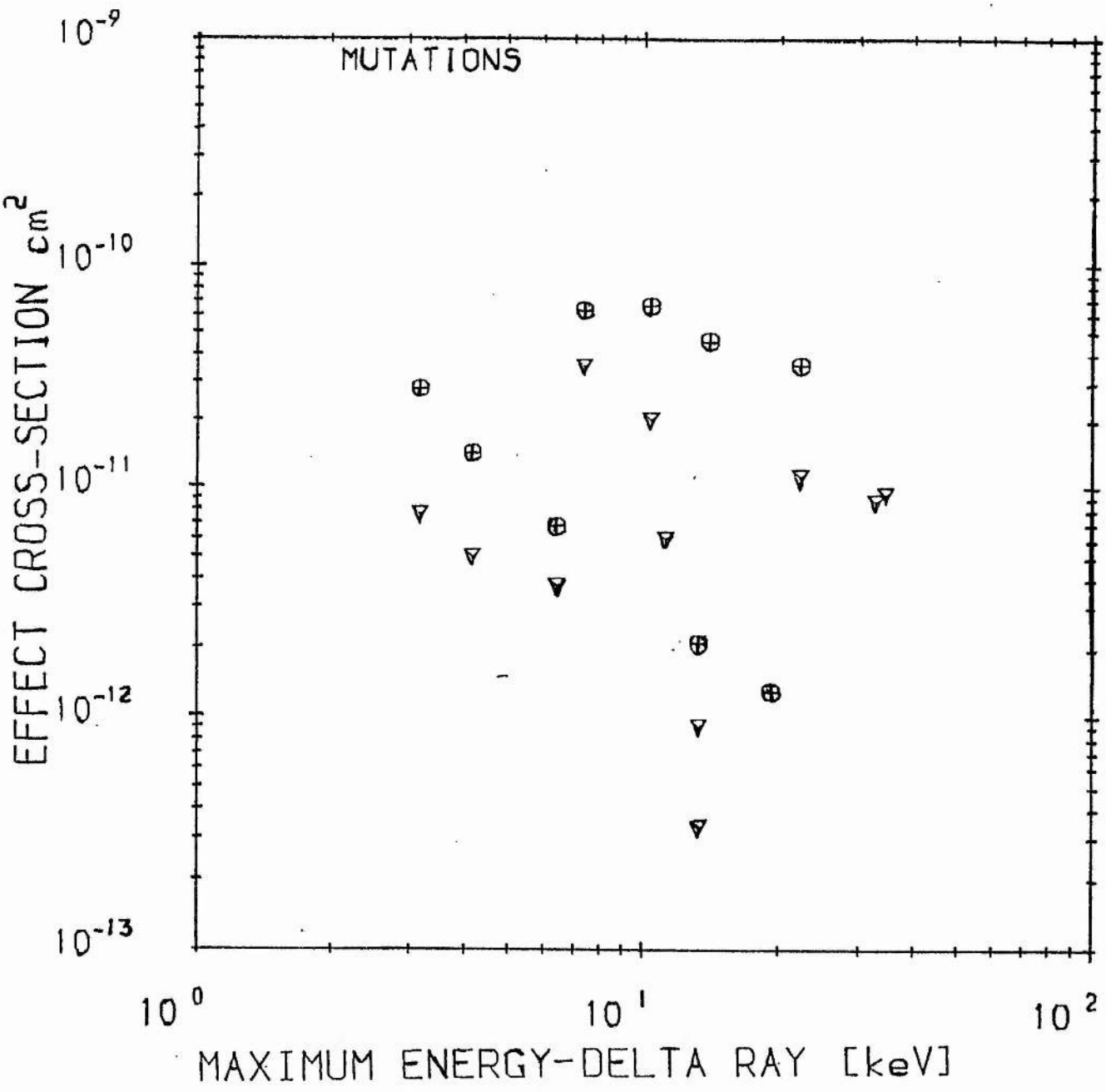


FIGURE 2.12 : The effect cross section for the induction of 6-TG$^r$ mutation in mammalian cells plotted against the maximum energy of the delta rays generated by the ions. The sources of data and symbolic designation is similar to figure 2.8.

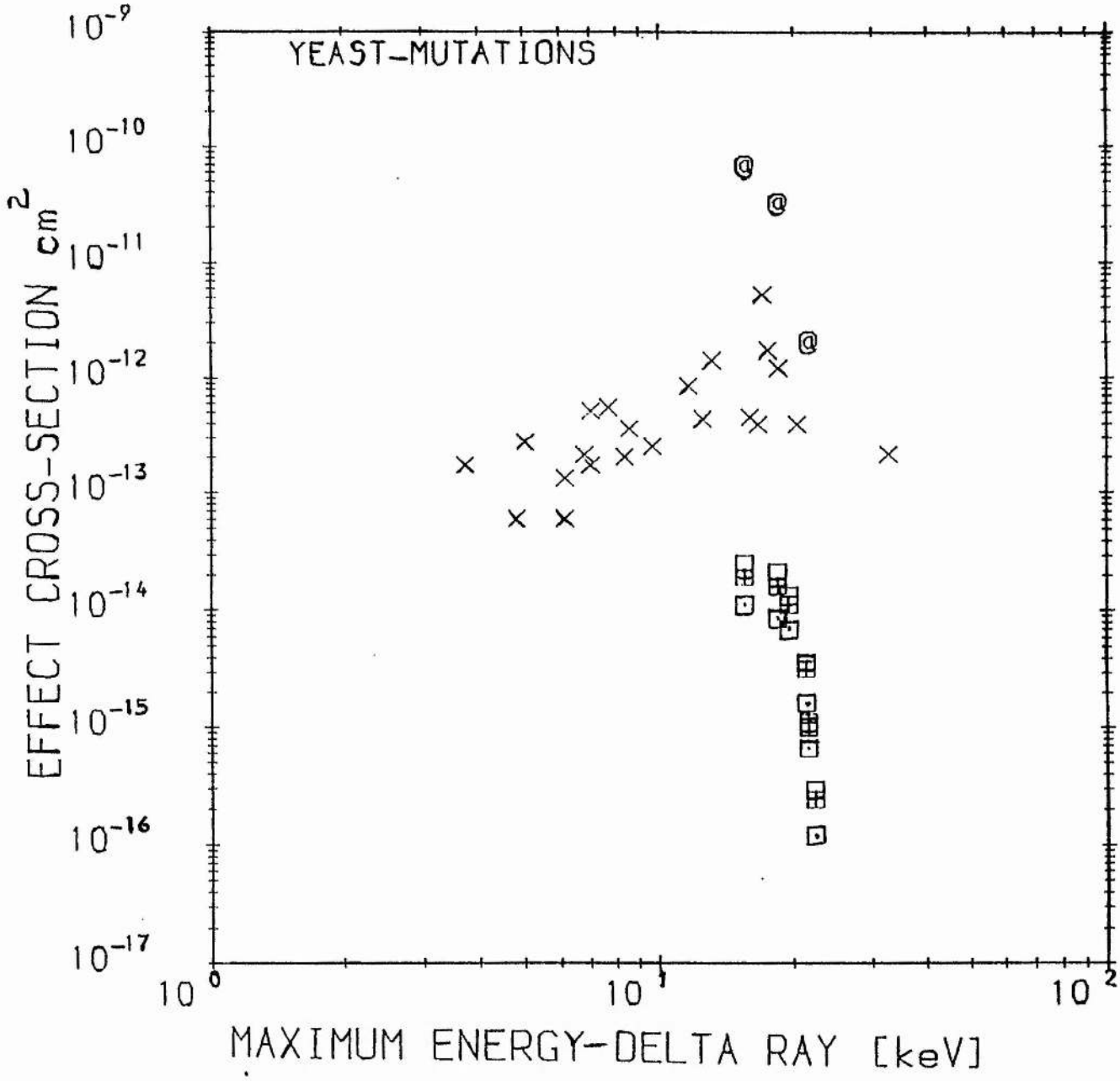


FIGURE 2.13 : The effect cross section for the induction of mutation in yeast cells plotted against the maximum energy of the delta rays generated by the ions. The sources of data and symbolic designations is similar to figure 2.9.

## 2.7. CELLULAR TRANSFORMATION:

The general public and radiation workers are exposed to low doses (less than 0.IGy) of radiation the biological effects and mechanism of which are not yet well understood. But even for the moderate doses (0.1-10Gy), the data currently available on cellular transformation in-vitro are few and inconclusive. For instance the phenomenon of reverse dose effect remains unresolved. However with an approach based on considerations similar to the foregoing, Sykes and Watt (1989) were able to interpret the phenomenon and outline conditions under which it may occur. Encouraged by this and by the significance of the in-vitro investigations as a model for the in-vivo situation, the few suitable data available on oncogenetic transformation are analysed. This analysis is restricted to those data sets obtained through the standardised procedures of Resznikoff et al (1973) in respect to mouse embryonic cells C3H10T1/2.

### 2.7.1. TREATMENT OF DATA.

The radiosensitive parameter, $\alpha$, is taken as the mean number of induced transformed cells per survivor cell per gray. The fitted values of the parameter provided by some investigators for irradiation with nearly monoenergetic neutrons and X-rays (see caption of figure 2.14) were used. By taking $\alpha$(per Gy) as equivalent to $1/D_0$, the effect cross-sections were evaluated in accordance with relation 2.2. In many of the publications on the induction of this endpoint the reported data were not fitted to any model (e.g. Yang et al, 1985). Apparently, the observed dose response data can neither be satisfactorily fitted with linear nor curvilinear models and were therefore not used. This consequently limits, severely, the data evaluated.

For all the considered data, the exposures are acute (lasting less than 20minutes), single and in air. The doses are generally less than 5Gy; the cells were not synchronised.

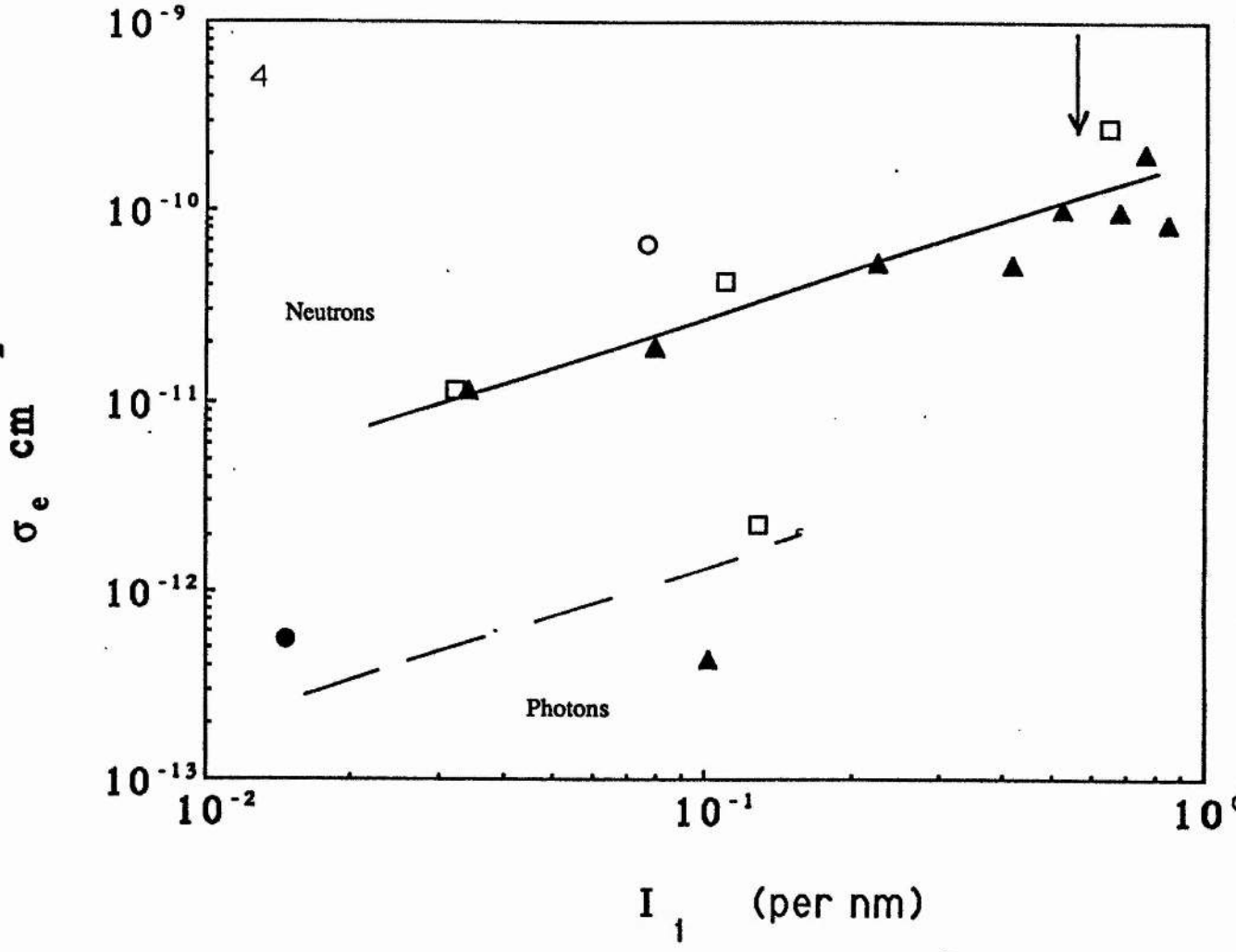


Figure 2.14: The effect cross section for the induction of transformations in C3H10T1/2 cells plotted against the $I_i$ of the different radiations. Data were from (▲) Miller et al (1989), (□) Barendsen and Gaiser (1985) for exposure with monoenergetic neutrons and X-rays; (○) Kolman et al (1979) for $^{137}$Cs γ-rays; and (●) Hieber et al (1985) for $^{241}$Am α-particles treatment.

## 2.7.2. CELLULAR TRANSFORMATION: RESULTS.

The $\sigma_e$ for the induction of cellular transformation are plotted against the $I_i$ in figure 2.14. There is an indication of some correlation between $\sigma_e$ and $I_i$, although there is some scatter of data points, indicative of interlaboratory differences. The $\sigma_e$ increase with the increase of $I_i$. The existence a point of inflection at $I_i$ equal to 0.55 per nm is not clear. Probably, because there are few data in respect to fast ions and neutrons with $I_i > 0.55$ per nm. This limitation of data is more acute for the photon radiations. But despite of this shortcoming, there is an indication of a difference in the damaging cability of the photons radiations relative to those by fast ions and neutrons. At equal values of $I_i$ the $\sigma_e$ for transformation by the neutrons and fast ions are an order of magnitude greater than those for photons. Since these trends were also observed in the case of the extensive data for inactivation (figure 2.1), chromosome aberration (figure 2.7) and mutation (figure 2.10), the tentative conclusion that can be drawn from figure 2.14 is that cellular transformation induction may involve simultaneous damage to the two strands of the DNA and could be dsb.

## 2.8. DNA STRAND BREAKAGE :

### 2.8.1 DNA STRAND BREAKAGE : TREATMENT OF DATA.

In the published literature the induction of DNA strand breaks are often reported either in terms of yield per absorbed dose per g/mol of the unirradiated DNA or in terms of the yield per absorbed dose per cell. In order to provide a common denominator for comparison, the former were converted into yield per Gy per cell by multiplying the number of breaks per gray per g/mol with the molecular weight of the unirradiated DNA of the pertinent cell. The molecular weights quoted by the original investigators of the various data sources were used. For the data from Kampf and Eichhorn (1983) the molecular weight of the DNA was not provided, hence the value quoted by Ritter at al (1977) for the same cell line was used.

The yield of DNA breaks per gray per cell are then taken as equivalent to the radiosensitive parameter $1/D_0$ in relation 2.2, and was used in calculating the effect cross sections. The sources of data, types of radiations and strand breaks scored are given in the figure caption.

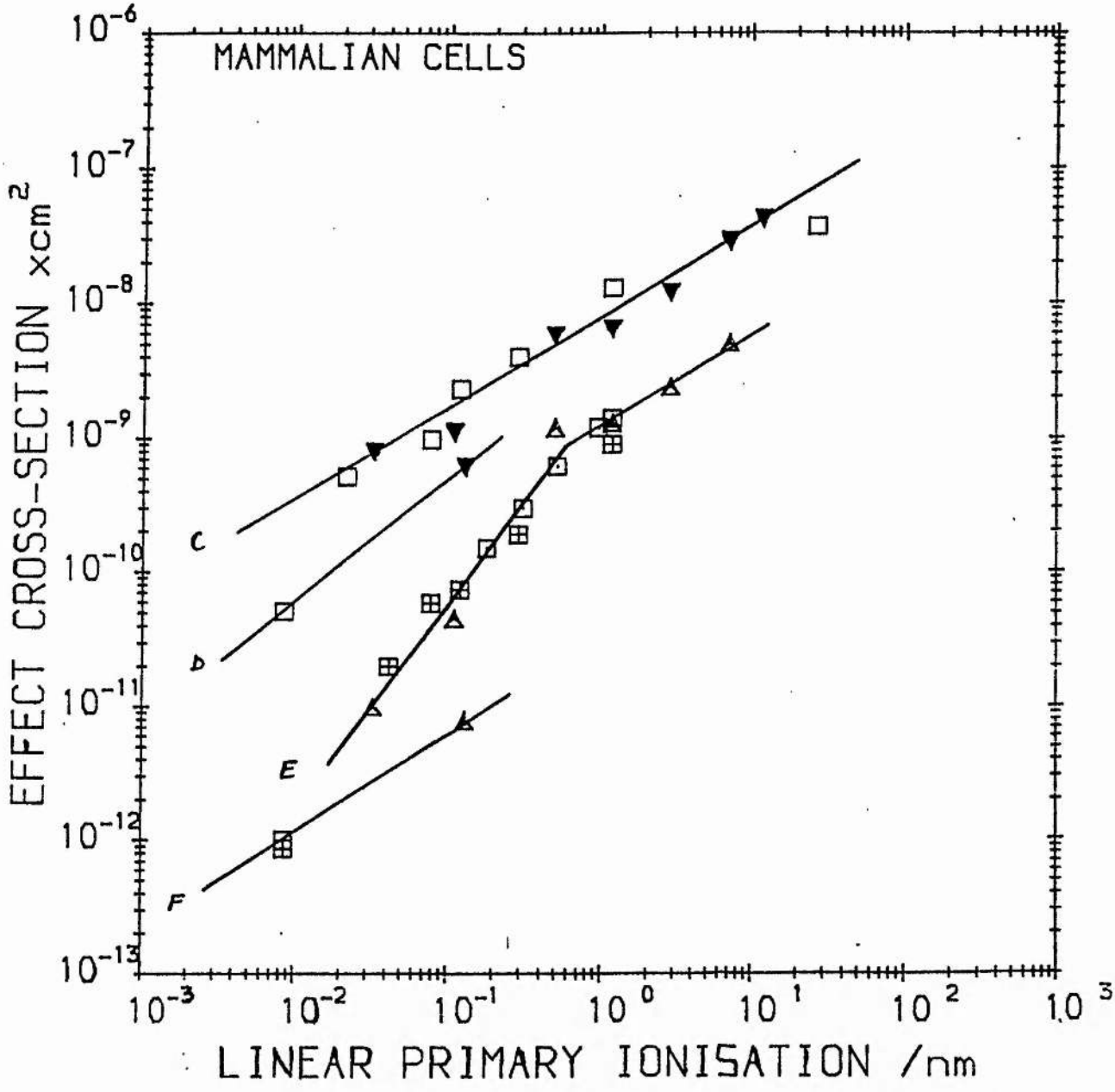


Figure 2.15: The effect cross section for the induction of strand breaks in mammalian (V79) cells plotted against the $I_i$ of the different radiations. Data were from Kampf and Eichhorn et al (1983) for 'single strand breaks '(□) and 'double strand breaks' (⊡) with cells irradiated in suspension and 'double strand breaks' with celss irradiated in monolayer (⊞); Ritter et al (1977) for 'total initial' breaks (▼) and for 'non-rejoined' breaks (▲).

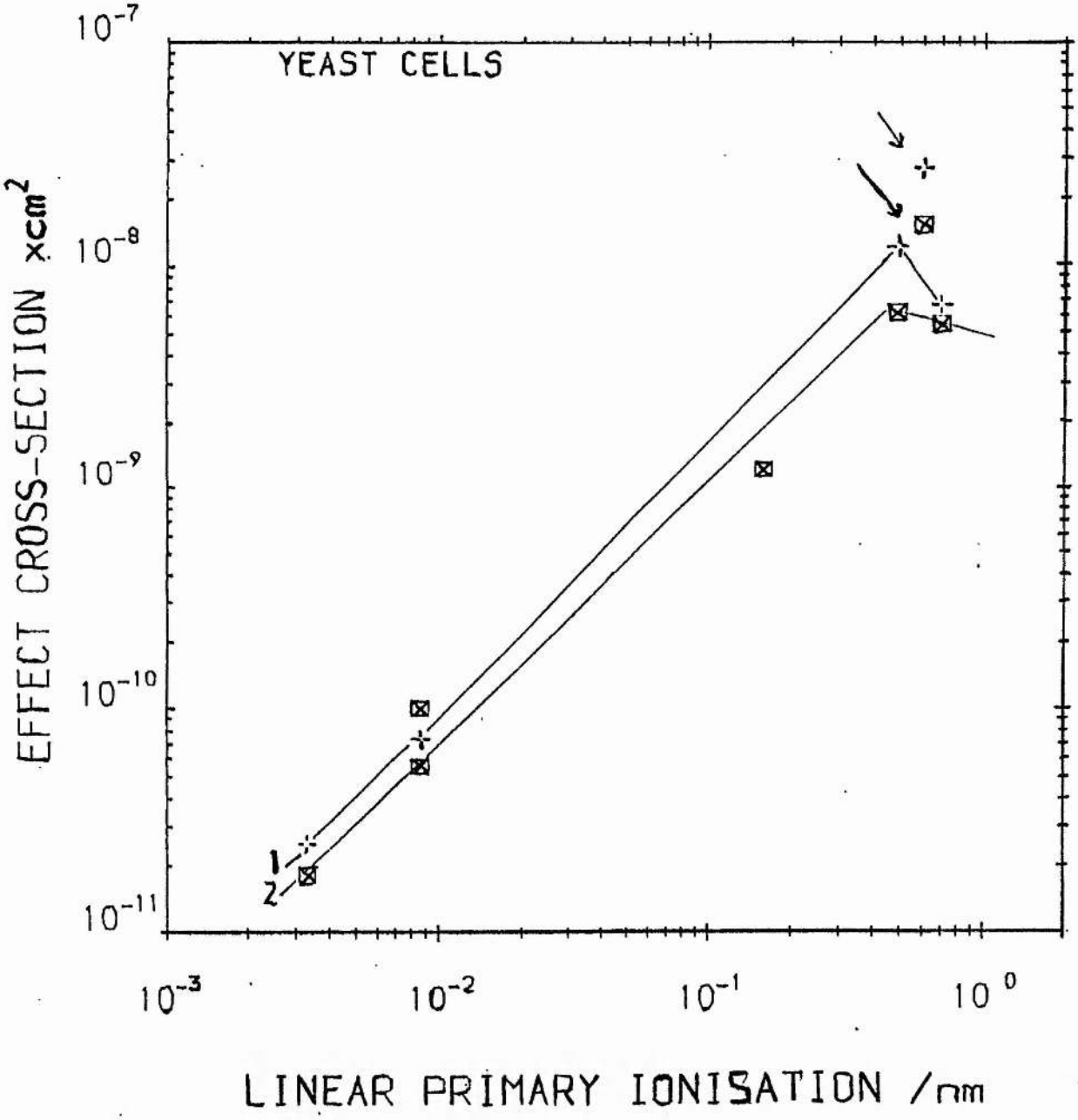


Figure 2.16: The effect cross section for the induction of strand breaks in wild and inactivation in mutant yeast cells plotted against the $I_i$ of the different radiations. Data for the survival of mutant strain rad54-3 (⊠) were from Frankenberg et al (1986), Budd and Mortimer (1982), Resnick and Martin (1976); those for dsb in wild sc211*b (-/-) were obtained from Frankenberg et al (1986). The data refers to photon radiations, except , those pointed which were obtained with $^{241}$Am α-particles.

## 2.8.1 DNA STRAND BREAKAGE: RESULTS

The $\sigma_e$ for the induction of DNA strand breaks in mammalian cells is plotted against the $I_i$ in figure 2.15. The curves (labelled C, D, E and F) were fitted by eye in order to enable reference. It is clear that both the effect cross section for the initial breaks and the non rejoined breaks (NRB) generally increase with the $I_i$. Comparison of curves C with D and curve E with F indicates an order of magnitude difference in the $\sigma_e$ for strand breakage induction by fast ions (curves C and D) and by photon radiation (curves D and F). Better estimate cannot be made due to the limitation of data in respect to exposure to photons of different qualities.

The nonexistence of the a point of inflection at $I_i$ of about 0.55 per nm is conclusive in respect to the initial breaks as scored by Ritter (1977) and the 'single strand breaks ' reported by Kampf and Eichhorn (1983). There is a clear indication of a change in slope at the critical point in the curve pertaining to nonrejoined breaks and double strand breaks scored the same authors.

It may however be observed that no hard and fast conclusions may be drawn from the data of mammalian cells because:

(a) The effects measured are the total number of initial breaks induced by the radiations and the number of breaks remaining unreconstituted after a certain period of post irradiation incubation in a medium that enables repair. The total initial breaks include ssb, dsb and breaks from alkaline labile lesions. It is probable that a greater fraction of the initial breaks may be ssb. The nonrejoined breaks (NRB) are closely related to the dsb but may not be the same (Radford, 1986; Goodhead et al 1978).

(b) The techniques of quantifying breakage yields are insensitive and have poor resolution. Very large doses have to be used (e.g. 20Gy by Ritter al, 1977) in order to produce quantifiable effects. With these supralethal doses the particle fluences are very high and the single tracks action inherently assumed in the relation (2.2) may not apply.

However in yeast cells, DNA strand breaks can be induced at doses not necessarily higher than those required for cellular inactivation (Frankenberg et al, 1986) and DNA repair

deficient species are available. The data in respect to induction of dsb in wild and mutant yeast cells (figure 2.16) show a similar pattern for the dependence of $\sigma_e$ on $I_i$. The $\sigma_e$ increase with the increase in $I_i$ of the radiations. Further, for the two data points in respect to $^{241}Am$ $\alpha$-particles (indicated by the arrow in figure 2.16), the in $\sigma_e$(cm2) is about thrice greater than those of photons, at equal value of $I_i$. However, the occurrence of a point of inflection at $I_i$ equal to to 0.55 per nm is not clear. There is a limitation of data for photons with $I_i > 0.55$ per nm.

It may be observed that there is an order of magnitude difference between the $\sigma_e$ for the induction of initial total breaks compared to that for the induction of non-rejoined breaks, and ssb compared to dsb for most of the data sets plotted in figure 2.15. This corresponds to the difference observed between the intrinsic efficiency for the inactivation of phages containing single stranded nucleic acids compared to those containing double stranded nucleic acids (point d in section 2.3). Allowing for the limited resolution of the experimental techniques, and that total breaks may include ssb, dsb and alkali-labile lesions, one can tentatively infer that the results obtained in this section supports the contention that the observed occurrence of a point of inflection at 0.55 per nm indicates the significance of dsb.

## 2.9. GENERAL DISCUSSIONS.

### 2.9.1. INTER-TRACK AND INTRA-TRACK ACTIONS.

In the foregoing analyses the empirically fitted parameter $\alpha$ (per gray), quoted by the original investigators, was taken as equivalent to the radiosensitivity parameter ($1/D_0$) in relation 2.2, and representative of the biological effectiveness of the different radiations; in other words a linear dose-response relation is presumed. The justification for neglecting the higher fitted parameters, if any, irrespective of the types of ionising radiations is the following.

A survey of the published data on dicentric aberration induction (Lloyd and Edwards, 1983) shows that 'high' LET and 'low' LET radiation induced dose response curves are respectively better fitted to the 'linear' and 'linear-quadratic' functions (that is relations of the type 1.1.1 and 1.1.2). But the demarcation between the two is not consistent and a number of other factors such as the range of doses and the dose rates determine the shape of the dose response curves.

Sevankaev et al (1979), in a study of chromosome aberration induction by nearly monoenergetic neutrons ($\gamma$-rays contribution less than 10%), have noted a linear relationship between the number of chromosome aberrations and dose for neutrons having energy from 0.025eV up to 0.35MeV. 14.7MeV neutrons and $^{60}Co-$rays produce linear-quadratic dose-response curves; whereas 0.85MeV neutrons induce dose-effect curves that can be fitted to either models. Lloyd et al (1976) obtained a shouldered dose response curve for $\gamma$-rays. With neutrons the shoulder decreases with increase in LET, but at $L_T > 20keV/\mu m$ it becomes exponential.

The shape also depends on the range of the doses considered and the nature of the exposed cells. The data of Cox et al (1977b) indicate that the induction of 6-TG resistance in cultured Chinese hamster cells and in freshly isolated human fibroblast cells showed dose-response curves that are better fitted to the curvilinear and linear models, respectively, for equal dose ranges. The induction of dsb in repair deficient yeast cells was shown by Frankenberg-Schwager et al (1979) to be linear up to doses of 2400Gy. This therefore suggests that the curvature may be related to the sensitivity of the different cells.

Experiments with protons (Bettega et al, 1981), neutrons (Fabry et al, 1985) and X-rays (Virsik et al, 1983) of different energies and under different experimental conditions such as temperature (Virsik et al,1983) and dose protraction and fractionation (Bauchinger et al, 1979; Virsik and Harder, 1980) indicate that it is only the '$\alpha$' term that varies with the radiation quality in the induction of dicentric aberrations. Miller et al (1979) also determined that the nonlinear coefficients do not vary with neutron energy in the killing and transformation of mammalian cells.

Since the higher the number of parameters used the better will be the fitting a biophysical interpretation of the mechanism can not be reliably deduced from the shape of the dose-effect curves. It can also be argued that if the radiosensitive sites are taken to be of nanometer dimension within the cell nucleus, then the probability of inter-track action within such small dimensions is negligibly small, at least for the low fluences common in most experimental conditions (e.g Goodhead et al, 1980).

The foegoing implies that it is very likely that only the '$\alpha$-term' that may be biophysically significant. The observed curvature of dose-effect curves is not due to inter-track action, and must be as result of other factors (Watt, 1989). This means that one of the main assumptions of the dual action models (Kellerer and Rossi, 1972 and 1978; Neary, 1965; Chadwick and Leenhouts, 1981) is not tenable.

## 2.9.2. THE INAPPROPRIATENESS OF ABSORBED DOSE, RBE AND LET

The results shown in figures 2.3, 2.4 and 2.5 indicate that the radiosensitive parameter ($\alpha$ per gy) cannot by itself clearly predict the biological effectiveness of radiation at least judged by its poor correlation with the three parameters $L_T$, $L_D$ and $I_i$ . Similar observation was made in the case of cellular inactivation (figure 1 in Watt and Kadiri, 1990 and figure 3 in Watt et al, 1989). The poor correlation can be ascribed to the fact that the probabilities for charged particles not transiting the site or transiting the target more than once are not considered. The effect cross section represents the probability of a single transversal of the sensitive site by the radiation track. The improvement obtained by expressing biological damage in terms of $\sigma_e$ (or the charged particle fluence), as compared to the dose, can be realised by comparing the scatter in figures 2.6 with 2.4, 2.7 with 2.3

and 2.8 with 2.5. This results implies that the absorbed dose, a mean value, is not a unifying parameter. It therefore also indicates the ambiguity inherent in the parameter RBE and belittles its use as a dosimetric parameter.

By definition, absorbed dose is the product of the particle fluence and $L_T$, so if absorbed dose is a satisfactory parameter for the prediction of biological damage as may be required for dosimetry then radiosensitivity ($\alpha$) should show inverse proportionality to the $L_T$. Figure 2.3 in the present work and Figures 2 and 3 in Watt (1989) showed that this is not so. This yet again indicates the need for more suitable parameters for chracterisation of radiation damage. Watt (1989) argued that the particle fluence could be a more appropriate parameter.

ICRU-30 (1979) and Blohm and Harder (1985) recommended the parameter $L_D$ for the specification of radiation quality. Figure 2.5 and 2.6 indicate that both the $L_T$ and the $L_D$ correlates well with the $\sigma_e$ for dicentric aberration induction. The $L_D$ appears to be slightly better than $L_T$. In both however there is no distinction between the damaging potentials of the heavier charged particles from those of the lighter electronic charged particles. The distinction is evident in the plots of $\sigma_e$ against $I_i$. At equal $I_i$ the $\sigma_e$ of damage by the neutrons and fast ions are about an order of magnitude greater than those of photons and electrons radiations. Furthermore in such curves a point of change of slope are indicated at $\lambda$ corresponding to the mean chord length of the DNA strand separation (about 1.8nm). The universality of this observation for all the end points investigated indicates the superiority of the parameter $I_i$ as a basis for biophysical analyses compared to the total LET and the mean LET.

The saturation of biological effectiveness, expressed in terms of RBE, at high LET was observed in cellular inactivation (Cox et al , 1977a), chromosome damage (Skarsgard et al, 1967), mutations (Mortimer et al, 1967), strand breakage (Ritter et al, 1977). It generally occurs at an LET between 100 and 200keV/$\mu$m, but the onset varies depending on the end point, cell type and the identity of the ion (ICRU-16, 1970). A concise interpretation of the occurrence has not hitherto been made, because the analyses were based on the LET and because the mean energy expended per effect depends on the ion type.

Katz et al (1972) suggested that the parameter $z^2/\beta^2$ is a good parameter for the

specification of radiation quality. It was also shown by Thacker et al (1979) in a plot of effect cross section against the parameter indicates saturation at the same value of $(1.95\pm0.05).10^3$ for fast ions. Such plots remove the difference in the dependence of RBE-LET relationship on the ion type for fast ions of different type and LET. But they do not offer a clear explanation of the saturation phenomenon. The reason being the parameter $z^2/\beta^2$ is directly proportional to the $I_i$ for fast particles. It is however dimensionless; it provides no indication on either the spatial distribution or energy of the delta rays; it is also less well defined for slow charged particles. The parameter $I_i$ has all the advantages of $z^2/\beta^2$, and yet it is a dimensioned parameter. Thus it can be concluded that the $I_i$, a zeroth moment of energy transfer, is more suitable for the characterisation of radiation quality than the higher moments of energy transfer. It was infered in chapter 3 that with suitable instrumentation the parameter $I_i$ (or its inverse, $\lambda$) need not be measured. Consequently, a sytem of dosimetry that requires no quality parameter was proposed.

## 2.9.3. THE ROLE OF ELECTRONS AND DELTA RAYS.

The plots of $\sigma_e$ against $I_i$ indicate that for each of the endpoints analysed, two distinct curves can be discerned: one for fast ions and neutrons radiations and another for electron and photon radiations. The curves show, within the limit of the experimental accuracy, a similar trend. Where the data are extensive (figures 2.7, 2.10 and 2.11) both curves indicate a point of inflection when the radiations mean intra-ionisation distance matches the mean separation distance of the DNA strands. The more coherently ionising particles are usually an order of magnitude more efficient than the 'electronic' type of radiations at equal $I_i$. These observations provide a basis on which an assessment of the role of (a) the primary electrons and the electrons in transient equilibrium in the case of electronic and photons exposure and (b) the delta rays generated in the interaction of fast and heavy ions, can be made.

A probable explanation for the observation that electrons are an order of magnitude less efficient in inducing damage than fast charged particles at equal $I_i$ may lie in the fact that to induce damage, the electrons must reach the nucleus. Cole et al (1980) showed that this requirement can be attained by electrons having energy of about 10keV. Since most of the delta rays have lower energies than this, and are at a grazing incidence to the whole nucleus

of a nearby cell their net damaging power is much less than the corresponding increase of their yield.

Given that dsb are the critical lesions, then to induce damage the individual electron tracks must be capable of servering both strands of the DNA. Electrons are most damaging when their energies are between 50eV and 250eV. At those energies the mean free path between their ionisations is about 2nm but their penetration range is only a few nanometers. Hence they can just interact with both strands of the DNA. An electron with energy $\geq$ 250eV can induce a break in the first strand but may not damage the second strand due to deviation of the electron from its previous direction and/or increased $\lambda$ as a consequence of its reduced energy. Thus multiple scatter processes and geometry combine to reduce the net probability for the induction of dsb through intra-track action of electrons with energies greater than 250eV and they can therefore just attains saturation. The equilibrium slowing down spectrum contains a large number of low energy (< 250eV) electrons for photons of all energies (McGinnes, 1959) and can induce ssb. But have low capacity of inducing dsb and damages that may originate from the latter (e.g. inactivation and chromosome aberrations) due to the scatter. Consequently the net efficiency for biological damage by electrons can be an order of magnitude less than those of heavy ions of the same mean free path.

The significance of the δ-ray contribution depend on whether the charged particles are fast and unsaturated or heavy and saturated. Figure 2.12 showed that the efficiency of damage did not depend on the maximum energy of the δ–rays for the case of mutation induction in mammalian cells by fast ions. Similarly, with inactivation as an endpoint, Watt et al (1985) showed that for unsaturated ions of approximately the same $I_i$, but greatly different charge and therefore different $\beta^2$ (proportional to the yield of δ-rays), have the same effect cross section. In the case of the smaller yeast cells (figure 2.13) there is a two orders of magnitude decrease in the efficiency of damage when the maximum energy of the secondary electrons increases from 10keV to 20keV.

This suggest that the role of the δ-rays may actually decrease with the increase of its energy depending on the cell's size . The δ-ray yield of the saturated ions is very high. The data of Kiefer et al (1982) in figure 2.13 indicates that mutation induction efficiency in yeast cells increased by an order of magnitude as the maximum energy of the secondary electrons increased from about 4keV to 20keV. However, the increase in the damage is not

commensurate with the increase in the yield of the secondary electrons. The plots of the damage per δ-ray (the ratio of intrinsic efficiency to $I_i$) against the $I_i$ , or $L_D$, or $L_T$ reveals that the enhancement in the total probability of damage per δ-ray is only three times, even though the yield of the δ-rays increased by several hundred times (Watt et al, 1985).

A plausible explanation for this may lie in the transport of energy out of the cell by the δ-rays. Results from theoretical considerations have indicated a decrease in the efficiency of biological damage with the increase in the δ–ray energy, of fast ions, as the sensitive site's size decreases (Blohm and Harder, 1985). Monte Carlo simulation of proton tracks, having energies of 1-2MeV, in water vapour (Wilson and Paretzke, 1980) indicates that that as the dimension of the simulated volume decreases the fraction of the energy of the δ-rays transported away from the site increases; for sites of a few nanometers almost all the energy of the δ-rays are carried out of the site, and it is only the single individual interactions of the proton with the absorber target that takes place.

The foregoing suggests that it is the frequency of the interaction that dominates the damaging processes rather than the total energy transferred. One of implications is that in the design of detectors for a unified system of radiation dosimetry the corrections for δ-rays effects necessary in conventional microdosimetry, need not be made. All that will be required is for the twin-detectors to efficiently count the frequencies of time coincident energy deposition events in two tissue equivalent detectors.

# CHAPTER THREE: APPROACHES TO INSTRUMENTATION IN UNIFIED DOSIMETRY.

In this chapter the conceptual and physical requirements (section 3.1) of detectors for the unified system of radiation dosimetry are first defined. It is followed by an evaluation of the potential of various radiation detector systems for satisfying the defined requirements. Section 3.2 contains a brief review of the principles, limitations of, and modifications to, gas based detectors, including those based on light emission and the multistep avalanche process. The remaining part of the chapter considers detectors constructed in the condensed phase. A more extensive and quantitative treatment of organic scintillators, the plastics in particular, was made separately in chapters four and five.

## 3.1. REQUIREMENTS OF A DETECTOR FOR UNIFIED DOSIMETRY.

In the preceding chapter it has been convincingly shown that the biological effects of ionising radiations are determined by their interactions in the DNA. Consequently a physical detector must be identified which has effective size and whose detection principle reflects this finding.

The occurrence of optimum damage efficiency at an inter-ionisation distance equal to the DNA interstrand separation for all the biological endpoints investigated suggests that it is a dominant damage process. The induction of damage is attributed to a stochastic process, whose relative yield, P, for fully penetrating charged particles is given by

$$P = \frac{1}{\sigma_g}\left[1 - e^{-\lambda_o/\lambda}\right].\phi_s$$

Where $\lambda$ is the mean free path for ionisation along the charged particle track and $\lambda_o$ (= 1.8nm) is the mean chord length between the DNA strands. $\sigma_g$ is the saturation cross section, that is the effect cross for the induction of the specified damage by radiations with $\lambda_o = 1.8$nm. $\phi_s$ is the pertinient charged particle fluence, the inverse of the effect cross section.

The DNA consists of two lengthy polymeric chains of nuclear tides that have flexible

configuration. Helical in shape, it is wound round protein structures (histones), from which more complex structures are formed. It can, for the present purpose of simulating the DNA response, be considered simply as a complex made up of similar basic units: the segments of the two DNA strand base pairs at risk in mammalian cells. The basic unit is essentially a tri-laminar entity of DNA strand segments, each about 1-2nm thick, interfaced by a layer of water molecules of the same thickness. Thus to achieve good emulation, the appropriate detector should be two detectors operated in coincidence (twin-detectors). The use of two wall-less detectors of submicron dimensions was previously suggested (Fowler, 1967) and explored (Burlin et al, 1972).

Alper (1979) suggested that the membranes of the cell and nucleus are the most probable targets for interphase death, especially in the presence of oxygen. Although this is ruled out by the results obtained from the inactivation of T1 phages (Watt et al, 1985), it is interesting to note that since the membranes are also tri-laminar, each layer being a few nanometers thick, the present considerations adequately represents that possibility also.

### 3.1.1. PHYSICAL REQUIREMENTS.

a. In order to mirror the DNA segments physically, the desired detector should consistt of two thin detectors separated by an non-sensitive layer of 1.8nm. The inference that the induction of double strand breaks can only be by single track action in the DNA (chapter two) suggests that the response of the detector should be restricted to single interaction events by the pertinent charged particles occurring in time coincidence in the separate detectors. The two thin detectors that form the system should have similar physical and chemical properties. The other desired properties of each of the detectors are as follows:

b. The interaction of radiation with the detector should generate charged particles (or corresponding entities) all of which can be conveniently and efficiently collected. This also ensures sufficient resolution. It is deduced in section 3.1.2 that unlike the sensitivity, the energy response resolution is not a critical requirement of the detector, provided that the signal is greater than the threshold value.

c. Ideally every radiation interaction should be detected. Rauth and Simpson (1960) showed that the minimum energy involved in effecting significant radiochemical action is 10 to 15eV, which is about half the average energy required to produce an ion pair in a

gas. The threshold for unified dosimetry will be taken as the energy involved in the induction of a single strand break of the DNA. A single OH radical (involving an energy as low as 4 eV) may cause a single strand break. But most single strand breaks can be efficiently repaired and may not lead to dsb (Elkind, 1984). For the latter to occur concentrations of energy deposition, of about 30eV, are required; this will therefore will be considered as the threshold energy for unified dosimetry.

d. The noise level of the detector and associated interference should be less than the threshold level, so that every interaction equal to, or above the threshold level should be detectable. For optimal signal-to-noise ratio some form of internal and external amplification may be required. The use of coincidence techniques will reduce the noise background and is advantageous.

e. The entities or charged particles produced and collected should ideally be linearly related to the number of interaction events.

f. The time it will take the radiation to transverse the segments of the DNA, which are a few nanometers thick, is very short; hence for meaningful simulation the response of the detector should be correspondingly fast. If coincidence techniques are used the coincidence resolving time should be of the order of nanoseconds or less.

g. Interest will be centred on the stochastics of radiation interactions which determines the detector's ultimate resolution. Consequently, a high degree of uniformity in composition and physical thickness of the material in each of the two detectors is a requisite. This will minimise fluctuations of signal generations due to structural inhomogeneity.

h. The molecular DNA within the cell is essentially in a concentrated liquid solution. As the physical properties of liquids are closer to solids than gasses, the required detector should preferably be in the condensed phase.

i. Electrical conduction, availability, amenability to routine preparation, good tensile strength and aging properties are other desired properties.

h. The interaction cross-section and mass stopping power to charged particles of the detector material should be the same as the DNA. Mass-stopping powers generally depend on energy hence consideration for it has to be made. Equality in electron density is also

desirable. The detectors should indicate both the mean and stochastics of radiation interactions hence similarity in geometrical form as well as equivalence in electron density are necessary. Tissue (actually DNA) equivalence is required.

### 3.1.2. MODE OF OPERATION AND INTERPRETATION OF RESPONSE.

The conventional object of radiation dosimetry (at macro, micro and nano level) is the measurement of the total energy deposited in a specified mass (the dose). The transferred energy is taken as athe parameter descriptive of the radiation interaction with matter. This has the inherent advantage that comparison with other physical measurements can be made. But other parameters such the momentum transferred were also proposed (Turner and Hollister, 1962). However, not all the deposited energy is radiobiologically relevant. Excitations, for example, are deemed less effective (Jagger, 1967).

The results presented in chapter 2 showed that the absorbed dose and RBE are not the most appropriate parameters with which biological damage can be quantified. It is also well known that in the present radiation dosimetric system has not satisfactorily handled the δ-rays. For targets of nanometer size, Monte Carlo simulation of radiation interactions indicates that most of the delta-rays produced in heavy ion tracks transport their energy out of the volume (Wilson and Paretzke, 1980). In such volumes the statistical variation of energy deposition, which sets an absolute limit to the precision of dose measurements (Kellerer, 1985), is very large. Taken together, these imply that the measurement of total energy deposition in the DNA (i.e. in detectors simulating the DNA) cannot be realistic.

More realistic measurements can be made if some form of threshold can be identified and used. It is a fundamental finding of the analyses reported in chapter two that it is the frequency of events, not the energy deposition, that determines the biological effectiveness of radiation and which is relevant to unified dosimetry. The events are (by the deductions previously made) the induction of coincident ssb in the DNA duplex. The energy involved in the induction of ssb can therefore be taken as the threshold sensitivity required of each of the two-volume detectors (operating in time coincidence) in the unified dosimetric system. Interpretation of the detectors response can therefore be made by just counting the interaction frequencies. Measuring, or rather converting such data in to the total energy deposited is not required.

This deviates from the normal methods of radiation dosimetry. But based on the facts presented in section 3.1.1, it is more realistic. In retrospect, it may be observed that the primary data provided by most detectors are the interaction frequencies. In proportional counter microdosimetry the pulse height spectra are the ionisation interaction frequency spectra. Energy deposition spectra are obtained by a conversion based on the assumed mean energy for the production of ion-pairs. It is well established that the mean energy required to produce an ion pair is not constant for slow particles (Goodman, 1978); it depends on the ion type and its energy (ICRU-31, 1979). So the conversion of the frequency measurements to energy deposition introduces uncertainties.

Detectors operated in counting mode are liable of having high sensitivity to the variations of radiation quality (Kellerer, 1985). This is an advantage if other sources of the fluctuations besides those due to the radiation interaction are minimised. The use of coincidence techniques, an essential element in the simulation of simultaneous damage to the two strands of the DNA, also enables the signal-to-noise ratio to be reduced. It was shown in chapter five that by counting in time coincidence the signal-to-noise ratio of a detector can be enhanced. The same is expected in the operation of two nanodosimeters operating in time coincidence.

Thus ideal detectors for unified dosimetry are not necessarily required to measure the total energy deposited. Rather it is more appropriate and convenient to count the coincident "ionisation" events. Conversely such detectors are not nanodosimeters in the usual sense of the term (ICRU-36, 1983). Indeed the term is used here only as an indication that the segments of the DNA are of nanometer dimensions.

For operation and implementation in the unified dosimetric system, such twin-volume detectors will be required to provide coincidence pulse height spectra. The pulse height of the individual events will be proportional to $\sigma_e/\sigma_g$. The number of events per pulse height interval corresponds to the effective cross-section $(\sigma_e/\sigma_g)$ per interval of $(\lambda_0/\lambda)$. Where $\sigma_e$ and $\sigma_g$ are, respectively, the effect cross-section and the saturation cross section (see Chapter two) for the induction of the specified effect.

By this approach the integral of the response spectrum to radiation (s) of mean free path $\lambda$ is is given, approximately, by

$$\sum (\sigma_e / \sigma_g).(1 - \exp(-\lambda_o / \lambda).\phi_s \qquad 3.2$$

For $\lambda = \lambda_0 = 1.8$nm, the ratio of $\sigma_e/\sigma_g$ can be made equal to unity. Thus the integral of the response spectrum of an ideal instrument is a direct measure of the Absolute Biological Effectiveness (ABE) of the given radiation.

The above relation implies that the integral of the area under the peak of a single radiation depends on its mean free path and charge particle fluence (determined by $\sigma_e/\sigma_g$). For a radiation beam composed of more than one component multiple response peaks will be obtained, some of which may be (fully or partially) superimposed on each other, depending on the difference in the component's $\lambda/\lambda_0$ and resulting into more intense and/or broader peaks.

The foregoing has two implications. First, since the area of the peaks (of the response spectra) is additive, the resolution of the detector is not of fundamental significance in so far it has a high sensitivity. Second, the net absolute biological effectiveness of the mixed radiation fields is simply given by the integral of their response spectra. Thus direct additively of the net biological effectiveness, without fore knowledge of the composition of the mixed radiation field, is obtained in this formalism in contrast to the radiation macrodosimetry (see section 1.2). An observed limitation (Goodhead, 1987) in the utilisation of proportional counter microdosimetry and the related quantities to biological systems is the absence of an explicit relationship between the stochastic quantities and the biological damage. Expression (3.2) provides the relationship between biological effects and the detector response parameters in the case of unified system of radiation dosimetry.

So far, we have shown the limitation of the conventional dosimetric system, proposed an alternative radiation dosimetric system, which is based on extensive radiobiological data, suggested a plausible biophysical interpretation and shown its potential advantages in operation. In the following sections we assess the potentials of various detector systems in realising an appropriate detector, an essential element, for the proposed system.

## 3.2. GAS BASED DETECTORS.

### 3.2.1. THE BASIC PRINCIPLES OF THE ROSSI'S COUNTER.

The Rossi counter is the most widely used detector for microdosimetry. It is a proportional counter made of tissue equivalent (TE) conducting plastic of 6 to 20cm diameter. The chamber is filled with a TE gas and has an electrically biased central anode. To simulate spherical tissues of desired dimensions, the pressure of the gas is lowered so that its mass is the same as that of the tissue. From the number of ionisations, as indicated from the pulse height spectrum, and the assumed mean energy to produce an ion pair, a direct measurement of the approximate total energy deposited by the radiation within the simulated tissue volume is obtained. For an ideal gas, the density is proportional to the pressure.

The prerequisite for quantitative simulation is the equality of the energy loss by the charged particle passing through the counter gas with that for a corresponding trajectory in the tissue volume. Thus

$$\Delta E_g = S_g.\rho_g.P_g = S_t.\rho_t.P_t = \Delta E_t$$

Where S is the mass stopping power, $\rho$ is the density, P is the path length; with subscript denoting gas (g) or tissue (t). $\Delta E_g$ and $\Delta E_t$ are the mean energy losses from the charged particles in gas and tissue, respectively.

With complete TE, the density of the gas required for simulating a tissue is equal to the ratio of the path length in the gas to the path of the radiation in the tissue. By reducing the diameter of the sphere by a factor equal to the ratio of the diameters of sphere to the tissue, the mean energy loss of charged particles is the same in both spheres. The special feature of proportional counter microdosimeters is the inherent signal amplification due to increased frequency of interaction (ICRU-36, 1983).

### 3.2.2. THE ROSSI COUNTER AND NANODOSIMETRY.

In principle, with sufficiently low-pressures, very small tissues with diameters of the order of nanometers may be simulated. In practice, the lower limit of tissue dimensions which can be accurately simulated is a bout 0.1μm (Coulautti et al, 1985), except the recent results

of Kliauga et al (1990). since simulating smaller volumes means that the proportional counter have to be operated with very high gain and low pressures. The gas multiplication region avalanche then covers a considerable fraction of the detector volume. Thus adequate multiplication with sufficient uniformity of response throughout the detector volume is not obtainable. A helical grid anode wire was used but could not overcome this limitation when the dimensions of tissues to be simulated is a few tens of nanometers in diameter. The variance and the variance-covariance techniques could be used but they provide limited data (see section 3.23). The other problem with the Rossi's counter is the existence of a density gradient between the solid wall and its gaseous content. It is a problem common to all gas based detectors, and its severity depends on the radiation. For low energy electrons whose energy degradation deviates from the csda, and high LET radiations having a high yield of delta rays, wall effects are severe. One method of overcoming wall effects is to separate the detection from the multiplication region (ICRU-36, 1983). Another method of eliminating the density effect is to use wall-less counters . In the latter, the boundary of the gas volume is defined either by a fine grid or by an electric field from small field electrodes (ICRU-36, 1983).

### 3.2.3. THE VARIANCE AND VARIANCE-COVARIANCE TECHNIQUES.

The variance technique is based on the fact that the relative variance ($V_{r,1}$) of a single event distribution $f_1(z)$ is related to the relative variance ($V_{r,n}$) of the multi event distribution, $f_n(z)$, by

$$v_{r,n} = \frac{V_{r,1} + 1}{n} \qquad 3.5$$

where n is the number of events. Given that the variance contributions from other sources are less significant, the measurement of the relative variance for a detector signal will indicate the mean of the single event distribution. The measurements are however limited only to time non varying radiation fields.

The variance-covariance technique is used for the determination of the microdosimetric parameters in time varying radiation fields (Kellerer and Rossi, 1984; Lindborg et al, 1985). The $y_D$ is determined from observations of the specific energies from two independent detectors A and B, operating in phase during a series of measurements.

$$y_{DA} = k[V_r(Z_A) - C_r(z_A, z_B)]\, z_A$$

where $z_A$ is the mean specific energy measured by counter A; k is the conversion term from Gy to keV/μm. $V_r$ and $C_r$ are the total relative variance and the relative covariance respectively. The $C_r$ indicates the difference between the macroscopic dose variance and the beam fluctuations variance. Similar expression as above can be written for the detector B, such that if the detectors are symmetrically positioned, that is $z_A = z_B$, the $y_D$ is the mean of the two.

These techniques can be used to measure the $y_D$, without determination of the explicit spectra, of simulated tissues that are less than 0.3μm diameter (Bengsston, 1970; Forsberg and Lindborg, 1981); mainly because little or no amplification of the charges is required if the detector is adjusted to integrate the response over finite dose increments. But the techniques are subject to all the other inherent problems of gas based microdosimetry (Forsberg and Lindborg, 1981).

Recently, the combination of the variance-covariance technique with a pair of wall-less spherical ionisation chambers was reportedly used by Goldhagen et al (1990) for the measurements of $y_D$ for 15MeV neutrons in site diameters ranging from 4.7μm to 19nm. Albeit these techniques can provide information on the $y_D$, a quantity of fundamental importance to radiation protection in nanometer size targets the operational basis of the technique is not consistent with the requirements of detectors for unified dosimetry as outlined in section 3.1.

### 3.2.4. DETECTORS BASED ON ION RECOMBINATION.

These detectors are based on the fact that the initial recombination of ions in a gas or liquid is a process determined by the distance between the ions formed along the tracks of the charged particles and hence on the rate of energy deposition and LET. Thus, an ionisation chamber exposed to radiations of different qualities shows different saturation curves of ion collection efficiency as a function of polarising voltage.

The principle and design requirements of this detector was outlined by Zielcynski et al (1981). They showed that the measurements of the recombined fractions of an ionisation chamber at two operating voltages can be used to determine the parameter Radiation Quality Index, RQI, which they defined in analogy to the RBE. The investigators showed that the RQI for some alpha and neutron sources, $^{60}Co$ γ-rays can be made such that they are equal

to the ICRU assigned quality factors of those radiations. Makrigiorgos and Walker (1985) reported the measurement of dose restricted LET, cut-off 500eV, of 30 to 100kVp x-rays relative to $^{60}Co$ γ-rays. They used tissue equivalent ionisation chambers at a constant pressure of 8atm to measure the ionisation currents for two high voltages.

Due to their low sensitivity, detectors based on ion recombination cannot be relevant in instrumentation for unified dosimetry.

### 3.2.5. THE MULTISTEP AVALANCHE COUNTERS.

The multistep avalanche counter (MSAC) is a variant of a gas proportional counter with at least two multiplication stages (Charpak and Sauli, 1978). The first stage, the preamplifier, functions as a parallel plate avalanche counter (PPAC), the separation between the cathode and the anode being only very few mm. The second stage is usually a multi-wire proportional counter (MWPC), but can also be a PPAC. In between the two stages a transfer region of few cm width is usually, but not necessarily, incorporated. The function of the transfer region is to absorb photons produced in the gas during the multiplication process, to block the back drifting of positive ions, and, if required, gating the counter.

The PPAC and/or the MWPC are usually constructed with grids or meshes. This enables electrons magnified by Townsend avalanche in the preamplifier to be transferred to the amplifier for further gain. The total gain ($G_t$) attained by the electrons is given by

$$G_t = G_p \cdot G_a \cdot \varepsilon_t$$

Where $G_p$ and $G_a$ refers, respectively, to the gains in the preamplifier and the amplifier. $\varepsilon_t$, the transfer efficiency of the preamplified charge, is approximately equal to the ratio of the field strengths in the transfer to that in the amplifier region. It has been shown (Brenskin et al, 1979) that MSACs operated at low pressures (2-10 torr) have fast response (few microseconds) and thus allow high frequency operation; the positive ions in the high E/p fields leads to a reduction of space charge and shorter electronic occupation time. MSAC can attain a high charge multiplication ($10^7$ to $10^8$) in pure hydrocarbons and are, therefore, efficient in the detection of single electron avalanches produced from the cathode. The prerequisite for the double step process is the occurrence of a substantial electron diffusion from the preamplification stage. Brenskin et al (1979) showed that this occurs if the lateral spread of the avalanche is about or exceeds the wire spacing of the 'anode' to the preamplifier. It is therefore determined by the type and pressure of the gas and the field

applied.

The MSAC is owing to its geometry, inappropriate for unified dosimetry. However, it can be coupled to the two sides of a low Z solid or liquid cathode for the detection of the low energy secondary electrons (section 4.4), and thus forms multiplication volumes of a dual volume nanodosimeter. The MSAC could be used for measurement of linear primary ionisation and radial dose distribution as in tissue equivalent gasses (see Chapter 6).

### 3.2.6. THE GAS SCINTILLATOR PROPORTIONAL COUNTER.

This is a hybrid of a proportional counter (it can in principle be ionisation) with a scintillator detector (Policarpo, 1977; Birks, 1964, chapter 14). It has similar characteristics, such as the possession of a prompt and a delayed component, to the solid scintillators (section 4.8 and Chapter 5). Its main advantage over the latter is the ability to magnify the light by electrostatic means. The gas scintillators show better resolution compared to the solid and liquid scintillators. It is also established that the light response is linear with increase in radiation energy for different radiation types, unlike the solid phosphors.

The most efficient gas scintillators are the noble gases, so there is thus little flexibility in the choice of detector gas and tissue-equivalence can hardly be realised. Furthermore, their emission is usually in the ultraviolet region hence wavelength shifters have to be painted on the inside of the chamber cavity. This complicates wall effects. It can therefore be inferred that such detectors are not appropriate for instrumentation in unified dosimetry.

## 3.3. DETECTORS BASED ON SECONDARY ELECTRON EMISSION.

The irradiation of a material generates an internal electron degradation spectrum. The secondary electrons have very limited ranges due to interaction with phonons. However at the peripheral layer of the material some electrons may escape through the barrier potential. It is established that the layer, termed as the escape zone, is characteristic of the material and is usually only a few nanometers in thickness (e.g. 4nm for C). The depth of the escape zone is independent of the energy of the radiation and of its type (quality).

The term secondary electrons refers to those electrons that escape the barrier potential of the material with energies less than 50eV. The type of energy distribution is independent of the primary electron energy (for those greater than 20eV). The number of secondary electrons, $n_{SE}$, ejected from the surface per incident primary electron can be correlated to the initial energy of the incident electrons for all materials (Burlin, 1974). The $n_{SE}$ depends on the depth of the escape zone, but the probability of escape $P(n_{SE})$ is a function of depth. $P(n_{SE})$ therefore reflects the statistics of energy deposition in the escape zone. The yields secondary electrons are generally very low (0.6 to 1.7 in metals and semiconductors, about 20 in insulators) and can be considered as single electrons. The secondary electrons yields are not a linear function of energy; it first increases rapidly, passes through a maximum and then declines.

The potential of secondary electron emission for radiation micro- and nanodosimetry was first shown by Burlin (1974). He observed that the secondary electrons emerging from a surface reflect energy deposition within volumes with effective linear dimensions of a few nanometers; the entrance and exit surfaces form two detectors separated by an interaction distance formed by the interior layer. Burlin (1974) presented theoretical and empirical data which indicated that the energy and angular distribution of the electron are separable, and within the medium the angular distribution is isotropic. In addition, he observed that the yield due to electrons irradiation is much less than that for heavier ions. This is analogous to the relationship between RBE and LET.

Forsberg and Burlin (1978) presented results of monte carlo simulation of the phenomenon. A comparison of the computed pulse height spectra with those obtained from the gas proportional counters of similar mean chord length indicates fair agreement and therefore good prospects of the phenomenon for radiation micro- and nanodosimetry.

It can be envisaged that a film of LiF connected on either side with a MSAC (section 4.2.7), will enable the efficient detection of the the usually low energy (about 3eV) secondary electrons. It can also be envisaged that the use of aluminised polyethylene can enable the detection of neutrons. A number of problems however remains.

The first is the influence of the rediffused electrons. Pulse height discrimination can be used to reject them but the chance exists that they may ionise the gaseous detection medium and complicate the resultant spectra. In radiobiology such electrons do not lead to biological effect and should not, therefore, be detected.

Secondly, the only well known secondary electron emitter which is approximately tissue equivalent is LiF, but its escape zone thickness is 24nm and its density is 2.625gm/$cm^2$. Thus direct simulation with a detector of appropriate size can not be achieved.

Thirdly, the separate detection of secondary electrons from the entrance and exit sides of the film, does not necessary reflect radiation interactions within two volumes, in that the electrons ejected from the opposite sides may actually originate from events in the inner layer. Thus the two escape zones cannot be distinguished unambiguously as the two strands of the DNA .

Fourthly, the gap energy in LiF is 12.1eV, the mean energy required to produce an electron-hole pair is therefore about 36eV. Considering that only a few electrons can escape, it is plausible that the practical value is much higher. Thus the secondary electron emission is likely to have very low sensitivity and single interaction events can hardly be detected. Thus the phenomenon is not suitable for instrumentation in the unified radiation dosimetric system.

## 3.4. DETECTORS BASED ON SEMICONDUCTIVITY.

The main advantage of these detectors is the low energy required to produce an electron-hole pair (e.g. 3.7eV in Si). This improves their energy resolution and the prospects of detecting minimum ionising particles. Experience exists on the use of semiconductor detectors as transmission detectors for charged particle identification (Goulding and Harvey, 1975). Their high atomic number is an advantage for detecting electrons; however the minimum thickness obtainable is in the order of mg/$cm^2$, which exceeds the ranges of these minimum ionising particles. Prospects for having thinner films, in the order of a few nanometer has greatly improved recently. Submicron semiconducting structures are presently being produced.

These are fabricated using optical beam, electron beam, ion beam or x-ray lithography depending on the minimum size of the device required. At present, extremely thin and precisely well defined layers of semiconducting alloys such as GaAs and $Au_{60}Pd_{40}$ can be fabricated. GaAs wires as thin as 9$nm^2$ cross-sectional area (Wilkinson and Beaumont, 1986; Lee et al, 1987) and evaporated $Au_{60}Pb_{40}$ wires of 25-40nm effective width (square

root of cross sectional area) are fabricated (Heraud et al, 1987). It can be envisaged that two such wires, each connected to current or voltage measuring devices, and placed at nanometer separation may thus serve as a two-volume detector.

This idea was explored at the initial phase of this work. An arrangement was made with the Nanodevices Research Centre, Glasgow, to provide two thin GaAs wires separated at a distance of 25nm, the separation distance will be progressively reduced. The response of the wires to $\alpha$-particles will the be sought. It was not carried through because of three envisaged obstacles. First, the electronic properties of the ultra small structures is dominated by quantum phenomena. The Boltzmans transport formulation for conductivity is not obeyed even at low temperatures (Bergman, 1984). At present their electronic properties are not well characterised (Bergman, 1984). It is not known how the quantum effects, and the corrections to conductivity of these highly disordered semiconductors may affect their potentials as radiation detectors.

The second problem has to do with the leakage currents, that occur due to the limitation in the degree of purity of the semiconductor materials. It is determined that the number of electron-hole pairs that can be produced by 5MeV $\alpha$-particles passing through a semiconductor (Si or GaAs) of $9nm^2$ in cross-sectional area and 9nm in thickness is about 2000. Where, the mean energy to produce an electron-hole pair is taken as 5eV; and following Northcliffe and Schilling (1970) the mass stopping power of the semiconductor to 5MeV $\alpha$-particles is taken as $627.2 MeV cm^2 gm^{-1}$ and its density as $2.33 gm/cm^3$. This therefore generate a current of only $4.21.10^{-17} A$.

On the otherhand, the leakage current is given by

$$\frac{\text{Voltage applied}}{\text{Resistivity . cross-sectional area}}$$

It is reasonable to assume a moderate voltage of 50V. The resistivity of the submicron devices are not available to the author, however it is known that the resistivity of the highly purified Si is about 50,000$\Omega$cm. For the present purpose of making estimates the same value can be assumed. Based on these values and the previously specified dimension of the sample the leakage current is estimated to be about $10^{-10} A$.

It is probable that the resistivity of the submicron semiconductors may be two or three orders of magnitude less than the value assumed above, but even if exceptionally high purity semiconductors are available, the leakage currents are still many orders of magnitude

greater than the radiation induced current. Leakage may also be increased due to contamination in the handling of the wires. Thus, unless the wires are provided with rectifying contacts rather than with ohmic contacts, as presently produced, leakage currents will inhibit the detection of ionising radiations. Similar problems were previously encountered in the use "crystal counters" such as bulk diamond detectors (Fowler, 1966).

For semiconductor detectors operating as rectifying diodes, the potential at any point is given by the Poisson's equation (Dearnaley and Northrop, 1963).

$$V^2\phi = -\rho^*/\varepsilon_d$$

where $\varepsilon_d$ and $\rho^*$ are, respectively, the dielectric constant and the density of the material. At equilibrium, the potential difference across the junction, the "contact potential" is about 1Volt. The accompanied electric field, -grad$\phi$, extends over the width of the depletion region. The latter, which represents the effective sensitive region of the detector, has a significantly reduced concentration of electrons and holes and therefore higher resistivity. It is the electrons and holes created within this region by the radiation and driven by the the electric field that forms the signal. The thickness, $d_d$ of the depletion region is given by (Dearnaley and Northrop, 1963).

$$d_d = \left[\frac{2\varepsilon_d V}{eN}\right]^{1/2} = \left[2\varepsilon_d V \mu \rho^*\right]^{1/2} \qquad 4.5.2$$

Where N is the dopant (donor or acceptor) concentration on the side of the junction that has lower dopant level, but for surface barrier detectors it refers to the bulk crystal; $\rho^*$ and $\mu$ are the resistivity of the doped material and the mobility of the majority carriers respectively. In conventional detectors it is usually required to have a high depletion depth but small detector capacitance ($C = \varepsilon/d$). Relatively high electric fields are therefore applied. For detectors in unified dosimetry however the priority is to have a low depletion depth (only pn junctions are therefore relevant) and low capacitance; but reverse bias has also to be applied to the junction for minimising the noise. The solution therefore is either to use materials of low dielectric constant or low resistivity.

The use of conventional rectifying diodes, operated at low voltages, will inadvertently be limited by low-level noise discrimination and tissue equivalence (Orlic, 1990). As for unified dosimetry, it can be envisaged that the former can be overcome by careful selection of the semiconductor and manipulation of its fabrication and operation conditions (as outlined in the preceding paragraph). However, the problem of tissue equivalence due to

the high atomic numbers of conventional semiconductors remains and novel materials have to be used. Detectors made with armophours semiconductors are not a panacea. It is shown (Equer and Karar, 1989) that they provide no significant advantage over crystalline semiconductors, although they can be laid down in nanometer layers.

However, organic semiconductors are potentially good. They have most of the characteristics of semiconductors (Kryszewski, 1980) including conductivity in the range $10^{-12}$ to $10^{-14}\Omega^{-1}cm^{-1}$, negative temperature coefficient of resistivity, dielectric behaviour at low temperatures, nonohmic and often rectifying contact with other substances, e.g. metals, high thermoelectric power, photoconductivity and resistivity that depends on the impurities introduced. Most organic semiconducting materials have conjugated systems of double bonds. Their behaviour can therefore be described by 'band' theory. Examples of such materials are dyes, anthracene, benzene, napthalene, various aromatic cyclic compounds and their derivatives containing metal free atoms and containing coordination bounded metals.

There are however some slight differences (Kao and Hwang, 1981). It is established that although impurities influence the conductivity of organic semiconductors, the conductivity is determined by the structure of the host. Organic semiconductors may be monomers or polymers. Polymers with conjugated bonds have only half of their allowed states occupied, therefore show metallic conduction. However polymers with all allowed energy levels filled, show semiconductivity. In both types conductivity increases with the length of the polymer.

The advantage of exploring the use of organic semiconductors for instrumentation in unified dosimetry is the low atomic weights of their constituents. Tissue equivalence may thus be approximated. Being solid and semiconducting, all the requirements enumerated in section 3.1.2 can be satisfied. In addition their high hydrogen content indicates good prospects for neutron detection. It can be envisaged that the Langmiur-Blodgett technique of making ultra thin films on solid substrates (Roberts et al, 1981) can be used in making the host layer, which is then doped with suitable ionic material. Both can be carried out under vacuum conditions and the detector's covered at the front and back with a thin film of metal. Thus leakage due to impurities can also be minimised.

## 3.5. DETECTORS BASED ON SUPERCONDUCTIVITY.

### 3.5.1. PRINCIPLE.

Radiation passing through a superconductor deposits its energy through the production of excess quasiparticles by electromagnetic interaction. The quasiparticles generate phonons through electron-phonon interaction or they break Cooper pairs by the direct electron-electron interaction. Thus radiation interaction, like any other means of supplying energy to the system, results in a nonequilibrium distribution of quasiparticles in the superconducting electrode. The "charge" producing mechanism in a superconductor is the breaking up of the Cooper pairs, which are the bound states of the conducting electrons responsible for the superconducting effect. The main feature of superconductors in radiation detection is the very low energy gap at the Fermi surface. This reduces the energy required for charge carrier formation and improves the energy resolution. Barone et al (1985a) reported that for Nb-$Nb_xO_y$-Nb junctions irradiated with natural alpha particles the value is about 20meV. Kurakado and Mazaki (1981) estimated the signal-to-noise ratio for the exposure of Sn-SnO-Sn junctions to 5MeV alpha particles, to be about 3600.

### 3.5.2. TUNNEL JUNCTIONS AS RADIATION DETECTORS.

The early detectors were mainly evaporated thin films of a few micrometers in widths and nanometers in thickness (Crittenden and Spiel, 1971). Their operation was attributed to local heating and a transition to the normal state by the impinging radiation. This transition spreads out across the transverse section of the film, so that a voltage pulse arises at the end of the strip. Thus a switching action due to the transition from superconducting to normal state, corresponding to the absence and presence of radiation of sufficient energy, serves as a particle detector and energy threshold discriminator. The main limitation of superconducting films in radiation detection is the fact that the transition from superconducting to normal state involves a significant delay in time for the phase boundary propagation. It prolongs the dead time of the detector. The superconductive tunnel junctions (STJ) offer more concrete possibilities for both radiation detection (that is as a fast switch) and spectrometry (that is with response proportional to the energy loss).

A STJ can be either of the Giaver or Josephson type. In the former, the width of the insulator layer is about 5-10nm; DC current flows from one superconductor to the other as

a result of quantum mechanical tunnelling (figure 3.1). In the Josephson type device, the barrier thickness is reduced down to 1-2nm, and consequently, in addition to the single electron current flowing up to a maximum value (AC Josephson effect), the I-V characteristic exhibits another curve (the DC Josephson effect) due to tunnelling of Cooper pairs.

In principle either a Giaver or a Josephson type of STJ can be used. However, due to the requirements of high tunnel probability, in practice Josephson junctions are actually employed where the zero voltage current (DC Josephson supercurrent) is quenched by a suitable externally applied magnetic field (Barone, 1985b). Wood and White (1969, 1971), Kurakado and Mazaki (1980, 1981), Barone et al (1985a), and Twenrenbold et al (1984) reported investigations on the use of STJs as radiation spectrometers. Various soft electrode materials (e.g. Pb, Sn, Al) were irradiated with alpha particles and with X-rays from $^{55}Fe$.

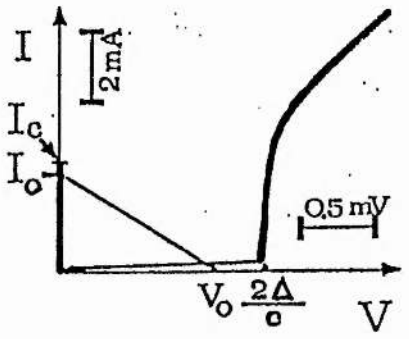


FIGURE 3.1: Current-voltage characteristics of a Josephson tunnel junction (Sn-$Sn_xO_y$-Sn). Also indicated is a load line suitable for a fast switching detector. Adapted from Barone et al (1985).

The functional basis of the investigations was explained (Barone, 1985) as follows. For a given STJ at a temperature, T and the insulating layer of which is suitably thin, there exists a well-defined relation I=I(v, t) between the direct current, I, passing from one film to the other by electron tunnelling and the voltage, V, developed across the insulating layer. At bias voltages $0 < \Delta(T)/e$, where e is the electronic charge and $\Delta(T)$ is the magnitude of the temperature dependent superconducting energy gap, this current varies with temperature

approximately as $\exp(-\Delta(T)/kT)$, k being the Boltzman constant. On irradiation of the STJ, charged particles transverse the films comprising the junction but lose a certain amount of energy while doing so. After a short relaxation time (the order of one nanosecond), this energy decays to zero in some characteristic time as the junction relaxes back to helium bath temperature. The resulting current pulse, after suitable amplification and shaping may then be analysed for information about the energy loss which produced it and the time within which it was produced using standard nuclear data acquisition electronics. Although not conclusive, these experiments give just cause for optimism on the use of STJ for energy spectroscopy.

### 3.5.3. JOSEPHSON JUNCTION AS FAST SWITCHES.

The use of the Josephson junction as an "on-off" device for radiation detection (Barone and DeStefano, 1982) takes advantage of the extremely fast switching (few picoseconds) occurring between a zero voltage (on the DC Josephson supercurrent branch ) and the finite voltage state (on the quasi-particle branch). The operation (figure 3.1) can be explained as follows. For a junction polarised at a current $I_0$ just below the critical current $I_C$ the deposited energy produces a breaking up of Cooper pairs into quasiparticles along a roughly cylindrical region coaxial with the track of the impinging radiation. This reduction of pairs will, in turn, produce a lowering of the Josephson current down to $I_R$. If $I_R < I_0$ the device is no longer in a stable state and it has to switch to another state, that is on the finite voltage branch of the I-V characteristic.

The actual detection mechanism has to take into account the quite intricate nature of the three fluid system (Cooper pairs, quasiparticles and phonons) and the properties of the non-equilibrium superconducting state (Barone et al, 1985b). A particular feature is that since the energy of the incident radiation is large compared to either the Debye or the gap energies, the electrons excited by the radiation decay in a very fast process, relaxing their energy through electron-electron interactions and electron-phonon interactions. The first step, an extremely fast process, determines the switching action. The operation does not involve any superconducting-normal transition. Rather, the time is expected to be given by the uncertainty relation: $\Delta E.\Delta(t) > h/2\pi$, where h is the planck's constant.

Barone and DeStephano (1982) pointed out the two possible modes of operating the device, depending on the specific loading values $V_0$. The "non-latching" or "self-resetting"

mode occurs when $V_o < V_m$, where $V_m$ is a certain minimum voltage. The junction will readily switch back to the original state (the one before irradiation) as soon as the effect of the radiation is over. The "latching-mode" occurs for $V_m < V_o < \Delta/e$. In this case, after "one detection", namely after the occurrence of the switching, the junction will remain in the finite voltage state and extra operations are required to reset the junction to zero voltage state. The former is the most suitable mode of operation of the detector. Magno et al (1981, 1983) reported experimental investigations concerned with the effects of alpha particles on Josephson junctions of Nb-Si-Nb configuration. (Si at liquid helium temperatures behaves like a dielectric).

### 3.5.4. REMARKS ON SUPERCONDUCTIVE DETECTORS.

The superconductors offers the possibility of high energy resolution, extremely fast response and high detection efficiency. In addition, methods of optimising one or more of these qualities are established. Some are the following. One, the resolution of a STJ may be improved by a) decreasing the normal junction resistance by using insulators of smaller dielectric constants and energy gap, and/or by minimising the insulator thickness. Or by (b) decrease the recombination probability of phonons to the substrate and superfluid helium liquid by surrounding the junction with a phonon insulator such as a cross-linked polymer (Crittenden and Spiel, 1971). It is also observed (Wood and White, 1973) that the symmetric junction is a more promising configuration than the asymmetric ones because it has reduced noise.

The practical limit of energy resolution is, however, determined by the stochastic variations in insulator thickness across the junction overlap area. One advantage of using Josephson junctions compared to the Giavier types, observed by Barone et al (1985b), is the possibility of performing supercurrent versus applied magnetic field measurements. This represents a very efficient probe to establish "a posteriori" the degree of the barrier junction uniformity. In twin volume detectors of nanometers in size, this is certainly advantageous. Two, the mean intrinsic noise in the STJ is proportional to the square of the junction impedance (Kurakado and Mazaki, 1981). Three, the sensitivity of a STJ, of a given thickness and detection area, can be improved by using the junction at a lower temperature (Kurakado and Mazaki, 1981a). It is notable that both the current through a STJ at a fixed bias voltage $V_o$ ($k_BT/q << Vo << \Delta/q$ ) and the reciprocal of the recombination time T have approximately the same temperature dependence as the number

of thermally exited electrons at temperature T.

There are some problems which may render the use of superconductive junctions inconvenient for radiation dosimetric purposes. They have high atomic number, Al is the lightest; recycling problems; sensitivity to magnetic fields; and the low transition temperatures (Sn:3.72K, In: 3.4K). The recent development of high temperature superconductors offers a ray of optimism for the future. The theoretical considerations of Kurakado and Mazaki (1981) indicate that in order to optimise the use of the Josephson junction as an "on-off" switch a low noise amplifier with a time constant much smaller than the relaxation times of the induced signals ($10^{-6}$s) is required. Economically, this is a severe limitation. Because of the deposition techniques employed, the STJs are thermally coupled to the substrates. Hence some of the energy expended in the substrate as the impinging particle comes to rest, can diffuse back to the junction in sufficient time to contribute to broadening the spectrum. This problem may not be easily solved; recent investigations showed that the substrate may degrade the theoretical resolution obtainable from the STJ detectors.

Having two conducting layers interfaced by an insulator of 1.8nm thickness, the STJ possesses the geometrical form required of detectors for unified dosimetry. However the radiation detection is based on the induction of quasiparticles tunnelling across the barrier, with a contribution of phonons in the breaking of Cooper pairs. The low energy involved in the latter suggests that the induced signal may represent approximately the total energy deposited, including those lost to vibrational modes. This contrasts sharply with other detectors. It may however be observed that there is a possibility that quantomechanical tunnelling between the two strands of the DNA may occur. Superconductivity in biological membranes, proteins and other substances of similar physical form to the DNA is well established (Lewis, 1982). The experimental and Monte Carlo simulation results cited earlier indicate that superconductors offer a possibility of an alternative and superior system of radiation detection including the detection of the heavy recoils of neutrons interactions. But their role in dosimetry is most probably only for the future. As of present little is known of their response to radiation of different types and energy and most of the known superconductors are high Z materials.

## 3.6. OTHER SOLID STATE DETECTORS.

The so-called exoelectron emitting detectors are based essentially on the emission of trapped secondary electrons from a material after thermal or optical simulation (Ennov, 1974). Materials such as LiF, BeO, CsI, $SiO_2$, $CaSO_4$ are examples. The mean energy required to eject an exoelectron varies between 1 and 10KeV. This is due to the fact that almost half the exoelectrons are emitted instantly when the sample is irradiated. The exoelectrons themselves have low energy (about 1eV), hence have to be associated with a proportional counter or a Geiger-Muller tube. Such materials can be used to measure total doses and in interface dosimetry, but can not be suitable for accurate radiation dosimetry or unified dosimetry. The same arguments hold true for thermoluminescent and radiophotoluminescent materials.

## 3.7. REMARKS ON THE VARIOUS DETECTION SYSTEMS.

The foregoing considerations indicate that gas based detectors offer a lot of flexibility for radiation dosimetry; various parameters such the radial dose and the linear primary ionisation can be measured. Their main advantage is the ease with which the detector's thickness and type of gas used, can be varied. Uniformity can also be easily attained. For their use in counting ionisation events, the mean energy required to produce an ion pair need not be known. The state is however not ideal and there are wall effects. Geometrical problems further limit their use as two-volume detectors.

A more promising configuration among detectors in the gaseous phase is a twin-volume wall-less proportional counter. Such a detector was reported by Burlin et al (1974). The device consists of similar, cylindrical, wall-less proportional counters operated in TE gas (64.4% $CH_4$, 32.4%$CO_2$, 3.2%$N_2$). The separation and orientation of the detectors to the radiation is variable. Burlin and collaborators presented tentative data for 5μm simulated volumes, using a coincidence resolving time of 2μs, exposed to α-particles of about 3.8MeV. Their results show that the coincidence gating of the second detector with the first one, decreases the total energy detected in comparison to those of the converse gating and to those of ungated detectors. Smaller volumes can not be simulated due to the difficulties related to inter-electrode disturbances that inhibits the determination of the detector's sensitive volume.

In effect, gas based detectors can be used for single-volume operation. Their potential for twin-volume function is very low. Detectors in the liquid state require containment unlike the solids. The principle of simulation by the reduction in gas pressure is also inapplicable. Such detectors are therefore inappropriate. Thus only the semiconducting organic materials show early promise for application in the instrumentation for a unified dosimetric system.

# CHAPTER FOUR: ORGANIC SCINTILLATORS FOR UNIFIED DOSIMETRY.

The usefulness of the scintillation detector in dosimetry depends on relationship between the fundamental process of light emission in the phosphor and radiation prompted processes in the tissues, or in the DNA in particular in the case of unified dosimetry. The objective of the present chapter is to determine this relationship using published data on the response of scintillators to radiations of different types and energy. This complements the experimental evaluation reported in chapter five.

## 4.1. BASIC CONSIDERATIONS.

Although inorganic scintillators are efficient light producers, they are however somewhat slower (typical response time: microseconds) than organic scintillators and are generally harder to handle. Sodium Iodide, the most commonly employed inorganic crystal for gamma spectroscopy is hydroscopic, hence cannot be used conveniently. The organic scintillators are quite fast and are relatively easy to handle. The crystalline organics, like anathracene and stilbene are brittle and have anisotropic response to radiation which complicates measurements. Liquid scintillators are inconvenient due to the need for a container and geometry. The Scintillation fibres are made either from organic or inorganic scintillators and do not offer different properties (White, 1988).

Among the scintillators, the organic plastic phosphors have the best potential. They are easy to handle, cheap, are in condensed phase and there are no radiation damage problems. They have densies very close to those of tissues; have low atomic weight constituents. They are widely used in the spectroscopy of heavy charged particles in nuclear physics. The main feature being their fast response (ns) and the relative ease of fabricating (in the laboratory) films of a few $mg/cm^2$ , which is less than the range of weakly ionising particles. They are used as transmission detectors (TFD) which respond only to the fraction of the energy lost by the particles as it passes through the film (Goulding and

Harvey, 1975). Wide experience has been acquired from such investigations.

Aspects of the thin film detector (TFD) that have been investigated are its potential as a device for identifying particles and its time response for possible use in time-of-flight experiments. These investigations (Goulding and Harvey, 1975 and Brooks, 1979) confirm the well known nonlinearity of the light output with energy loss suggesting the inappropriateness of the TFD as a transmission detector in the dE/dX and dE technique of identifying low energy nuclear species. Since the plastics produce sufficient light output, at least to the passage of densely ionising radiation, and they can be easily made in ultra thin layers, it may helpful to explore ways (and limits) in which the plastic scintillators could be improved for application to unified dosimetry.

## 4.2. REVIEW OF EXPERIMENTAL DATA.

Birks (1964) has made an extensive review of the use of scintillators for radiation detection. The more recent developments have been reviewed by Brooks et al (1979) for organic scintillators, by Heath et al (1979) for NaI(Tl) detectors and by Harvey and Hill (1979) for neutron detection. The empirical data summarised here is restricted to that from laboratories which have published sufficiently extensive data. By so doing, problems such as differences in the scintillator concentration, light collection etc can be minimised.

### 4.2.1. RESPONSE OF THICK ORGANIC SCINTILLATORS.

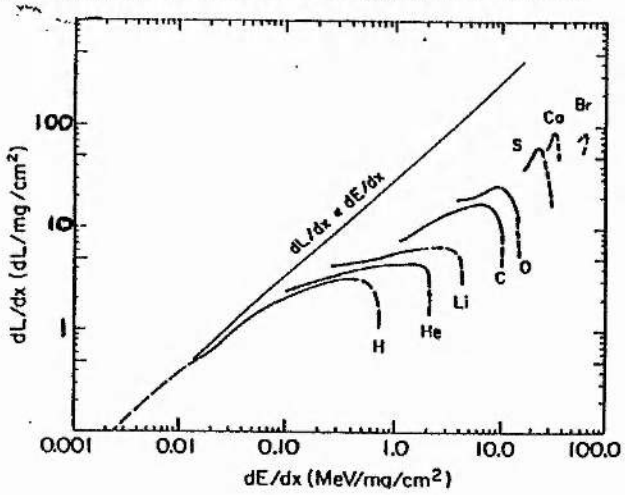


FIGURE 4.1: Specific fluorescence versus calculated specific energy loss in NE102. Adopted from Becchetti et al (1976).

The response of plastic scintillators to a variety of ions (Z=1-35) fully stopped in the phosphors was reported by Becchetti et al (1976). They exposed plastic scintillators to the ions of $E \leq 170$MeV at near normal-incidence, they observed the following.

(a) The intrinsic light output of three scintillators (NE102, NE111, NE110) is basically the same for given conditions of PM, light collection etc.

(b) At the same energy, lighter ions are more efficient light producers than heavy ion, figures 4.1 and 4.2. The nonlinearity of the light output with energy is similar for ions with energy less than 15MeV/amu, and is given by $L \alpha E^n$, where n is 1.6 independent of Z of the ions.

(c) The response is generally nonlinear with energy, but becomes linear for $E/A >>$ 6MeV/amu.

(d) The differential efficiency of fluorescence (dL/dX) is initially linearly related to dE/dX, but with increase in stopping power it saturates. (In the case of NaI(Tl), this occurs at about 7-8MeV per nucleon for the different ions (Newman and Steigert, 1960) there after it decreases, see figure 4.4). For ions of the same dE/dx, dL/dX increases with Z but is relatively independent of mass.

(e) The light output is slightly less (about 5%) for odd Z ions compared to that for adjacent even-Z ions.

(f) dL/dE is generally not constant except at high energies ( > 40MeV); its pattern of variation with energy is similar for the different ions, but its magnitude depends on Z and it decreases with increasing Z. This implies that the number of photoelectrons detected is proportional to the light output or, conversely, the photo-conversion efficiency depends on the ion energy and not the dE/dx and suggests a complicated mechanism of photon production in the scintillator.

(g) The pulse height resolution is given by $0.8L^{-1/2}$.

(h) The light output is best described as a function of the ion range, R, in the scintillator, with a strong dependence on Z but little dependence on isotopic mass; thus

$$L \alpha Z^{1.22} [R - 0.04Z]$$

The curve L against R shows curvature and non-zero intercept which indicates, according to Becchetti et al (1976) an effective light producing portion of the range $R_L$ which is less than the total range. The dead layer may be due to surface oxidation of the films. Its thickness increases with the increase in the ions charge, but is independent of its energy.

The response of organic scintillators to electrons is quite linear with particle energy above 100keV. There is however a strong dependence on the mode of irradiation: external or internal. This is due to the back scattering of electrons, surface effects and surface escape of photons (Brannen and Olde, 1962). Smith et al (1968) compared the response of different scintillators (anthracene, stilbene, NE123, NE230 and Pilot B) to external electrons of energies in the range (0.16-0.99MeV) with that to protons (0.24-15.0MeV). They reported that the response of the different scintillators to ionising particles of Z>1 is nonlinear, but the response to electrons is linear. They also observed that, at the same energy, the light output of the electrons is greater than those of protons. The investigators also noted that although there were large differences (a factor of three) in light output of the different scintillators, a similar trend in the energy dependence of the ratio of the light output of protons (or deutrons) to the response of electrons is observed. The ratio is constant at the same energy, but varied with energy. The ratio is about 0.1 for particles with energy 0.20-1.0MeV, increased to between 1.0 and 4.0MEV but levelled off to 0.5 in the energy range 10-15MeV.

---

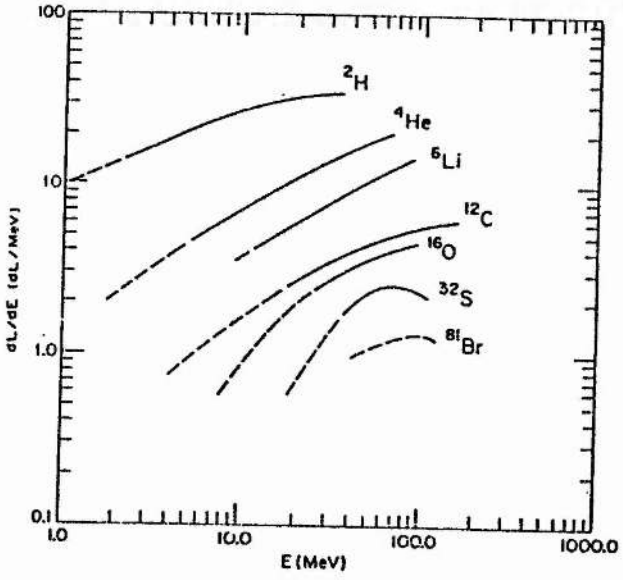


FIGURE 4.2: Scintillation efficiency versus energy. The light output are in a scale that the light output due ThC' exposure is arbitrary taken as 30. Adopted from Becchetti et al (1976).

---

## 4.2.2. RESPONSE OF THIN PLASTIC FILMS.

Unlike conventional sized phosphors, thin films have thickness less than the range of the ions. Thus, a more realistic measurement of dL/dx can be obtained. By their forms, they also have a greater surface-to-volume ratio, hence surface effects may play a more significant role than in the thicker films. Given that the light production is due mainly to delta-rays, as is assumed in most scintillation theories, it can be expected that their escape will reduce the light output. For ultrathin films the role of the delta-rays is expected to be simple. Unfortunately, while there is abundance of data on both thick and thin films, measurements of their absolute light output is restricted only to the conventional size phosphors exposed to electrons and photons. This hinders direct comparison.

It was noted however that although the saturation of luminescence in the TFD was observed (as in the conventional size plastic scintillator) the onset of saturation does not occur, consistently, at about 6-7MeV per nucleon as was observed with the conventional sized phosphors (Muga and Griffith, 1974; Kohl, 1975). Poorer resolution which improves with thickness, and in the regions that the different data overlaps, lower light conversion efficiency than those of the thick films, were reported (Becchetti et al, 1976), as expected. But otherwise, the TFD shows similar response characteristics, in general terms.

---

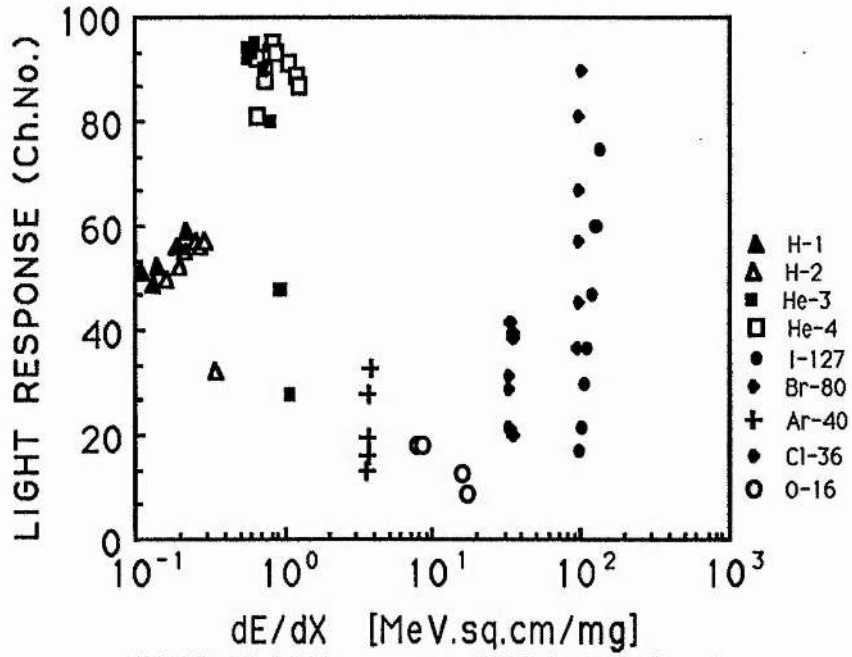


FIGURE 4.3: Light response of TFD to transiting ions plotted against the specific energy loss of the ions. Redrawn from Muga and Griffith (1973a and b).

Most of the investigations are concerned with the TFD response to fission fragments, e.g. from $^{252}Cf$, (Brooks, 1979). Batsch and Moszynski (1975B) investigated their timing properties. Their pulse height resolution was investigated by Batsch and Moszynski (1975) and by Muga and Griffith (1973a). Energy loss and energy loss straggling were investigated by Geissel et at (1977). Their response to different ions of different energies was investigated by Kohl (1975), Voltz et al (1966) and by Muga and collaborators (1973).

Muga and collaborators investigated the response of TFD (mainly NE102, but also NE111) to accelerated ions (Z=1-53) of different energies. Different laminations of the films were used to determine the effect of thickness on their specific luminescence. Their experimental set up is similar to that described in section 5.5, except that two photomultiplier tubes were used of instead of one. They observed (figure 4.3) features similar to those cited as (a) to (h) in section 4.2.1.

Muga and Griffith (1974) inferred: (1) that their results indicated the inadequacy of the parameter dE/dx for characterising the specific luminescence response; (2) that parameters related to ion charge and velocity may be better. They showed that the effective ion charge plotted against the energy can be superimposed on the curve of dL/dx versus E/m and inferred that the dependence of light production on dE/dx was a consequence of the decrease in effective charge of the transiting ion as it picked up electrons in slowing down.

## 4.3. RESPONSE OF INORGANIC SCINTILLATORS.

Newman and Steigert (1960) provided data on the response of NaI(Tl) to accelerated ions ($4 \leq Z \leq 20$) having energies from approximately 1.0 to 10.0MeV per nucleon. Figure 4.4 showed some of their results. The investigators reportedly observed features basically similar to those cited as (b) to (g) in the section 4.2.1. The resemblance in the relationship between the light output and ion energy in NaI(Tl) and plastic scintillators for ions of $5 \leq Z \leq 10$ was also noted by Becchetti et al (1976), at least where the energies overlap. In particular, the Becchetti et al (1976) observed that the expression

$$L = k(Z).R.[1 - \Delta(z)]$$

where R is the ion range in mg/cm2, k(z) is a Z-dependent coefficient and $\Delta(z)$ depends mainly on z but not on energy, fited both organic and inorganic scintillators by suitable adjustment of the constants.

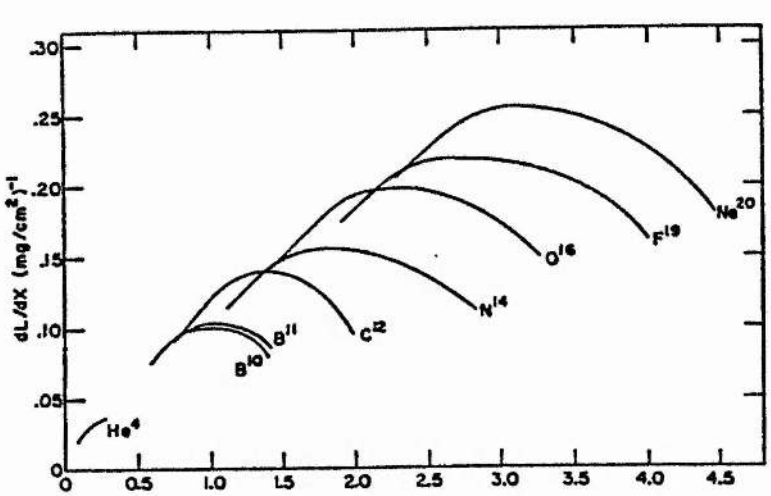


FIGURE 4.4: The specific fluorescence plotted as a function of the specific energy loss for various heavy ions in NaI. Adopted from Newman and Steigert (1960).

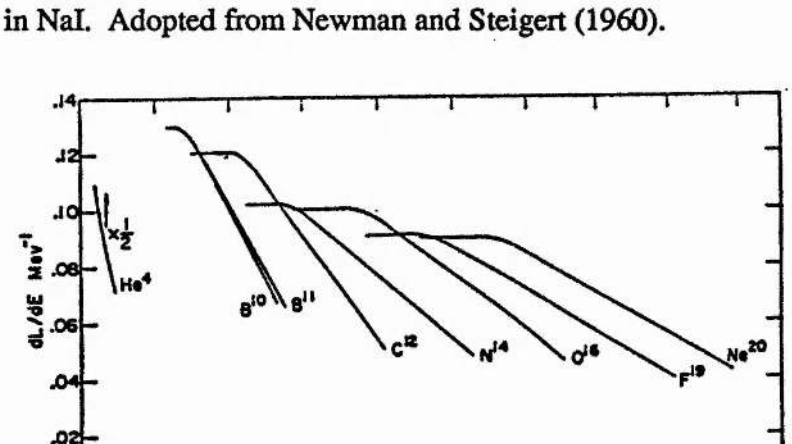


FIGURE 4.5: The conversion efficiency plotted as a function of the specific energy loss for various heavy ions in NaI. Adopted from Newman and Steigert (1960).

---

The response of NaI(Tl) to electrons having energies in the range 7-1000KeV was reported by Prescott and Narayan (1969). Their data indicate that the dL/dE increase with the energy of the electron in the range 1-20keV, thereafter it decrease with the increase in energy. However, a compilation of different data sets by Birks (1964) indicated that

saturation occurs in the range 30-70keV, in the different experiments.

The foregoing suggests that although the physical mechanisms of light production in crystalline inorganic scintillators differs from that for the organic ones, their response characteristics are basically the same. Scintillation theories developed for one are applicable to the other. In the following analysis the organics and NaI(Tl) are treated in a similar manner.

## 4.4. SPECIFIC LUMINESCENCE AND LINEAR PRIMARY IONISATION.

The preceding summary of empirical data suggests that light production in phosphors is not determined by the stopping power of the charged particles but by their ranges or by their charge and velocity. With the impetus of the success obtained in the correlation between biological damage and $I_i$ in chapter two, we seek to establish whether the light response of scintillators can also be characterised by the same parameter.

The underlying reasons for this approach is as follows. In scintillation detectors a saturation of luminescent response (see section 4.2) at higher dE/dX, whose onset depends on the ion type (at least on considerations based on the specific energy loss of the ion) was observed. An analogous effect is the well known relationship between RBE and LET (Chapter one). It was shown in Chapter two that by expressing $\sigma_e$ as a function of $I_i$, the onset of saturation was found to occur at the same value of 0.55 per nm for different radiation types. If the same can be achieved with the scintillation detectors, then knowledge of the point of the onset of saturation will enable the determination of the characteristic distance of the scintillators, which in turn, allows the following. First, the properties of the scintillator, the solute and or wave shifter concentration that determines the characteristic distance can be adjusted such that a characteristic distance of 1.8nm is obtained. Alternatively, the response can be scaled such that it corresponds to a scintillator with a characteristic distance of 1.8nm.

In analogy to the treatment carried out in chapter two correlation between dL/dx and $I_i$ will be sought; dL/dx being proportional to the cross section for light emission. The specific fluorescence (also referred to as the specific luminescence) is deduced from the scintillation efficiency and stopping power as

$$dL/dx = (dL/dE) \,.\, (dE/dx)$$

The early scintillation theories (e.g. Birks, 1964) assumed that dL/dx was a simple linear function of dE/dx, but as may be clear from the preceding disscussion this was observed only for low dE/dx particles. We expect the results to provide an alternative qualification of the role of δ-rays. We also seek to determine, if possible, features that can be manipulated and enhance the light output.

## 4.4.1. INPUT DATA AND CALCULATION.

The $I_i$ of the charged particles in the pertinent absorbers was calculated as explained in chapter two, but with due consideration of the absorber composition. Given in Table 4.1 are the physical data for the absorbers. The values of the ionisation potential of the phosphors were obtained from ICRU-37 (1984). The mean energy required to produce an ion pair was taken as 10eV and 20eV for the NE102 and NaI(Tl) respectively. The threshold energy for δ-ray production, and the mean excitation potential were taken to be 30eV. The gap energy of NaI is 5.8eV. By the empirical rule that the mean energy required to produce an electron-hole pair is about three times the band gap energy, 18eV would have been a better choice. The overestimation should not however affect the overall pattern of the results.

Table 4.1. The physical characteristics of NE102A and NaI(Tl) scintillators

| Parameter | NE102A | NaI(Tl) |
|---|---|---|
| Mean Ionisation potential (eV) | 64.68 | 452.009 |
| Mean (Z/A ) | 3.65 | 0.4270 |
| Density (gm/cm$^2$) | 1.032 | 3.667 |
| Molecular weight (dalton) | 118.178 | 149.89 |
| Molecular density (*10$^{20}$mol/gm) | 0.5096 | 0.04018 |
| Constituent number of atoms/molecule | H: 10; C:9 | Na: 1; I:1 |
| Constituent fractional weights | H: 0.0853; C: 9147 | Na: 0.1534; I: 0.8466 |
| Constituent atomic number | H: 1; C: 6 | Na: 11; I: 53 |
| Constituent atomic weight | H: 1.0079 C: 12.0110 | Na: 22.9898 I: 126.9045 |
| Constituent mean excitation potential | H: 19.200 C: 81.000 | Na: 168.370 I: 554.830 |

4.4.2. RESULTS .

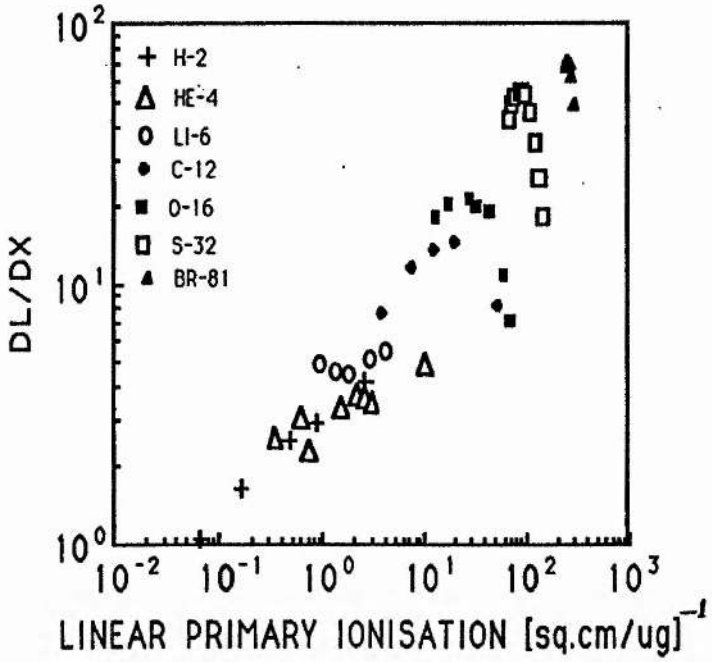


FIGURE 4.6 Specific luminescence plotted against the linear primary ionisation for ions stopped in NE102A scintillator.

Plotted in figure 4.6 is the relationship between the calculated specific luminescence and the $I_i$ of the fast charged particles of different energy in conventional sized plastic scintillator (NE102A). The original data (the same as that in figures 4.1 and 4.2) were obtained from Becchetti et al (1976). The absolute light was not measured, but was calibrated relative to the light output induced by ThC' α–particles-arbitrary assigned a value of 30. There is a clear dependence of dL/dx on the ion type. For a given ion type the specific luminescence increases with the increase in the $I_i$ of the charged particle, attains a peak value then decreases. In the case of the lighter ions ($^2$H, $^4$He, $^6$Li) and the heavier ions ($^{81}$Br, $^{32}$S, and $^{16}$O) the respective final decrease and initial increase is not evident.

The corresponding plot for ions passing through a thin film of the scintillator NE102A, originally reported by Muga and Griffith (1973a and 1974) is given figure 4.7. The ordinate values are actually the peak's channel of the pertinent scintillation spectra recorded in the multichannel analyser. The spectra were not calibrated. Since the films are much

thinner than the ranges of the charged particles, it can be taken as proportional to the dL/dx. The data for the lighter ions ($^1H$, $^2H$, $^3He$ and $^4He$) refer to films that are about 0.65mg/cm$^2$ thick. The data for the other ions refers to films that are about 1mg/cm$^2$ thick. The general trend is similar to that of the conventional size detector (figure 4.6). The initial increase in dL/dx for ions heavier than oxygen is not evident. They are saturated and their specific fluorescence decreases slowly with the increase in the $I_i$ of the charged particles.

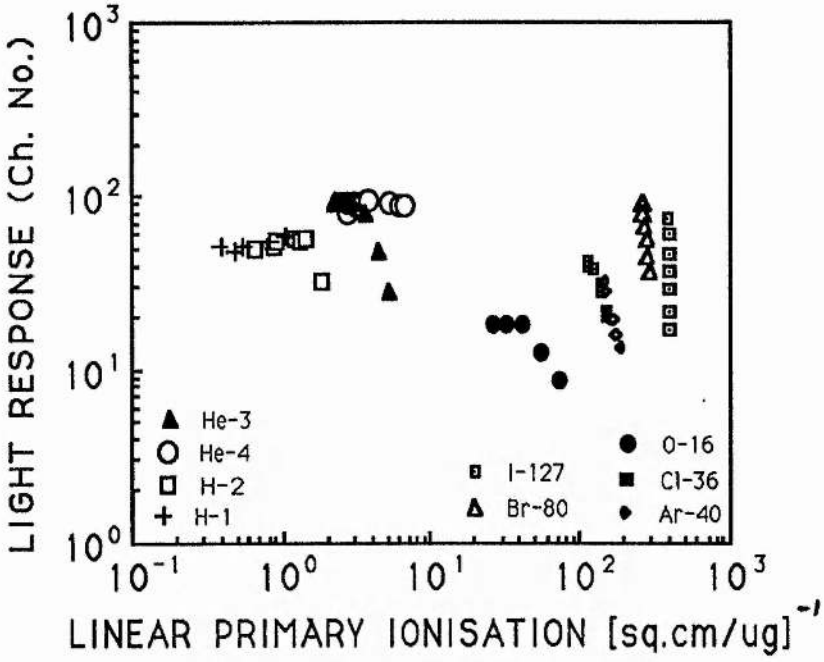


FIGURE 4.7: Light response of TFD to transversing ions is plotted against the linear primary ionisation of the ions.

A similar plot for conventional size NaI(Tl) is provided in figure 4.8 for the treatment of fast ions of different energies. The heavy ion data were taken from the original investigations by Newman and Steigert (1960).

In all the plots there appears to be some form of ion dependent relationship between the two parameters. The dL/dX initially increases with $I_i$ until saturation parameter due to ionisation quenching, is attained. Thereafter it decreases. The onset of saturation varies with the ion type and it appears that the value of the $I_i$ at which it becomes evident increases with the mass (or charge) of the ion. The trends are similar in both the organic and inorganic phosphors, and is generally similar to the relationship between dL/dX and dE/dX shown in figure 4.1 to 4.4.

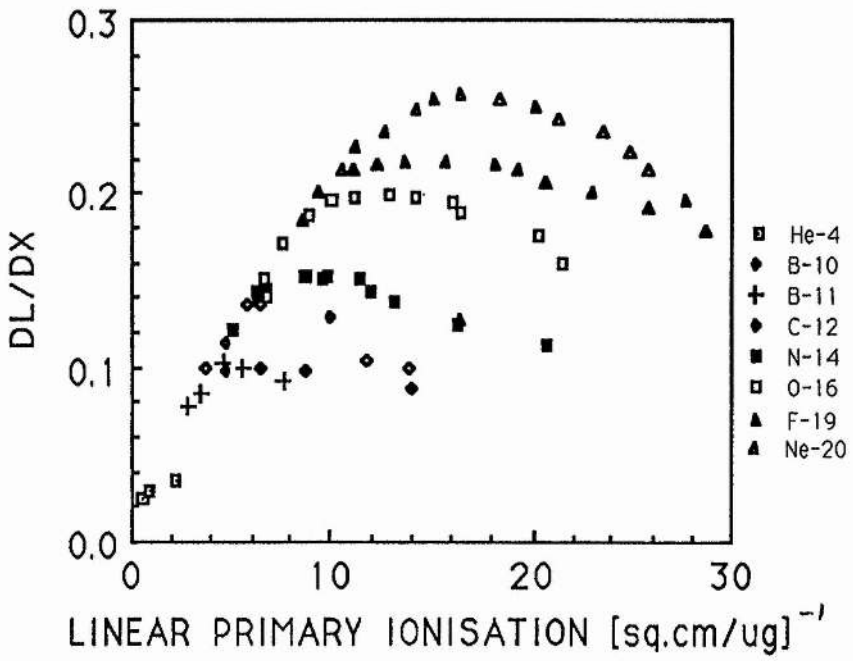


FIGURE 4.8: Specific fluoresence and linear primary ionisation of fast ions stopped in NaI(Tl).

## 4.5. DISCUSSIONS

These results show that although some form of correlation can be obtained between the $I_i$ and the dL/dX, universality in the value of the radiation's $\lambda$ at which the onset of light response saturation occurs is not obtained. This contrasts with the results obtained from the biological damage, and is explainable as follows.

### 4.5.1. DIFFERENCE IN THE DAMAGE PROCESSES.

In organic phosphors the production of useful photons arises mainly from the $S_{10}$-$S_{0x}$ transitions in $\pi$-electronic energy levels of the scintillator; it accounts for 90% of the prompt scintillation component (the fluorescent part). The $S_{10}$ states are populated from the instantaneous deexcitation of higher lying energy states, excited by the ionising radiation. There are however other channels that compete with the population of the $S_{10}$ state. These alternative channels (Brooks, 1979) are $\pi$-electron ionisation, $\sigma$-electron ionisation and $\pi$-electron excitations.

Ionised $\pi$-electrons recombine into either excited triplet or singlet states. The resultant singlet states contribute little (at most 10%) to the main scintillation component. Recombination into the triplet state is the dominant (80-90%) process (Brooks, 1979). This process, termed intersystem crossing, is probably the main channel of populating triplet states (Brooks, 1979). Higher lying triplet states decay nonradiatively, rapidly and efficiently to the $T_1$ states. The decay from $T_{1x}$ to $S_{0x}$ is however spin forbidden. The $T_{1x}$ state decays by triplet annihilation process:

$$T_1 + T_1 \dashrightarrow S_1 + S_0 + \text{phonons} \qquad 4.1$$

The light emitted in this transition $T_{1X} \rightarrow S_{0X}$ is delayed by the diffusion process involved in the intersystem crossing and has longer wavelength than the main scintillation component. This slower and weaker emission (termed phosphorescence), does not play a significant role in scintillation detectors, for the clipping time of amplifiers is usually shorter, except in pulse shape discrimination. The $S_{1X}$ states produced via the triplet annihilation generate, on decay to $S_{0x}$, photons having the same wavelength as those of fluorescence, but the decay is different: it is nonexponential. Its intensity and rate are respectively proportional to the concentration of the $T_1$ states and the rate of the annihilation reaction. This emission corresponds to the delayed fluorescence in luminescent materials and does not play a significant role in scintillation spectra recorded under normal conditions.

Thus light production depends on the excitation of the singlet state energy levels, rather than on the total energy deposited. The ionisation of both the $\sigma$– and the $\pi$–orbitals do not lead to useful photon production. Thus an increase in the mean energy deposition per charged particle interaction will not necessarily lead to photon emission. Rather it increases the occurrences of the processes that compete with the population of the $S_{10}$ state, and therefore there is a decrease in the efficiency of conversion of the radiation energy to light.

Electrons deposit less energy per interaction than ions of the same energy, and are therefore more efficient light producers (section 4.3). The maximum energy deposited per interaction by an ion is proportional to the ion's energy and mass. At the same energy a heavy ion deposits more energy per interaction than both a lighter ion and an electron. Much of this will be expended in $\delta$-ray production, but the accompanied ionisation quenching into channels that competes with the population of $S_{10}$ states renders heavy ion

($Z \geq 6$) less efficient light producers than a lighter ion ($Z<6$), and light ion in turn less efficient than an electron of the same energy. It can therefore be expected that with ionising radiation of low dE/dx and small δ-ray yields both the ions track core and the penumbra formed by the δ-rays plays a role in photon production (Birks, 1964). However with the increase in dE/dx of the ions the role of the track core decreases.

4.5.2: THE ROLE OF DELTA-RAYS.

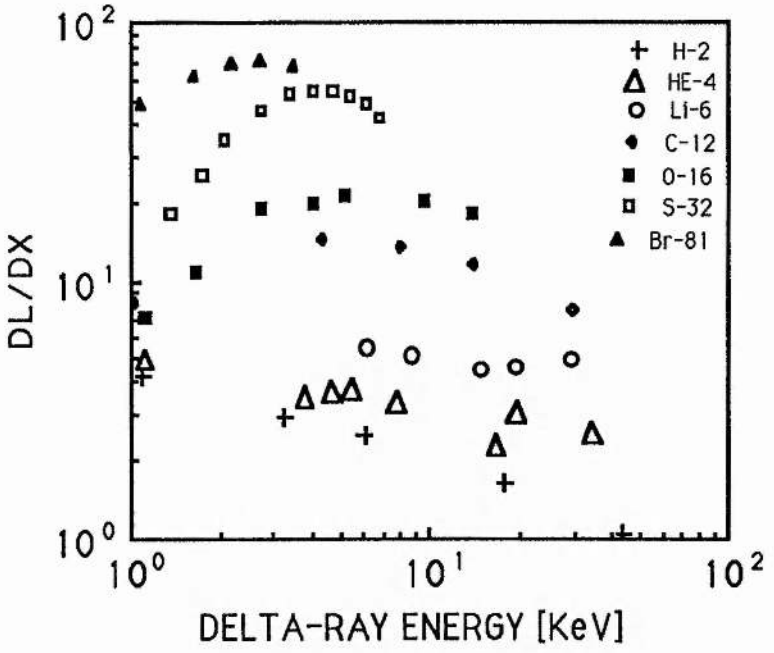


FIGURE 4. 9: The specific luminescence plotted against the delta-ray maximum energy for ions stooped in NE102A.

Plotted in figures 4.9, 4.10 and 4.11, and 4.12 is the relationship between specific luminescence and the maximum energy of the δ-rays in the respective cases of ions stopped in NE102A scintillator, heavy ions passing through films of NE102A, light ions passing through films of NE102A and ions stopped in NaI(Tl). The same data as in the preceding subsection are used. In each, there appears to be an initial increase of dL/dx with the energy of the δ-rays, then at higher values of kinetic energies of the latter the light production decreases. The extent to which the different increases and decreases are manifested depends on the ion type in the different scintillators; in the case of the TFD (figure 4.10 and 4.11) the initial shape of dL/dx is very steep for the very heavy ions (Br, Ar, I and Cl). Thus, unlike biological detectors (Chapter two), in all cases, the specific

fluorescence is related to the range or energy of the δ-rays.

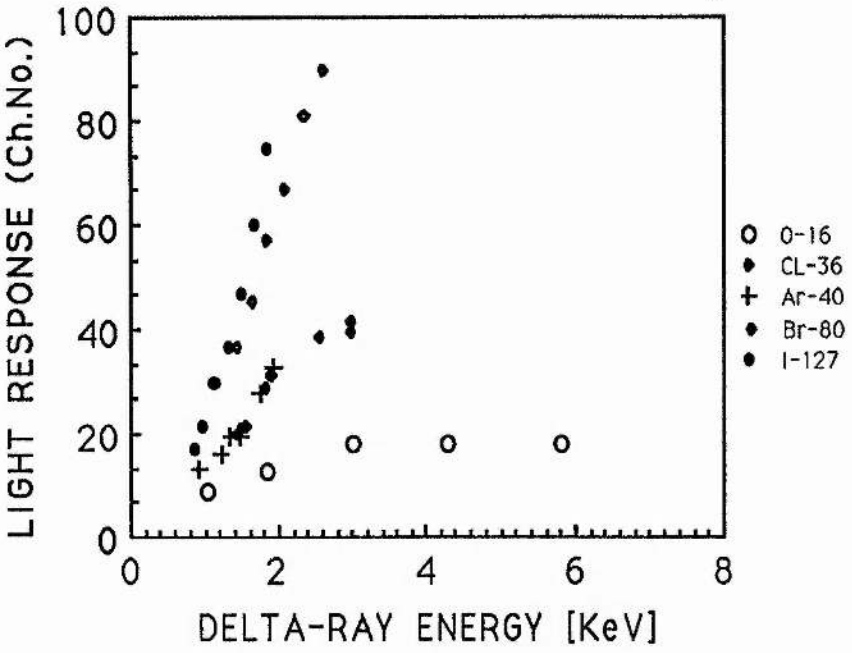


FIGURE 4.10 : Light response and energy of the delta-rays for heavy ions transversing the TFD of NE102

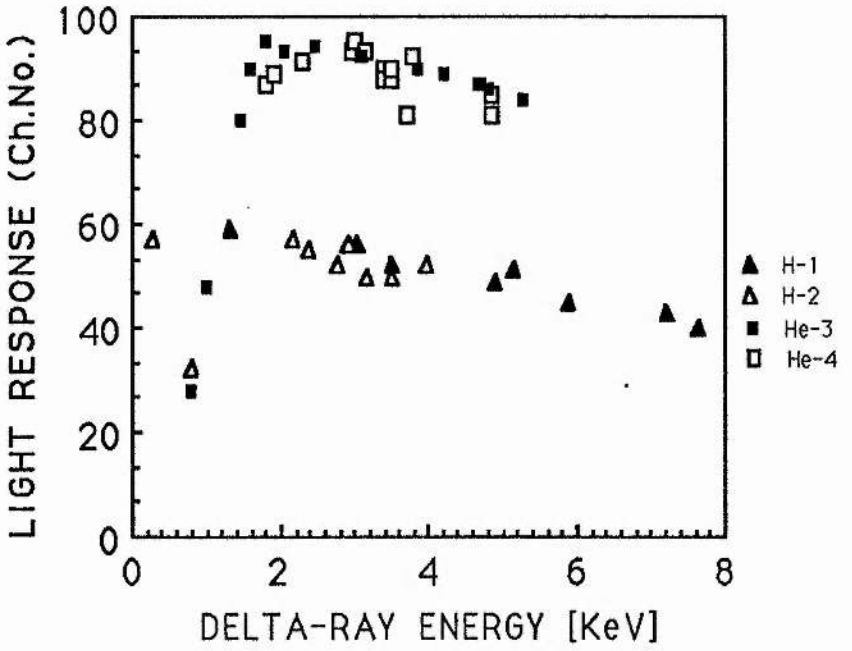


FIGURE 4.11 : Light response and energy of the delta-rays for light ions transversing the TFD of NE102

The observed dependence of light response on an ion's charge and velocity (see figure 4.13) or its range (section 4.2) is due to the fact that the δ-ray extension and yield per unit path length are, respectively, proportional to the ion's velocity and $Z^{*2}/\beta^2$. Thus in this detector, the effect cross section is determined predominantly by the δ-ray response.

This is consistent with the track structure theory of Katz and collaborators (Katz et al, 1972). Those investigators showed that their theory can predict the specific luminescence of inorganic (Katz and Kobetech, 1968) and mineral based liquid scintillators (Katz et al, 1972); the inactivation effect cross of biological cells (Butts and Katz, 1967) and various other detectors. They proposed the parameter $Z^{*2}/\beta^2$ for the specification of radiation quality. We have therefore compared and contrasted the parameters $Z^{*2}/\beta^2$ with $I_i$ in terms of their ability to characterise radiation damage in the cell and in the scintillating phosphors as follows.

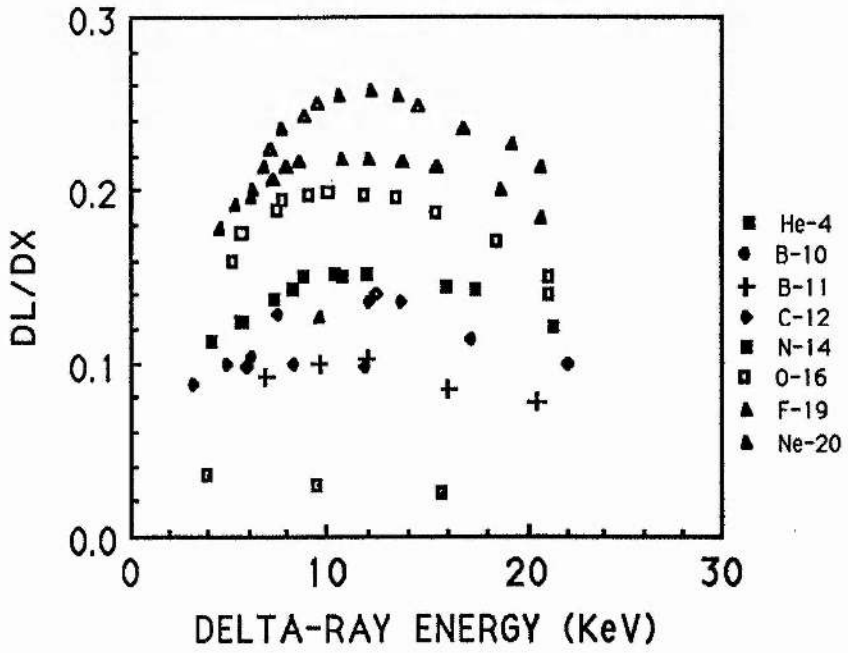


FIGURE 4.12: The specific luminescence of ions stopped in NaI(Tl) scintillator represented as function of the ion's delta ray energy

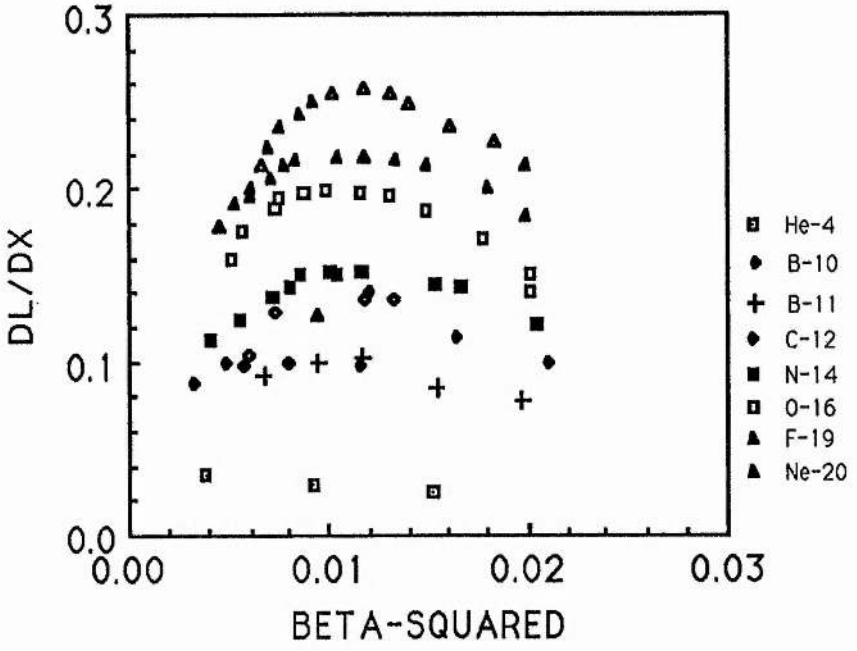


FIGURE 4.13 : The relationship between specific luminescence and the yield of delta-rays in NaI(Tl).

## 4.5.3 : $Z^{*2}/\beta^2$ AND LINEAR PRIMARY IONISATION

In chapter two it was shown that there is universality in the value of the radiation mean free path at which optimal damage is induced, independently of the ion type. It consistently, occurs when the mean free path of the charged particles inducing the damage is about 1.8nm. The observation was attributed to the need for interaction between two single strand breaks for the formation of a double strand break. The biological detector's sensitivity (the effect cross section for biological damage) is therefore determined by the matching of the mean free path of the pertinent charged particles ($\lambda$) with the mean chord length of the DNA ($\lambda_0$ = 1.8nm). The latter defines the detector's sensitive volume and is constant independent of the radiation type.

In the case of the scintillator detector, each energy deposition event that leads to the population of the $S_{10}$ states may lead to photon emission; interaction between the excited states is not required. The existence of sensitive volumes in the scintillation detectors arise from quite different circumstances, as explained in the following.

## 4.5.4. CHARACTERISTIC DISTANCES IN PLASTIC SCINTILLATORS.

Most practical scintillators are not unitary systems. NE102A and NaI(Tl) are binary and ternary systems respectively. The fractional weight of Tl in the alkali halide is usually 0.01%, and the composition of NE102A is given Table 4.2. The scintillation emission of those scintillators arise from energy transitions in the activator or solute(s). The latter are introduced because it has more favourable energy levels for light emission, and are usually only a small fraction by weight of the phosphors. Most of the energy of the incoming radiation is therefore deposited initially in the bulk host. Energy transfer from the host to the impurity or solute, which are effectively the luminescent centres, has to take place. The efficiency of the transfer of the energy determines the usefulness of the scintillator. The transfer can be intramolecular or intermolecular; it can also be radiative or nonradiative (Brooks, 1979). Competion between energy transfer from the matrix to the luminescent centres, with the radiationless decay of excitation energy, define a characteristic distance and sensitive volume in association with a luminescent centre. The volume is therefore not fixed and varies with the concentration of the activator or solute as was deduced by Katz and Kobetiech (1967).

Table 4.2 The chemical composition of NE102A.

| | | |
|---|---|---|
| Solvent | PVT (polyvinyltoluene) | 97.00% |
| Primary solute | PT (p-terphenyl) | 3.0% |
| Secondary solute | POPOP (p-bis[2-5-phenyloxazole]benzene) | 0.05% |

Data obtained from Nuclear Enterprises (1987).

In addition, the present author observed that, since the nonradiative decay pathways increase with the ionising density of the radiation, the sensitive volume cannot be fixed even for a given solute, or activator, concentration but varies with the radiation type and energy. This will explain the dependence of the value of the ion's mean free path at which the onset of dL/dx ionisation quenching occurs on the ion type and is consistent with the mechanism of light production in the phosphor.

## 4.5.5: SCINTILLATION AND UNIFIED DOSIMETRY.

The present results show that the parameter $I_i$ can be correlated with dL/dx of organic and

inorganic phosphors, just as much as $Z^{*2}/\beta^2$ can, due to their proportionality and the simplicity of the damage mechanism. Individual energy deposition events in the isolated luminescent centres are all that is required to produce the light photons. However in detectors that require coincident energy deposition events in composite volumes, e.g. the strand segments of DNA, for the induction of damage, then the $I_i$ is the better parameter for the specification of radiation quality due to its dimensional property.

The facts that photon emission depends on the excitation of σ-electrons' singlet states and that, at the same energy electrons are more efficient light producers than heavy charged particles, cast a fundamental doubt on the usefulness of scintillators for instrumentation in the unified system of radiation dosimetry. For excitation energy deposition is less likely to break a chemical bond, and induce a single strand break, and, consequently, less relevant in effecting significant biological damage. If however it can be established that the ratio of the effect cross section for excitations and ionisations remains unvaried over a defined range of energy, then improvision can be made with the organic plastic scintillators.

Pertinent data are few (e.g. Swanson and Powell, 1963) . In gases, it is often assumed (e.g. ICRU-31, 1979) that the yields of the two are approximately equal, at least for ions with energies greater than the Bragg ionisation peak. It may be less relevant for organic scintillators in that it is only the excitations of the σ-electronic levels that lead to useful photon production; π-electrons excitations do not. The availability of such data will throw more light on ionisation quenching, aid in the development of better scintillation theories and be used to optimise the light output.

# CHAPTER FIVE:

# EXPERIMENTAL WORK

## 5.0 OBJECTIVES OF EXPERIMENTAL WORK.

The purpose of the following investigation is to evaluate, experimentally, the viability of thin film plastic scintillators as a detector system for unified dosimetry. The aspects investigated are;

1) The feasibility of making plastic films that are a few nanometers thick, uniformly thin and which have a good homogenous composition.

2) The response characteristics of thin films to radiation beams. At this stage only α–particles are used, they are taken as a 'model' for fast ions. Aspects of response characteristics specifically examined are light output, the resolution and the detection efficiency. These were investigated as a function of the thickness of the scintillator films and of the energy of the alpha particle beams.

3) The investigation was restricted to single films of plastic scintillator, and therefore corresponds to 'single strand break' detector. The results were used in evaluating the viability of realising a double strand break detector as desired in the unified system of radiation dosimetry described in chapter three.

## 5.1 THIN FILM FABRICATION

### 5.1.1. OVERVIEW AND SELECTION OF FABRICATION TECHNIQUE

Thin films are widely used in nuclear physics and chemistry research. Several fabrication techniques are therefore known. The common methods are vacuum evaporation , dissolution and evaporation, rolling, electrospraying and sputtering (Yaffe, 1962). The appropriateness of a given technique may depend on whether the material is organic, inorganic (essentially, metals) or it is one of the forms of carbon. Other criteria are the desired range of thickness and degree of uniformity, the integrity and stability of the material, its amenability to routine preparation and the relative cost of the process.

There are three general methods of making thin organic films: drain-coating and dip-coating, stretching and vacuum evaporation. Thin organic films of a few microns thickness were reportedly stretched down to fractions of a micron (Al-Ahmad, 1984). Though simple and convenient at large scale, the technique has little laboratory use due to the difficulty in controlling the quality of the films made. Vacuum evaporation is applicable only to materials that do not decompose on heating (e.g. polyethylene).

Drain coating and dip-coating involve the deposition of a film from a suitable solution. Several variations of each of the two techniques were reported (Al-Ahmad, 1984). Generally, both techniques are easy and amenable to routine laboratory work, provided that a suitable solvent can be identified. Of the two methods, the dip-coating is more convenient and wastes less material. The most commonly used solvent for plastic scintillators is a mixture of ethyl acetate and amyl acetate. The other established solvents are cyclohexanone, xylene, and toluene (Muga et al, 1972; Yaffe, 1962).

Ajitanand and Iyenger (1976) described a method in which 15mg of plastic scintillator is dissolved in $1cm^3$ of toluene. Portions of the solution are then spread directly over a carefully levelled and cleaned face of a photomultiplier tube mounted inside a vacuum chamber. After the solvent evaporated in a dust free environment, the chamber is slowly evacuated, leaving behind a clear uniform film. If desired, the film may be floated off by dipping the photomultiplier face in distilled water. Alternatively, its quality and response may be determined by exposing it to a radiation source.

The main advantage of this technique is its simplicity. That the film can be directly tested in the chamber circumvents the problems of handling and it is reported that since the films adhere to the photomultiplier face, the light collection efficiency is high. To prepare films of different thicknesses the concentration of the solution is proportionately altered. For NE111 scintillator with the cited concentration, 0.5ml of the solution spread over an area of about $20cm^2$ provides a film of $4\mu m$ thick. By this one-step technique films having thickness ranging from $2300\mu g/cm^2$ to $30\mu g/cm^2$ were reportedly prepared. The same technique was used by Brooks et al (1985), but with xylene as the solvent. They reportedly reproduced films having thickness within 10% and uniformity better than 5% over an area of $5cm^2$.

In another procedure described by Cormier et al (1974), the films were made by dropping off a drop of the scintillator solution on a distilled water surface. The solvent evaporates leaving a film floating on the water surface. The range of thicknesses reportedly made through this method is $2\mu g/cm^2$ to $25\mu g/cm^2$.

In the method described by Muga et al (1972), a few drops of the organic scintillator solution were squeezed out onto the centre of a very clean glass plate partly immersed at one end of a water pan and inclined at an angle to the water surface. Surface tension forces the droplets to spread. After a few seconds the solvent is absorbed by the water and a solid film floating on the water surface emerges. The film is picked off the water by means of a target frame. Thinner films were reportedly made by increasing the flow rate, achieved by dipping the thumb and the fore finger onto the leading edge and gently dragging the the film across the surface at a faster pace. Films having thickness of about $0.1mg/cm^2$ were reportedly prepared. Thicker films were made by laminating thin ones together.

For the purpose of the present investigation plastic scintillator films with thickness less than $5\mu m$ are required. The films are also desired to have high purity, homogeneous composition and uniform thickness better than one percent. A first hand appraisal of the different versions of the drain-coating and dip-coating techniques outlined above in satisfying these criteria was made. It was determined that the procedure reported by Ajitanand and Iyenger (1976) is not suitable. The prerequisite for a horizontally levelled surface is difficult to fulfil. Films made under inadequately levelled substrates are not uniform and unsuitable. The fabrication version reported by Cormier et al (1974) and by Muga et al (1972) have a common limitation viz reproduction of films having thicknesses within a few percent cannot be conveniently realised and the films are not uniform. For the present investigation, the method adopted for making the thin films is a slightly modified version of the procedure reported by Geissel et al (1977); it was described below.

## 5.1.2. THE MAKING OF THIN FILMS

Two types of plastic scintillator were used, NE102A and NE104. Both were supplied in the form of chips by Nuclear Enterprises, Edinburgh. The chips were kept in a dark, clean and air-tight environment. Following the recipe of Muga et al (1972), 12g of the scintillator chips was completely dissolved in 100.0ml of ethyl acetate and amyl acetate

(8.0ml) in a closed conical flask. Just before the films were made the solution was carefully stirred and gently poured out into a beaker. After the bubbles disappeared, a glass slide, typically 0.15cm by 3.7cm by 7.7cm, was gently inserted into the solution. The plate was then gently pulled out of the solution at a steady pace stabilised by an electronic device. This consisted of a motor and a gear box (supplied by Radiospares, U.K.). A schematic diagram of the experimental setup was drawn in figure 5.1.

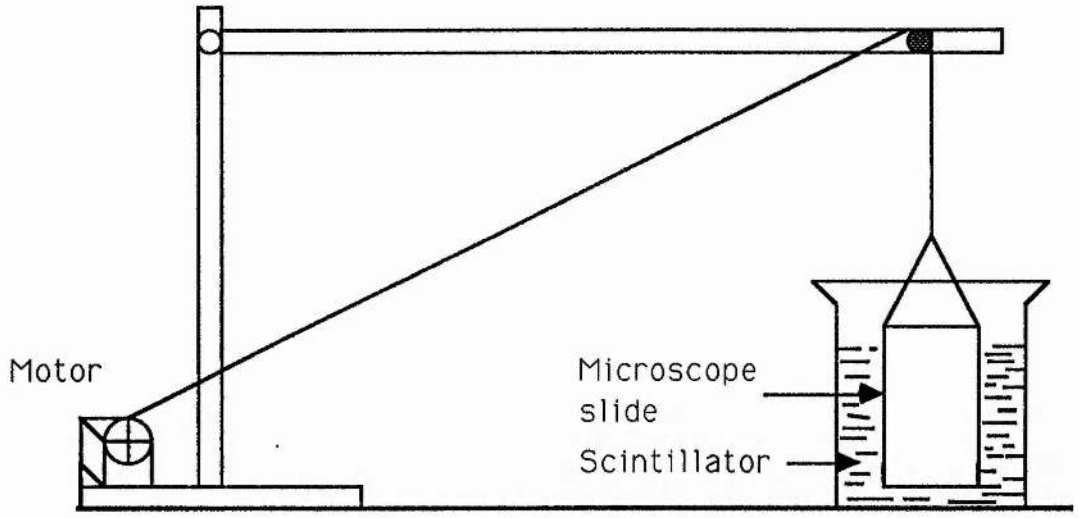


FIGURE 5.1 The dip coating method of making thin films.

The film coated slide was then dipped into a pan of distilled water, at an angle (about $30^0$) with the water surface. After a few minutes, depending on the thickness of the film and the quality of the glass substrate, the film peeled itself off the plate and floats on the water surface. It is then picked up with a solid, rectangular, target frame. The frame was slightly larger than the glass slide but has a hollow circular centre of two to three centimetre radius. The films, attached to their frames, were dried and kept in a vacuum chamber containing a drying agent, silica gel or calcium chloride. Films of different thicknesses were made by varying the rotation frequency of the gear box (see results in the next section).

## 5.1.2. RESULTS AND COMMENTS ON FILM FABRICATION.

Figure 5.2 shows the dependence of the film thickness on the speed of pulling the film-coated glass plate out of a 2% NE102 and NE104 solutions. The symbols designate films made from different solutions, but prepared under similar conditions. The difference between ordinate values of the different symbols for a particular withdrawal speed indicate the reproducibility of the method, which is evidently good. The thicknesses of the films made with a pulling speed that exceeds 0.60cm/sec were measured by weighing (section 5.3.1). Those of the thinner films were obtained through α-particle (calibrated) transmission (section 5.3.3) or by optical method (section 5.2.1).

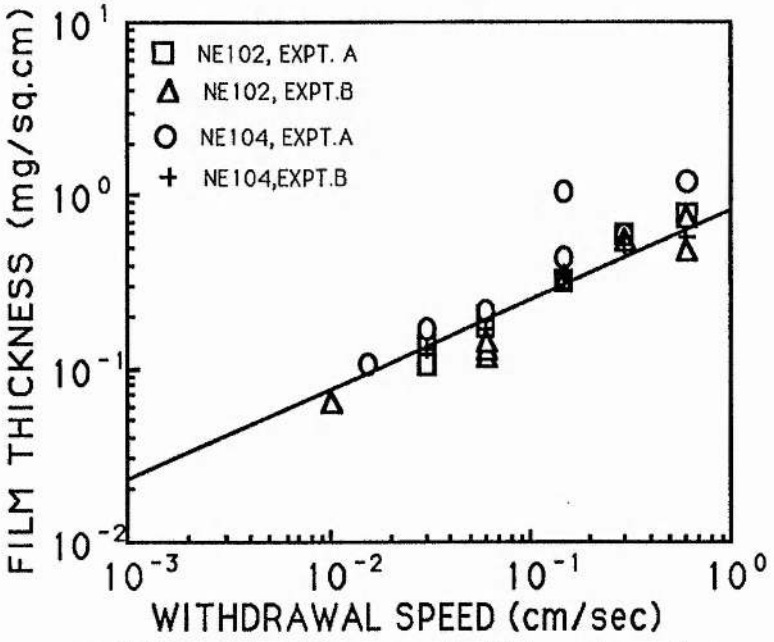


FIGURE 5.2: Film thickness and withdrawal speed of a microscope slide out of the scintillator solution.

A feature of the method is the convenience of producing films of different thickness by just changing the rotation frequency of the gear box. The data shown in figure 5.2 were obtained at rotation frequencies ranging from 1rev/3sec to 1rev/3min. Regression analysis of the data showed the film thickness, t, is given by

$$t(mg/cm^2) = (0.804 \pm 0.005) + v\ (cm/s) \cdot (0.517 \pm 0.008)$$

where v is the extraction speed of the glass slide.

The facility can be rotated as slowly as by 1rev/24 hours, indicating that films having thickness of a few nanometers can in principle be made using the present setup. However the removal from the glass substrate, of intact films made with rotation frequencies less than 1rev/3 mins is difficult. Those films that were removed usually got torn or folded by ambient air circulation in the process of mounting them in the detector assembly. The author suggests that, for future investigations, the films should be formed directly on the Lucite block or ring holder that supports the film in the final detector assembly. This was not practicable in the present setup due to the size of the perspex block and of the photomultiplier window.

A number of precautions were taken. In order to obtain films of high purity only clean, distilled water was used. The glass slides and the containers were thoroughly cleaned, rinsed with distilled water, and dried in an oven prior to use. The scintillator solution was covered whenever possible. The laboratory in which this work was carried out is almost dust free. Nonetheless, it would have been desirable to work in a dust free fume chamber, for this would also limit the flow of air and improve the uniformity of the films.

Geissel et al (1977) reportedly made the films by wetting the glass slide with a water soluble detergent prior to its insertion into the scintillator solution. The need for this step was determined by using Typhoon (supplied by ALF, U.K.), diluted to one part in a 100. The present investigator observed that the coating of the glass slide eased the removal of the film off its substrate in to the water. It is particularly useful for films thinner than a micron.

However the main hindrance to the removal of the films is the formation of the film layer on all the sides of the plate that get into the scintillator solution. Cutting off those parts of the film formed on the two edges and on the base of the glass plate prior to its dipping in the water eased the difficulty. With this modification, the detergent was no longer required and doubts on the contamination of the films and on the purity of the remaining solution were therefore minimised. It is also observed that films of good uniformity cannot be obtained using fire polished glass slides. Optically flat microscope slides have to be used.

## 5.2. THICKNESS AND UNIFORMITY MEASUREMENTS.

## 5.2.0. OVERVIEW AND SELECTION OF PERTINENT METHODS

Although several methods of measuring the thickness of thin films are known (Yaffe, 1962), only a few are simple and accurate. Many of the methods, e.g. the use of quartz crystal oscillator are not pertinent to this work. In addition, in many of the methods knowledge of one or more secondary quantities, e.g. the refractive index in Michelson interferometry, is required. The accuracy of the values of the secondary quantities determines the accuracy of the particular technique.

For the pertinent case of self supporting films interest is on the measurement of areal density of the films. The ideal technique must be nondestructive so that the same film can be used for mounting in the irradiation chamber. It should also indicate quantitatively the film's uniformity. Devices which depend on mechanical contact are liable to contaminate and deform the surfaces of the films. They are therefore not appropriate. Transmission methods are most suitable but are seldom absolute and require some form of calibration. Consequently, no single method is by itself sufficient, and a combination of methods, namely weighing, Michelson interferometry and $\alpha$–particles transmission, were used.

The integrity of thin films was first determined visually for hairline cracks, folds and other blemishes. Inferior films were discarded. Following Muga et al (1972) a first hand appraisal of the films' uniformity and thickness was made through the interference colours they produce under fluorescent light. Films of high quality produced regular colours and were used for weighing, optical measurements and alpha particles absorption measurements as the case may be.

## 5.2.1. OPTICAL MEASUREMENTS OF FILM THICKNESS.

A schematic diagram of the Michelson interferometer used for the measurement of film optical thickness is given in figure 5.3. It is determined as follows. With the two mirrors at about equal distances from the half silvered glass block localised fringes of a sodium light source were sought using the linear drive attached to the movable mirror. The fine drive was then used to position the mirrors at equal optical path length. A few (10 to 20) bright, symmetrical circular fringes of the sodium light source (with the white light fringes

on either side) were observed and the reading of the linear drive $L_1$ noted. The film was then introduced in front of the movable mirror and the new reading $L_2$ of the linear drive taken at the new position of the set of symmetrical circular fringes.

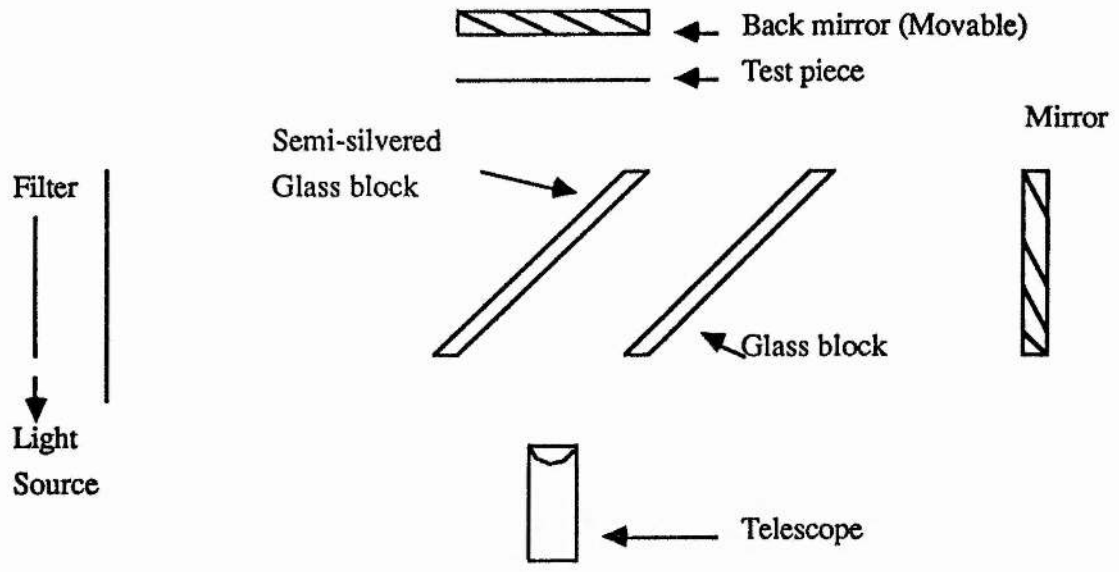


FIGURE 5.3: The set up of the Michelson interferometer for measuring optical thickness

The physical thickness, t, of the sample is obtained from the relation,

$$L_2 - L_1 = (\mu - 1)\, t \qquad 6.1$$

where $\mu$ is the refractive index of the sample, taken as 1.58, according to Nuclear Enterprise, Edinburgh 1978 catalogue. The linear drive attached to the interferometer has a minimum scale division of a micron. Thus the minimum physical thickness determinable (with an accuracy of 10% ) using the setup is half one micron. The main uncertainty of this method is the assumption that the refractive index of the bulk material is the same as that of the film.

## 5.2.2. WEIGHTING

From the selected, good quality films, disc samples of about $(0.51\pm0.01)cm^2$ were cut out with a "disc cutter". The diameter, $(2.54 \pm 0.02)$cm, of the circular knife was measured with vernier callipers and a travelling microscope. The same knife was used for cutting all the samples. Samples that were at least 10μg were weighed with a semimicron balance (Stanton Instruments). Usually at least four samples, prepared under similar conditions, were weighed separately and the mean determined. This enabled the subsequent measurement of the thickness of at least one of the set of four films by interferometry or by α–particle transmission. The weights generally agreed within 10%. Samples whose weight did not agree within this limit were discarded.

The minimum areal density that can be determined with 5% accuracy is $(20.0\pm1.0)\mu g/cm^2$. The minimum sample weighed in this investigation is 0.1mg. Samples lighter than this, even though their weights exceeded the minimum weigh of 10μg, were not weighed. The thickness of such samples was determined using the calibrated alpha particle transmission device, described in the following. This precaution enabled the accuracy attained in the measurements of the thicknesses by weighing method to be better than 5.0%.

## 5.2.3. ALPHA PARTICLE TRANSMISSION METHOD.

The experimental set up (figure 5.4) is typical for energy loss measurement. It consist of a vacuum chamber aligned with a semiconductor detector, a collimator, the sample on its holder, a second collimator and an α–particle source. The sample holder is rotatable, between the two collimators, across the radiation beam. The upper and lower collimators are, respectively, 3.3mm and 1.3mm thick, each with a collimation hole of 1mm diameter.

The surface barrier detector, SBD, ORTEG model BA-18-300-100, has a nominal active area of $300cm^2$ and depletion depth of 100μm when operated at the recommended bias of +75volts. The solid state detector has a leakage current of 0.40μA. The charge sensitive preamplifier (ORTEG model 124) has a load resistance of 10MΩ. The dial reading on the high voltage supply (ORTEG model 459) at which the semiconductor detector was operated was therefore +110volts. The appropriateness of this voltage was confirmed by comparing the noise width measured with the MCA as the bias voltage was varied.

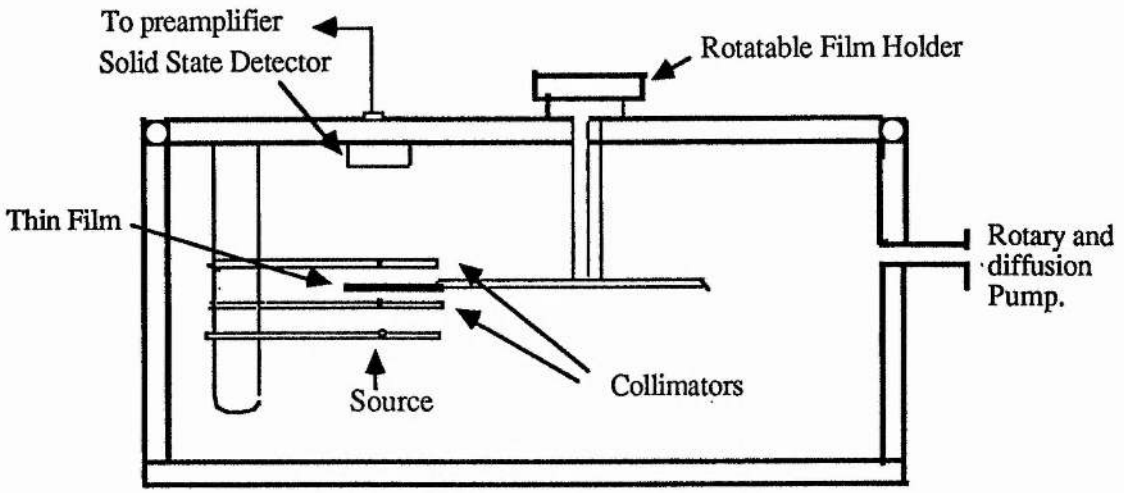


FIGURE 5.4 : The vacuum chamber for film's uniformity and thickness measurements.

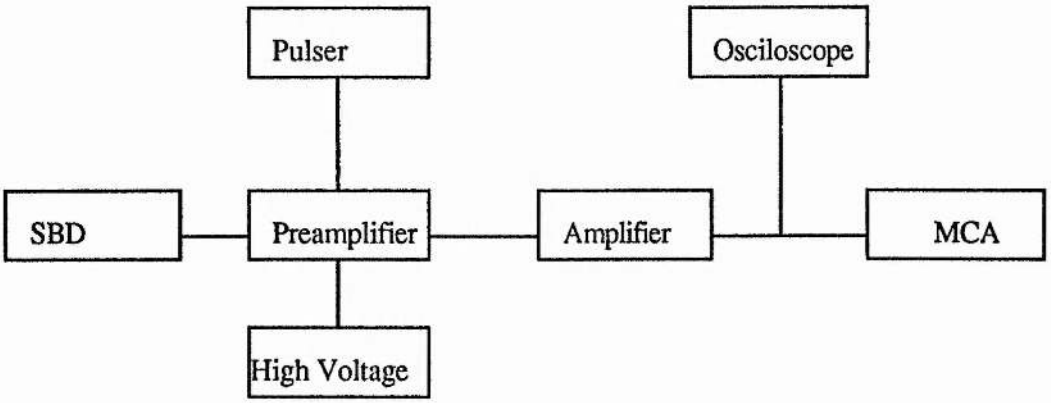


FIGURE 5.5: The electronic set up for the measurement of film's thickness and uniformity.

The preamplifier was followed by a linear amplifier (ORTEG model 572) and a voltage sensitive MCA (ORTEG model 6220). A schematic diagram of the electronic set up is given in figure 5.5. Initial adjustments included the selection of the gain of the linear amplifier for which the undegraded $\alpha$-particle pulses are 8 to 9 volts, as observed on the ossciloscope. Following established procedures (EGG linear amplifier 472A manual, 1987) the pole-zero, baseline restoration and the DC input zero offset were appropriately

adjusted. A shaping time constant of 0.5μsec was selected as being consistent with the pulse rise time (1μs) of the detector and from observation of the pulse amplitudes (on an oscilloscope) at different clipping times. Noise was reduced by using high impedance cables (RG 62/U ) with characteristic impedance of 93Ω/cm; a short cable (about 10cm) links the detector with the preamplifier. All intercomponent connections were impedance matched (Knoll, 1979).

The MCA was calibrated into energy per channel with mixed α–particle source. It consists of $^{241}Am$, $^{244}Cm$ and $^{239}Pu$ that emit nearly monoenergetic particles of effective energies 5.485MeV, 5.805MeV and 5.115MeV respectively (Lederer and Shirley, 1979). To provide a means of checking the operational stability of the system and the faithfulness of the calibration, a pulser (ORTEG model 448) was calibrated against the $^{241}Am$ source peak. The pulser was also used in determining the linearity of the amplifier and the electronic noise of the system (figure 5.6).

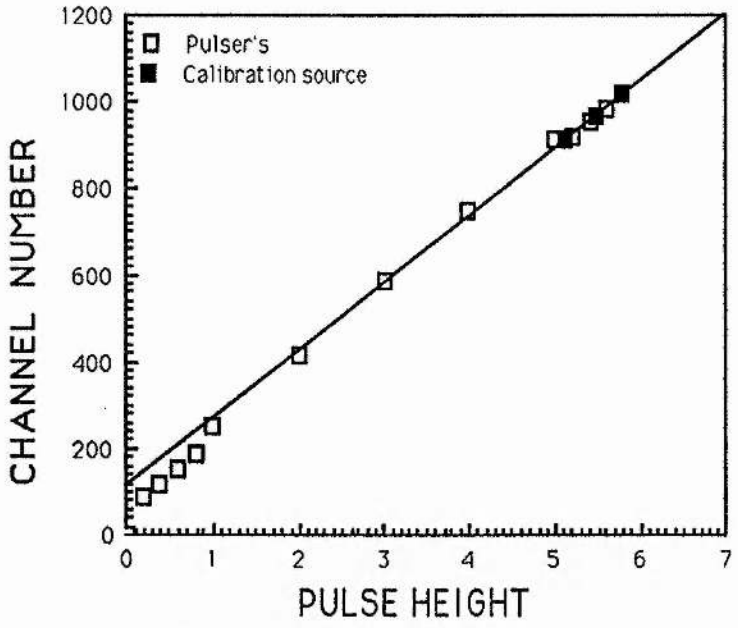


FIGURE 5.6 : Calibration and linearity test of theMCA.

The integral linearity of the MCA is better than 0.1% except at the lower 250 channels, for which deviation up to 30% was observed. Correction for this was made in the relevant data. Apart from the calibration, all other investigations was made using an $^{241}Am$

α–particle source of about 1.35μCi, at room temperature (about 23 to 25 degrees centigrade) and under vacuum better than $10^{-4}$ torr. Both the mixed nuclide and the $^{241}Am$ sources are thin and have negligible difference in thickness. Self absorption and energy losses in the source window (at most 150keV) were neglected.

For the determination of the film thickness the residual energy spectrum of the α–particles that passed through the film is accumulated in the 1024 channels of the MCA. With films of known mass per unit area a calibration curve of the energy loss as a function of the film thickness is obtained (see section 5.6.2). The areal density of other films were then determined accordingly.

## 5.2.4. DETERMINATION OF FILM UNIFORMITY.

In principle the interferometer can be used to compare, qualitatively, one film with another in terms of the pattern of the interference fringes each film produce. Since no particular film can be designated as a 'standard', this technique was not exploited. The quantitative determination of the film's uniformity relied essentially on the α-particle transmission measurement. The same experimental set up, as described in section 5.2.3, was used. Basically the spectra of the residual energy of the α-particles was measured at five points randomly selected across the film. From the usually gaussian spectra, the energy loss $\Delta E_i$ and the energy loss straggling width, $\Omega_i$, at each point was determined. The mean value of energy loss $\langle \Delta E \rangle$ averaged over the total number of points was calculated. Deviations of the individual energy loss datum from the mean reflects the uniformity of the film. The degree of uniformity is quantitatively expressed in terms of the percentage standard deviations $S_{\Delta E}(\%)$ of the energy loss distribution of the selected points from their mean viz:

$$s_{\Delta E}(\%) = \left[ \frac{\Delta E_i - \Delta E}{\Delta E} \right]_i * 100$$

An analogous procedure was followed in expressing the uniformity in terms of the standard deviations of the energy loss straggling, $S_{\Omega i}(\%)$, of the specified point from the their mean values as:

$$S_{\Omega}(\%) = \left[ \frac{\Omega_i - \Omega}{\Omega} \right]_i * 100$$

Table 5.1 illustrates the uniformity measured for a typical plastic film. The thickness of the film as determined by weighing is 0.517mg/cm$^2$. The incident energy of the $^{241}$Am α–particles was taken as 5.485MeV; energy loss in the source widow is neglected. The total area of the sample is (4.909±0.003)cm$^2$. Each of the points represents an area of 1.1mm$^2$. The samples mounted in the detector assembly are about 1.2cm by 2.6cm and the actual portion irradiated is 2.2mm$^2$. The overall degree of uniformity is better than 5%, judged by the energy loss data. If points 4 and 6, could be discarded, the table indicates that agreement within 1% in uniformity of film is obtained.

TABLE 5.1 : Illustration of the uniformity measured for a foil

| Point | $\Delta E_i$ (keV) | $\Delta E_i - \langle\Delta E\rangle$ (keV) | $S_{\Delta E}(\%)$ | $\Omega_i$ (keV) | $\Omega_i - \langle\Omega_i\rangle$ (keV) | $S_{\Omega i}(\%)$ |
|---|---|---|---|---|---|---|
| 1 | 501.5 | +2.0 | +0.40 | 59.6 | +1.42 | +2.43 |
| 2 | 501.5 | +2.0 | +0.40 | 38.3 | -19.88 | -34.17 |
| 3 | 497.5 | -2.0 | -0.40 | 59.6 | +1.42 | + 2.43 |
| 4 | 486.7 | -13.5 | -2.70 | 46.9 | -11.28 | -19.39 |
| 5 | 493.3 | -6.2 | -1.24 | 59.6 | +1.42 | +2.43 |
| 6 | 516.5 | +17.0 | -3.40 | 85.1 | +26.92 | +46.26 |

$\langle\Delta E\rangle$ = 499.5keV $\quad\quad$ $\langle\Omega_i\rangle$ = 58.18keV

$S_{\Delta E}(\%)$ = 10.21 $\quad\quad$ $S_{\Omega i}(\%)$ = 15.83

The standard deviation of the energy loss across the film is about 10keV which suggests a spread in film areal density of about 2%. It can be observed that although the energy loss at points 1 and 2 are the same, the energy loss straggling widths are different. A similar trend was observed with other films examined. It can therefore be taken that the uniformity of the films made and exposed are generally about 5%.

## 5.3. THE PHOTOMULTIPLIER AND ITS PARAPHERNALIA.

For the objectives enumerated in section 5.0 the following considerations were made in the selection of the photomultiplier, the design of the voltage divider network (VDN), and the system for the transport of the photons to the photomultiplier.

## 5.3.1. THE PHOTOMULTIPLIER

For the detection of very weak light, as may be expected from films that are less than a micron thick it is imperative to have a high signal to noise ratio (SNR) . This implies that the tube should have a low dark count and be capable of single photon counting (Foord et al 1969; Bendiscioli et al, 1984). It also means that the signal should be linearly and optimally amplified. The plastic scintillators investigated in this work emit photons in the blue/green region of the visible spectrum (figure 5.7). This matches with the spectral response of a photomultiplier with bialkali photocathode.

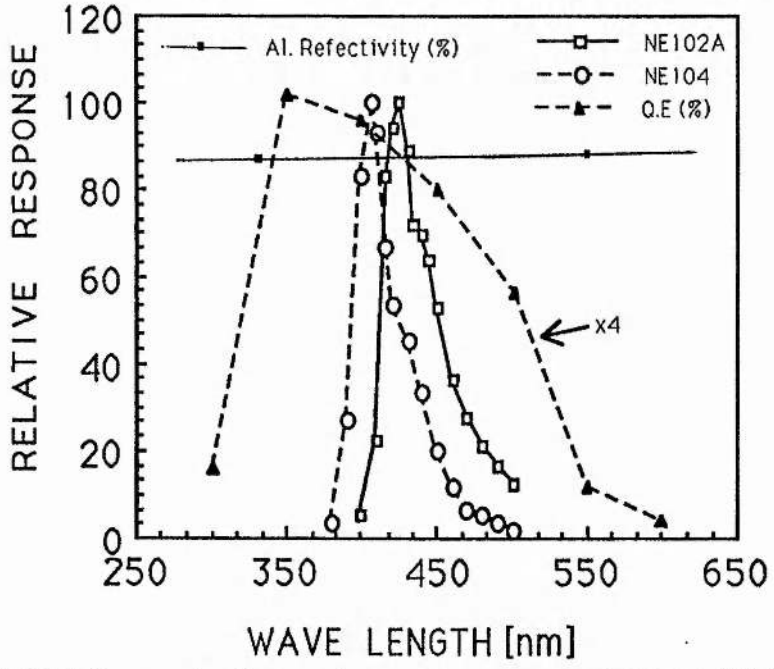


FIGURE 5.7: The wavelength dependence of the responses of NE102A, NE104A, bialkali photocathode (% Q.E.) and reflectivity of evaporated aluminium.

The photomultiplier selected is Thorn EMI model 9893B/350. It was primarily meant for wide band and high gain photon counting. It has a 14 stage fast linear dynode structure, with BeCu secondary emitting surfaces.

TABLE 5.2 : Electrical characteristics and ratings of the EMI9893B/350.

| | |
|---|---|
| Typical cathode sensitivity | 60μA/lm |
| Minimun corning blue cathode sensitivity | 7.00μA/lm |
| Typical corning blue cathode sensitivity | 8.5μA/lm |
| Typical corning red cathode sensitivity | 1.00μA/lm |
| Quantum efficiency (Peak) | 22% |
| Nomial anode sensitivity (at total voltage of 3000 volts) | 5000A/lm |
| Typical anode sensitivity (at total voltage of 3000 volts ) | 2250A/lm |
| Maximum anode sensitivity (at total voltage of 3000 volts) | 2700A/lm |
| Anode nomial gain | $83.10^6$ |
| Nomial dark emission (typical) | 0.20nA/lm |
| Nomial dark emission (maximum) | 1.00nA/lm |
| Maximum dark counts | 150cps |
| Nomial dark emission count rate(typical) | 40 cps |
| Response rise time | 2.5ns |
| Response transit time | 45ns |
| Response time FWHM | 4ns |
| Maximum rated sensitivity | $10^4$ A/lm |
| Maximum rated voltage between cathode and first dynode | 450volts |
| Maximum rated interdynode voltages | 450volts |
| Maximum rated voltage between cathode and anode | 3.0 kvolts |
| Maximum rated average cathode current ($I_K$) | 1.5nA |
| Maximum rated average anode current ($I_a$) | 200μA |
| Maximum-Minimum ambient temperature | (-30 to 60 )°C |

The tube's nominal photocathode diameter is 52mm but reduced, by internal focusing, to an effective diameter of 9mm. This reportedly (Thorn EMI Catalogue, 1988) results in negligible cathode dark count, at room temperature, while still preserving the wide spectral range of a bialkali photocathode. The tube was supplied coated with graphite, connected to the cathode pin, and sleeved with black plastic for electrostatic insulation purposes. Linear focused tubes have poor immunity to magnetic fields. As the laboratory is in the

vicinity of high pulsed magnetic fields, the tube was therefore fitted with a 'mu' metal shield. The container of the tube provides rf shielding. Listed in Table 5.2 are the electrical characteristics and ratings of the photomultiplier as provided in the manufacturers catalogue.

## 5.3.2. THE VOLTAGE DIVIDER NETWORK.

The two main considerations used in the design of the voltage divider network are
a) the attainment of maximum gain without loss of linearity;
b) the input requirements of the preamplifier.
Current linearity depends on the nature of the photocurrent and its magnitude relative to the voltage divider current ($I_D$). For the pertinent case of pulsed currents (AC) the transient current can be larger than $I_D$ in so far as a constant interdynode current is maintained for the duration of the pulses. The incorporation of stablizing capacitors, $C_s$, across the last three dynodes can therefore maintain current linearity. The charge stored by the stablizing capacitors must be larger than the maximum charge supplied by each dynode. The minimum value of the capacitance $C_s$ is given by

$$C_s = \frac{\Delta Q}{V} \Big/ \frac{\Delta V}{V} \qquad 5.5$$

where $\Delta Q$ is the anode output pulse charge, and $\Delta V/V$ is the desired degree of stability of the voltage.

The charge produced by each photoelectron at the anode is G.e, where G and e are respectively the gain of the photomultiplier and the electronic charge ($1.6.10^{-19}$ coloumbs). The average DC anode current, $i_a$ is given by

$$i_a = \frac{e\,G}{\tau} \qquad 5.4.1$$

The pulse width, $\tau$, depends on the pulse shape and the transient time spread in the photomultiplier. According to Bengston and Moszynski (1974), the decay time and the FWHM of the main scintillation component of NE102 are respectively 2.4ns and 3.3ns. It is therefore assumed that $\tau$ for the plastic scintillators is 5ns. The yield of photoelectrons from a scintillator depends on the irradiation geometry and the light collection efficiency. There is little published data on plastic scintillators (Bengston and Moszynski, 1974).

Consequently a maximum operating frequency, $f_{max}$, of 1Mhz is assumed. The corresponding maximum anode current [$I_a$(max)], is given by

$$I_a\,(max) = e.\,G.\,f_{max} \qquad 5.4.2.$$

It is envisaged that space charge problems can not arise if $I_D$ is two orders of magnitude greater than the maximum anode current. Thus

$$I_D = 100.\,e.\,G.\,f_{max} \qquad 5.4.3$$

The high voltage supply can provide DC currents ($I_D$) up to 10mA, therefore in principle the tube gain of $10^8$ can be attained. The recommended voltage between the cathode and the first dynode is 300volts. This implies that for a linear network of 14 dynodes, the resistance of each dynode should be 1.5kΩ. However large dynode currents may lead to large heat dissipation within the VDN resulting in poor performance with an increase in the dark current. The network was therefore redesigned for a moderate gain of $10^7$ (figure 5.8). The individual resistors could be 714kΩ but the available resistors of 680kΩ were used.

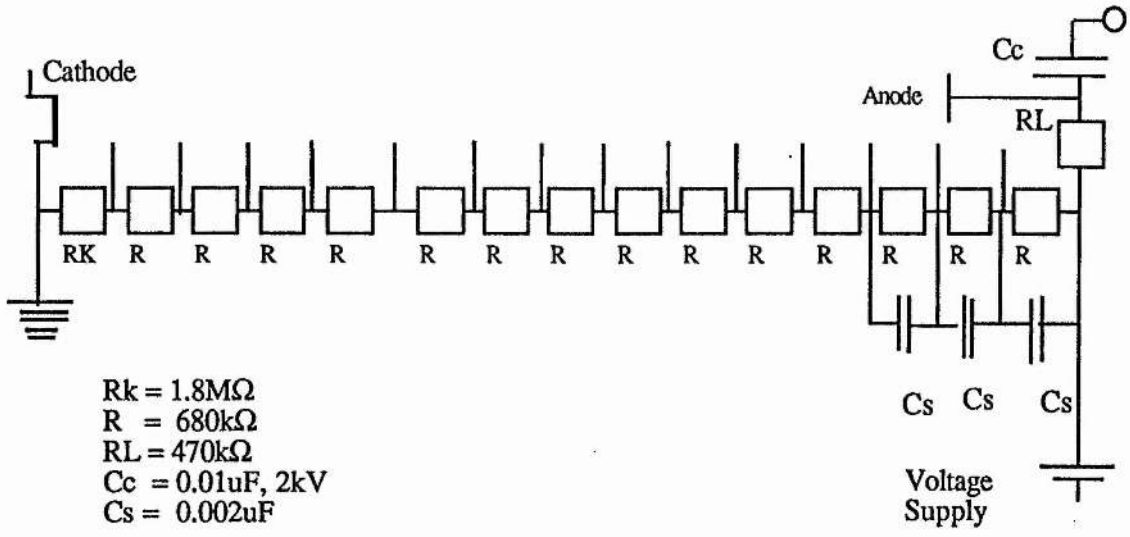


FIGURE 5.8: The voltage divider network for the photomultiplier.

A fast, linear focused photomultiplier of the type used in this investigation should, ideally, be operated with the anode at ground potential and a negative high voltage applied to the

cathode (Meade, 1981). Such an arrangement would be suitable for both DC and AC operation. It would not however allow any contact with the cathode, unless electrical insulation is provided. Due to the requirements that the source, light guide and the SBD have to be held together and in contact with the photocathode (see next section), and that the preamplifier (ORTEG model 121) accepts only AC coupled signals, the VDN was designed with the cathode grounded and a positive high voltage applied to the anode. Thus coupling capacitors ($C_c$) for the isolation of the signal from the high voltage supply were employed. This created rate effects and overshoot problems, even at moderate voltages, due to the fast rise time (Table 5.2) of the photomultiplier. The appropriate voltage for operation was obtained from the differential bias curves (section 5.5.1).

## 5.4. THE DETECTOR ASSEMBLY.

The detector assembly refers to :
a) the facility that enables collimated radiations of predetermined energy to interact with the sample;
b) the system for the collection and focusing of the light produced on the photomultiplier window;
c) the SBD that stops alpha particles that passed through the scintillator film; and
d) the collimators and energy moderators, if any, used.

A facility for holding all the different components appropriately aligned at fixed positions was made (Figure 5.9); it enabled the irradiation geometry to be convenient reproduced whenever the scintillator foils or the energy of the $\alpha$-particles were changed.

### 5.4.2. THE ALUMINIUM MIRROR.

Two systems for the collection of the light output, and focusing it on the photomultiplier were explored. The first follows the approach of Gelbe et al (1971) and Ettling and von-Witsch (1978). Its basic requirements are to have a scintillation film held vertically inside a reflecting tent, with the open end viewed by a photomultiplier. The emission spectra of NE102 and of NE104, and the peak of the quantum efficiency (QE) of bialkali photocathode matches those of aluminium reflectivity (figure 5.7). Aluminium has a reflectivity of about 90% within the range of wavelengths of interest, it is the best known

specular reflector (Birks, 1964).

The mirror (figure 5.10) that was built for this work is essentially an aluminium cylinder. The foil holder is attached to the closed, upper, circular top. The lower, open end rests on, and focuses the light on to the photomultiplier window. Halfway along the cylinder's length, two aligned holes (each 0.2cm diameter) were drilled. They serve as entrance and exit ports for the radiation beam and provide additional collimation. The lower end of the vertically held plastic foil, is lightly smeared with silicone oil, and just rest on the photomultiplier window. To ensure high reflectivity, the inside of the mirror is hand polished with a metal polishing cream known as "Brasso".

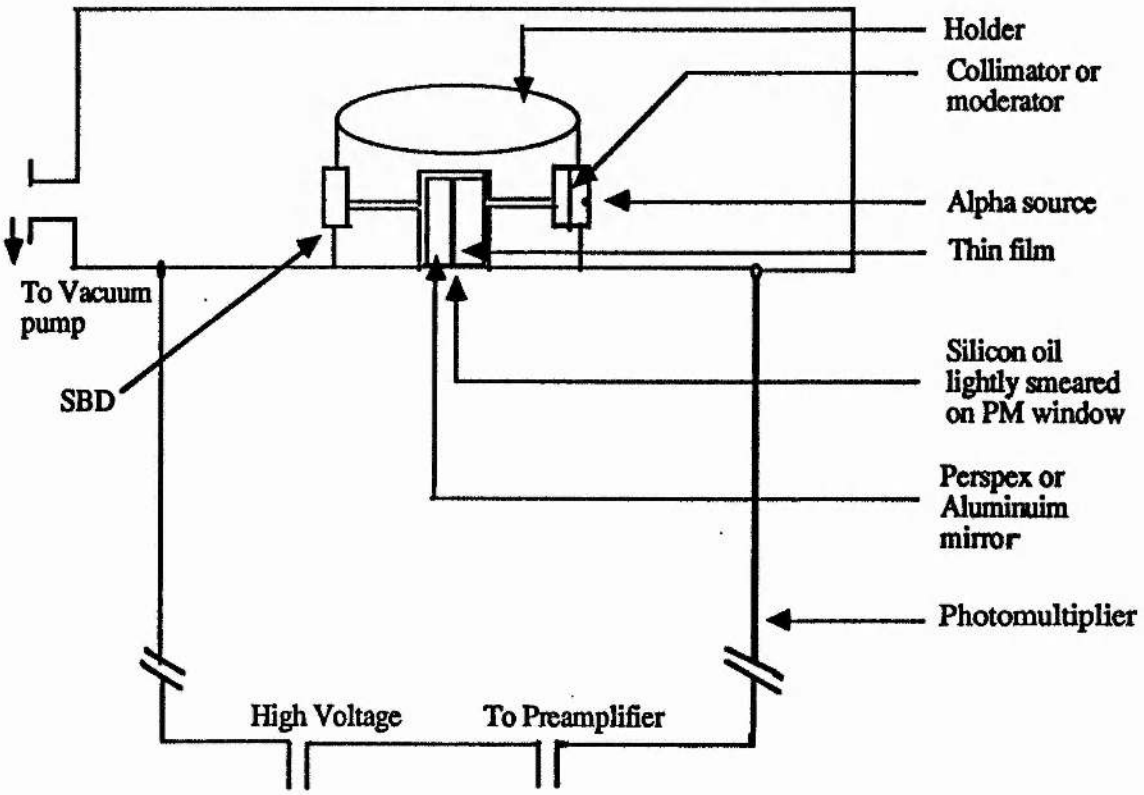


FIGURE 5.9: The Irradiation chamber for thin film detector.

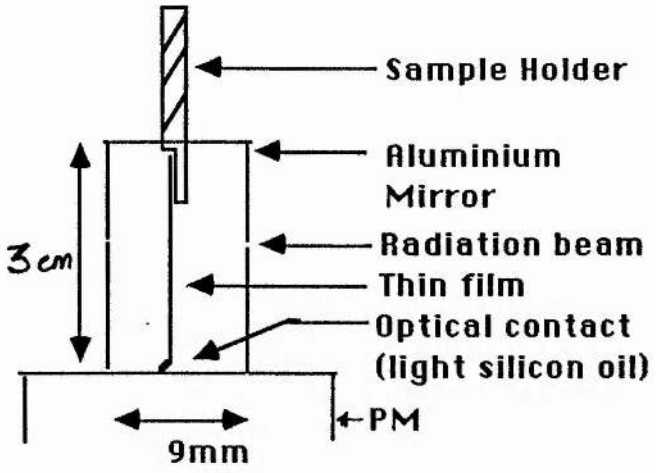


**FIGURE 5.10: The Aluminum mirror.**

The light pulses obtained using this system are low and unstable. Irregular and poorly shaped pulses were observed on the oscilloscope, even with the same foil. The inconsistency of response is most probably due to the shifting of the foil under vacuum conditions. Thus the incoming radiations passed through different effective thicknesses of the foil and therefore there were different energy losses in the foils and hence variable light output. These problems can be attributed to the size and shape of the mirror which, in turn, were determined by the size of the photomultiplier window (9mm). This aspect of the photomultiplier is discussed in section 5.6.4. The results reported and discussed in this work pertain only to those obtained with an alternative system.

## 5.4.3. THE LUCITE LIGHT GUIDE

The second light collection system consisted of two hemi-cylindrical perspex halves (figure 5.11). In each a hole of diameter 0.2cm was drilled perpendicularly through the large flat face. The holes enable the radiation to pass through. The plastic film is laid flat on one of the Lucite halves. In operation, one hemicylinder covers the other forming a whole 'cylinder', with two aligned holes that serve as collimators and entrance and exit channels for the radiation. Normally, the flat faces of the perspex halves were lightly, and evenly, smeared with silicone oil before a foil was laid. To obtain optical coupling, the base of the "cylinder" that rests on the photomultiplier window was also smeared. The "cylinder's"

top, and all the curved surfaces of the 'cylindrical' perspex were painted with white, optical paint ( NE460, Supplied by Nuclear Enterprises, Edinburgh). The complete cylinder was inserted into an aluminium bushing (figure 5.11) for further minimisation of light loss.

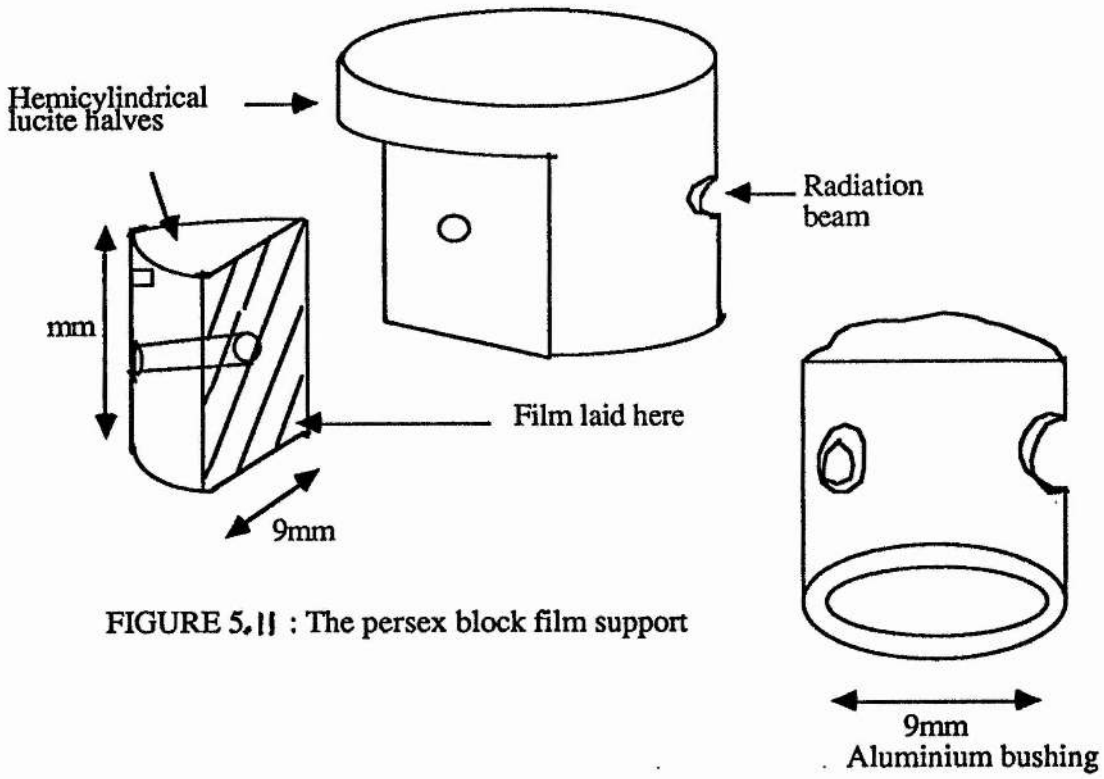


FIGURE 5.11 : The persex block film support

## 5.5. ADJUSTMENTS AND OPTIMISATION OF THE EXPERIMENTAL CONDITIONS.

Described in the following are the procedures taken for obtaining the appropriate condition under which the experiments were made. The manufacturers recommended an operating voltage of 1.9kV for the Photomultiplier. Since this was obtained with NaI(Tl), whose light output differs from those of the present work, a more appropiate bias and amplifier

gain (ORTEG model 472A) for the present investigation was sought.

## 5.5.1. THE OPERATING CONDITIONS FOR THE PHOTOMULTIPLIER .

The general counting characteristics and the operating voltage of the photomultiplier was obtained from a plot of the count rate in response to weak light source as a function of the applied voltage. For this, the single channel analyser, SCA, (J & P model NIM 213), following a linear amplifier, was operated in a differential mode. The lower level discriminator was adjusted to exclude pulses due to electronic noise. Counting curves were obtained in respect of:

a) The response of foils of 5μm and 100μm thickness in the TFD arrangement.

b) A thick NE102A (6.35mm thick) slap directly and optically coupled to the photomultiplier with silicone oil.

Responses frequencies were obtained in the presence and absence of the source and at different amplifier gains. In all instances the size of the pulses formed were monitored on an oscilloscope. The desired counting point was located by:

1) Constructing the differential characteristic, dN/dV, obtained by subtracting adjacent points on the plateau, and giving the change in frequency per given interval of applied voltage (Oliver and Pike, 1968); the minimum value indicate the region of optimal stability.

2) plotting the ratio of the signal to the square root of the noise at the same applied voltage and under similar conditions.

The results indicated that the appropriate voltage that can be applied to the photomultiplier can range from 1.7kV to 1.9kV. The gain range of the linear amplifier that yields detectable signals from the thick foil without exceeding a 10volt limit is $2.10^2$ to $2.10^3$. In all instances the shaping time constant of the linear amplifier was kept at 0.5μs. Having identified the ranges, the actual voltage and gain were obtained by observing the response of the thinnest and thickest plastic foil investigated. Two conditions were identified as suitable for both: (1.5kV, gain: 2800) and (1.8kv, gain: 180). These will be referred to as ExptA and ExptB respectively. Most results were obtained under these conditions, the exception being the thick films (section 5.5.4) whose scintillation response spectra were determined at a bias of 1.8kV, linear amplifier gain of 45 and in the absence of coincidence

gating.

## 5.5.2. MODERATION OF ALPHA PARTICLE ENERGY.

In some of the investigations (sections 5.6.6 and 5.6.7) the energy of the α–particles, incident on the foil, were varied. This was achieved by inserting absorbers, aluminium foils, just in front of the source. The foils were stacked together and glued in between two annular discs. The subsequent scattering of the α-particles was reduced by inserting a collimator just in front of the aluminium foils. To facilitate the same irradiation geometry as in the instances that the energy of the $^{241}Am$ α-particles was not reduced, dummy dicks having similar thicknesses were inserted in between the source and the collimator.

## 5.5.3. THE DETERMINATION OF SCINTILLATION SPECTRA FOR TFD.

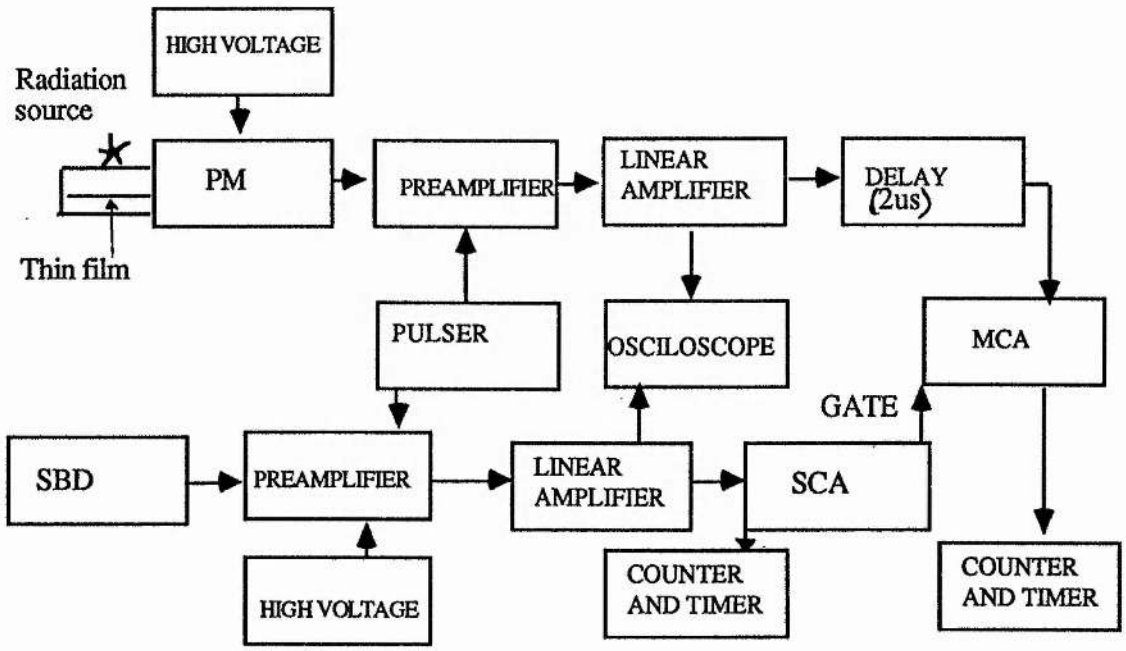


FIGURE 5.12: The electronic set up for scintillation counting

Figure 5.12 shows the electronic setup for determination of the light response of the thin film detector (TFD). For convenience the chain of electronic components in between the Photomultiplier and the MCA are referred to as the photomultiplier channel. The other part of the set up which will be referred to as the SBD channel, provides a signal for gating the response of the photomultiplier channel. The SBD channel is essentially similar to the electronic set up for thickness and uniformity measurements (section 5.2.3). The residual energy spectra of the α–particles, and therefore the energy loss and the thickness of the foil, can be obtained provided the perspex light guide is not, or is only lightly, smeared with the silicone oil.

The light guide, detector, high voltage supply, photomultiplier and preamplifier are described in the preceding sections. In principle, scintillation spectra can be obtained without gating the MCA with the pulses from the other arm of the setup. However the difference between the signal and noise is small particularly for films that are less than a micron thick (see section 5.6.1 and figure 5.14). Therefore to reduce the accumulation of dark count due to photomultiplier noise and light pulses due to cosmic radiation, the gate (figure 5.12) was applied. Chance coincidence events, due to the electronic noise in the SBD channel, were minimised by passing the signal from the linear amplifier of the SBD channel through a SCA operated in the differential mode. The lower and upper windows of the discriminator were selected by determining the count rates of the SCA output at successive window widths of 0.5volts. Each time a sample of different thickness and/or the energy of the radiation was varied the appropriate discriminator setting was determined.

Spectra were usually accumulated in the 256 channels of the MCA over a period of 800seconds, at room temperature and under a vacuum better than $10^{-4}$ torr. During the collection of spectra in the MCA the count rates of the SCA output, $C_{SBD}$, and those of the pulses that occur in coincidence, as registered by the ADC of the MCA, $C_c$ were determined. Casual coincidence count rates ($C_a$) in the absence of the scintillator foil were also obtained. Each spectrum was recorded at least two hours after the chamber was closed. This enabled the decay of ambient light that the photomultiplier may be exposed to during the changing of the foils or energy of the radiations.

## 5.5.4. THE DETERMINATION OF OTHER SCINTILLATION SPECTRA.

The response characteristics of 100 and 50μm, NE102A films (obtained from Nuclear Enterprises, Edinburgh) were also investigated. Since, their thickness exceeds the range of the natural α-particles their scintillation response was collected ungated. Two irradiation geometries were explored. In one, referred to as the set up A, the films were held just like in the TFD arrangement, except the coincidence gating. In the other, referred to as set up B, the films were laid directly on the photomultiplier whose window was previously lightly smeared with silicon oil for optical coupling. Collimation and energy moderation of the TFD arrangement (set up A) was achieved as described in the preceding section. For exposures in the set up B, discs samples of 9mm diameter were used. The arrangement is shown in figure 5.13.

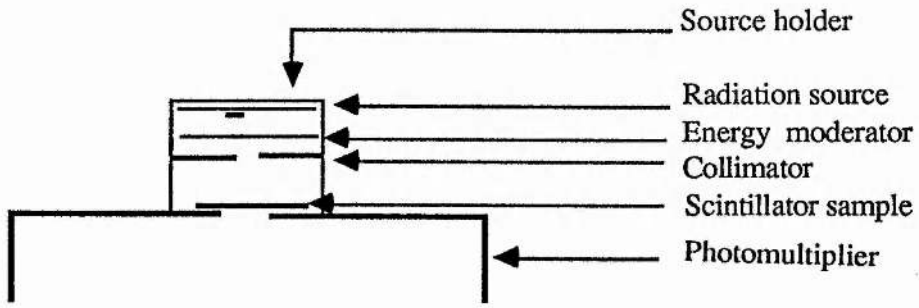


FIGURE 5.13: The set up for the irradiation of thick films mounted directly on the photomultiplier.

## 5.6. RESULTS AND DISCUSSIONS.

### 5.6.1. DARK NOISE AND THE SIGNIFICANCE OF COINCIDENCE COUNTING.

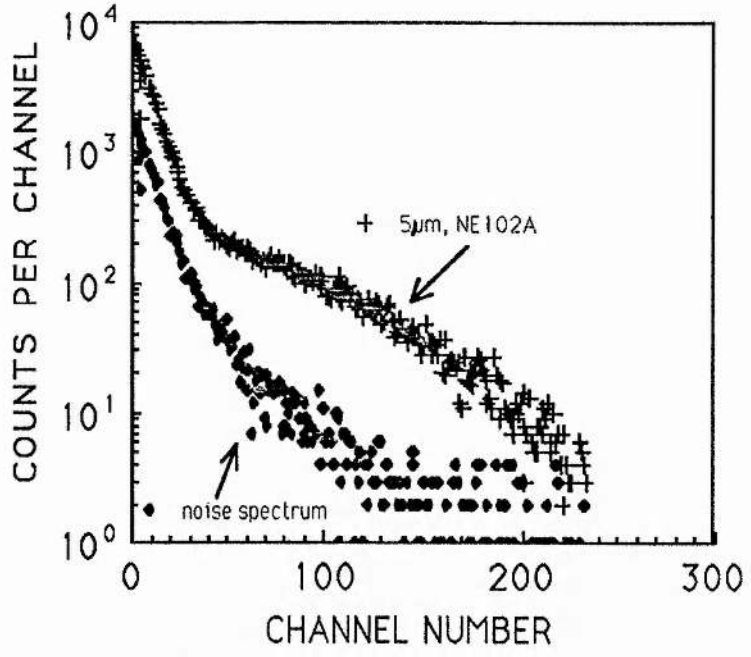


FIGURE 5.14: The response of 5um thick NE102A film in the absence of coincidence and the noise spectrum.

In figure 5.14 the scintillation spectrum obtained under normal conditions, that is without the use of coincidence gate to the MCA with pulses detected in coincidence in the stopping detector (SBD), is compared with the dark spectrum. The latter refers to the spectrum recorded in the absence of the source and the film, and, in order to enable the decay of any absorbed light, with the chamber closed for the previous five days. The scintillator is a 5μm film of NE102A. The plot indicates that the two spectra can be distinguished. However, the difference in the two spectra vanishes with the decrease in the thickness of the film. The merging of the signal into the dark count indicates that only a few of the light photons produced from the film are actually collected and converted into photoelectrons by the photocathode. To determine if that is true, and is not due to a 'bad' response by the photomultiplier the various components of the dark spectrum were investigated.

It was observed that there is, essentially, no difference between the spectra obtained in the absence of the source but with the scintillating film present from that accumulated under the converse situation. If either the spectrum obtained in presence of the source but without the film or in the absence of the source but with the film present is compared with that obtained in the absence of the source and the film and with the chamber closed for the previously five days a significant difference is observed. A substantial reduction in the intensity of the dark count was evident. Furthermore, a good response spectrum was obtained for a 6.35mm thick slap of NE102A. This indicates that the photomultiplier response is not "bad", but the photomultiplier is highly sensitive and a significant portion of the dark count is from the ambient light absorbed by the detector assembly holder, the scintillator film itself, the perspex block and the photomultiplier window. This light decays over a period of five days.

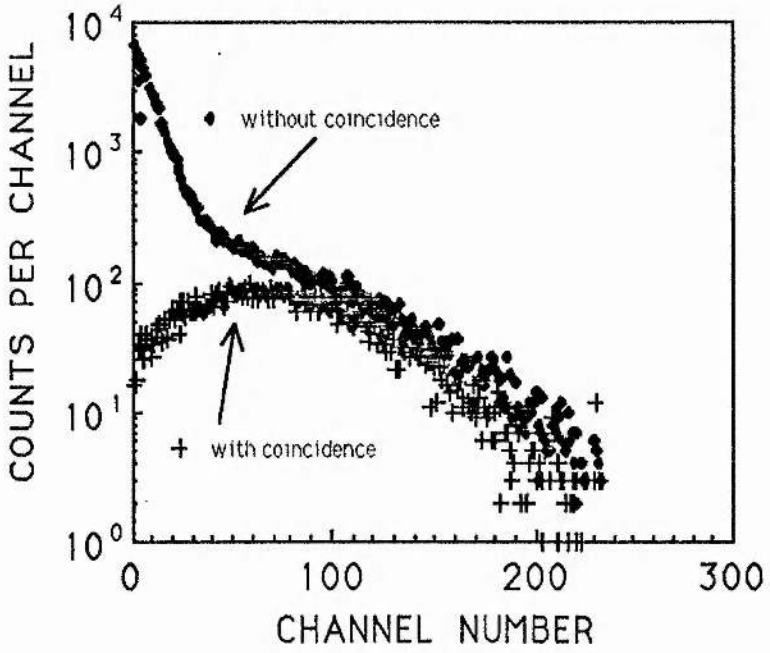


FIGURE 5.15: The spectra of 5μm NE102A film obtained with and without the use of coincidence.

Shown in figure 5.15 are typical scintillation spectra obtained when the gate was applied and in its absence. In both, the same sample, NE102A of 5μm thick, and experimental conditions refer. It is evident that the blocking of the MCA with coincident pulses completely stopped in the SBD helps in reducing the electronic noise (the more numerous pulses at channel numbers that are less than 50). It was also observed that there is no

difference between the anticoincidence spectrum of the same film from the dark count spectrum. This suggests that most of the real pulses detected by the photocathode occur in coincidence with the pulses stopped in the SBD; the majority of the dark counts pulses in the photocathode occur in anticoincidence. To reduce the frequency of chance coincidences and the broadening of the scintillation spectra, noise events in the SBD were eliminated by careful selection of the discriminator windows (section 5.5.3).

With the signal just greater or about the dark count level it is impractical to subtract the dark count from the signal. However, the foregoing results show that by using a photomultiplier with single electron response (in photon counting mode), in conjunction with coincidence technique, relatively good spectra can be obtained, albeit very few photoelectrons (see discussion in section 5.7) are produced or detected. Cooling, the other method of enhancing the signal-to-noise ratio, is impractical due to the peculiar nature of the irradiation chamber. It would therefore be expected that the minimum thickness of films that can give a detectable light pulse is limited mainly by the electronic threshold.

## 5.6.2. ENERGY LOSS AND FILM THICKNESS.

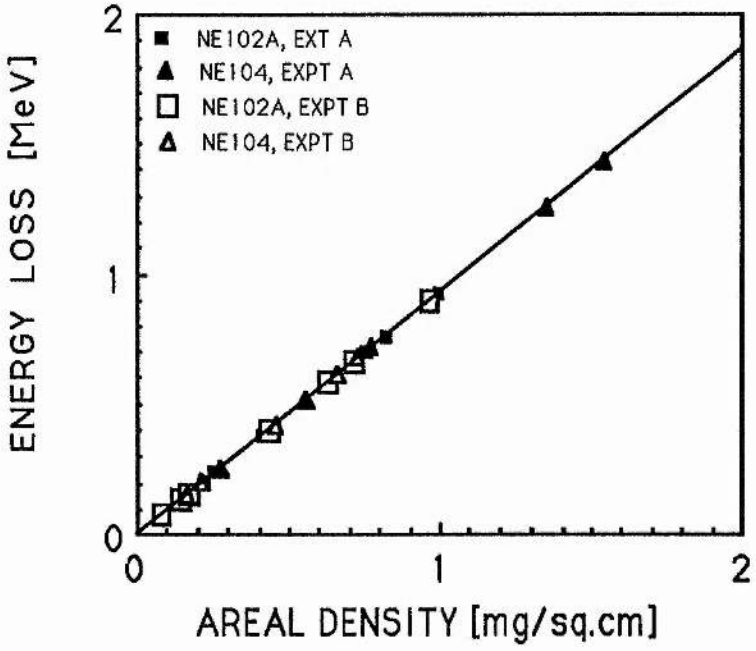


FIGURE 5.16: Film's thickness and energy loss in the film.

Shown in figure 5.16 is the relationship between the energy loss in the thin films and their thickness. For the sake clarity the uncertainties in the energy loss determinations, which are about 5-10%, are not indicated in the same picture but see figure 5.17. The data in figure 5.16 shows that there is no difference in the energy absorption characteristics of the two plastics, as far as we can determine. This expected result follows from the similarity in their chemical composition and physical characteristics.

Clearly the energy deposited in the films is linearly related to their physical thickness (t). The following relationship fits the data:

$$\Delta E \text{ (MeV)} = (8.4108 \pm 0.005).10^{-6} + (0.9332 \pm 0.003).t(mg/cm^2)$$

The intercept, being so small can be neglected and has no significance. By the above relation, the α-particles lose on average 0.933MeV for each 1mg/cm$^2$ of the plastic film.

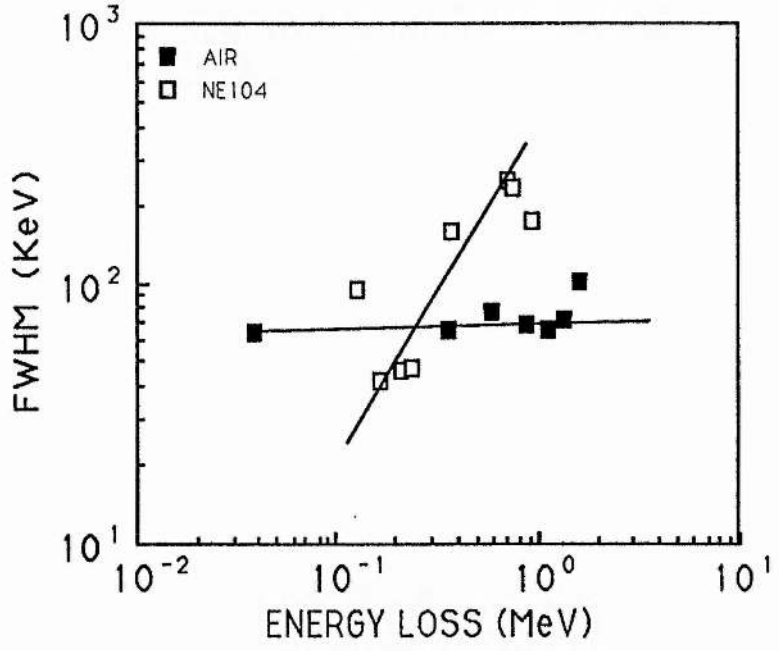


FIGURE 5.17: Energy loss and energy loss straggling in air and thin film.

The relationship between the energy loss straggling, represented by the response peak's full width at half maximum (FWHM), and the energy loss (or the film's thickness) is indicated in figure 5.17. For comparison purposes the straggling in energy loss measured

in air at different pressures, and therefore variable thicknesses and energy loss, is also indicated. The instrumental contribution (about 31.55keV, based on measurement in the absence of the film) to the straggling was not deducted. The energy loss straggling measured in the films is about the same as in air, for energy loss of few hundreds keV. However as the thickness of the solid films increases the straggling in the energy loss increases rapidly at least compared to that in air of comparable thickness. It is not clear whether this indicates a poor uniformity of the relatively thicker films or a nonuniformity of air. However, it has been visually observed that the quality of films produced by the dip-coating technique tends to deteriorate as the glass plate on which the film is deposited is withdrawn at a faster pace as is required for making the relatively thicker films.

## 5.6.3. THE RESPONSE AND THICKNESS OF THIN FILM DETECTOR.

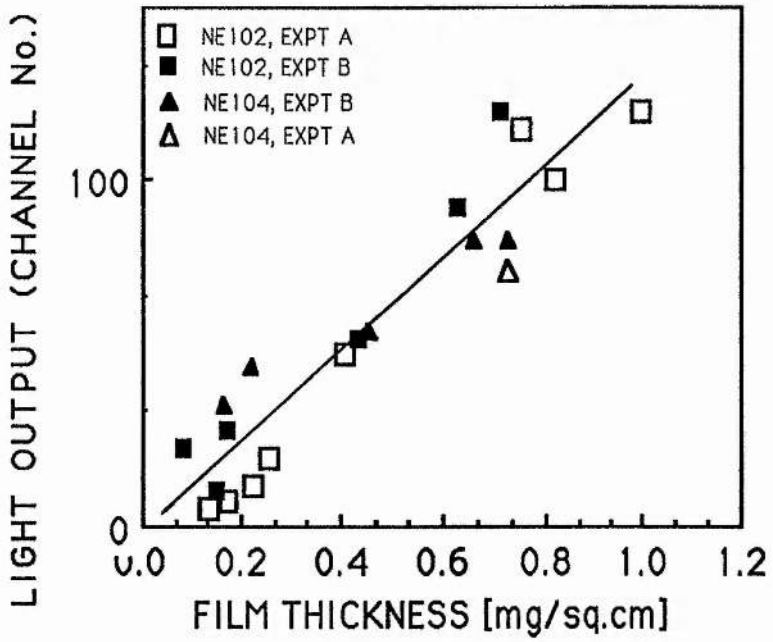


FIGURE 5.18: Thin film detector light output and thickness.

Figure 5.18 shows the pulse height response of the TFD to α-particles of about 5.485MeV as a function of the film thickness. The response was given in terms of channel number (pulse height) at which the peaks of the pertinent spectra fall on the MCA. All the spectra were obtained with the coincident gate applied. The bias to the photomultiplier and the linear amplifier gain differ slightly (see section 5.5.1). However the light pulses obtained

from a given scintillator under the two conditions agree within about 5%. For the sake of clarity, the broadening in the response, the FWHM, which are very wide, were not indicated in figure 5.18. The extend of response spectrum broadening and its dependence on the film thickness is given in figure 5.19. The latter represents the unmodified spectra of NE104 films of different thickness but obtained under as similar experimental conditions as possible.

Clearly the light output increases linearly with the plastic film thickness. For films having thickness (t) in the range 0.6mg/cm$^2$ to 8mg/cm$^2$ the light response, in terms of channel number , $L(C_p)$, is given by:

$$L(C_p) = (6.204 \pm 6.845) + (99.49 \pm 10.86).t(mg/cm^2)$$

The intercept value of 6 channels is consistent with the known (determined with a pulse generator) zero off-set of the MCA (10 channels). The four channels difference may be due to uncertainties in the determination of the response spectra peak channels. This is particularly true for the scintillation spectra of the very thin films (see figure 5.19) which form their peaks, if any, within the lower 50 channels. (It can be suggested that this may also be the factor responsible for the large uncertainty in the regressed value of the intercept. Other contributing factors such as slight variations in optical coupling can not be eliminated completely.

In section 5.6.2 it was shown that the mean energy loss per unit thickness of the scintillator is 0.933MeV per mg/cm$^2$. Using the above expression, the relationship between the TFD light output, expressed in terms of the response channel number, $L(C_p)$, is given by

$$L(C_p) = 6.204 \pm 0.103 + (106.63 \pm 10.52).\Delta E(MeV)$$

This relation implies that for the particular setting of the MCA, one channel difference in the response spectra corresponds to a difference of 9.38kev of absorbed energy or alternatively to the 0.053mg/cm$^2$ difference in the film's thickness.

Statistical analysis and Figure 5.18 indicate that there is no difference in the light response of NE102A from that of NE104 for the thicknesses investigated in this work and for exposure to unmodified $^{241}$Am $\alpha$–particles. This probably because two plastics have essentially similar physical composition, although NE104 is known to have faster response than NE102A (Nuclear Enterprises, Edinburgh, 1987).

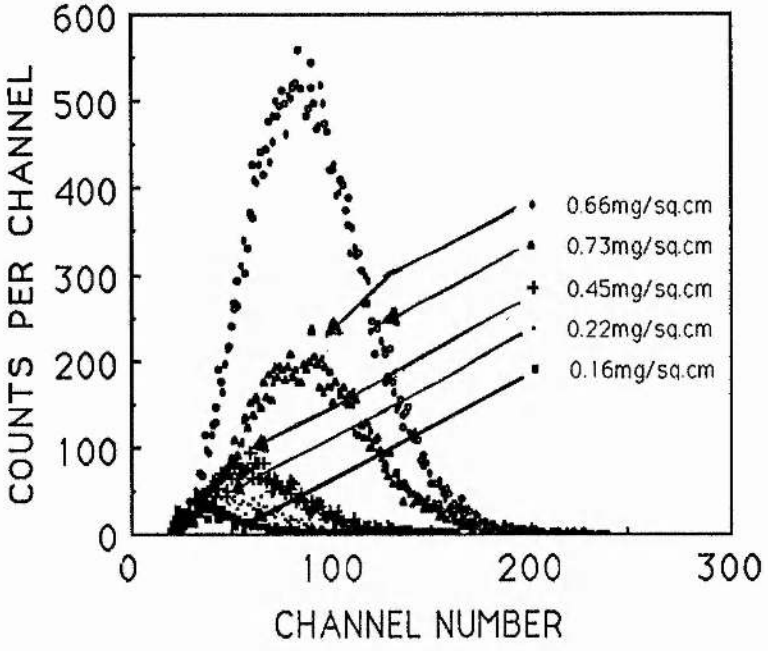


FIGURE 5.19: The coincident spectra of NE104 films of different thickness.

As evident in figure 5.19, the scintillation spectra decreases with decrease in the scintillator thickness. The ability to observe the 'complete' spectra also decreases. The minimum thickness of the scintillator film that can give a "complete" scintillation spectrum, that is for which both the leading and the tail ends of the spectrum can be discerned, is 500nm. Scintillator films that are less than 0.05mg/cm$^2$ produce coincident pulses that can be recorded on the MCA, but the spectrum is triangular, that is without the leading edge and hence the peaks cannot be discerned. Various attempts were made to extend this lower limit (see section 5.8), but none yielded successful results. Thus, 500nm is the lower limit of film thickness that can be investigated using the available facility.

The total energy deposited in a scintillator of thickness t mg/cm$^2$ is given as

$$\Delta E = 0.88.\ S_\rho.\ t\ (mg/cm^2)$$

The factor 0.88 was introduced as a correction for the difference in the amount of hydrogen compared to carbon in polyethylene and NE102A. According to Northcliffe and Schilling (1970), the stopping power of 5.485MeV helium ions in polyethylene is 1.0605MeV cm$^2$mg$^{-1}$. Thus the energy lost in a film of 500nm is about 46.65keV. This represents the minimum energy deposition that can give a quantifiable signal with the present set up.

## 5.6.4. THE RESOLUTION AND THICKNESS OF THIN FILM DETECTOR .

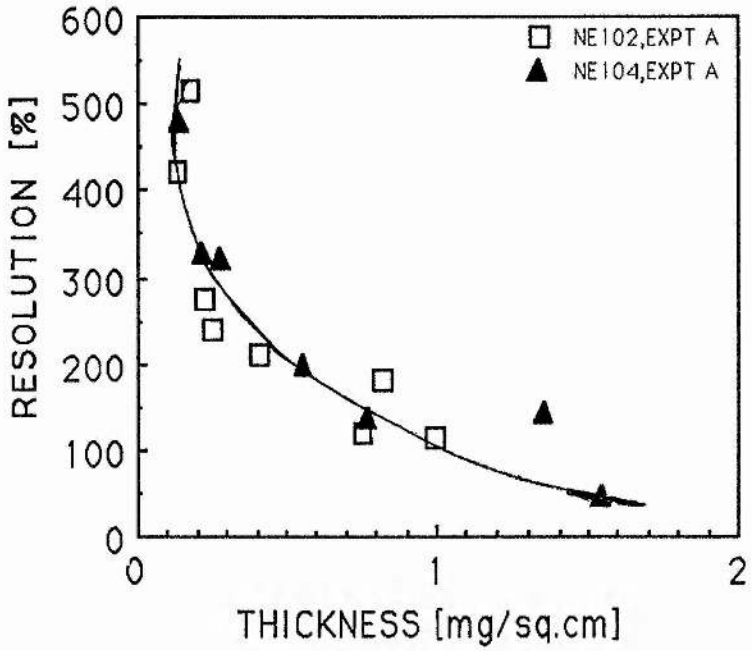


FIGURE 5.20: Pulse-height resolution of TFD and film thickness.

The broadening of the response spectra can be expressed in percentage resolution by

$$\eta(\%) = [\text{FWHM / peak channel}] .100$$

The dependence of the response resolution of the TFD on the scintillator thickness is given in figure 5.20. The resolution improves with the thickness of the scintillator. Like the light output, there is no apparent difference in the dependence (on the thickness) of the spectrum broadening of the two scintillators. Figure 5.16 showed that the energy lost in the film increased linearly with the foil's areal density. The improvement in the resolution and light output with increased scintillator thickness is due to the increase in the number of ionisation energy depositions.

Regression analysis indicates that the resolution, $\eta(\%)$, is given by

$$\eta(\%) = 102.03 \pm 10.56 + t^{-0.585 \pm 0.123}$$

Given that the energy deposited in the film is linearly related to the film thickness, a similar

relationship would be expected between the resolution and the energy loss, $\Delta E$. It is determined that (data not shown) the dependence of the resolution on energy deposited can be expressed as

$$\eta(\%) = 113.79 \pm 12.51 + \Delta E(MeV)^{-0.585 \pm 0.102}$$

The above expression imply that the resolution $\Delta L/L$ can be expressed as

$$\Delta L/L = \text{constant} + (t)^{-1/2}$$

Since energy deposited in the films is linearly related to the thickness, it follows that

$$\Delta L/L = \text{constant} + (\Delta E)^{-1/2}$$

Thus, the resolution is proportional to the square root of the energy loss. A similar conclusion was reached by Beechetti et al (1976) for the case of conventional sized NE102A.

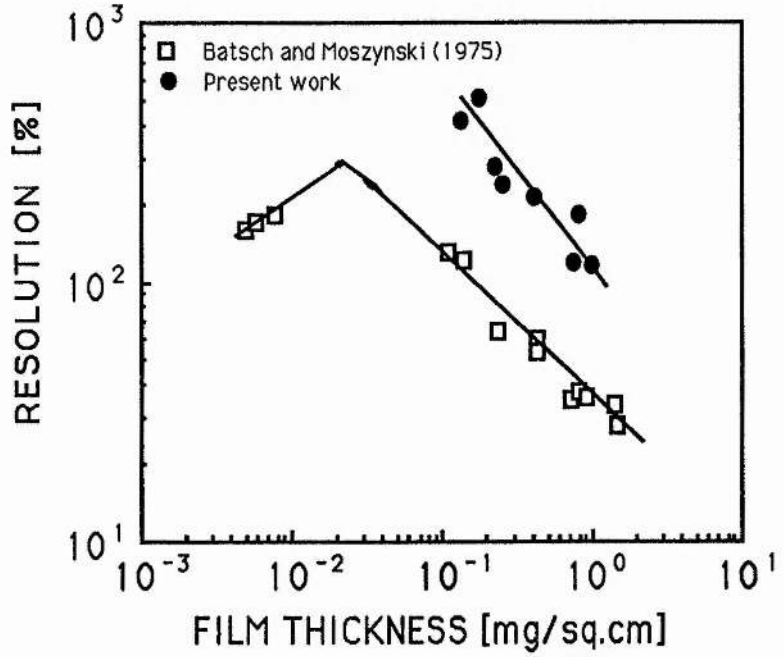


FIGURE 5.21: The TFD response resolution and film thickness.

The results obtained from this investigation is compared to that of Batsch and Moszynski (1975) in figure 5.21. In both investigations, unmoderated $\alpha$-particles and NE102A scintillator films were used. A similar trend in the dependence of the resolution on the film thickness is evident. But, for films of comparable thickness, the present results indicate inferior resolution. There are however differences in the experimental conditions, eg the

photomultiplier, electronics etc. Birks (1964) listed the various factors that might contribute to the broadening of scintillation spectra (see also section 5.7). Of these the light collection system employed plays a fundamentally important role.

The two requirements of a light guide in scintillation counting are optimal light collection and minimisation of the maximum photon transit times in the light guide or reflector relative to the combined photomultiplier transit and scintillation decay time. Both can be satisfied if the shape and size of the mirror ensures only one light reflection between the film and the photocathode. Thus a parabolic mirror with inner diameter similar to the photocathode window is appropriate. The cylindrical mirror was a compromise between these requirements and technical feasibility. A parabolic mirror of 9mm inner diameter could not be machined. Even if it could be obtained, a provision for entrance and exit of the $\alpha$-particles and a holder for the film cannot be facilitated. Thus the present results were obtained using a Perspex block.

Batsch and Moszynski (1975) compared the two light collection systems. They observed that in the case of two Perspex block halves supporting the film, the photons produced in the film were transferred to the photocathode within the scintillator. The photons collection characteristics depended on the optical coupling between the film and the photocathode, the state of the surface of the perspex block in contact with the scintillator film and the quality of the film. In the mirror system, on the other hand, the photons are transferred outside the film. Its characteristics therefore depend on the reflectivity of the aluminium cavity, on its size, on light losses through the edges that rest on the photomultiplier window and through the entrance and exit ports of the beam in the mirror.

The investigators claimed that their aluminium mirror system ensured a twice better scintillation efficiency compared with the perspex block system. Since the resolution is related to amount of light output, with lower light yield the resolution may be poorer. This may be cause of the systematic disparity in the pulse-height resolution of the films as obtained in the present investigation from those of Batsch and Moszynski (1975).

It is noted that the other advantages of the mirror cited by Batsch and Moszynski (1975) are ease of fabrication, simplicity in exchange of films, insensitivity to background radiation and Cerenkov radiation. Clearly these advantages were not exploited in the present setup. Our fundamental consideration in the selection of a photomultiplier with small window is

based on dark count reduction. It is subjective whether it is a misplaced priority.

## 5.6.5. THE EFFICIENCY AND THICKNESS OF THIN FILM DETECTOR.

Various forms of detector efficiency (eg intrinsic, absolute, total, peak, etc) can be defined. Following Batsch and Moszynski (1975) the TFD efficiency, $S_\varepsilon$, is defined as the probability for the release of one photoelectron from the photocathode by a quantum of the radiation energy absorbed in the scintillator.

In the present investigations a quantity proportional to the number of photons emitted per particle passing through a thin plastic film is determined, following Voltz et al (1966) and Geissel et al (1977). It is based on the assumption that only a fraction of the photons emitted by the scintillator is detected by the fast photomultiplier. The number of photons hitting the photocathode are so few that they may be regarded as single photons, each contributing individual electrical pulses at the anode. Hence, the current density is proportional to the light intensity and the photomultiplier can be assumed to have single electron response for a given experimental condition. The efficiency, $S_\varepsilon$, is given by

$$C_c = k . S_\varepsilon$$

$C_c$ is the actual count rate, k is a factor that depends on the counting efficiency, the geometrical arrangements of the counters, but presumably independent of the radiation's nature. Thus if $C_p$ and $C_a$ are, respectively, the coincidence rates in the presence and absence of the scintillator, the true coincidence rate $C_c$ is given by

$$C_c = C_p - C_a$$

The detection efficiency

$$S_\varepsilon = (1/ 2 . \tau_c . k)((C_p - C_a) / C_{SBD})$$

where $C_{SBD}$ is the count rate of pulses stopped in the SBD. The constant, $\tau_c$, is the coincidence resolving time of the MCA. It is observed that for all the experimental runs, the coincidence count rates in the absence of the film are at least three orders of magnitude less than those in the presence of the film. Furthermore the irradiation geometry and coincidence resolving time remains the same. Thus the detection efficiency is proportional

to the ratio of the coincidence count rates in the presence of the film to the frequencies of the particles stopped in the SBD. This ratio is expressed in percentage, and referred to as the 'detection efficiency' in this work:

$$S_e(\%) = (C_p / C_{SBD}).100$$

In the foregoing, the SBD is assumed to have a detection efficiency of 100%. This is acceptable in that the range of α-particles of 5.485MEV in silicon is about 30μm, according to Northcliffe and Schilling (1970), is less than the depletion depth of the SBD (100μm).

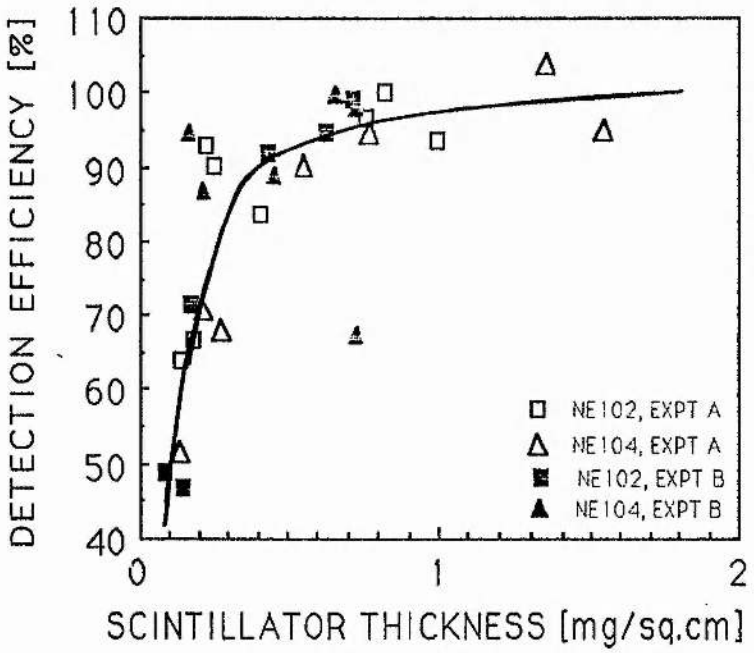


FIGURE 5.22: Detection efficiency and film thickness.

Figure 5.22 indicate the relationship between the detection efficiency of the TFD and the film thickness. For very thin films, the detection efficiency increase rapidly with the thickness, until a saturation value is attained. Like the other parameters investigated in the preceding section, there is no basic difference in the detection efficiency of the two types of plastics.

Some determinations of the scintillation efficiency of the TFD have been reported. Kohl (1975) reported that individual photoelectron peaks could be distinguished in the noise spectrum of the photomultiplier tube, hence he gave the light output in terms of the number of photoelectrons. His results can not therefore be compared with those of the present work. Batsch and Moszynski (1975) determined the average number of photoelectrons released from a given film by comparing the centre of the spectrum of one photoelectron, obtained by illuminating the photocathode with attenuated daylight, with the centre of the spectrum of the alpha particles detected in a given film. It is not clear how they established that the attenuated daylight response spectrum corresponded to a single photoelectron. Their results also cannot be compared with the present work.

The only investigations comparable to the present work are those of Geissel et al (1977). The procedure with which they determined the detection efficiency is similar to the present work. The investigators inferred that the detection efficiency of the scintillators becomes 100% at film thickness of about 200$\mu g/cm^2$, which correspond to an energy loss of 150keV by 5.48MeV alpha particles. In the present set up the maximum detection efficiency of 100% is attained at 0.3$mg/cm^2$ of either NE102A or NE104 films. This corresponds to an energy loss of 280keV based on the stopping power data of Northcliffe and Schilling (1970). Given the differences that may exist in the two investigations, it may be inferred that close agreement is obtained.

## 5.6.6. INCIDENT ENERGY AND RESPONSE CHARACTERISTICS.

Figure 5.23 indicate the response of the TFD as the energy of the natural α-particles is gradually moderated to 0.6MeV, as described in section 5.5.4. NE104 films of $0.5mg/cm^2$ and $1.0mg/cm^2$ were used. The results suggest that the light output increases slightly with the incident energy of the radiation in the range 1 to 3 MeV, thereafter it decreases. Similar results were obtained by Kohl (1975), Muga and Griffith (1973) and Voltz et al (1966) for accelerated α-particles of corresponding energy. It may be observed that at these energies, the light response to the radiation has already attained saturation. Related results for films having thickness greater than the charged particles ranges is given in the following section.

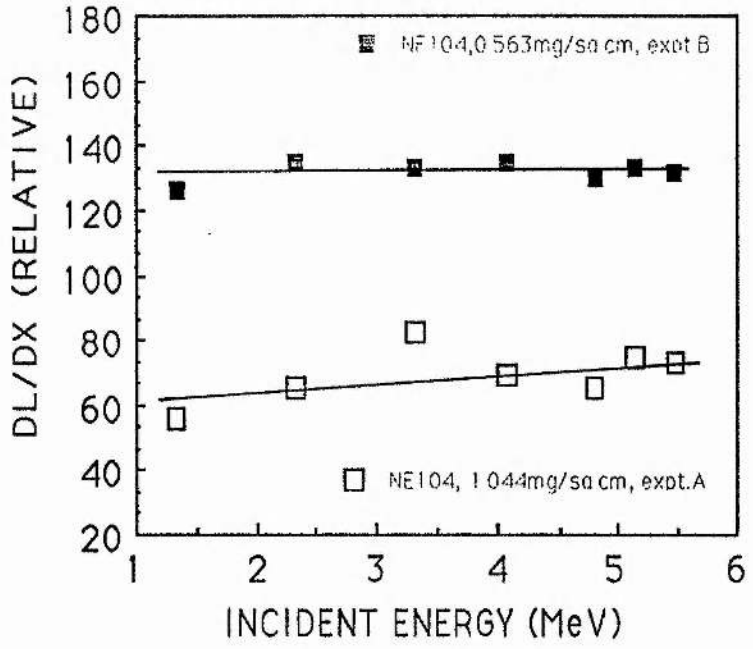


FIGURE 5.23: Relative scintillation efficiency and energy of the radiations.

The relationship between energy loss by the transiting charged particles and their incident energy is given in figure 5.24.

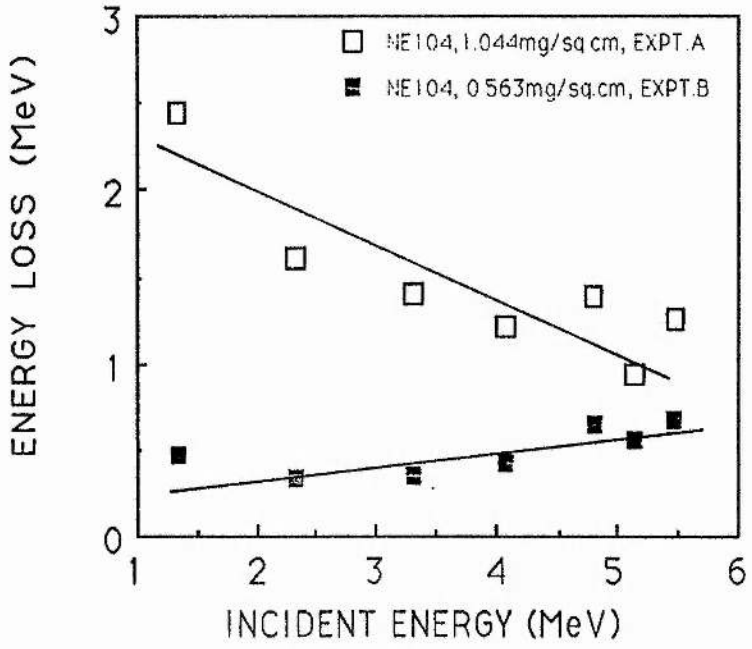


FIGURE 5.24: The energy loss in films and the energy of the radiations.

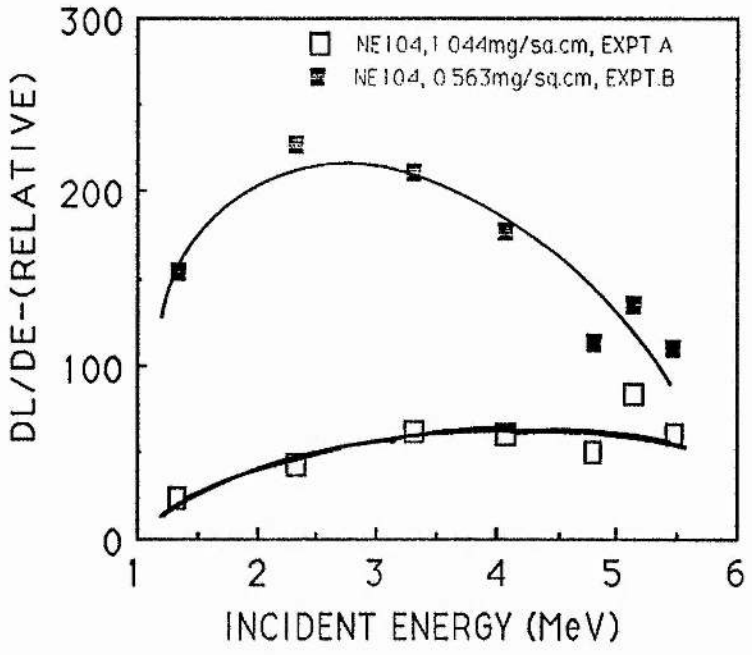


FIGURE 5.25: The relative DL/DE and the energy of the radiations.

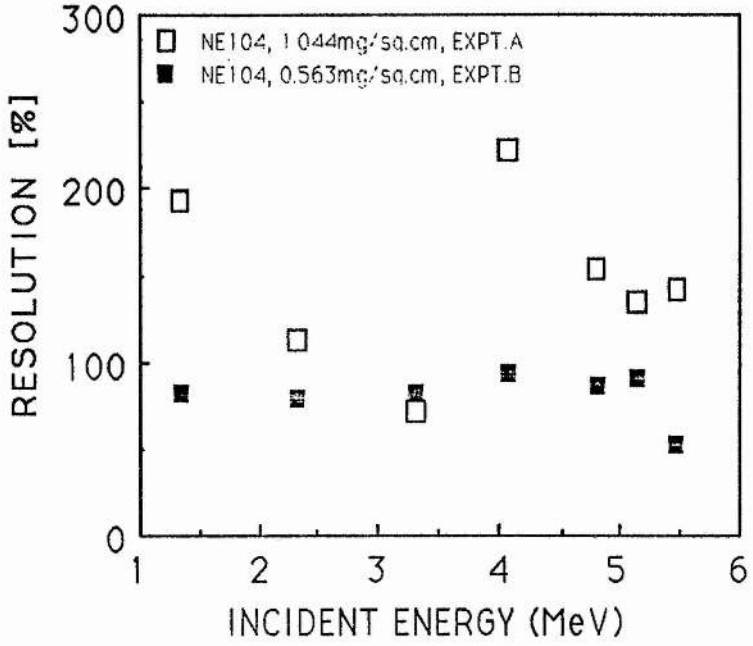


FIGURE5.26: The pulse-height resolution and the energy of the alpha particles.

Figure 5.25 and 5.26 show that the TFD detection efficiency and resolution are independent of the energy of the incoming beam. Thus, the resolution and detection efficiency both depends mainly on the thickness, and therefore on the energy deposited in the scintillator.

## 5.6.7. COMPARISON OF TFD AND CONVENTIONAL SCINTILLATOR DETECTOR.

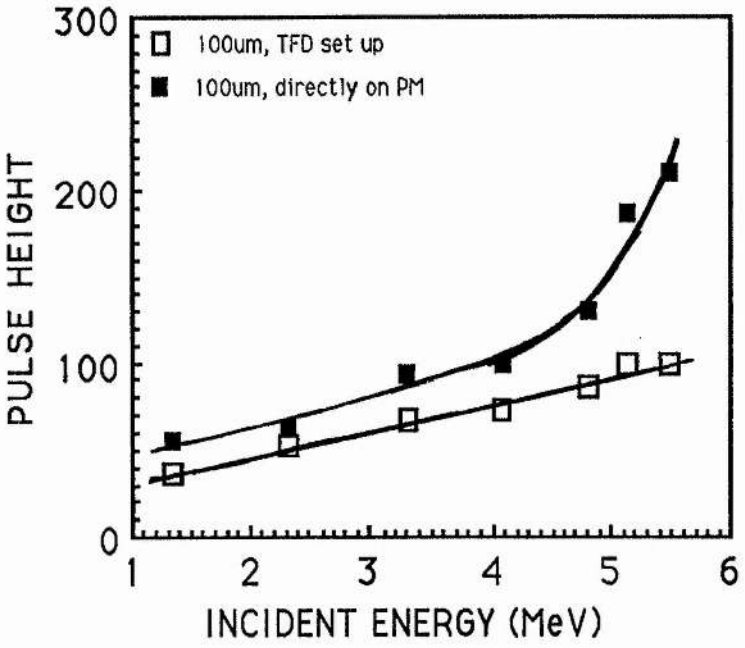


FIGURE 5.27: Light response of a film in the TFD set up compared with that directly laid on the PM.

In general, the light response of the conventional size phosphors is much better than those of the TFD, indeed the gain of the external linear amplifier had to be reduced to 45 (and the bias to 1.8kV). Figure 5.27 compares the pulse height response of 100μm NE102A laid directly on the photomultiplier (Set up A), with that of the TFD arrangement. The corresponding plot for a 50μm film is given in figure 5.28. It appears that the difference in the light output of the two arrangements is small for α-particles having energies between 1 and 3MeV. However the difference is significant for more energetic α-particles. Greastest difference is obsereved for unmoderated α-particles, for which the film laid dirctly on the photomultiplier gives twice as much light ouput as the film in the TFD arrangement.

At the energies considered, the ranges of the α-particles are less than the thickness of the films, hence all the energies of the incoming radiation are deposited within the films. Since the same scintillator was used, it can be taken that the intrinsic conversion efficiency of the energy deposited into luminescent output remains the same for a given incident energy. The difference in the light output can therefore arise only from the differences in the geometries of the two detectors. In the TFD only the bottom edge of the film and the

perspex block are in optical contact with the photomultiplier window. Thus, the transfer of light depends on the optical quality of the perspex block, the homogeneity of the scintillator film and the relative significance of light emission from the different sides of the scintillator.

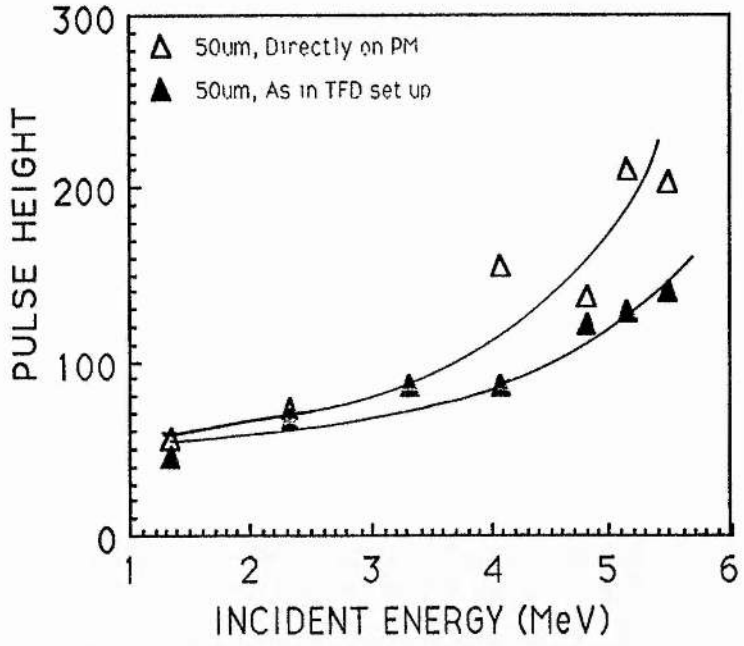


FIGURE 5.28: The light response of TFD set up compared with that directly laid on the PM.

The investigations of Bendisciolli et al (1984) reveal that when a 10μm film of NE104 is exposed to accelarated protons, 75% of the light is emitted from two faces of the scintillator film. The same may apply to the present situation. Thus the collection of light in the TFD geometry depends on the optical contact between the film and the perspex block, and between the block and the photomultiplier window and on the quality of the perspex. On the other hand, for a film laid directly on a silicone smeared photomultiplier window, these were avoided, and most of the light emmitted fom the face of the film is transferd directly to the window of the photomultiplier, and consequently a higher light output is obtained.

When the same data is used to compare the luminescent yield of 50μm and 100μm films held in the TFD arrangement the results (figure 5.29) differ. The thinner film yields more light per absorbed energy than the thicker film. The difference in the light output increases with the increase of absorbed energy. For the unmoderated natural α-particles, the 50μm

film gives as much light as the 100μm film. This observation is consistent with the contentions made in the preceeding section. It shows that if the film's thickness exceeds the range of the radiation, then the unpenetrated portion of the scintillator does not contribute to the light production, as expected, rather it weakens it through absorption.

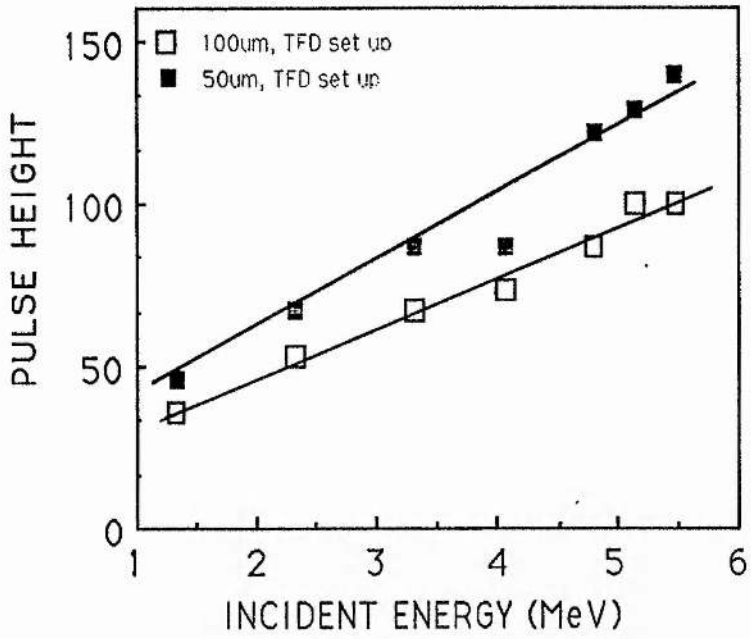


FIGURE 5.29: The light output of a 50um and100um thick films, in the TFD set up, as the incident energy is varied.

The same data indicate (figure 5.30) that there is no difference in the light output of 50μm and 100μm films if either is laid directly on the photomultiplier. This suggests that for the case that the film is laid directly on the photomultiplier, if the thickness of the film exceeds the range of the incident radiation, the light output from the scintillator remains the same.

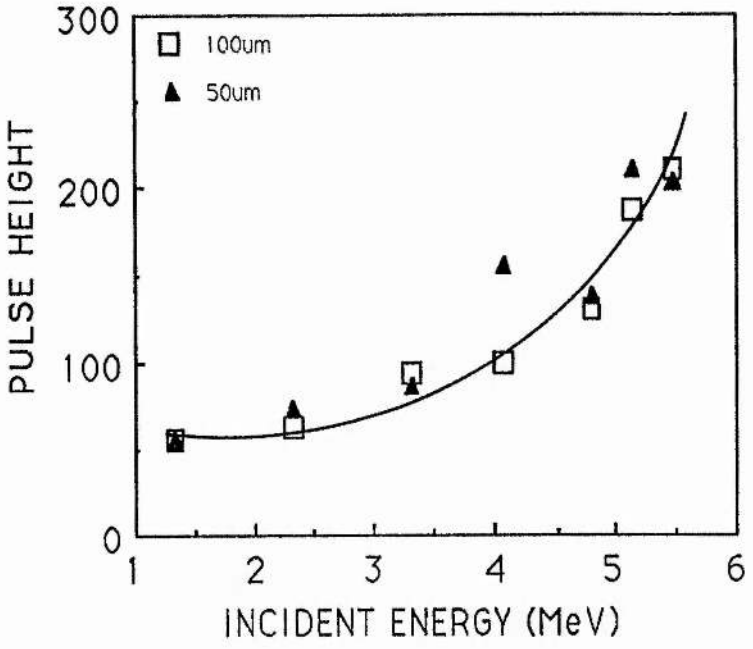


FIGURE 5.30: The light output of a 50um and a 100um thick films, laid directly on the PM, as the incident energy is varied.

## 5.7: THIN FILM DETECTOR AND UNIFIED DOSIMETRY.

The requirements of an ideal detector for the unified system of radiation dosimetry are enumerated in section 3.1. In the following the use of a thin film plastic scintillator (TFD) as a single-detection volume and as a twin- detection volume detector is discussed.

a) PHASE: The main constituent of cells is liquid water; the intranuclear DNA is a colloid. Mammalian tissue is usually regarded as solid. Thus the solid plastic phosphors satisfy the need for a detector in condensed phase.

b) TISSUE EQUIVALENCE: The main constituents of some plastic scintillators are carbon and hydrogen. In some scintillators, eg NE102 (see Table 4.2) there is also oxygen and in others nitrogen. Thus, elemental tissue tissue equivalence is also satisfied approximately.

c) DETECTOR VOLUME: It is shown in section 5.1 and 5.2 that solid films as thin as $0.05 mg/cm^2$ (about $0.5 \mu m$) can be readily made using commonly available laboratory

materials, and be easily mounted in the chamber. Films having thickness about 0.05μm were also made but could not be mounted in the chamber due to their low tensile strength, but suggestions with regard to improvement were given (section 5.1.2). Thus the present results showed that condensed phase detector of 0.5μm sensitive volume (microdosimeters) is at hand and those of 50nm (nanodosimeters) can be practically realised with some improvements in the film fabrication technique and electronics.

d) LINEARITY BETWEEN LIGHT OUTPUT AND ENERGY DEPOSITED: It was shown in sections 5.6.2 and 5.6.6 that the light response of the TFD is proportional to the energy deposited in the film, at least for the energies of the alpha particles and thicknesses of the films considered in the present investigation. However more extensive investigations (see section 4.2) with different types of accelerated ions having a wider range of energies indicate that the fluorescence response of organic scintillators is a nonlinear function of the ion energy. For ions fully stopped or transiting through the plastic film, the light output saturates with increases in ion energy. That the saturation of specific luminescence, dL/dx, at high stopping power, dE/dX, depends on the ion type is one of the main hindrances in the use of scintillators as a single or twin volume dosimeters. For linear correlation between the charged particles mean free path and the response will not be achieved in a radiation field comprising ions of two or more different types for at least one of the different ions will saturate before the others.

e) LIGHT LOSSES: The absolute light output was not measured in the present investigation, and there is scarcity of relevant published data. It is reported (Wright, 1984) that the mean energy required to produce photoelectrons from conventionally sized films of NE102A and Pilot B optically coupled to a photomultiplier is about 1.5keV. This is 30 times greater than the mean energy required to produce an ion pair in a gas. But, the investigations of Batsch and Moszynski (1975) indicate that the energy required to produce a useful photoelectron from films of NE102A (and NE111) of thickness in the range $0.02mg/cm^2$ to 2mm, with the TFD, varies with the thickness but is within the range 18keV to 32keV. Thus the mean energy required to produce a useful photon in the TFD is 17 times greater than that required in the conventional scintillation detector arrangement. The experimental conditions differ hence conclusive deductions cannot be made. Nonetheless, this appears to suggest that considerable amount of light losses occur in between its production and conversion at the photocathode in the thin film detector set up. This is believed to be one of the main limitations of the TFD as a practical radiation

nanodosimeter or microdosimeter.

f) DETECTION EFFICIENCY: It is determined (section 5.6.5) that the thin film plastic scintillator can detect every particle stopped in the surface barrier detector (that is its detection efficiency attains a 100% level) at minimum thickness of 0.3mg/cm$^2$. This represents an energy loss of 0.3MeV by the $\alpha$-particles (of 5.485MeV) in the film. Thinner films (0.05-0.3mg/cm$^2$) have very low detection efficiencies but produce detectable light nonetheless.

The observation (section 5.6.5) that the minimum thickness of the plastic scintillator that can give a 'complete' spectrum is 0.05mg/cm$^2$ means that a minimum energy deposition of 56keVis required to produce a quantifiable response with the TFD set up.

g) RESOLUTION: In microdosimetry and nanodosimetry interest is in the measurement of both the mean energy deposited and the stochastic of energy deposition within a specified site. To achieve the latter, it is required of a potential detector have negligible or small inherent fluctuations. In the case of TFD, apart from energy loss straggling in the film, the stochastic of response arises from the following.

1. Statistics of secondary electron emission from the photocathode.
2. Variations in the proportion of light collected from different parts of the scintillator film.
3. The reflections and transmissions of photons in the mirror or light guide.
4. Variations in the number of secondary electrons due to thermionic emission.
5. Current nonlinearity in the voltage divider network.

The main causes of disparity in light output from different portions of a film are nonuniformities in the thickness and inhomogeneity in the composition of the scintillator. Given that a good fabrication method is used, and precautions taken such as careful stirring of the scintillator solution (section 5.1), the contribution of energy loss straggling due to film inhomogeneities can be minimised. Another expidient measure is to expose only small portions of the film to a well collimated beam. Variations due to multiple reflections of the light photons in the mirror or due to absorption in the perspex block can be decreased by using, respectively a well polished mirror and a short, optical grade Perspex block.

Thermionic emission depends on the photocathode and the temperature at which the

photomultiplier is operated. Because of the small area of the photomultiplier's photocathode (section 5.3) and that the present investigations were carried out at room temperature (section 5.5.3) these can be neglected. Similarly current nonlinearity due the instability of the high voltage supply to the photomultiplier and to high anode currents (section 5.3.2) are insignificant. Thus, the main source of inherent detector response fluctuations is in SEE from the photocathode. This is a fundamental limitation analogous to charge multiplication near the anode wire in gas based proportional counters.

h) SIGNAL TO NOISE RATIO: It was shown in section 5.6.1 that the coincidence gate of the MCA with pulses stopped in the SBD reduces the dark count significantly. However casual coincidences cannot be eliminated completely, and the effectiveness of the technique depends on the response times of the two detectors and the coincidence resolving time. In the present investigations a 2μs delay was applied to the photomultiplier channel in consideration of the delay introduced by the single channel analyser; the combined response time of the photomultiplier and the scintillator is about 50ns. The consequent use of a long coincident resolving time is not significantly detrimental considering that the elimination of photomultiplier noise or background count rate minimises one of the main contributors to the variation in the light production. Alternative methods (discussed in section 5.8) of reducing the dark count such as cooling, are most probably less effective. Thus improvement in the potential of TFD of nanometers in thickness can only be attained by the enhancement of the light output relative to the noise.

## 5.8: ENHANCEMENT OF THE LUMINESCENT RESPONSE

The foregoing results and discussions indicate that the main limitation of TFD in radiation microdosimetry and nanodosimetry is the loss of light produced from the film as a consequence of radiation perturbation, before it is collected and converted into secondary electrons by the photocathode. These losses reduces the photo-conversion efficiency of the TFD. Methods of redeeming the situation are required. The use of an optical grade perspex block or an aluminium mirror on a photomultiplier with a wider window may decrease the losses but offers no significant improvement.

The cooling of the photomultiplier is inconvenient, and will provide little improvement as

most of the pulses due to thermionic emission will occur in anticoincidence with pulses detected by the SBD. The pulse amplitude depends on the time constant, $\tau = R.C$, of the anode output circuit; where R and C are the effective load resistance and capacitance, respectively. The latter is determined mainly by the stray capacitance and may not be varied at will. Various load resistances were tried. None increased the pulse amplitude without accompanied pulse accumulation and distortion.

Figure 5.7 indicates that the peak quantum efficiency of the spectral response of bialkali photocathode did not precisely match the wavelength of the peak of the scintillators. However the same figure also indicates that even if a wave shifter is added to the scintillators, the improvement in the light output would hardly exceed 3%. The other photocathode material, S20, has an absorption peak that matches those of the scintillators (450nm) but with reduced (4%) quantum efficiency. Thus it offers no overall improvement. The use of a fused silica window, in contrast to glass, will extend the range of response of the bialkali cathode up to 200nm. It is however irrelevant, in that it is beyond the response range of the scintillators.

With technological advance, the threshold limits of the electronic components, the photomultiplier window and the photocathode may be decreased but none are the panacea to the problem. The fact that films less than 100nm can also give a detectable signal, but with an incomplete spectrum indicate that the real remedy is the amplification of the luminescent response. Attempts were made to achieve this through electrostatic means. An electric field was gradually applied across a 0.6mm thick NE102A scintillator optically coupled to a photomultiplier. The response of the scintillator to $\alpha$-particles was observed as the voltage was gradually increased. No change in the response was observed for fields up to 1.0kV/cm, at which sparks were generated. It is probable that the negative results and the occurrence of the sparks may be due inappropriateness of the electrodes used (copper wires). In the future this approach requires further considerations with better electrodes and perhaps other scintillators.

# CHAPTER SIX

# CONCLUSIONS AND SUGGESTIONS FOR FUTURE WORK

Summarised in the following are the inferences made in this work and list of suggestions for future investigations.

## 6.1 INFERENCES MADE IN CHAPTER TWO.

It was shown in chapter two that the induction of biological damage per unit dose can neither be expressed as a simple function of the $L_D$ (figure 2.3) nor of the $L_T$ (figure 2.2). The poor correlation, it was inferred, indicated a non reliability of the present radiation dosimeric system as based on the concepts of RBE and LET in fulfilling its expected role of determining the likely consequences of radiation exposure.

It was determined that the charged particle fluence, or its inverse, the effect cross section ($\sigma_e$) for the induction of the endpoints can be correlated with the $L_D$ (figure 2.5), or with the $L_T$ (figure 2.6, 2.8, 2.9) , or with the $I_i$ (figure 2.7, 2.10, 2.11, 2.14, 2.15 and 2.16) of the charged particles. The parameter $I_i$ was assessed to be more convenient for biophysical analyses because of its ability in showing the following, which were not indicated by figures 2.5, 2.6, 2.8, and 2.9.

The curves correlating $\sigma_e$ with $I_i$ indicates a biphasic behaviour, the $\sigma_e$ initially increase with $I_i$, until $I_i$ is about 1.8nm, thereafter the $\sigma_e$ no longer increase or increase but less rapidly with further increase in $I_i$. It was inferred that the matching of the mean free path ($\lambda$) of the charged particles at which the point of inflection occurred with the mean inter strand distance of DNA indicates that dsb of the DNA is the common critical lesion involved in the induction of the different end points.

The curves correlating $\sigma_e$ with $I_i$ indicated that ions and neutrons radiations are by order of magnitude more damaging than photons and electrons of equal $I_i$. This was observed for all the endpoints considered and was independent of the ion type.

Radiation damage was inferred to be through intra track action of the pertinent charged particles in the cell nucleus. Electrons were shown to be capable of just attaining saturation at $I_i = 0.55$ per nm. The damage per δ–ray were shown to be disproportionately less than the energy of the δ–rays. It was attributed to the transport of energy out of the cell nucleus by the δ–rays and that although they secondary electrons can induce single strand breaks, they have low efficiency of inducing dsb in the nuclear DNA through intra-track action.

## 6.2 INFERENCES MADE IN CHAPTER THREE.

A new system of radiation dosimetry (termed as unified dosimetry, and shortened as unidosimetry) was proposed. It was based on the observation that for each the biological endpoints considered in chapter two an Absolute Biological Effectiveness (ABE) for damage by the relevant charged particles can be defined as

$$ABE = \frac{\sigma_e}{\sigma_g} = \left[1 - e^{-\lambda / \lambda_o}\right] \Phi_z \cdot \sigma_g^{-1}.$$

Where $\lambda_o$, about 1.8nm, is the mean inter-strand distance of the DNA. $\sigma_g$ is the effect cross section for the induction of the endpoint by electrons or photons radiations with mean free path of $\lambda_o$. Two features of the proposed system are its ability to unify the biological effectiveness of radiations in a manner that is independent of the ion type (section 3.1.2) and its non requirement for radiation quality parameter.

The main physical requirements for its instrumentation (named as unidosimeter) were outlined. The unidosimeter should emulate (and quantify) the induction of dsb in the DNA segments at risk. It should consists of two tissue equivalent (TE) detectors, each of 1nm thickness, separated at a distance of 2nm. The twin-detector should operate in time coincidence and have a high sensitivity at least to radiations interactions that may be sufficient for the induction of a single strand break (about 30eV). The unidosimeter is also

a nanodosimeter in the sense that its sensitive volume is in order of nanometers.

The feasibility for its realisation using one or more of the various systems of radiation detection was assessed. It was inferred that such a dosimeter can hardly be obtained from the gas based detectors, mainly due geometrical factors. Superconductive detectors, the Josephson junctions in particular, have the geometric form and the required sensitivity. But there are the inconvenience of its sensitivity to heat and magnetic fields, the high atomic weights of most superconductor materials, which hinders the attainment of tissue equivalence, and that the superconductors are fabricated on a substrate whose role in radiation detection is not clear.

Other detection systems such as thermoluminescence, radiophotoluminescence, secondary electron emission were determined unsuitable due to poor sensitivity, in compactabilty of their operational mechanism with the induction of dsb through intra-track action and geometrical factors.

It was shown that the use of submicron thick films of semiconductors in the form of two transmission detectors operating in time coincidence is handicapped by leakage currents, unless the submicron semiconductors were made in the form of rectifying junctions. It was deduced that (doped) organic semiconductors appeared to have the best potentials, although such materials are not yet available in physically characterised form as may required for detector construction.

## 6.3 INFERENCES MADE IN CHAPTER FOUR.

A correlation, independent of the ion type of specific luminescence ( proportional to the cross section for light production) with the charged particle's mean free path was not obtained. It was inferred that ionisation quenching, the process that leads to the saturation of luminescence response, differs from the radiobiologically known saturation of RBE with LET. The results, it was inferred indicated that the induction of light from a phosphor by radiation differ fundamentally from the induction of dsb in the cell. The former is a single hit process, the latter involves the induction of coincident single strand breaks in two DNA strands laying close together.

It was shown that unlike the induction of biological damage (figures 2.12 and 2.13) δ-rays are efficient light producers. This was attributed to the fact the energy deposition per event by electrons are just sufficient for population of the $S_{10}$ singlet states without populating other states whose decay are radiationless. The heavy ions generate a number of delta rays but the accompanied higher energy loss per event which leads to the population of states with radiationless decay makes the heavier ions less efficient light producers than electrons and lighter ions of the same energy.

The fact electrons are more efficient light producers than ions at the same energy and that saturation of specific luminescence depends on the ion type were suggested as the fundamental limitations to use of phosphors as system of instrumentation in unidosimetry. For it contradicts the mechanism of biological damage as determined in chapter two.

## 6.4 INFERENCES MADE IN CHAPTER FIVE.

The experimental investigations have shown that by using coincidence techniques, the plastic scintillators can be used as single volume microdosimeters (0.1-10μm thick). Its use as a single detection volume nanodosimeter is handicapped by

(a) its weak tensile strength, but suggestion on circumventing this limitation was made.

(b) inherent weakness of the light response, which can be minimised with better photomultipliers and electronic interface.

(c) light losses in the detector assembly, which may not reduced.

It was determined that the minimum energy loss that can give a quantifiable signal in the thin film detector assembly is 56keV. This poor sensitivity is another factor indicative of the unsuitability of the plastic scintillators for instrumentation of proposed system of dosimetry.

However, the technique developed for the fabrication of high quality films can be used in fabricating organic semiconductors (see section 6.2) in future investigation.

## 6.5 SUGGESTIONS FOR FUTURE INVESTIGATIONS.

A closer examination of the saturation cross section need to be made. A first hand appraisal of its magnitude suggests that it may be associated with the net size of the DNA genome whose damage may lead to the expression of the particular end point. In the case of 6-TG$^r$ mutation induction in mammalian cells estimates based on the amount of DNA bases in a cell showed about equal to the the estimated size of the HGPRT gene as determined by Monte Carlo simulation (Goodhead, 1987) and estimates based on the target theory (Fuscoe et al 1987). It can be surmised that from the fact that the saturation cross section for cellular transformation is greater than those of mutation induction suggests that oncogenic transformation may not arise from mutations.

The present results showed that radiations are most damaging when their $I_i$ is about 0.55 per nm. It can be predicted that for radiotherapy optimal efficiency of the radiations will be obtained when the relevant charged particles have energies that satisfies this requirement. Oxygen effects have always been a factor for consideration in radiotherapy treatment. An extension of the present analyses to data on the induction of different endpoints under anoxic and oxygenated conditions could be of value for cancer treatment.

In the calculations of the physical data for neutrons the role of the heavier recoils has been neglected (section 2.4), in more detailed calculations their contribution needs consideration.

In the 'distance' version of the 'Dual Theory of Radiation Action' (Kellerer and Rossi, 1978) the parameter proximity function which depend on the type of the radiation was introduced. The relationship between the parameter and the linear primary ionisation need to be established. It may turn out that there are the same.

The multistep avalanche counter (MSAC) described in section 3.2.6 can be developed for measurement of delta-rays radial extension, linear primary ionisation, and for for ionisation cluster counting.

Given that the limitations identified in the use of plastic scintillators can be overcome, and appropriate wave shifters can be obtained, then consideration can be made for developing it into a dsb counter as required for unified dosimetry. The counter may consist of three layers of plastic films laminated together. The outer two layers being 1nm thick and emits nearly monoenergetic photons of widely different wavelength, say in the infrared and in the ultraviolet region. The middle layer of about 2nm thick, can be a plastic with poor

scintillation and light transmission properties. The laminated film can be coupled to a photomultiplier with high sensitivity in the infrared at one end, and another photomultiplier with high sensitivity in the ultraviolet region at the other end. An appropriate stopping detector, as in the thin film detector can be used, and the three should be operated in time coincidence.

With the organic semiconductors, identified to have good potentials for instrumentation for unified dosimetry it is suggested that physical characterisation, identification of appropriate organic compounds and methods of rectifying the organic materials deserves future investigations.

# REFERENCES

AJITANAND, N. N. and K. N. IYENGAR. 1976. On the technique of preparation of high quality thin film scintillators. *Nucl. Instr. Meth.*, **133**, 71-74.

AL-AFFAN, I. A. M. 1989. Calculated effective stopping powers and projected ranges for H, He, C, N, and O projectiles (0.05-500KeV) in some elements and materials of dosimetric interest. South Bank Polytechnic, London SE1 0AA.

AL-AHMAD, K. O. 1984. Ph.D Thesis, University of Dundee, Dundee, U.K.

AL-AHMAD, K. O. and D. E. WATT. 1984. Stopping powers for low energy electrons (< 10KeV) in solid polyethylene. *J. Phys. D: Appl. Phys.*, **17**, 1899-1904.

ALPER, T. 1970. Mechanisms of lethal radiation damage to cells. IN: Proc. Second Symp. on Microdosimetry. (H.G. Ebert, editor).pp 5-36. EURATOM, 14452 d-e-f.

ALPER, T. 1979. Cellular Radiobiology. Cambridge University Press, London.

ANDERSEN, H. H. and J. F. ZIEGLER. 1977. Stopping powers and ranges in all elements. Volume 4 of the Stopping and Ranges of Ions in Matter. Pergamon Press. New York.

ASHLEY, J. C. 1982. Stopping power of liquid water for low energy electrons. *Radiat. Res.*, **89**, 25-31.

BARENDSEN, G.W. 1964. Impairement of the proliferative capacity of human cells in culture by α-particles with differing linear energy transfer. *Int. J. Radiat. Biol.*, **8**, 453-466.

BARENDSEN, G. W., and J. F. GAISER. 1985. Cell transformation i*n-vitro* by fast neutrons of different energies: Implications for mechanisms. *Radiat. Prot. Dosim.* **13**, 145-148.

BARENDSEN, G. W., C. J. COOT, G. R. van KERSEN, D. K. BEWLEY, S. B. FIELD and C. J. PARNELL. 1966. The effect of oxygen on the impairement of the proliferative capacity of human cells in culture by ionising radiations of different LET. *Int. J. Radiat. Biol.* **10**, 317-327.

BARJAKTAROVIC, N.and J. R. K. SAVAGE. 1980. R.B.E. for d(42MeV)Be neutrons based on chromosome type abberations induced in human lymphocytes and scored in cells at first division. *Int. J. Radiat. Biol.*, **37**, 667

BARONE, A., and S. DE-STEFANO. 1982. More on the possibilities of nuclear Radiation detection by superconductors. *Nucl. Instr. Meth.*, **202**, 513-514.

BARONE, A., S. DE-STEFANO and K. E. GRAY. 1985b. Superconductive Detectors. *Nucl. Instr. Meth. Phys. Res.*, **A235**, 254-265.

BARONE, A., G. DARBO, S. DE-STEFANO, G. GALLIANANO, A. SIRI, R. VAGLIO and S. VITALE. 1985a. Superconductor Nb-$Nb_xO_y$-Pb Tunnel Junctions as high resolution detectors for nuclear spectroscopy: Preliminary Results. *Nucl. Instr. Meth. Phys. Res.*, **A234**, 61.

BATSCH, T. AND M. MOSZYNSKI. 1975. Pulse-height resolution of thin film scintillator foils. *Nucl. Instr. Meth.*, **125**, 231-236.

BATSCH, T. AND M. MOSZYNSKI. 1975B. Timing properties of thin scintillator foils. *Nucl. Instr. Meth.*, **123**, 341-352.

BAUCHINGER, M., E. SCHMID and J. DRESP. 1979. Calculation of the dose-rate dependence of the dicentric yield after Co-γ irradiation of human lymphocytes. *Int. J. Radiat. Biol.*, **35**, 229-233.

BECCHETTI, F. D., C. E. THORN and M. J. LEVINE. 1976. Response of plastic scintillator detectors to heavy ions, $Z \leq 35$, $E \leq 170$MeV. *Nucl. Instr. Meth.*, **138**, 93-104.

BETTEGA, D., S. DUBINI, A. M. FUHRAM-CONTI, T. PELUCCHI, and H. TALLONE-LOMBARDI. 1981. Chromosome aberrations induced by protons up to 31Mev in cultured human cells. *Radiat. Enviro. Biophysics*, **19**, 91-100.

BENDISCIOLI, G., V. FILIPPINI, C. MARCIANO, A. ROTONDI and A. ZENONI. 1984. Performance of a thin scintillator detector. *Nucl. Instr. Meth. Phys. Res.*, **227**, 478-482.

BENGSTON, B. and M. MOSZYNSKI. 1974. Energy transfer and light-collection characteristics for different types of plastic scintillators. *Nucl. Instr. Meth.*, **117**, 227-232.

BELLI, I. M., R. CHERUBINI, S. FINOTTO, G. MOUCHINI, O. SAPORA, G. SIMONE and M. A. TABOCCHINI. 1989. RBE-LET relationship for the survival of V79 cells irradiated with low energy protons. *Int. J. Radiat. Biol.*, **55**, 93-104.

BENGTSSON, L. G. 1970. Assessment of dose equivalent from fluctuations of energy deposition. IN: Proc. Second Symp. Microdosim. (H. G. Ebert, editor). EUR 4452. pp 375-379. Brussels.

BERGMAN, G. 1984. Weak localization in thin films. *Physics Reports* **107**, 1-58.

BEWLEY, D. K. 1968. Fast neutrons - LET distributions and the response of mammalian cells. IN: Panel on Biophysical Aspects of Radiation Quality, Second Panel Report. pp 65-85. IAEA. Vienna.

BIRKS, J. B. 1964. *The Theory and Practice of Scintillation Counting*. Pergamon Press. Oxford. 1964.

BURLIN, T. E. 1974. The characteristics of secondary electron emission and some potential applications to microdosimetry. IN: Proc. Fourth Symp. Microdosimetry. (J. Booz et el, editors) Commission European Communities. Brussels. Belguim. EUR-51222-d-e-f. pp 35-58.

BURLIN, T. E., D. M. J. BENSTOCK AND M. HADDOW. 1972. A twin volume

apparatus for microdosimetric studies. IN: Proc. Third Symp. Microdosimetry. (H.G. Ebert, editor) Commission European Communities. Brussels. Belguim. EUR-4810 d-f-e. pp 657-674.

BLOHM,R. and D. HARDER, 1985. Restricted LET: Still a good parameter of radiation quality for electrons and photons. *Radiat. Protect. Dosim.*, **13**, 377-381.

BOAG, J. W. 1975. Time scale in Radiobiology. IN: *Radaition Research*. Fifth Int. Congress of Radiation Research, Seattle, 1974, (Nygard et al, editors). Academic Press. pp. 9-29. London.

BOHNE, L., T. COQUERELLE, and U. HAGEN. 1970. Radiation sensitivity of bacteriophage DNA. II. Breaks and cross-links after irrradiation in-vivo. *Int. J. Radiat. Biol.*, **17**, 205-215.

BRANNEN, E. and G. L. OLDE. 1962. The response of organic scintillators to electron energy deposited in them. *Radiat. Res.* **16**, 1-6.

BRENSKIN, A., G. CHARPAK, S. MAJEWSKI, G. MELCHART, G. PETERSEN and F. SAULI. 1979. The multistep avalanche chamber: A new family of fast, high-rate particle detectors. *Nucl. Instr. and Meth.*, **161**, 19-34.

BROOKS, F. D. 1979. Development of Organic Scintillators. *Nucl. Instr. Meth.*, **162**, 477-505.

BROOKS, F. D., W. A. CILLIERS and D M. S. ALLE. 1985. Response of thin NE102A scintillator films to fission fragments. *Nucl. Instr. Meth. Phys. Res.*, **A240**, 338-342.

BRYANT, P. E. 1984. Enzymatic restriction of mammalian cell using PvuII and BamHI: evidence for the double-strand break origin of chromosomal aberrations. *Int.J. Radiat. Biol.* **46**, 57-65.

BRYANT, P. E. 1985. Enzymatic restriction of mammalian cell DNA : evidence for double-strand breaks as potentially lethal lesions. *Int.J. Radiat. Biol.* **48**, 55-57.

BUDD, M. and R. K. MORTIMER. 1982. Repair of double- strand breaks in temperature conditional radiation-sensitive mutant of saccharomyces cerevisiae. *Mutat. Res.* **103**, 19-24.

BUTTS, J. J. and R. KATZ 1967. Theory of RBE heavy ion bombardment of dry enzymes and viruses. *Radiat. Res.* **30**, 855-871.

BURKI, H. J. 1976. Critical DNA damage and mammalian cell reproduction. *J. Mol. Biol.*, **103**, 599-610.

CANNELL, R. J. and D. E. WATT. 1985. Biophysical mechanisms of damage by fast ions to mammallian cells *in vitro*. *Phys. Med. Biol.*, **30**, 255-258.

CHADWICK, K. H. and H. P. LEENHOUTS. 1981. The Molecular Theory Of Radiation Biology (Heidelberg: Springer-Verlag).

CHARPAK, G. and F. SAULI. 1978. The multistep avalanche chamber: A new high-rate,

high-accuracy gaseous detector. *Physics Letters.*, **78B**, 523-528.

CHATTERJEE, A. and J. L. MAGEE. 1985. Theoretical investigation of the production of strand breaks in DNA by water radicals. *Radiat. Prot. Dosim.*, **13**, 137-140.

CHEN,C. Z. and D. E. WATT. 1986. Biophysical mechanism of radiation damage to mammalian cells by γ-and x-rays. *Int. J. Radiat. Biol.* **49**, 131-142.

CLEAVER, J. E., 1977. Induction of thioguanine and ouabain ressistant mutants and single-strand breaks in the DNA of chinese hamster ovary cells $^{3}$H-thymidine. *Genetics* **87**, 129-138.

COLAUTTI, P., M. CUTAIANA, M. MAKEREWICZ, H. SCHRAUBE, G. TALPO, and G. TORNIELLI. 1985. Neutron microdosimetry in simulated volumes less than 1μm in diameter. *Radiat. Prot. Dosim.*, **13**, 117-121.

COLE, A., R. E. MEYN, R. CHEN, P. M. CORRY, W. HITTELMAN. 1980. Mechanisms of cell injury. IN: *Radiation biology in cancer Research*, edited by R. E. Meyn and H. R. Withers. New York: Raven Press, 33-58.

CORMIER, T. M. R. S. GALIK, E. R. COSMAN and A. J. LAZZARINI. 1974. Performance of a heavy-ion time-of-flight spectrometer. *Nucl. Instr. Meth.*, **119**, 145-150.

COX, R. and W. K. MASSON. 1978. Do radiation induced thioguanine-ressistant mutants of cultured mammalian cells arise by HGPRT gene mutation or X-chromosome rearrangements? *Nature (London), 276*, 629-631.

COX, R., J. THACKER and D. T. GOODHEAD. 1977a. Inactivation and mutation of cultured mammalian cells by aluminium characteristic ultrasoft X-rays. II. Dose response of chinese hamster and human dipliod cells to aluminium X-rays and radiations of different LET. *Int.J. Radiat. Biol.* **31**, 561-567.

COX, R., THACKER, J., GOODHEAD, D. T., and R. J. MUNSON. 1977. Mutation and inactivation of mammalian cells by various ionizing radiations . *Nature (London), 267*, 425-427.

CRITTENDEN, E. C. Jr and D. E. SPIEL. 1971. Superconducting thin film detector of nuclear particles. *J. Appl. Phys.*, **42**, 3182-3188.

DEARNALEY, G. and D. C. NORTHROP. 1963. Semiconductor counters for nuclear radiations. Spon. London.

EDWARDS, A. A., R.J.PURROT, J. S. PROSSER and D. C. LLOYD. 1980. The inductionof chromosomal aberrations in human lymphocytes by alpha radiation. *Int.J. Radiat. Biol.* **38**, 83-91.

EDWARDS, A. A., LLOYD, D. C., PROSSER, J. S., FINNON, P., and J. E. MOQUET, 1986. Chromosome aberrations induced in human lymphocytes by 8.7 MeV protons and 23.5 MeV helium-3 ions. *Int.J. Radiat. Biol.*, **50**, 137-145.

EDWARDS, A. A., D. C. LLOYD and J. S. PROSSER. 1985. The induction of chromosome aberrations in human lymphocytes by accelarated charged particles. *Radiat.*

*Prot. Dosim.*, **13**, 205-209(1985).

EGG ORTEG, Oak Ridge Technical Enterprises Corporation, Oak Ridge, Tennesse.U.S.A.

ELKIND, M. M. 1984. Repair Processes in Radiation Biology. *Radiat. Res.*, **100**, 425-449.

ENNOW, W. R. 1974. Measurements of the variance of energy deposition by means of exoelectron emitting materials. IN: Proc. Fourth Symp. Microdosim. (J. Booz et al, editors). Comm. Eur. Comm. EUR 5122. pp 925-929. Luxembourg.

ETTLING, K. and W. VON WITSCH. 1978. A thin-film scintillator detector for light ions in low-energy nuclear Physics. *Nucl. Instr. Meth.* **148,** 299-301.

EQUER, B. and A. KARAR. 1989. Amorphous semiconductors for particle detection: physical and technical limits and possibilities. *Nucl. Instr. Meth. Phys. Res.* **A275,** 558-563.

FABRY,L., A. LEONARD, AND A.WAMBERSIE. 1985. Induction of chromosome aberrations in Go human lymphocytes by low doses of ionizing radiations of different quality. *Radiat. Res.*, **103**, 122-134.

FOLKARD, M., K. M. PRISE, B. VOJNOVIC, S. DAVIES, M. J. RORER and B. D. MITCHAEL. 1989. The irradiation of V79 mammalian cells by protons with energies below 2MeV. *Int. J. Radiat. Biol.*, **56**, 221-237.

FOORD, R., R. JONES, C. J. OLIVER and E. R. PIKE. 1969. The use of photomultiplier tubes for photon counting. *Appl. Opt.*, **8**, 1975-1989.

FORSBERG, B. J. and T. E. BURLIN. 1978. Relations of secondary electron emission to microdosimetry and applications to two-target theory. IN: *Proc. of the sixth symp.on microdosim.*. Brussels. EURATOM 6064. pp 207-216.

FORSBERG, B. J. and LINDBORG, L., 1981. Experimental limitations in microdosimetry measurements of the dose mean lineal energy in a neutron beam. *Radiat. Protec. Dosim.*, **13**, 347-351.

FOWLER, J. F. 1966. Solid state electrical conductivity dosimeters. IN: *Radiation Dosimetry*. Vol.II (F. H. Attix and W. C. Roesch, editors). Academic Press. London. 291-324.

FOWLER, J. F. 1967. Biological significance of shape and volume of microdosimeters. IN: *Proc. of the symposium on microdosimetry*. Ispara (H. G. Ebert, editor). EURATOM 3747 d-f-e. pp 93-112.

FRANKENBERG, D., M. FRANKENBERG SCHWARGER., D. BLOECHER. AND R. HARBICH, R., 1981. Evidence for DNA Double strand breaks as the critical lesions in yeast cells irradiated with sparsely or densely ionizing radiation under oxic or anoxic conditionts. *Radiat. Res.*, **88** , 524-532.

FRANKENBERG, D., D. T. GOODHEAD, M. FRANKENBERG-SCHWARGER., R. HARBICH, R., D. A. BANCE and R. E. WILKINSON. 1981. Effectiveness of 1.5keV

Aluminium K and 0.3keV carbon characteristic X-rays at inducing double strand breaks in yeast cells. *Int. J. Radiat. Biol.*, **50**, 727-741.

FUSCOE, J. C., C. H. OCKEY and M. FOX. 1986. Molecular analysis of X-ray-induced mutants at the HPRT locus in V79 Chinese hamster cells. *Int. J. Radiat. Biol.*, **49**, 1011-1020.

GEISSEL, H., K. GUTTNER, S. HOFMAN and G. MUNZENBERG. 1977. Energy loss and straggling of alpha particles in thin homogeneous NE-111 scintillator foils. *Nucl. Instr. Meth.* **144**, 465-468.

GELBE, C. K., K. D. HILDENBRAND AND R. BOCK. 1971. Time-of-flight spectrometer for heavy ions. *Nucl. Instr. Meth.*, **95**, 397-402.

GOLDHAGEN, P., S.A. MARINO, G. RANDERS-PHERSON and P.KLIAUGA. 1990. Variance-covariance measurements of $y_D$ for 15-MeV neutrons in spherical sites with a wide range of sizes. IN: Proc. Tenth Symposium on Microdosimery. In Press.

GOODHEAD, D. T. 1987. Relationship of microdosimetric techniques to applications in Biological systems. IN: *The Dosimetry of Ionizing Radiations*. Vol. II (K. R. Kase et al, editors) Academic Press. London. 1-89.

GOODHEAD, D.T., J. THACKER. and COX, R. 1978 Non-rejoining DNA breaks and cell inactivation. *Nature (London)* **272**, 379-380 (1978).

GOODHEAD, D. T., J. THACKER and R. COX. 1979. Effectiveness of 0.3Kev carbon ultrasoft X-rays for the inactivation and mutation of cultured mammalian cells. *Int.J. Radiat. Biol.*, **36**, 101-114.

GOODHEAD, D.T., R.J.MUNSON, J. THACKER. and COX, R., 1980. Mutation and inactivation of cultured mammalian cells exposed to beams of accelerated heavy ions IV. Biophysical interpretation. *Int.J. Radiat. Biol.* **37**, 135-167.

GOODMAN, L. J. 1978. $W_N$ computed from recent measurements of W for charged particles. IN: *Proc. 3rd Symp on neutron dosimetry in biology and medicine.*, (G. Burger and G. Ebert, editors) Comm. Eurpean Communities, EUR-5848.

GOULDING, F.S. and B. G. HARVEY. 1975. Identificatication of Nuclear Particles. *Annual Review of Nuclear Science,* **25**, 167-240.

GUENTHER, K. and W. SCHUTZ. 1983. Biophysical Theory of Radiation Action - A Treatsise on Relative Biological Effectiveness. Akademic-verlag, Berlin.

HARVEY, J. A. and N. W. HILL. 1979. Scintillation detectors for neutron physics. *Nucl. Instr. Meth.* **162**, 507-529.

HEATH, R. C., R. HOFSTADLER and E. B. HUGHES. 1979. Inorganic scintillators. A review of techniques and applications. *Nucl. Instr. Meth.* **162**, 431-476.

HERAUD, A. P., S. P. BEAUMONT, C. D. W. WILKINSON, P. C. MAINT, J. R. OWERS-BRADLEY, AND E. J. EAVES. 1987. Inelastic electron scattering in pseudo-one-dimensional metal wires. *Phys. C: Solid State Phys.*, **20**, L249-L255.

HIEBER, L., G. PONSEL, H. ROSS, S. FENN, E. FROMKE, and A. M. KELLERER. 1985. Absence of a dose-rate effect in the transformation of C3H10T1/2 cells. *Int.J. Radiat. Biol.* **52,** 859-869.

HOLT, P. D. 1987. Interpretation of the variation of bacterial sensitivity with radiation quality at high LET using a two-ionisation Target theory. IN: *Nuclear and Atomic Data for Radiotheraphy and Related Radiobiology.* IAEA. Vienna. pp 69-80.

HOWARD-FLANDERS, P. 1958. Physical and chemical mechanisms in the injury of cells by ionising radiation. *Adv. Biol. Med. Phys.* **6,** 553-603.

HUTCHINSON, F., 1985. Chemical changes induced in DNA by ionising radaition. *Progress in Nucleic Acid Research and Molecular Biology,* **20,** 115-154.

INOKUTI, M. 1983. Radiation Physics as a basis of Radiation Chemistry and Biology. IN: *Applied Atomic Collision Physics.* Vol. **4** (S. Datz, editor) Academic Press. London. 179-236.

ICRU, 1969. Neutron Fluence, Neutron Spectra and Kerma. Report 13, (ICRU Publications, 7910 Woodmont Ave., Bethesda, Maryland, 20814,USA).

ICRU, 1970. Linear Energy Transfer. Report 16, (ICRU Publications, 7910 Woodmont Ave., Bethesda, Maryland, 20814,USA).

ICRU, 1983. Neutron dosimetry for Biology and Medicine, Report 26 (ICRU Publications, 7910 Woodmont Ave., Bethesda, Maryland, 20814,USA).

ICRU, 1979. Quantitative concepts and Dosimetry in Radiobiology. Report 30, (ICRU Publications, 7910 Woodmont Ave., Bethesda, Maryland, 20814,USA).

ICRU, 1979. Average energy required to produce an ion pair. Report 31, (ICRU Publications, 7910 Woodmont Ave., Bethesda, Maryland, 20814,USA).

ICRU, 1983. Microdosimetry, Report 36 (ICRU Publications, 7910 Woodmont Ave., Bethesda, Maryland, 20814,USA).

ICRU, 1984. The Stopping powers of electrons and positrons. Report 37, (ICRU Publications, 7910 Woodmont Ave., Bethesda, Maryland, 20814,USA).

ICRU, 1986. The Quality Factor in Radiation Protection. Report 40, (ICRU Publications, 7910 Woodmont Ave., Bethesda, Maryland, 20814,USA).

ICRP, 1978. RECOMMENDATIONS OF THE INTERNATIONAL COMMISSION ON RADIOLOGICAL PROTECTION. Reference Man, Publication 23. Pergamon, Oxford.

ISKEF, H., J. W. CUNNINGHAM and D. E. WATT. 1983. Projected ranges and effective stopping power of electrons with energy between 20eV and 10KeV. *Phys. Med. Biol.,* **28,** 535-545.

JACOBS, G. P., A. SAMUNI and G. CZAPSKI. 1985. The contribution of endogenous and exogenous effects to radiation-induced damage in the bacterial spore. *Int.J. Radiat. Biol.* **47,** 621-627.

JAGGER, J., 1967. *Introduction to research in ultraviolet photobiology*. Prentice Hall. Englewood Cliffs, New Jersey.

JANNI, J. G. 1982. Proton range-energy tables, 1keV - 10GeV. *Atomic Data and Nuclear Data Tables*, **27**, (2/3).

JAWAD, H. H. and D. E.WATT. 1986. Physical mechanism for inactivation of metallo-enzymes by characteristic X-rays. *Int.J. Radiat. Biol.*, **50**, 665-674.

JOHANSEN, I. and P. HOWARD-FLANDERS. 1965. Macromolecular repair and free radical scavenging in the protection of bacteria against X-rays. *Radiat. Res.*, **24**, 184-200.

KAMP, G. and K. EICCHORN. 1983. DNA strand breakage by different radiation qualities and relations to cell killing. *Studia Biophysica*, **93**, 17-26.

KAO, K. C. and W. Hwang. 1981. Electrical Transport in Solids. Pergamon Press. Oxford.

KAPLAN, H. S. and L. E. MOSSES. 1964. Biological complexity and radiosensitivity. *Science*, **145**, 21-25.

KATZ, R. and E. J. KOBETICH. 1968. Response of NaI(Tl) to energetic heavy ions. *Phys. Rev.* **170**, 397-400.

KATZ, R., S. C. SHARMA and M. HOMAYOONFAR. 1972. Detection of energetic heavy ions. *Nucl. Instr. Meth.* **100**, 13-22.

KELLERER, A. M. 1985. Fundamentals of Microdosimetry. IN: Dosimetry of Ionizing Radiation. (K. R. Kase et al, editors). Vol. 1, pp. 77-162. Academic Press. Orlando.

KELLERER, A.M., CHMELEVSKY, D. 1975. Creteria for the applicability of LET. *Radiat. Res.*, **63**, 226-234.

KELLERER, A. M. and H. H. ROSSI. 1972. The theory of dual radiation action. *Curr. Top. Radiat. Res. Q.* **8**, 85-158.

KELLERER, A. M. and H. H. ROSSI. 1978. A generalised formulation of dual radiation action. *Radiat. Res.* **75**, 471-488.

KELLERER, A. M. and H. H. ROSSI. 1984. On the determination of microdosimetric parameters in variable radiation fields. The variance-covariance method. *Radiat. Res.* **97**, 237-245.

KIEFER, J. 1985. Cellular and subcellular effects of very heavy ions. *Int.J. Radiat. Biol.* **48**, 873-892.

KIEFER, J., S. RASE, E. SCHNEIDER, H. STRAATEN, G. KRAFT and H. LIESEM., 1982. Heavy ion effects on yeast cells:induction of canavanine-ressistant mutants. *Int. J. Radiat. Biol.*, **42**, 591-600.

KLIAUGA, P. 1990. Measurement of single event energy deposition spectra at 5nm to 250nm simulated site sizes. IN: *Proc. Tenth Symposium on Microdosimetry*. Rome, 1989.

KOHL, J. W. 1975. Response of various thin-film scintillators to low-energy alpha particles. *Nucl. Instr. Meth.* **125**, 413-417.

KOLMAN, A., M. NASLUND, S. OSTERMAN-GOLKAR, G-P. SCALIA-TOMBA, A. MEYER. 1989. Comparative studies of *in-vitro* transformation by ethylene oxide and gamma-radiation of C3H /10T1/2 cells. *Mutagenessis,* **4**, 58-61.

KRAFT, G., 1987. Radiobiological effects of very heavy ions: inactivation, induction of chromosome aberrations and strand breaks. *Nuclear Science Applications*, **3**, 1-28.

KRANERT, T., J. KIEFER, E. SCHNEIDER. 1987.Mutation induction in mammalian cells by heavy ions: Preliminary investigations. *GSI-Scientific Report 1986*. GSI Darmstadt.

KRYSZEWSKI, M. 1980. Semiconducting Polymers. PWN-Polish Scientific Publishers. Warsaw. Poland.

KURAKADO, M. 1982. Possibility of high resolution detectors using superconducting tunnel junctions. *Nucl. Instr. Meth.* **196**, 275-277.

KURAKADO, M. and H. MAZAKI. 1980. Quasiparticle excitation in a superconducting tunnel junction by α-particles. *Phys. Rev.* **B22**, 168-173.

KURAKADO, M. and H. MAZAKI. 1981a. Possibility of high resolution detectors using superconducting tunnel junctions. I. Mean energy per excess quasiparticle. *Nucl. Instr. Meth.* **185**, 141-147.

KURAKADO, M. and H. MAZAKI. 1981b. Possibility of high resolution nuclear radiation detectors using a superconductor tunnel junctions. II. Tunnel junction. *Nucl. Instr. Meth.* **185**, 149-155.

LEDERER, C. M. and V. S. SHIRLEY. 1979. *Table of Isotopes*, 7th edition. Wiley-Interscience, New York.

LEE, K. Y., J. FROST, C. STANLEY, W. PATRICK, W. S. MACKIE, S. P. BEAUMOND and C. D. W. WILKINSON. 1987. Fabrication of ultrasmall devices on a thin active GaAs membranes. *J. Vac. Sci. Technol.* **B5**, 322-325.

LEWIS, T. J., 1982. The saventeenth Douglas Lea Lecture. Electronic processes in biolgy. *Phys. Med. Biol.*. **27**, 335-352.

LINDBORG, L., P. KLIAGA, S. MARINO and H. H. ROSSI. 1985. Variance - covariance measurements of the dose mean lineal energy in a neutron beam. *Radiat. Prot. Dosim.* **13**, 347-351.

LLOYD, D. C., R. J. PURROT, G. W. DOLPHIN and A. A. EDWARDS 1976 Chromosome aberrations induced by neutron irradiations. *Int. J. Radiat. Biol.* **29**, 169-182.

LLOYD, D.C. and A.A. EDWARDS. 1983. Chromosome aberrations in human lymphocytes: Effects of radiation quality, dose and dose rate. IN: *Radiation Induced Chromosome Damage in Man* (T.Ishihara and M.S.Sasaki, editors) New York: Alan

R.Liss. pp 23-49.

LLOYD, D. C., R. J. PURROT, G. W. DOLPHIN, D. BOLTON, A. A. EDWARDS, and M. J. CORP. 1975. The relationship between chromosome aberrations and low LET radiation dose to human lymphocytes. *Int. J. Radiat. Biol.*, **28**,75-90.

LLOYD, D. C., and R. J. PURROTT. 1981. Chromosome aberration analysis in radiological protection dosimetry. *Radiat. Prot. Dosim.*, **1**,19-28.

MAGNO, R., M. NISENOFF, R. SHELBY, A. B. CAMBELL, J. KIDD. 1981. Upset events in Josephson digital devices under alpha particle irradiation. *IEEE Trans. Nucl. Sci.* **NS28**, 3994.

MAGNO, R., M. NISENOFF, R. SHELBY, A. B. CAMBELL, J. KIDD. 1983. Alpha particle induced switching in Josephson tunnel junctions. *IEEE Trans. Mag.* **Mag 19**, 1286-1290.

MAKRIGIORGOS, G. and A. J. WALKER. 1985. The measurement of the restricted dose mean LET ratios of two photon spectra on the basis of initial recombination theory. *Radiat. Prot. Dosim.*, **13**, 383-386.

McGINNES, R. T. 1959. Energy spectrum resulting from electron slowing down. Circular 597, NBS Washington DC, 1959.

MEADE, M. L. 1981. Instrumentation aspects of photon counting applied to photometry. *J. Phys. E: Sci. Instrum.*, **34**, 909-918.

MILLER, R. C., C. R. GEARD, D. J. BRENNER, K. KOMATSU, S. A. MARINO and E. J. HALL. 1989. Neutron energy dependent oncogenic transformation of C3H10T1/2 mouse cells. *Radiat. Res.*, **117**, 114-127.

MIYAZAKI, N. and Y. FUJIWARA, 1981. Mutagenic and lethal effects of [5-$^{125}$I]Iodo-2'-deoxyurridine incorporated into DNA of mammalian cells, and their RBEs. *Radiat. Res.*, **88**, 456-465.

MORTIMER, R., T. BRUSTAD, and D. V. CORMACK, 1965. Influence of linear energy transfer and oxygen tension on the effectiveness of ionizing radiations for induction of mutations and lethality in Saccharomyces Cerevisiae. *Radiat. Res.*, **26**, 465-482.

MUGA, L. and G. GRIFFITH. 1974. Specific luminescence studies in plastic scintillators. *Phys. Rev.* **B9**, 3639-3649.

MUGA, L. and G. GRIFFITH. 1973a. Response of thin film scintillator to light and heavy ions. *Nucl. Instr. Meth.* **109**, 289-295.

MUGA, L. and G. GRIFFITH. 1973B. Double valuedness of specific luminescence as a function of stopping power. *Phys. Rev.* **B8**, 4069-4071.

MUGA, M. L., D. J. BURNSED and W. E. STEEGER. 1972. Recipe for making a thin film detector. *Nucl. Instr. Meth.* **104**, 605-610.

MUGA, L., G. L. GRIFFITH, H. L. SCHMITT and H. E. TAYLOR. 1973. Thin film detector response to the passage of accelarated heavy ions. *Nucl. Instr. Meth.* **111**,

581-585.

MUSSA, T. A. K., B. SINGH AND P. BRYANT. 1990. Enhanced mutability at the tk locus in the radiosensitive double-strand break repair xrs5. *Mut. Res.* In press.

NEARY, G. J. 1965. Chromosome aberrations and the theory of RBE. I. General considerations. *Int. J. Radiat. Biol.*, **9**, 477-502.

NEWMAN, E. and F. E. STEIGERT. 1960. Response of NaI(Tl) to energetic heavy ions. *Phys. Rev.* **118**, 1575-1578.

NORTHCLIFFE, L. C. and R. F. SCHILLING. 1970. Range and stopping power Tables for Heavy ions. *Nuclear Data Tables.* **7**, 233-463.

NUCLEAR ENTERPRISES. Sighthill, Edinburgh. Scotland EH11 4BY.

OKADA, S. 1970. DNA as a target responsible for cell killing. IN: *Radiation Biochemistry,* edited by K. I. Altman, G. B. Gerber and S. Okada, Vol. I. New York: Academic Press, pp. 103-155.

OLIVER, C. J. and E. R. PIKE. 1968. Measurement of low light flux by photon counting. *J. Phys. D: Appl. Phys.* **1**, 1459-1568.

ORLIC, M. 1990. A microdosimetric semiconductor Counter. IN: *Proc. Tenth Symposium on Microdosimetry.* Rome, 1989.

PLATZMAN, R., 1967. Energy spectrum of primary activations in the action of ionizing radaitions. IN: *Radiation Research*, Proc. 3rd. Int. congress. Cortina d'Ampezzo, Italy, 1966, pp 20-42, (North Holland Publishing Company, Amsterdam).

POLICARPO, A. J. P. L. 1977. The gas proportional scintillation counter. *Space Science Instrumentation,* **3**, 77-107.

PRESCOTT, J. R. and G. H. NARAYAN. 1969. Electron responses and intrinsic line-widths in NaI(Tl). *Nucl. Instr. Meth.* **75**, 51-55.

PRISE, K. M., S. DAVIES and B. D. MITCHAEL. 1989. Cell killing and DNA damage in Chinese hamster V79 cells treated with hydrogen peroxide. *Int. J. Radiat. Biol.*, **55**, 583-592.

PURROTT, R. J., E. J. REEDER and S. LOVEL, 1977. Chromosome aberration yields in human lymphocytes by 15MeV electrons given at conventional dose-rate and in microsecond pulses. *Int. J. Radiat. Biol.*, **31**, 251-

RADFORD, I. R. 1986. Evidence for a general relationship between the level of DNA double strand breakage and cell killing after X-irradiation of mammalian cells. *Int. J. Radiat. Biol.*, **49**, 611-620.

RAJU, M. R. 1980. Heavy Particle Radiotherapy. Academic Press. New York.

RAJU, M. R., M. GNANAPURANI, and B. STACKLER, 1971. Induction of Heteroallelic Reversions and Lethality in *saccharomyces cerevisiae* Exposed to Radiations

of Various LET ($^{60}$Co γ-rays, Heavy ions and π⁻mesons) in Air and Nitrogen Atmospheres. *Radiat. Res.*, **47**, 635-643.

RAUTH, A. M. and J. A. SIMPSON. 1964. The energy loss of electrons in solids. *Radiat. Res.*, **22**, 643-661.

RBE COMMITTEE. 1963. Report of the RBE commitee to the International commission on Radiological Protection and Radiological Units and measurements. *Health Physics*, **9**, 357-386.

RESNICK, M. A. and P. MARTIN. 1976. Repair of double-strand breaks in the nuclear DNA of saccharomyces cerevisiae and its genetic control. *Molecular and General Genetics*, **143**, 119-129.

REZNIKOFF, C. A., J. S. BETRAM, D. W. BRANKOW, C. HEIDELBERGER. 1973. Quantitative and qualitative studies of chemical transformation of clonal C3H mouse embro cells sensitive to post confluence inihibition of division. *Cancer. Res.* **39**, 123-130.

RITTER, M.A., J. E. CLEAVER and C.A. TOBIAS. 1977. High-LET radiations induce a large proportion of non-rejoining DNA breaks. *Nature (London)* **266**, 653-655.

ROBERTS, C. J. and P. D. HOLT. 1985. Induction of chromosome aberrations and cell killing in syrian hamster fibroblasts by γ-rays, X-rays and fast neutrons. *Int. J. Radiat. Biol.*, **48**, 927-939.

ROBERTS, G. G., P. S. VINCETT and W. A. BARLOW. 1981. Technological applications of Langmuir-Blodgett films. *Physics Technology*, **12**, 69-87.

ROOTS, R. AND S. OKADA. 1975. Estimation of life times and diffusion distances of radicals involved in X-ray induced DNA strand breaks or killing of mammalian cells. *Radiat. Res.*, **64**, 306-320.

ROOTS, R., A. CHATTERJEE, P. CHANG, L. LOMMEL AND E. A. BLAKELY. 1985. Characterization of hydroxyl radical-induced damage after sparsely and densely ionizing irradiation. *Int. J.Radiat. Biol.*, **47**, 157-166.

ROSSI, H. H. 1968. Microscopic energy distribution in irradiated matter. IN: Radiation Dosimetry (F.H.Attix and W.C.Roesch, editors) Volume **I**, 43-92. Academic Press, New York.

ROSSI, H. H. 1970. Experimental limitations of microdosimetry. IN: *Proc. second symp. on microdosimetry* (H. G. Ebert, editor) Comm. of European communities. EURATOM. EUR 4452-d-f-e. Brussels. pp 303-326.

SCHMID, E., G. RIMPL and M. BAUCHINGER. 1974. Dose-response relation of chromosomal aberrations in human lymphocytes after in-vitro irradiation with 3MeV electrons. *Radiat. Res.* **57**, 228-

SEVANKAEV, A., E. A. ZHERBIN, N. V. LUCHNIK, G. M. OBATUROV, V. M. KOZLOV, E. G. TYATTE, S. P. KAPCHINGASHEV. 1979 Neutron-induced cytogenetic effects of neutrons of different energies on various types of chromosome aberrations. *Genetica*, **15**, 1046-1052.

SEELANTAG, W. W., W. PANTHER, G. DREXLER, L. PLATZ and F. SANTER. 1979. A catalogue of spectra used for the Calibration of Dosimeters. GSR Report S-560.

SKARSGARD, L. D., B. A. KIHLMAN, L. PARKER, C. M. PUJARA and S. RICHARDS. 1967. Survival, chromosome abnormalities and recovery in heavy ion- and X-irradiated mammalian cells. *Radiat. Res.*, **7**, 208-221.

SMITH, D. L., R. G. POLK, and T. G. MILLER. 1968. Measurement of the response of several organic scintillators to electrons, protons and deutrons. *Nucl. Instr. Meth.*, **64**, 157-166.

SONNTAG, von C. 1987. *The Chemical Basis of Radiation Biology.* Taylor and Francis. 94-115. London.

SPARROW, A. H., A. G. UNDERBRINK and R. C. SPARROW. 1967. Chromosome and cellular radiosensitivity. I. Relationship of $D_0$ to chromosome volume and complexity in seventy-nine different organisms. *Radiat. Res.*, **32**, 915-945.

SWANSON, N. and C. J. POWELL. 1963. Excitation of $\pi$ electrons in polystyrene and similar polymers by 20keV electrons. *J. Chem. Phys.*, **39**, 630-634.

SYKES, C. E. and D. E. WATT. 1989. Interpretation of the increase in the frequency of neoplastic transformations observed for some ionising radiations at low dose rates. *Int. J. Radiat. Biol.*, **55**, 925-942.

TAKATSUJI, T. and M. S. SASAKI. 1984. Dose-effect relationship of chromosomal aberrations induced by 23MeV alpha particles in human lymphocytes. *Int. J. Radiat. Biol.*, **45**,237-243.

TAKATSUJI, T., H. TAKAKOSHI, and M. S. SASAKI. 1983. Induction of chromosome aberrations by 4.9MeV proton in human lymphocytes. *Int. J. Radiat. Biol.*, **44**, 553-562.

TAKAHASHI, E., M. HIRAI, I. TOBARI, T. UTSUGI and S. NAKAI. 1982. Radiation-induced chromosome aberrations in lymphocytes from man and crab-eating monkey: The dose-response relationships at low doses, *Mutat. Res.*, **94**,115-

TODD, P., 1967. Heavy-ion irradiation of cultured human cells. *Radiat. Res. Supplement*, **7**,196-207.

THACKER, J., M. A. STEPHENS and A. STRECH. 1976. Factors affecting the efficiency of purine analogues as selective agents for mutants of mammalian cells induced by ionising radiation. *Mutat. Res.*, **35**, 465-478.

TOLKENDORF, E. and K. EICHHORN. (1983) Effect of ionizing radiation of different linear energy transfer on the induction of cellular death and chromosomal aberrations in cells of chinese hamster. *Studia Biophysica*, **95**, 43-56.

THACKER, J., A. STRETCH and D. T. GOODHEAD. 1982. The mutagenecity of $\alpha$-particles from Plotonium-238. *Radiat. Res.*, **92**, 343-352.

TUNG, C. J. and P. J. CHEN. 1983. Energy loss and range stragglings for electrons in water. IN: *Proc. Eighth Symposium on Microdosimrtry*, Harwood Academic Publishers,

London, Commission for European Communities, EUR 8395, pp 243-254.

TURNER, J. E. AND H. HOLLISTER. 1962. The possible role of momentum in radiation dosimetry. *Health Physics,* **8,** 523-532.

TWENRENBOLD, D., A. ZEHNDER, and R. ZACEK. 1984. Development of high resolution superconductive detector for KeV radiation at SIN. IN: *4th Int. School of Physics of exotic Atoms*. Enice, Italy. (Plenum Press, New York) pp 421-434.

UNITED NATIONS SCIENTIFIC COMMITTEE ON THE EFFECTS OF ATOMIC RADIATIONS (UNSCEAR), 1977. Sources and Effects of Ionizing Radiation. New York.

UPTON, A.C., 1977. Radiobiological effects of low doses. Implications for radiological protection. *Radiat. Res.*, **71,** 51-74.

VIRSIK,R.P., R. BLOHM, K. P. HERMANN and D. HARDER.1981. IN: *Proc. Seventh Symposium on Microdosimrtry*, Oxford 1980 (H.G.Ebert, editor) Harwood Academic Publishers, London, Commission for European Communities, EUR 7147 DE-EN-FR.

VIRSIK, R.P., D. T. GOODHEAD, R. COX, J. THACKER, C. H. SCHAER, and D. HARDER. 1980. Chromosome aberrations induced in human lymphocytes by ultrasoft $Al_k$ and $C_k$ x-rays. *Int. J. Radiat. Biol.*, **38,** 545-557.

VIRSIK, R. P., R. BLOHM, K. P. HERMAN, H. MODLER and D. HARDER. 1983. IN: Radiation Protection. *Proc. Eighths Symposium on Microdosimetry* (J. Booz and H. G. Ebert, Editors). 409-422. Harwood Academic Publishers. Comm. European Communities, Luxemburg.

VIRSIK, R. P. and D. HARDER. 1978. Chromosome aberrations in human lymphocytes induced by photon and electron radiations, and the sublesion interraction model. IN: *Proc. Sixth Symposium on Microdosimery* (J. Booz and H. G. Ebert, editors) pp.869-881. Harwood Academic Publ. for Comm. of European Comm., London.

VIRSIK, R. P. and D. HARDER. 1980. Recovery kinetics of radiation-induced chromosome aberrations in human $G_0$ lymphocytes. *Rad. Envirom. Biophsics,* **18,** 221-238.

VIRSIK-PEUKERT, R. P.,1983. Inducibility of chromosome abberrations by ultrasoft X-rays. IN: *Radiation Induced Chromosome Damage in Man* (T. Ishihara and M. S. Sasaki, editors) New York : Alan R. Liss. pp 23-49.

VOLTZ, R., J. LOPES DA SILVA, G. LAUSTRIAT and A. COCHE. 1966. Influence of the nature of ionizing particles on the specific luminescence of organic scintillators. *J. Chem. Phys.* **45,** 3306-3311.

VULPIS, N., L. TOGNACCI, G. SCARPA. 1978. Chromosome aberrations as a dosimetric technique for fission neutrons over the dose-range 0.2-50 rad. *Int. J. Radiat. Biol.*, **33,** 301

WARD, R. L. 1980. Mechanism of poliovirus inactivation by direct and indirect effects of

ionizing radiation. *Radiat. Res.* **83**, 330-344.

WARD, J. F. 1985. Biochemistry of DNA lesions. *Radiat. Res.* **104**, 103-111.

WARTERS, R. L., K. G. HOFER, C. R. HARRIS and J. M. SMITH. 1977. Radionuclide toxicity in cultured mammalian cells: Elucidation of the primary site of radiation damage. *Curr. Top. Radiat. Res. Q.*, **12**, 389-407.

WATT, D. E. 1975. Hit cross-sections in single target theory. *Phys. Med. Biol.*, **20**, 944-954.

WATT, D. E. 1988. Absolute biological effectiveness of neutrons and photons. *Radiat. Protec. Dosim.*, **23**, 63-67.

WATT, D.E., 1989. On absolute biological effectiveness and unified dosimetry. *J. Soc. Radiol. Protect.* **9**, 33-49.

WATT, D. E. and L. A. KADIRI. 1990. Physical quantification of the biological effectiveness of ionizing radiations. *Int. J. Quantum Chemistry,* **xxvii**, In press.

WATT, D. E., A. T. AL-KAZWINI, H. M. A. AL-SHAIBANI and D. A. A. TWAIJ. 1981. Studies in enzyme inactivation as prelude to damage modelling. IN: *proc. of 7th symposium on microdosimetry,* EUR 7147 (London: Harwood Academic). 1475-1488.

WATT, D. E., I. A. M. AL-AFFAN, C. Z. CHEN and G. E. THOMAS.1985. Identification of biophysical mechanisms of damage by ionizing radiation. *Radiat. Prot. Dosim.*, **13**, 285-294.

WATT, D. E., R. J. CANNELL and G. E. THOMAS. 1984. Ion Beams in Quality Determination for Radiation Protection. IN: Int. Symp. on 3-day in depth Review on the Nuclear Accelarator Impact in the Interdisplinary Field. Laboratoire Nazionali di Legnaro, Padova, Italy.

WHITE, T. O., 1988. Scintillating fibres. *Nucl. Instr. Meth. Phys. Res.*, **A273**, 820-825.

WILKINSON, C. D. W. and S. P. BEAUMONT. 1986. Electron Beam Nanolithography. IN: The Physics and facrication of microstructures and microdevices (C. Weisbuch and M. J. Kelly, editors). Springer-verlag. Heidelberg. pp 36-50.

WILSON, W. E. and H. G. PARETZKE, 1980. Calculation of ionisation frequency distributions in small sites. *Rad. Res.*, **81**, 316-335.

WOOD, G. H. and B. WHITE. 1969. Pulses induced tunneling currents between superconductors by alpha-particle bombardment. *Appl. Phys. Lett.*, **15**, 237-239.

WOOD, G. H. and B. WHITE. 1973. The detection of alpha particles with superconducting tunnel junctions. *Can. J. Phys.*, **51**, 2032-2046.

WRIGHT, A. G. 1984. Design of photomultiplier output circuits for optimum amplitude or time response. Thorn EMI R/P065.

YAFFE,Y. 1962. Preparation of thin films, sources and targets. *Ann. Rev. Nucl. Sci.*

**12**, 153-188.

YANG, T. C-H., L. M. CRAISE, L. M., M-T. MEI and C. A. TOBIAS. 1985. Neoplastic cell transformation by heavy charged particles, *Rad. Res.*,**104**, S177-S187.

YOUNIS, A. R. S. and D. E. WATT. 1989. The quaility of ionising radaitions emitted by radionuclides incorporated into mammalian cells. *Phys. Med. Biol.*, **34**, 821-834.

YUSUI, L. S., and K. G. HOFER. 1986. Role of mitochondrial DNA in cell death induced by $^{125}$I decay. *Int. J. Radiat. Biol.*, **49**, 601-610.

YUSUI, L. S., K. G. HOFER and R. L. WARTERS. 1985. Inhomogeneity of the nuclues to $^{125}$IUdR cytotoxity. *Rad. Res.*,**102**, 106-118.

ZIEGLER, J. F. 1980. The Stopping cross-sections for energetic ions in all elements. Handbook of Stopping Cross Sections of Energertic Ions in Matter. Vol. 5. Pergamon. New York.

ZIEGLER, J. F., J. P. BIERSACK AND U. LITTMARK. 1985. The Stopping and range of ions in solids. Vol. 1 of The stopping and ranges of ions in matter (J. F. Ziegler, editor). Pergamon. New York.

ZIELCZYNSKI, M., N. GOLNIK, M. MARKAREWICZ, A. H. SULLIVAN. 1981. Definition of radiation quality by initial recombination of ions. IN: Proc. seventh symposium on Microdosimetry (Booz et al, editors). EUR 7147 (Luxembourg: CEC) 853-862.